PROTEIN-PROTEIN INTERACTIONS OF THE HUMAN IRON SULFUR CLUSTER BIOSYNTHESIS COMPLEX

A Dissertation

by

MICHAELLA JANE LEVY

Submitted to the Office of Graduate and Professional Studies of
Texas A&M University
in partial fulfillment of the requirements for the degree of

DOCTOR OF PHILOSOPHY

Chair of Committee,	David Barondeau
Committee Members,	Marcetta Y. Darensbourg
	Margaret E. Glasner
	David H. Russell
Head of Department,	David H. Russell

August 2014

Major Subject: Chemistry

ABSTRACT

Iron sulfur (Fe-S) clusters are integral cofactors responsible for a number of cellular processes including electron transfer, catalyzing substrate turnover, sensing small molecules, and regulating gene expression or enzymatic activity. Elaborate multi-component systems have evolved to protect organism from the toxic effects of free iron and sulfide ions while promoting the efficient biosynthesis of these cofactors. Previously, our lab discovered the human cysteine desulfurase complex (NFS1-ISD11, named SD) and the Fe-S assembly scaffold protein ISCU2 form a low activity Fe-S assembly complex (named SDU) that can be activated by the allosteric activator frataxin (FXN) to generate the high activity SDUF Fe-S assembly complex. Importantly, mutations in FXN result in the neurodegenerative disease Friedreich's Ataxia (FRDA), whereas mutations in ISCU2 lead to a disease characterized by myopathy with exercise intolerance.

The goals of this dissertation were to provide structural details for protein-protein interactions in the human SDUF complex, contribute to understanding how FXN binds and activates the assembly complex, and define how a clinical ISCU2 variant was compromised in Fe-S assembly activity. To address these questions, a multidisciplinary approach was initiated that included anaerobic biochemistry and kinetic assays, fluorophore incorporation for anisotropy measurements, and chemical modifications coupled to mass spectrometry experiments. First, protein interfaces were probed by hydroxyl radical footprinting experiments where the SD, SDU, and SDUF complexes

were exposed to different does of synchrotron radiation (generating hydroxyl radicals) and the resulting modified proteins were proteolytically digested and analyzed by MALDI mass spectrometry. These experiments revealed that ISCU2 binding to the SD complex results in a decrease in modification kinetics to for regions of ISCU2 near the N-terminus. Consistent with this assignment, kinetic assays revealed that the clinical ISCU2 variant, which has a mutation near the N-terminus, exhibits cysteine desulfurase and Fe-S assembly activities similar to native ISCU2, but compromised binding affinity to the assembly complex. Next, hydroxyl radical footprinting experiments revealed that FXN binding to the SDU complex resulted in the C-terminal α-helix of ISCU2 becoming more protected and suggested specific interactions associated with FXN activation. Next, fluorescence anisotropy experiments under different experimental conditions revealed both determinants for FXN binding and that the FRDA variant has compromised binding affinity to the SDU complex. Finally, this activation model was tested and supported by mutagenesis and binding studies that indicated residues in this C-terminal α-helix of ISCU2 interacts with residues on the β-sheet region of FXN, which are associated with FRDA. Together, these studies reveal details of the protein-protein interactions and function of the human SDUF complex that have implications for human disease.

ACKNOWLEDGMENTS

I would like to acknowledge the people who provided unwavering support and guidance through this process. Professionally and personally, I would like to thank Dr. Stephanie Cologna, Dr. Pei-Jing Pai, and Dr. Ashley Gucinski for sharing their knowledge of mass spectrometry, being patient teachers, and good friends. I would also like to acknowledge the excessive patience and confidence Dr. Michael Boyne has shown toward me and the encouragement of my career choices.

I wish to acknowledge the generosity of the David H. Russell research group for their help with experiments and their willingness to help me run samples in the mass spectrometry facility. I would like to acknowledge Dr. RhijutaD'Mello and Dr. Sayan Gupta of Brookhaven National Laboratory at beamline X28C for exposing my samples for the hydroxyl radical footprinting experiments and working closely with me over the course of more than a year to collect the samples that are the bulk of this dissertation. I would like to thank undergraduate students Mr. Andrew Winn for his assistance performing the fluorescence anisotropy titration experiments, Mr. Ryan Lake for his attempts to label ISCU2 with fluorophores, and Ms. Emily Carr for all of her work on the crystallization of NFS1-ISD11.

Lastly, but definitely not least, I would like to thank my family and friends for their support and love. It has been a long and sometimes tough but rewarding journey. To my rugby ladies, you are truest friends a person could ask for. I'm not sure I could have done this without friends like you. To my family, thank you for all the phone calls,

care packages, and trips to visit me, among all of the other support you've shown me through this process. I feel so blessed to be able to claim you as my family.

NOMENCLATURE

A. fulgidus	*Archaeoglobus fulgidus*
A. vinelandii	*Azotobacter vinelandii*
ADP	Adenosine diphosphate
ATP	Adenosine triphosphate
BLI	Bilayer interferometry
CD	Circular dichorism
CIA	Cytosolic iron sulfur cluster assembly
DNA	Deoxyribonucleic acid
DPD	*N, N'*-diphenyl-*p*-phenylenediamine
DTT	Dithiothreitol
E. coli	*Escherichia coli*
Fe-S	Iron sulfur
FRDA	Friedreich's Ataxia
FRET	Förster resonance electron transfer
FXN	Frataxin
ISC	Iron sulfur cluster assembly
ITC	Isothermal titration calorimetry
MS	Mass spectrometry
NIF	Nitrogen fixation pathway
NMR	Nuclear magnetic resonance
PDB	Protein data bank

PLP	Pyridoxyl-5'-phosphate
S. cerevisiae	*Saccharomyces cerevisiae*
SAXS	Small angle X-ray scattering
SD	NFS1/ISD11 protein complex
SDU	NFS1/ISD11/ISCU2 protein complex
SDUF	NFS1/ISD11/ISCU2/FXN protein complex
SPR	Surface plasmon resonance
SUF	Mobilization of sulfur pathway
TOF	Time of flight

TABLE OF CONTENTS

LIST OF FIGURES

LIST OF TABLES

CHAPTER I

INTRODUCTION AND LITERATURE REVIEW

Iron sulfur (Fe-S) clusters are integrals cofactors found in most, if not all, organisms and are commonly found with stoichiometries such as a rhombic 2Fe-2S, a 3Fe-4S, or a cubane 4Fe-4S (Figure 1-1, A-C).[1-3] Fe-S clusters play a critical role in many important biological processes including electron transfer or catalysis due to their ability to exist in multiple redox states. For example, 2Fe-2S clusters are found in proteins required for DNA repair,[4] gene regulation,[5] post-translational modifications,[6] and also in the biosynthesis of other iron containing proteins.[7] Proteins requiring 4Fe-4S clusters function in respiration and the tricarboxylic acid cycle among other roles in *E. coli*.[1, 8] Additionally, some clusters are required only for structural stability of proteins.[1] The functional properties of these clusters are tuned by their location, solvent accessible or buried in the protein, and also the characteristics of the residues that surround the Fe-S cluster. Other configurations have also been observed for highly specialized functions such as the complex [8Fe-8S] P-cluster in nitrogenase (Figure 1-1D) or systems in which a [4Fe-4S] cluster is linked to a nickel center (acetyl-CoA synthase), a siroheme (sulfite reductase), or a di-iron cluster ([FeFe]-hydrogenase).[9]

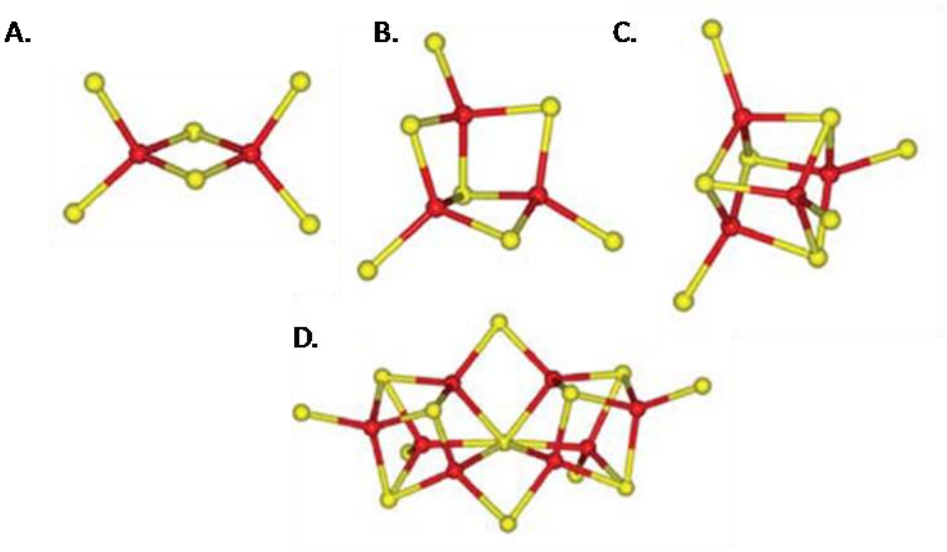

Figure 1-1. Common Fe-S cluster forms found in biological systems include the: A.) 2Fe-2S cluster; B.) 3Fe-4S cluster; C.) cubane 4Fe-4S cluster; and D.) 8Fe-8S cluster from nitrogenase. The iron atoms are shown in red and the sulfur atoms are shown in yellow. Reprinted with permission from *Annu. Rev. Biochem*., 74:247-281. Copyright 2005 Annual Reviews.[9]

It appears that prokaryotic organisms took advantage of the properties of iron and sulfur to perform cellular tasks in a reducing, anaerobic environment.[10-16] In fact, the Holm's group and others have demonstrated that the common biological forms of Fe-S clusters can be self-assembled from iron and sulfide in solution.[17] Unlike the early reducing environment in which there were high levels of ferrous iron and hydrosulfide ion, after the Great Oxidation Event both reagents became limited. As a consequence, bacteria developed three separate Fe-S assembly systems, the nitrogen fixation (NIF), mobilization of sulfur (SUF), and the iron-sulfur cluster assembly (ISC) pathways.[18-22] These Fe-S assembly systems have evolved to not only sequester and protect the cell from the potentially toxic effects of free iron and sulfide, but also synthesize and deliver different forms of Fe-S clusters to the appropriate apo targets.[11] Eukaryotic Fe-S cluster

assembly pathways that are found in organelles appear to have evolved from these bacterial systems (Figure 1-2).[22, 23] For example, the Fe-S assembly machinery inside plant and algae plastids is analogous to the SUF machinery, whereas mitochondria contain Fe-S cluster machinery with homology to the ISC system. Eukaryotes also contain an additional pathway termed the cytosolic iron sulfur cluster assembly (CIA), which can deliver Fe-S clusters to appropriate proteins in the cytosol and the nucleus.[22] The CIA pathway is unique in that it has no prokaryotic analog and does not appear to contain typical assembly components such as a cysteine desulfurase or Fe-S scaffold protein (see below).

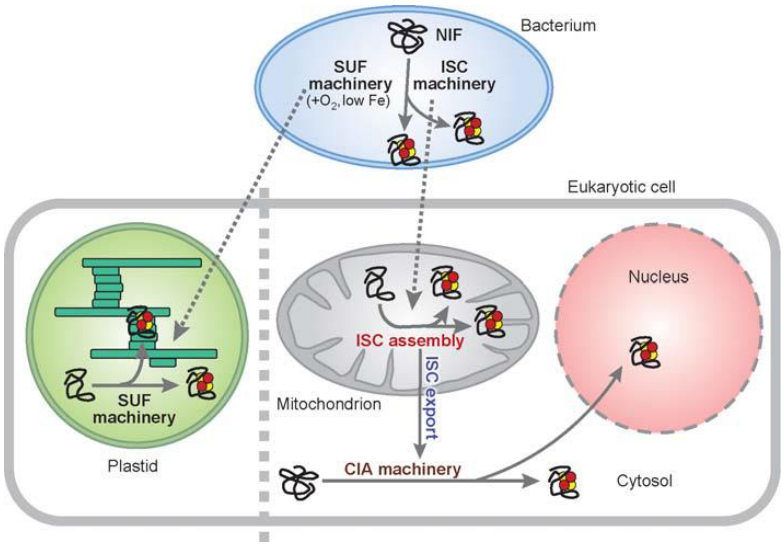

Figure 1-2. Iron sulfur cluster assembly pathways. Reprinted with permission from *Annu. Rev. Cell Dev.Biol*, 22:457-486. Copyright 2006 Annual Reviews.[22]

Fe-S ASSEMBLY PATHWAYS IN PROKARYOTES

The best studied iron sulfur cluster assembly system is likely the ISC pathway from *E. coli.* The ISC operon from *E. coli* (Figure 1-3)[24] contains the genes thought to be critical for Fe-S assembly, and many of the assembly proteins have functional analogs in the NIF and SUF systems. The cysteine desulfurase (IscS in Figure 1-3) is a PLP-dependent enzyme that converts cysteine to alanine and forms a transient persulfide intermediate with a cysteine on the mobile loop (Figure 1-4).[9, 25, 26]

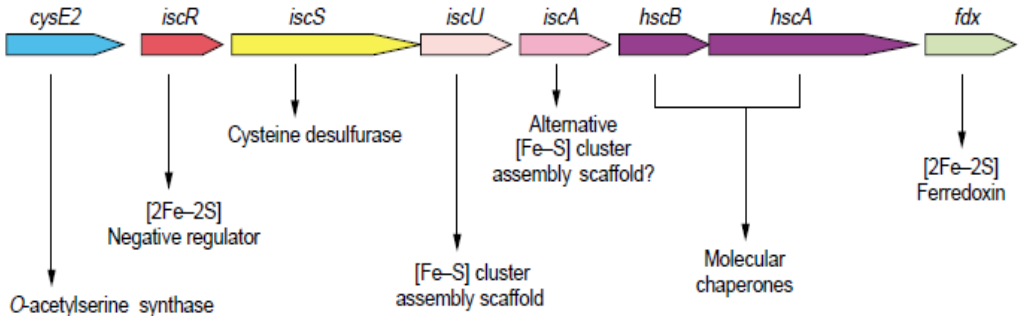

Figure 1-3. ISC operon from *E. coli*. Adapted with permission from *Current Opinion in Chemical Biology*, 7:166-173. Copyright 2003 Elsevier Science Ltd.[24]

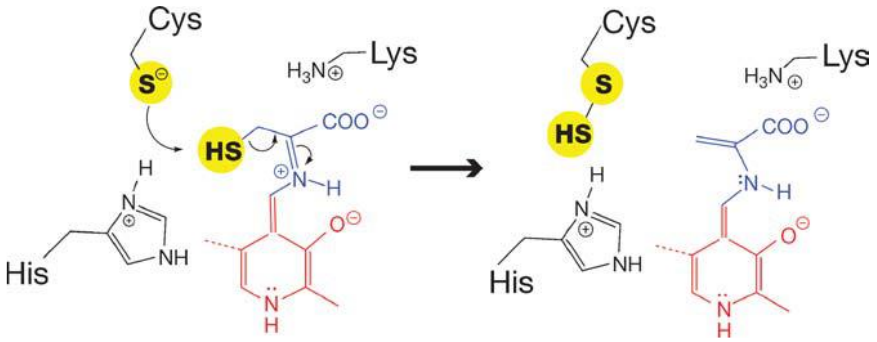

Figure 1-4. Cysteine desulfurase catalyzed sulfur carbon bond cleavage of a PLP-substrate adduct to form a cysteine bound persulfide. Reprinted with permission from *Annu. Rev. Biochem*., 74:247-281. Copyright 2005 Annual Reviews.[9]

The cysteine desulfurase transfers the sulfur to the second component of the system, the Fe-S cluster assembly scaffold protein. The scaffold protein (IscU, Figure 1-3) combines the sulfur atoms with iron and electrons to synthesize Fe-S clusters.[25] It has been shown that the scaffold can assemble a single $[2Fe\text{-}2S]^{2+}$ on a monomer of the scaffold that can be reductively coupled to form a $[4Fe\text{-}4S]^{2+}$ cluster, which is thought to bridge the subunits in a homodimeric IscU species.[9, 27-29] The $[4Fe\text{-}4S]^{2+}$ cluster can be oxidized back to the $[2Fe\text{-}2S]^{2+}$ upon exposure to O_2.[28]

Crystal structures of the *E. coli* IscS homodimeric[30] and IscS-IscU homotetramer[31] species reveal protein-protein interactions and provide a basis for the development of testable functional models. The crystal structure of IscS-IscU shows that the C-terminus of each subunit of the of IscS dimer interacts with the N-terminus of a IscU molecule to create an elongated S-shaped complex (Figure 1-5).[31] A crystal structure was also recently determined for the *Archaeoglobus fulgidus* (*A. fulgidus*) IscS-IscU complex that contains a [2Fe-2S].[32] Interestingly, the three conserved IscU

cysteines along with mobile loop cysteine of IscS ligated the Fe-S cluster. The D37A IscU mutant (discussed below), which is thought to stabilize the labile Fe-S cluster species and also form a tighter protein complex with IscS, was used for both of the IscS-IscU crystallographic studies. Gel filtration studies also support a heterotetrameric IscS-IscU complex in solution,[33] whereas the molecular envelope from small angle X-ray scattering (SAXS) curves suggest a solution structure consistent with the elongated S-shaped observed in the crystal structure.[34]

The co-crystal of the *E. coli* IscS-IscU has brought into question what oligomeric state of IscU is the biologically relevant form for cluster assembly and transfer. Johnson and co-workers have observed the formation of a $[4Fe\text{-}4S]^{2+}$ cluster that bridges a dimer interface of two IscU monomers from *A. vinelandii*.[27, 28]Based on this result, most Fe-S assembly models invoke a dimeric IscU species that interacts with chaperones for cluster transfer to apo target proteins. However, in the IscS-IscU crystal structure each molecule of the IscS dimer interacts with a single monomer of IscU. It will therefore be critical to determine if the scaffold protein is capable of forming a IscU dimer when bound to IscS, if IscU dissociates from the cysteine desulfurase after Fe-S cluster assembly but prior to cluster transfer, or if the dimeric form of IscU is not relevant for cluster transfer (see cluster transfer models below).

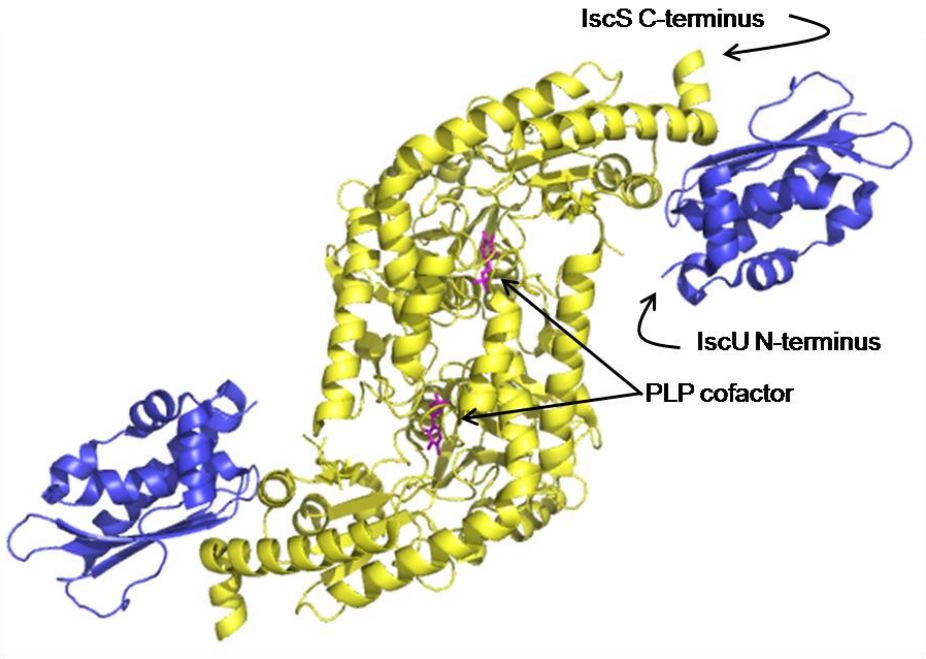

Figure 1-5. Cartoon model of the *E. coli* IscS-IscU protein complex based on the crystal structure (PDB code: 3LVL). The IscS dimer is shown in yellow and the IscU molecules are shown in blue. The PLP-cofactor is shown in magenta.

NMR studies of *E. coli* IscU indicate an equilibrium mixture between two conformational states, an ordered and a dynamically, disordered state that interconvert on the second time scale.[35] Determination of the NMR structure for the ordered state revealed a similar conformation to that of the Zn^{2+} bound IscU from *Haemophilus influenzaei*[36] and the IscU conformation found in the IscS-IscU complex structures.[31] Additionally, NMR studies showed that the D39A (*E. coli* numbering) IscU mutation, which is known to bind a Fe-S cluster tighter than wild-type IscU,[37-39] is primarily in the ordered state (Figure 1-6).[35]Consistent with this idea, circular dichroism (CD) measurements as a function of temperature revealed that mutations at position 39

(including D39A, D39L and D39V but not D39G) increased the thermal stability of IscU.[40] Three additional mutations to IscU were discovered that favored the ordered state (N90A, S107A, and E111A) and two that favored the disordered state (K89A and N90D) (Figure 1-6).[35]Interestingly, these NMR studies suggested that IscS preferentially binds and stabilizes IscU in the disordered state.[35] These results directly contradict previous experiments that indicate the D37A variant, which exhibits the ordered conformation, increases the binding affinity of IscS for IscU.[35]

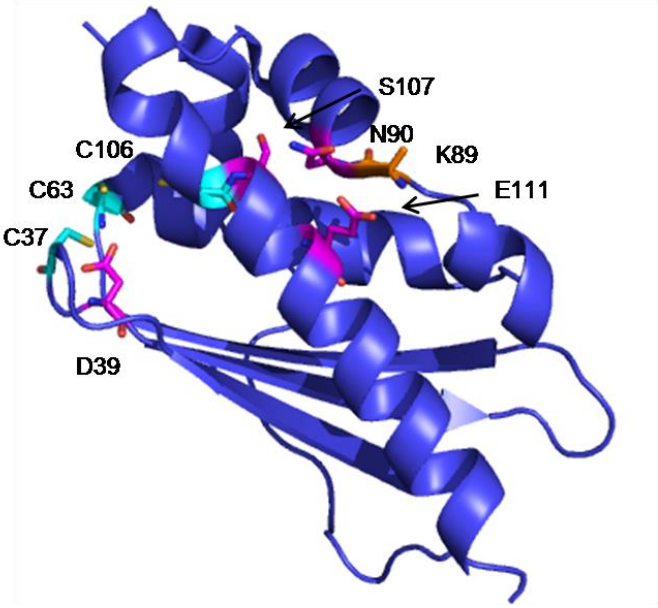

Figure 1-6. The crystal structure of *E. coli* IscU is shown highlighting the residues that are known to affect the protein stability by NMR. The active site cysteine residues are highlighted in cyan (C37, C63, C106). The residues that favored the ordered state of IscU are shown in magenta (D39, N90, S107, E111) and the residue that favored the disordered state is shown in orange (K89). PDB code 3LVL.

The iron donor and reducing electron source for cluster assembly have been widely debated and still have not been determined. In prokaryotes, IscA has been hypothesized to be an alternate scaffold to IscU[41, 42] or the iron donor for Fe-S cluster assembly[43, 44] due to its ability to bind Fe^{2+} and transfer the Fe^{2+} to IscU.[45] In eukaryotes, it has been hypothesized that frataxin (FXN) serves as the iron donor[46] and that a homolog of IscA is part of a three protein complex that is involved downstream of the chaperones and functions in delivering Fe-S clusters to a subset of [4Fe-4S]-containing targets.[47] A general scheme for the assembly and transfer of Fe-S clusters is shown in Figure 1-7.[33, 47]

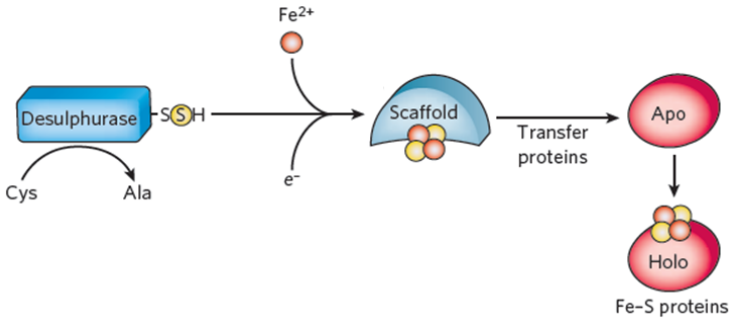

Figure 1-7. A cartoon representation of the minimum requirements for the general assembly and transfer of Fe-S clusters is shown. Reprinted with permission from *Nature*, 460:831-838. Copyright 2009 Macmillan Publishers Limited.[47]

After cluster assembly on IscU, the chaperones HscA and HscB are responsible for accelerating the transfer of intact Fe-S clusters to apo targets in *E. coli* in an ATP dependent manner.[48, 49] NMR experiments reveal that the DNA J-like protein HscB interacts with IscU through residues M31, V32, V40, K42, L43, K59, E111, D112, and

K115[50] and recruits and facilitates interactions with HscA.[48] Biophysical and functional studies reveal that HscA binds to the conserved LPPVK motif on IscU and that these IscU residues have no secondary structure when bound to HscA.[51-54] A model of cluster assembly and transfer has been proposed by Vickery *et al* (Figure 1-8).[48]

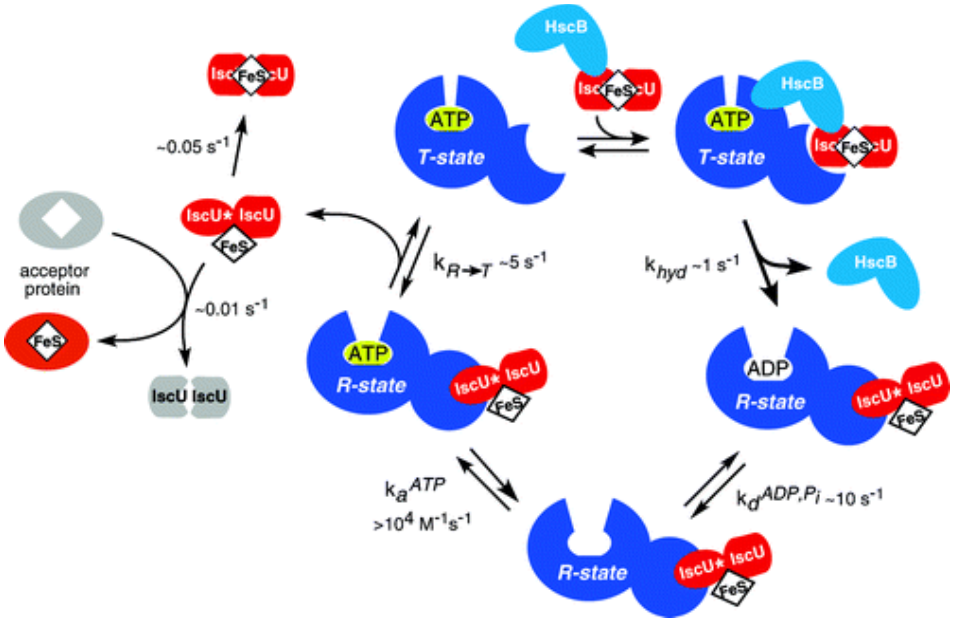

Figure 1-8. The proposed mechanism of cluster transfer from holo-IscU (red) to apo targets by the chaperones HscA (dark blue) and HscB (cyan) is shown with a dimer model of IscU. Reprinted with permission from *Biochemistry* 48:12795-12801. Copyright 2008 American Chemical Society.[48]

In this model, holo-IscU is recruited by HscB prior to binding the T-state of HscA that has ATP bound. Upon the hydrolysis of ATP to ADP, HscB is released and HscA undergoes a conformational change to the R-state. The HscA/holo-IscU in the R-state can then bind ATP causing the HscA to convert back to the T-state prior to IscU

being released for delivery of the Fe-S cluster to apo target proteins. Upon IscU release, the ATP bound HscA is returned to the T-state to accept another holo-IscU molecule.[48] This model presumes that IscU dissociates from IscS after cluster assembly and interacts with HscB as a homodimeric species. This hypothesis has yet to be evaluated.

Fe-S CLUSTER ASSEMBLY IN HUMANS

The prokaryotic and mitochondrial eukaryotic Fe-S cluster assembly machinery appears to have a common ancestor that has diverged over time.[23] In mitochondria, iron sulfur clusters are assembled and delivered to targets by the ISC machinery.[23, 55, 56] Additional machinery exists in the cytosol, aptly named the cytosolic iron-sulfur assembly pathway (CIA), which is responsible for the assembly and transfer of Fe-S clusters (Figure 1-9).[11, 57-59] The physical interactions between the CIA and ISC pathways are not well understood.

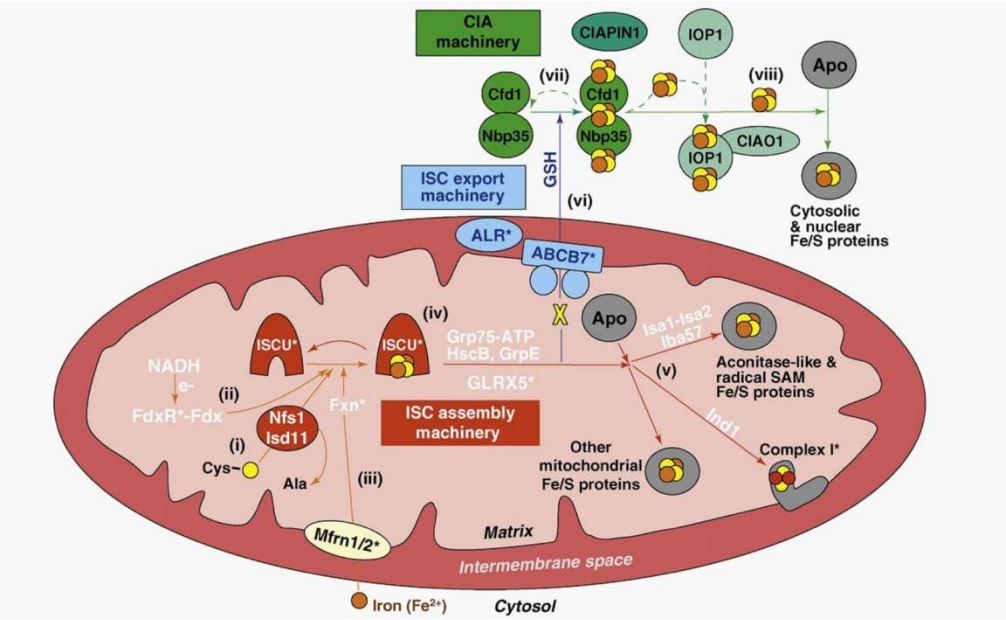

Figure 1-9. A model is shown of proteins in eukaryotic mitochondria and cytosol which are involved in Fe-S cluster assembly. Reprinted with permission from *Trends in Endocrinology and Metabolism,* 21:302-314. Copyright 2010 Cell Press.[11]

The human mitochondrial Fe-S assembly pathway appears to require four proteins, the cysteine desulfurase, NFS1, ISD11, the scaffold protein ISCU2, and FXN to efficiently synthesize Fe-S clusters.[33] The human mitochondrial Fe-S cluster assembly complex builds sequentially from the starting complex of NFS1/ISD11 (SD) which is unable to assemble Fe-S clusters. NFS1 in eukaryotes is the homolog to bacterial IscS proteins, which share an approximate 59% sequence identity to the *E. coli* IscS. Eukaryotic NFS1 co-purifies with ISD11, a small co-protein with which is hypothesized to activate NFS1[60] and is required for the stability and solubility of NFS1.[61-63] ISCU2 binding the SD complex forms the SDU complex, whereas binding both ISCU2 and FXN yields the SDUF complex. The SD, SDU, and SDUF complexes

were observed as distinct species by gel filtration chromatography indicating that these complexes are not made up of just dynamic or transient interactions and those stable assembly complexes can be isolated. The SDUF complex produced a slower migrating band on native gel electrophoresis and migrated with an estimated molecular weight of 190 kDa on a size exclusion column that suggests a stoichiometry of approximately $\alpha_2\beta_2\gamma_2\delta_2$.[33, 64]

The role of the cysteine desulfurase is to provide sulfur for Fe-S cluster biosynthesis by using a PLP cofactor to convert free cysteine into alanine (Figure 1-4), create a transient persulfide bound to a mobile loop, and then transfer the sulfur to the scaffold protein.[9] The activity of the cysteine desulfurase in the SD, SDU or SDUF complexes can be assessed by an assay modified from Siegel.[65] The persulfide species is reductively cleaved by DTT to release inorganic sulfide into solution, the released sulfide is reacted with *N, N'*-diphenyl-*p*-phenylenediamine (DPD), and the formation of methylene blue is quantitated using the extinction coefficient at 670 nm.[65] The SDUF complex has increased cysteine desulfurase activity compared to SD or SDU and the activity can be further increased by the addition of Fe^{2+}.[33] Additionally, the SDUF complex has increased Fe-S assembly activity compared to the SDU complex in an assay that monitors the increase in absorbance at 456nm, which is characteristic of [2Fe-2S] clusters.[33] Together these experiments suggest that FXN is an activator of the Fe-S assembly complex and that FXN may facilitate sulfur transfer from NFS1 to ISCU2.[33]

A scheme was proposed to explain the FXN based activation of the SDU complex.[66] In this scheme, the SDU complex can react with L-cysteine to form alanine

and a persulfide species (Figure 1-10, the persulfide sulfur is labeled red and attached to NFS1 label of S of the SDU complex). In the absence of FXN, the primary fate of the persulfide on NFS is the generation of sulfide through DTT-mediated cleavage (Figure 1-10, path 1). FXN binding is proposed to facilitate sulfur transfer from the persulfide on NFS1 to form a persulfide species on ISCU2 (Figure 1-10, path 2). The persulfide species on ISCU2 can then be reductively cleaved by DTT (Figure 1-10, path 3) or, in the presence of Fe^{2+} and an electron source, synthesize Fe-S clusters (Figure 1-10, path 4).[66] According to this model, the FXN-dependent acceleration of the cysteine desulfurase reaction is due to faster cleavage of the persulfide bound to ISCU2 (Figure 1-10, path 3) than the persulfide bound to NFS1 (Figure 1-10, path 1). In addition, an FXN-defendant conformational change could increase the access of the NFS1 persulfide to DTT and lead to an increased cleavage of the persulfide bound to NFS1 (Figure 1-10, path 1).

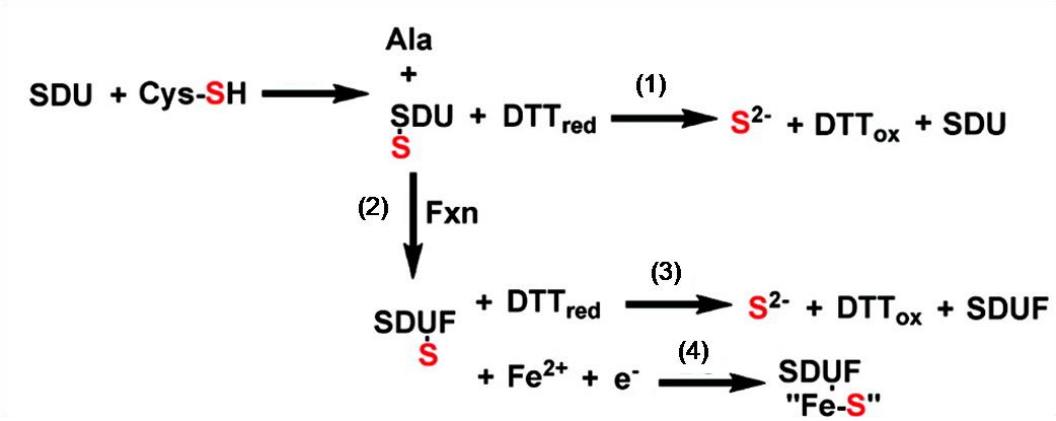

Figure 1-10. A hypothesized model of the fate of the persulfide on NFS1 to form the Fe-S cluster on ISCU2 is shown. The sulfur atom from cysteine that becomes the persulfide on the mobile loop of NFS1 is shown in red. Adapted with permission from *Biochemistry* 50:6478-6487.Copyright 2011 American Chemical Society.[66]

This scheme predicts that mutation of the sulfur acceptor on ISCU2 would eliminate the FXN-based activation of the cysteine desulfurase activity. Mutation and radiolabeling studies show that ISCU2 residue C104 (human numbering) is critical for this activation and sulfur transfer.[67] The identification of this cysteine as the sulfur acceptor was unexpected as this cysteine is located on a somewhat buried α-helix and is furthest from the mobile loop on NFS1 that contains the persulfide (Figure 1-6, C106 in *E. coli* numbering). Therefore, ISCU2 was proposed to undergo a conformational change upon FXN binding to position C104 to accept the sulfur from NFS1.[67]

Recently, a mutation on the scaffold has been identified at position M107I (yeast numbering) that is able to restore Fe-S cluster biosynthesis for a frataxin knockout strain of *Saccharomyces cerevisiae*.[68] The corresponding mutation (M106I, human numbering) was introduced into ISCU2 and the SDU_{M106I} complex exhibited 12-fold higher cysteine desulfurase and 3-fold higher Fe-S assembly activity than the wild-type SDU complex.[67] Thus, the human SDU complex with this ISCU2 mutant did not require the same level of FXN-based activation, consistent with the yeast frataxin bypass phenotype. This result is consistent with a pre-equilibrium model in which the inactive form is more stable than the active form, the role of frataxin is to bind and stabilize the active form, and that the M106I variant shifts the equilibrium similar to FXN binding (Figure 1-11). This model in which ISCU2 contains multiple conformation states is consistent with results on *E. coli* IscU from the Markley lab (see above). The nature of the conformational change in human ISCU2 is not known, but may be related to the helix-to-coil transition proposed to position C104 for sulfur transfer from NFS1 (Figure 1-11).[67] This model is especially attractive due to the close proximity of M106 to the chaperone binding motif, LPPVK (residues 97-101), and C104.

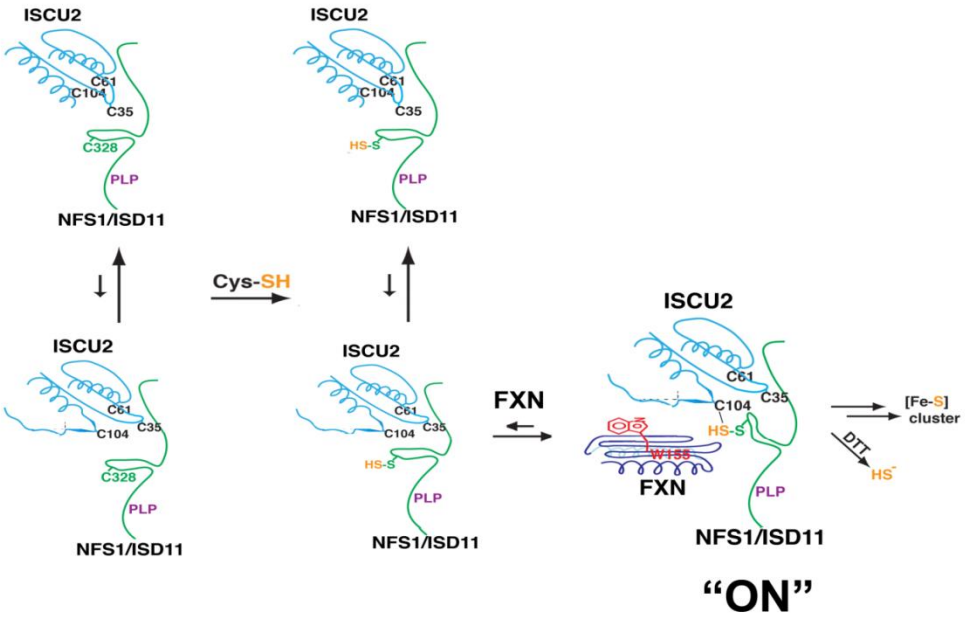

Figure 1-11. A model is hypothesized for the FXN-based selection of the active ISCU2 conformation. ISCU2 exists in two conformations with the helical, inactive, conformation being preferred. FXN binding interacts with and stabilizes the ISCU2 coil conformation that positions C104 to accept sulfur from NFS1.[69]

There is currently limited structural information for human FXN binding to the SDUF complex or the *E.coli* homolog CyaY to the IscS-IscU complex. Mutational and pull-down studies reveal that IscS substitutions R116E, R220E, R223E, R225E/E227R, G234L, R237E/M238E, A327V, and R340E diminish interactions with CyaY and provide a potential binding site (Chapter II).[31] Additionally, NMR studies indicate residues along the acidic patch on CyaY (residues D22, D23, S28, D29, E33, F43, and E44) were perturbed upon the addition of IscS indicating a potential binding interaction.[70] Mutation studies on human frataxin have also indicated that residues on the

acidic patch (E108, E111, D124) and also residue W155 are important for the interactions with the human cysteine desulfurase and scaffold proteins (Figure 1-12).[64]

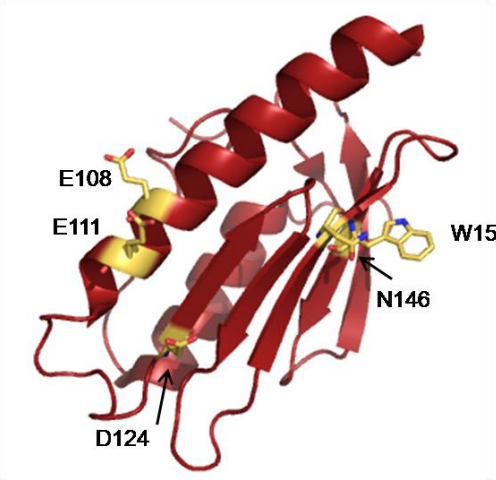

Figure 1-12. Frataxin mutated residues that diminish or lose binding affinity to NFS1 and ISCU2 are highlighted as yellow sticks on the wild-type structure (PDB 3S4M).

After cluster assembly, additional machinery is required to transfer the cluster from the SDUF complex to apo target proteins. In humans, the equivalent of the *E. coli* HscA chaperone is HSP70, which is also known as GRP75 and mortalin, whereas the equivalent to HscB is known as HSC20, also known as DNA J type-III co chaperone.[71] The interactions of HSP70 and HSC20 have been less well studied in the human system. The interactions determined by yeast two-hybrid and pull down studies indicate that Hsc20 interacts with ISCU2 and HSP70[71] and co-immunoprecipitation experiments indicate an interaction between FXN and GRP75.[72] There remains much to be learned

about the chaperone-facilitated transfer of Fe-S clusters from the SDUF complex to apo targets such as ferredoxin.[24]

CONNECTION BETWEEN Fe-S CLUSTER BIOSYNTHESIS AND HUMAN DISEASE

Mutations in the Fe-S assembly pathway in humans can manifest itself in a number of diseases (Figure 1-13).[11] The most commonly inherited ataxia, Friedreich's ataxia (FRDA), is an autosomal recessive neurodegenerative disease associated with deficiencies in the protein frataxin.[63] The most common mutation is a GAA repeat on the first intron of the gene.[63] In healthy individuals, the occurrence of this insert is between 6 to 36 but in diseased patients, the number of repeats is greatly increased to 70-1700 causing a phenotypic progressive gait and limb ataxia, muscular weakness in the legs, and dysarthria.[63] Most FRDA patients have GAA repeats on both alleles. A small subset of FRDA patients exhibits a GAA repeat on one allele and a missense (point mutant) on the other allele. Both classes of FRDA patients exhibit decreased amounts of functional frataxin that manifests as a decrease in iron sulfur cluster assembly.[73]

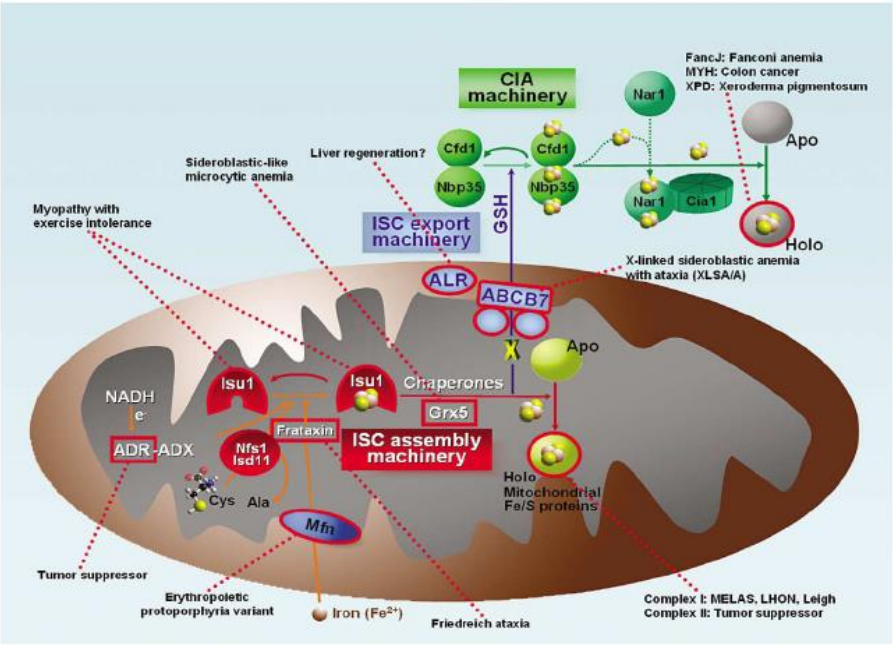

Figure 1-13 This model highlights the various diseases associated with deficiencies in Fe-S assembly. Reprinted with permission from *Trends in Endocrinology and Metabolism,* 21:302-314.Copyright 2010 Cell Press.[11]

The ability of these FXN mutants to bind its partner proteins through pull down assays,[72, 74] stimulate the cysteine desulfurase activity and Fe-S cluster assembly activities, and bind the SDU complex has been studied.[66, 75] The results of these studies indicate that there is a general correlation between the ability of the FXN mutants to bind the SDU complex and stimulate the cysteine desulfurase activity.[75] Mutations such as W155R that are highly compromised in both binding and activation of the SDU complex tend to have early onset disease progression, whereas mutants such as R165C and N146K that have a more modest loss of binding and/or activation tend to have an unusually mild disease progression.[75]

Frataxin has had many proposed roles from iron trafficking and storage to acting as an allosteric switch to regulate Fe-S biosynthesis (Figure 1-14).[76, 77] It has recently been discovered that the role of frataxin in the Fe-S assembly pathway differs between bacteria and humans.[78] In *E. coli*, the addition of the frataxin homolog, CyaY, decreases the Fe-S cluster assembly activity,[70, 78] whereas in humans, the addition of FXN stimulates the Fe-S cluster activity.[33, 78]

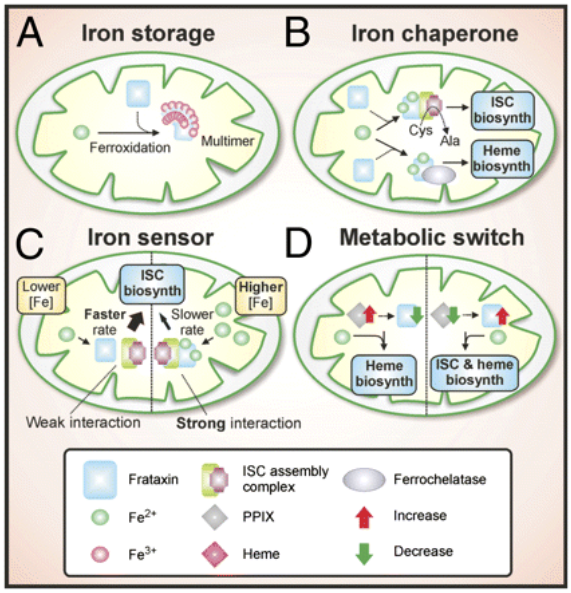

Figure 1-14. Various proposed roles of frataxin are shown from iron storage and chaperone roles to frataxin acting as a metabolic switch. Reprinted with permission from *PNAS*, 107:10775-10782. Copyright 2010.[76]

Additionally, a mutation on ISCU2 has recently been identified as the source of the disease Myopathy with exercise intolerance.[79, 80] This disease is an inherited autosomal recessive disease specific to northern Sweden, which has a phenotype of early

on-set fatigue, dyspnoea, and palpitations upon light exercise.[79] ISCU2 myopathy is caused by a homozygous point mutation on intron 4 that causes the intron to have a 100bp fragment insertion between exons 4 and 5 and also includes a premature stop codon in the open reading frame of the mRNA of ISCU2.[81] A more severe progression of the disease is caused by a heterozygous mutation to one allele in which a missense mutation in exon 3 is reported.[79, 81] The transcribed ISCU2 has a point mutation at a conserved glycine to glutamate. It is unclear how this mutation alters the functional properties of ISCU2.

CONCLUSION

Despite the information on the prokaryotic IscS-IscU complex, many questions remain in both prokaryotic and also eukaryotic Fe-S cluster biosynthesis. For example, there exists no structural information for the cysteine desulfurase, NFS1, its co-protein ISD11, or the scaffold, ISCU2. The interaction between NFS1 and ISD11 and the role that ISD11 plays in Fe-S cluster assembly are not known. Additionally, the surfaces of interaction for the regulator of activity of the human Fe-S cluster assembly complex, frataxin, is not well defined with either NFS1 or ISCU2 in terms of the protein complex. Therefore, one goal of this dissertation was to use hydroxyl radical footprinting to define the protein interfaces for the SDUF complex (Chapter II). This protein interface data provides an initial testable model for the complexes than can be evaluated through mutagenesis experiments and also coupled to other ongoing low-resolution approaches

in the Barondeau lab such as SAXS and electron microscopy to generate a more sophisticated model of the SDUF complex.

Very little is known about the Fe-S cluster transfer reaction in humans. Once the SDUF complex has assembled a Fe-S cluster it is unclear at what stage and oligomeric state ISCU2 interacts with the chaperones to deliver the Fe-S cluster to apo targets. Possible models include larger macromolecular complexes with interactions between SDU and SDUF Fe-S assembly complex and the molecular chaperones (Figure 1-15, top paths) and models in which ISCU2 dissociates from the SDUF complex before delivering the cluster to the target protein (Figure 1-15, bottom paths). In the dissociation models, the loss of ISCU2 from the SDUF complex could be induced by chaperone binding or occur spontaneously. In addition, the released ISCU2 could interact with the chaperones as a monomer or dimer. To understand the molecular choreography of these events, a strategy has been initiated in which an individual component, namely FXN, was labeled with a fluorophore. Labeling the component with fluorophore is a powerful approach that can allow the determination of protein binding constants, size information (fluorescence anisotropy experiments) and distance measurements (Förster resonance energy transfer, FRET, between appropriately labeled proteins). In Chapter III, fluorescence anisotropy experiments were initiated on labeled FXN and a FXN variant to help distinguish Fe-S transfer models.

ISCU2 variants were then designed to test aspects of the pre-equilibrium model in which ISCU2 exists as a mixture of function and non-functional states.[67] Recent experiments reveal *E. coli* IscU exists as a mixture of ordered and dynamically

disordered states, that the D39A (*E. coli* numbering) variant favors the ordered state, possibly by removing buried charge, and that this variant appears to enhance Fe-S cluster binding and complex formation with IscS.[35] Moreover, additional experiments suggest a model in which FXN favors an ISCU2 helix-to-coil transition, which may be a component of this conformational change, to activate the human Fe-S assembly system. In Chapter IV, variants of ISCU2 at position K101, which is hypothesized to be a component of the helix-to-coil transition and interact with FXN, were coupled to previously made ISCU2 and FXN variants to evaluate FXN binding and activation of the cysteine desulfurase and Fe-S assembly activities.

In addition to the structural studies of the SDUF complex, more specific experiments were designed to understand the impact of clinical (G16E) ISCU2 mutants on Fe-S cluster biosynthesis (Chapter V).

Previous experiments correlated defects in FXN missense mutations in binding and activation of the SDU complex with the severity of disease progression.[75] In Chapter V, similar experiments on the G16E ISCU2 missense mutant are described that reveal a significant loss in binding affinity of the clinical mutant to the Fe-S cluster assembly complex. Once the weaker binding is taken into account, this clinical mutant has cysteine desulfurase and Fe-S cluster assembly activities similar to wild-type ISCU2 and highlights the importance of a high affinity assembly complex for synthesizing Fe-S clusters.

Additionally in Chapter V, the human D37A and L107Q ISCU2 variants were designed to stabilize the structured state and test their ability to bind the SD complex and interact with FXN. The functional properties of the variant SDUF complexes were also evaluated with cysteine desulfurase and Fe-S cluster assembly experiments.

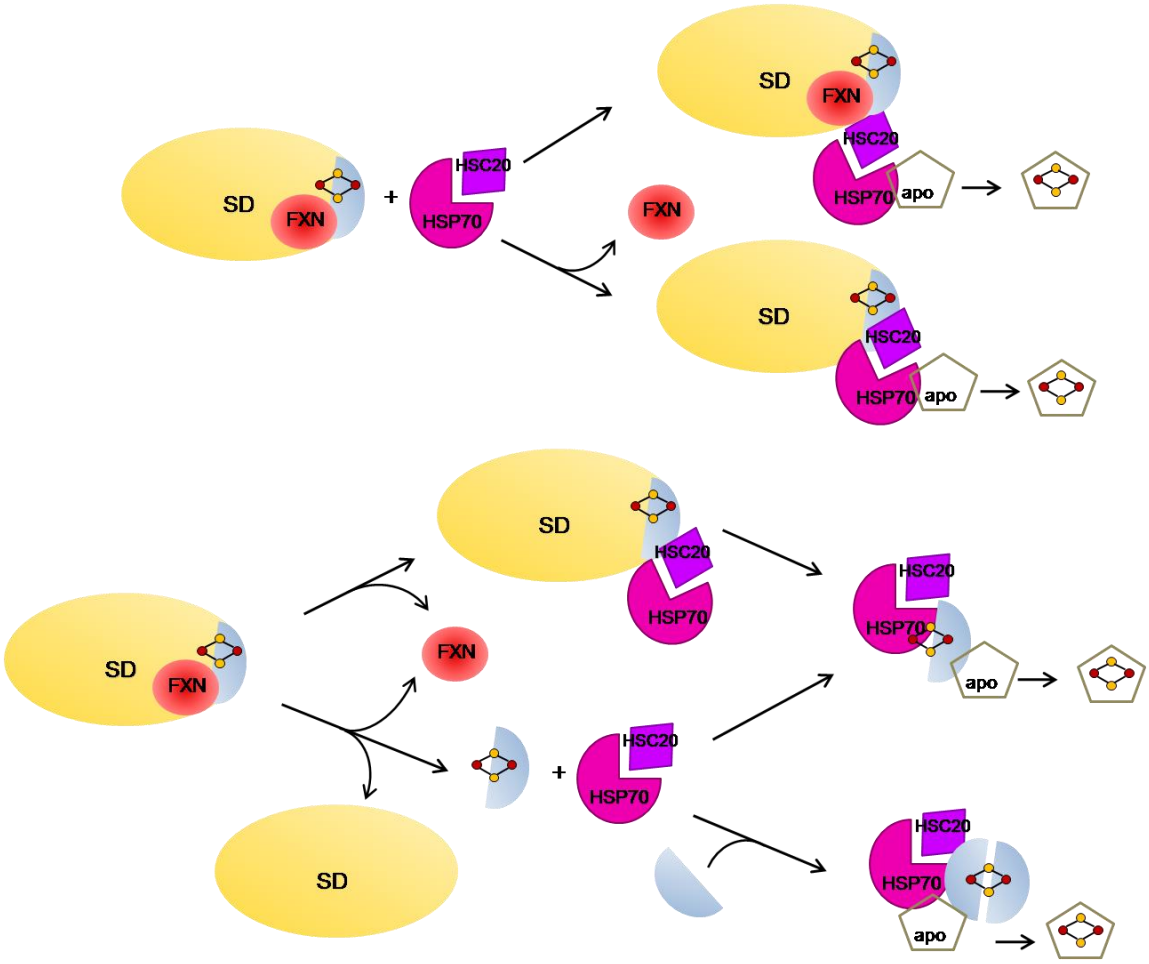

Figure 1-15. A model of Fe-S cluster transfer from the SDUF complex to apo target proteins. The NFS1/ISD11 (SD) is shown as a yellow sphere, ISCU2 monomer is shown as a blue crescent and FXN is shown in red. The chaperones HSP70 (pink) and HSC20 (purple) are shown as a complex that can interact with the Fe-S cluster biosynthesis complexes or its components to transfer the [2Fe-2S] cluster to apo target proteins.

CHAPTER II

PROTEIN-PROTEIN INTERACTIONS OF THE SDUF COMPLEX DETERMINED BY HYDROXYL RADICAL FOOTPRINTING

INTRODUCTION

Iron-sulfur (Fe-S) clusters are integral cofactors found in every life form from prokaryotes to eukaryotes, and are involved in critical cellular processes such as nitrogen fixation, respiration, DNA repair and sensing of reactive oxygen and nitrogen species.[1] In bacteria, Fe-S clusters are assembled through one of three pathways, namely the nitrogen fixation pathway (NIF), sulfur mobilization pathway (SUF), and the iron sulfur cluster formation pathway (ISC).[82] Homologues of many of the components from the prokaryotic system are conserved in eukaryotes.[22] Specifically, the primary pathway for Fe-S cluster assembly in humans is the ISC system located in the mitochondria. This Fe-S assembly system contains a cysteine desulfurase, NFS1, which, along with its co-protein ISD11, is responsible for the conversion of cysteine to alanine. During catalysis a persulfide is generated on a mobile loop cysteine on NFS1 and the terminal sulfur is then transferred to the scaffold protein ISCU2 for Fe-S assembly.[37, 83, 84]These three components, NFS1/ISD11 and ISCU2, form a low activity Fe-S assembly complex named SDU that can be activated by the binding of frataxin (FXN).[33]The active four protein component SDUF complex was first identified by native gel electrophoreses and has a molecular mass of approximately 190 kDa as determined by gel filtration chromatography and intact mass spectrometry, which suggests an approximate

stoichiometry of 1:1-2:1:1 for the NFS1/ISD11/ISCU2/FXN components, respectively.[33, 64]

In recent years, the ISC Fe-S cluster assembly system has been studied extensively *in vivo* and *in vitro* from a variety of organisms to gain a mechanistic understanding of this pathway and determine the effect of deficiencies in assembly components at the cellular or organism level.[77] In contrast, the structural features of many of the Fe-S assembly components and molecular details for Fe-S assembly complexes in eukaryotes are currently lacking. Elucidating the structures of the individual proteins and details of the protein-protein interactions of the associated protein complexes will aid in constructing testable models that will provide a deeper understanding and context for mechanistic studies. Moreover, such studies may also provide a basis to understand interactions between the core SDUF Fe-S cluster assembly complex and additional assembly, chaperone, and accessory proteins that assist in Fe-S cluster biosynthesis.[52, 85]

The largest subunit of the ISC Fe-S assembly complex is the cysteine desulfurase, which is named NFS1 in eukaryotes and IscS in prokaryotes. Crystal structures of the *E. coli* IscS (PDB 1P3W)[30] as well as the homolog from the NIF system, NifS, from *Thermotoga maritima* (PDB 1EG5)[86] reveal an overall dimeric structure, with active site PLP cofactor of each active site located more than 17 Å from the catalytic cysteine, Cys328(*E. coli* numbering).[30] This catalytic cysteine is on a mobile loop that is often disordered in crystal structures and is consistent with the required large-scale structural rearrangement required to transfer the sulfur from the PLP

at the active site to various acceptor proteins.[30, 31] In contrast, there is no known structure of a cysteine desulfurase from an eukaryotic system. The human NFS1 shares an approximate 51% sequence identity with *E. coli* IscS, exists as a ~90 kDa dimer based on gel filtration chromatography experiments[77] and have further been characterized by pull-down, biochemical and mutational studies to determine binding interactions with IscU and frataxin,[31] and NMR studies show complex formation between IscS and IscU.[34] Additionally, the co-protein ISD11 localizes to the mitochondria and is required for the stability and activity of NFS1 in eukaryotic organisms *in vivo,*[61, 87] and for the generation of functional recombinant NFS1 in bacteria.[77] Although experimental data for the 10.6 kDa ISD11 protein is lacking, secondary structure and *de novo* structure prediction support a 3-helix bundle protein fold.[88]The number, oligomeric state, and position of ISD11 molecules on the surface of NFS1 are not known.

The scaffold protein, which is named ISCU2 for humans andIscU in prokaryotes, is the second component of the ISC Fe-S assembly complex and has been primarily studied by NMR spectroscopy and X-ray crystallography in bacteria. Solution structures have been solved of homologous proteins from *E. coli* of wild-type and D39A (*E. coli* numbering), a mutant which is known to bind a Fe-S cluster tighter,[36, 40] a Zn^{2+} bound IscU from *Haemophilus influenza* (PDB 1R9P),[36] and also an unpublished structure from *Mus musculus* (PDB 1WFZ). These NMR and additional CD spectroscopy studies reveal that wild-type apo-IscU is purified as a monomeric protein with an αβ fold and high α-helix content,[89] a flexible N- and C-terminus, and exists in two freely interconverting

states in solution.[35, 40] Markley *et al* determined that wild-type apo-IscU exists approximately 70% in the structured and 30% in the disordered form but the equilibrium can be shifted by incorporating single amino acid point mutations, such as the D39A substitution, which shifts the equilibrium to ~95% structured.[35, 40] Markley *et al* further show that it is the disordered state of IscU that preferentially interacts with IscS.[35] Protein crystallization has been successful from a homolog from *E. coli* with a zinc bound to the three active site cysteine residues (PDB 1SU0)[90] and also from *Aquifex aeolicus* which was crystallized with a single [2Fe-2S] cluster between a trimer of IscU molecules (PDB 2X7E).[91]

Recently, groundbreaking crystallographic studies by two separate groups revealed the protein-protein interactions for the IscS-IscU complex from prokaryotes.[31, 32] The Cygler group published a crystal structure of the *E. coli* complex (PDB 3LVL)[31] that revealed the N-terminus of the scaffold protein IscU changes from a flexible coil to a short α-helix upon forming a complex with IscS. This conclusion is consistent with pull-down results that indicate the N-terminally truncated IscU loses binding affinity toIscS.[31] Additionally, the Fontecilla-Camps and Dean groups determined a 2.5 Å co-crystal structure of IscS-IscU from *A. fulgidus* that contained a bound 2Fe-2S cluster to one subunit (PDB 4EB5).[32] The protein-protein interactions of the scaffold and cysteine desulfurase from *E. coli* and *A. fulgidus* are very similar indicating that these interactions might be conserved across organisms.[31, 32]

The fourth component of the Fe-S cluster assembly complex is frataxin which has recently been identified as an allosteric activator for the SDU complex.[64, 77] In

contrast to the activator role for the human system, addition of the *E. coli* homolog CyaY to the IscS-IscU complex appears to inhibit Fe-S cluster assembly.[78, 92] Human FXN is the only component of the SDUF complex in which protein crystallography information is available.[75, 93, 94]The structures of FXN homologs from yeast (Yfh1)[95, 96] and *E. coli* (CyaY)[94, 97, 98] have also been determined and are very similar to human FXN. The overall sequence identity is relatively low between *E. coli* CyaY and yeast Yfh1 or human FXN at 26.4% and 24.5%, respectively, but share an overall compact αβ sandwich fold consisting of a 6 antiparallel β-sheets panel flanked on either side by 2 helices, α1 and α2 (Figure 2-1).[99, 100] The conserved residues between CyaY, Yfh1, and FXN are shown in blue on the orange CyaY molecule (PDB 1WE4) and the red FXN molecule (PDB 3S4M). Mutation of conserved residues on β3 and β4such as V144, N146, Q148, Q153, W155, and R165 (human numbering), diminish the ability of CyaY to pull down IscS,[64] decrease the ability of FXN to stimulate the cysteine desulfurase, Fe-S cluster biosynthesis activities, and FXN binding to the SDU complex[67, 75] revealing the importance of these residues in the Fe-S cluster assembly complex. There currently exists no model of the four-protein SDUF complex from eukaryotes.

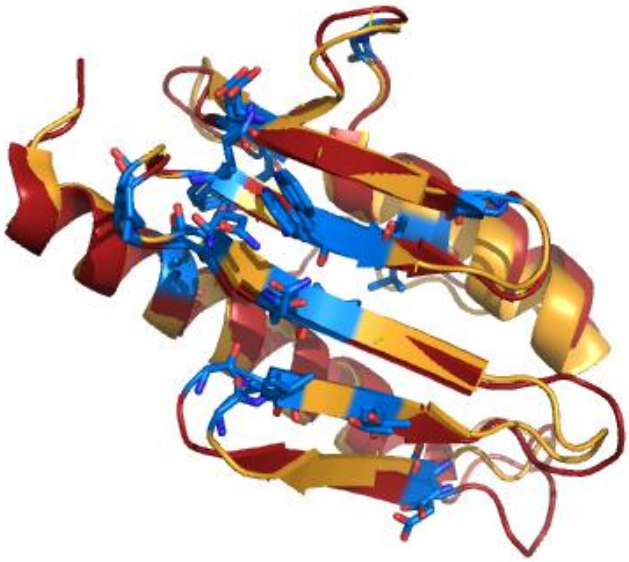

Figure 2-1.Structural overlay and conserved residues of human and *E. coli* frataxin homologs. Ribbon diagrams for *E. coli* CyaY (orange, PDB 1EW4) and human FXN (red, 3S4M) crystal structures reveal similar tertiary structures and a clustering of conserved residues (blue).

Many standard structural characterization techniques have been unsuccessful or are inappropriate for the proteins and complexes responsible for Fe-S assembly in humans. Specifically, protein crystallography has been unsuccessful for human NFS1, ISD11, and ISCU2 and the SD, SDU, and SDUF complexes. NMR requires very high protein concentrations, labeling of subunits in isotope rich media or buffers, and the size of the complexes pushes or exceeds the limitations of the technique. Techniques such as hydrogen deuterium exchange (HDX) mass spectrometry (MS) have gained popularity in determining protein dynamics,[101-104] protein-ligand,[105, 106] and protein-protein interactions[107] but this technique has limitations in that the label is labile and will readily exchange with protons in the buffer solution, known as back exchange. Additionally, the

conditions required to quench the exchange reaction make necessary the use of acid proteases, which do not cleave after specific amino acid residues making the data analysis complex. Recently, hydroxyl radical footprinting by synchrotron radiation monitored by mass spectrometry has been used to understand the multimerization reactions of insulin,[108] the interactions between myosin and actin,[109] or the conformation dynamics between protein and receptor or ligand complexes.[110, 111] Hydroxyl radical footprinting is an attractive alternative to other structure characterization techniques because it requires significantly lower protein concentration (~10 μM), the reaction times are short (<30 ms) and the modifications are covalent allowing for protein digestion with specific proteases such as trypsin. Additionally, generating the hydroxyl radicals by synchrotron radiation does not require the addition of radical forming species, such as hydrogen peroxide. The modifications are monitored by MS which also requires very little sample, has fast experiment time, and high sensitivity to low abundance species.

For these reasons, hydroxyl radical footprinting by synchrotron radiation monitored by matrix-assisted laser desorption ionization (MALDI) time of flight (TOF) mass spectrometry was used to probe the interactions of humanISCU2 withNFS1-ISD11 (SD) to form the NFS1/ISD11/ISCU2 (SDU) complex. Further, the addition of FXN to the SDU complex to form the NFS1-ISD11-ISCU2-FXN (SDUF) was monitored to better understand the interactions that are critical for complex formation and activation. Models for these complexes were generated and then evaluated using criteria such as electrostatic potentials and previous mutational studies. These structural models lead

directly to the generation of specific hypotheses that will be partially tested in later chapters of this dissertation and also with future studies in the Barondeau lab.

EXPERIMENTAL PROCEDURES

Sample Preparation for Hydroxyl Radical Modification. Human FXN, ISCU2, and SD were recombinantly purified as previously described[75] and were buffer exchanged into 1X PBS (10 mM Na_2HPO_4, 2 mM KH_2PO_4 pH 7.4, 137 mM NaCl, 2.7 mM KCl) using Micro Bio-Spin P-6 buffer exchange columns (Bio-Rad Laboratories), which had previously been conditioned with 1X PBS. To assemble the SDU or SDUF complex, SD was incubated with 5 equivalentsISCU2 (SDU) or 5 equivalents each ISCU2 and FXN (SDUF) on ice for 30 minutes. Excess ISCU2 (14 kDa) and/or FXN (14 kDa) were removed by applying the complex to a 30 kDa MW cutoff Vivaspin 500 (GE Life Sciences) concentrator and centrifuging for 5 minutes at 4 ^{o}C at 8000 x g. The protein complex that did not flow through the concentrator was buffer exchanged into 1X PBS as above. The protein samples at a final concentration of 10 μM in 1X PBS buffer were frozen in liquid nitrogen and were shipped overnight to Brookhaven National Lab (BNL) on dry ice. Sample concentrations were determined using the extinction coefficient at 280nm (ISCU2, ε_{280} = 8250 $M^{-1}cm^{-1}$ and FXN ε_{280} = 26,030 $M^{-1}cm^{-1}$) and 420nm (SD, SDU, SDUF; ε_{420} = 10.9 $mM^{-1}cm^{-1}$). Upon arrival to BNL, the samples were stored at -20 ^{o}C until X-ray exposure.

Sample Exposure. Synchrotron dose response was determined for each sample as previously described.[112] Briefly, a fluorescent molecule such as an Alexa fluorophore

was added to a small quantity of each protein or complex sample and exposed to synchrotron radiation. The fluorophore was quenched by the excess radicals not absorbed by the protein molecule or complex and rate of quenching was used to determine the amount of exposure required to label each sample. The exposure time determined using this method was then used to modify each sample or complex prior to quenching the reaction with 10 mM methionine amide to prevent further oxidation.[112] Specifics of the configuration of beamline X28C and sample exposure followed previously described protocols.[112] Three independent data sets for each sample were collected for analysis. Differences in beam flux and currents (approximate 10% decrease) could account for the modest differences in the rates of modification for the individual experiments.

Preparation and MALDI TOF Analysis of Irradiated Samples. After exposure to hydroxyl radicals and quenching, the samples were shipped from BNL on dry ice, thawed upon arrival, and digested with trypsin. For the ISCU2 and FXN samples, trypsin was added at a 1:50 dilution; for SD, SDU, and SDUF, trypsin was added at a 1:25 dilution to ensure efficient digestion of the complexes. The protein digests were incubated at 37 ^{o}C for 3.5 hours before the tryptic peptides were acidified to a final concentration of 0.1% trifluoroacetic acid (~pH 2-3). Approximately 60-70 µl of the sample was desalted using a C_{18} Zip-Tip® pipet tip (Millipore), eluted in 4 µl, mixed 1:1 with MALDI matrix (5 mg/ml α-cyano-4-hydroxycinnamic acid, 50% (v/v) acetonitrile, 10 mM ammonium dihydrogen phosphate, 0.1% trifluoroacetic acid), and 1 µl of the resulting mixture was spotted onto a MALDI sample plate in duplicate. Dr. Pei-Jing

(Peggy) Pai in the Dr. David Russell Biological Mass Spectrometry Laboratory performed the MALDI TOF MS and MS/MS experiments using a 4800 TOF/TOF Analyzer (Applied Biosystems, Framingham, MA). Collision-induced dissociation (CID) spectra were acquired using 2 eV of collision energy of the 30 most abundant peptides in each spectrum.

Theoretical masses and mass to charge ratios (*m/z*) were calculated from the known peptide sequence and used to identify the unmodified peptides for the different proteins and complexes. Peptides that were unable to be confidently assigned by the calculated *m/z* were confirmed by MS/MS if the data was collected. Modified peptides were identified by sequence-specific changes in mass compared to the unmodified peptide with 100ppm allowed error. Most often this change in peptide molecular weight was +16 Da mass increments due to oxygen incorporation. The fraction unmodified was calculated[113, 114] for each peptide of ISCU2, FXN and for the peptides in the SD, SDU, and SDUF complex by dividing the peak height of the monoisotopic peak for the unmodified peptide by the sum of the peak heights of the monoisotopic peaks for the unmodified and modified peaks (Equation 2-1).

$$fraction\ unmodified = \frac{RA_{unmodified}}{\left(RA_{unmodified} + \Sigma RA_{modified}\right)} \qquad (2\text{-}1)$$

The fraction unmodified was plotted as a function of exposure time and the graphs were fit to a first order process in KaleidaGraph software using Equation 2-2. The variable *y* represents the fraction unmodified at a given exposure time (*t*) and *k* is the rate

constant in s^{-1}.[112, 114, 115] The reported error for each rate value is an error in the fit of the data.

$$y = e^{-kt} \quad (2\text{-}2)$$

Homology Models for Human NFS1 and ISCU2. Homology models were generated for of human NFS1 and ISCU2 using SWISS-MODEL (http://swissmodel.expasy.org/).[116-118]Briefly, the model was based on the IscS and IscU coordinates from the *E. coli* IscS-IscU complex (PDB 3LVL)[31] and the sequence of human NFS1 and ISCU2. In addition, a model of the complex between NFS1 and ISCU2 was generated based on the same IscS-IscU co-crystal structure.

Ab initio Structural Model for Human ISD11. ISD11 has been predicted to have a high helical propensity[88] but there is no known solution or crystal structure of human ISD11 or a ISD11 homolog organism. Therefore, a structural model was generated using the Robetta Full-Chain Protein Structure Prediction Server http://robetta.bakerlab.org/. The predicted 3-helix bundle is consistent with a published structural model.[61]

Calculation of Electrostatic Potential for SDUF Components. The electrostatic surface potentials for the individual components of the human Fe-S cluster assembly complex were determined using CHARMM-GUI PBEQ Solver with the default input settings (http://www.charmm-gui.org/?doc=input/pbeqsolver). The generated coordinate files for human NFS1, ISD11, and ISCU2 models and the human FXN crystal structure (PDB 3S4M) were individually uploaded onto the CHARMM server and the

electrostatic potentials and solvation energies for each structure were generated. The electrostatic maps were displayed at the solvent accessible surface using PyMOL software (PyMOL Molecular Graphics System, Version 1.3 Schrödinger, LLC.). The electrostatic scale is from -1.0 to 1.0 kcal/(mol · unit charge). The regions with negative electrostatic potential are shaded red, whereas regions with positive electrostatic potential are shaded blue.

RESULTS

Here our objectives were (1) to identify the protein interaction interfaces for the cysteine desulfurase and scaffold proteins from the human Fe-S assembly complex, (2) to identify the binding interfaces between FXN and the proteins of the SDU complex, and (3) compare the interactions uncovered in these studies to what is already known from homologous proteins from the *E. coli* co-crystal structure. To fulfill these objectives, samples of individual proteins or complexes were exposed to synchrotron radiation for variable amounts of time to become labeled with hydroxyl radicals, quenched by the addition of 10 mM methionine, digested with trypsin, and the resulting peptides were subjected to analysis by MALDI TOF mass spectrometry (see Methods).

To ensure reproducibility, the only peptides included in the final analysis were those identified by their *m/z* in at least two of the three independent data sets. We classified peptides as becoming modified if their *m/z* value shifted by the amount corresponding to the addition of oxygen atoms (+16 Da, +32 Da, +48 Da, etc.) upon exposure to hydroxyl radicals. The peptides from each protein were identified from individual and complex analysis and were compared over the course of the three separate experiments. For the ISCU2 protein, eight unique peptides were identified in the hydroxyl radical footprinting experiments, corresponding to ~55% sequence coverage (Figure 2-2). The peptides identified are shown as bars over the protein sequence (Figure 2-2A) and are mapped onto the human model of ISCU2 protein (Figure 2-2B) with the identified peptides shown in blue with the regions unobserved in gray and the active site cysteines highlighted by sticks.. These peptides were observed in the individual ISCU2 experiments as well as in the SDU and SDUF complexes. The changes in rates of modification of these peptides were used to determine regions of interaction to NFS1 (SDU complex) and FXN (SDUF complex).

A.

```
1   MHKKVVDHYE NPRNVGSLDK TSKNVGTGLV GAPACGDVMK LQIQVDEKGK

51  IVDARFKTFG CGSAIASSSL ATEWVKGKTV EEALTIKNTD IAKELCLPPV

101 KLHCSMLAED AIKAALADYK LKQEPKKGEA EKK 133
```

B.

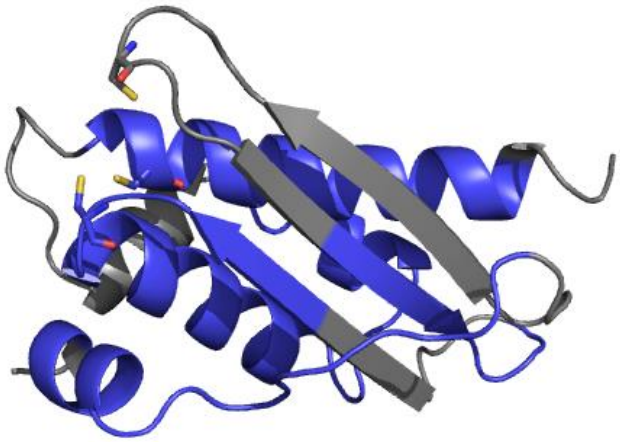

Figure 2-2. ISCU2 was digested with trypsin and the fragments observed from 3 separate hydroxyl radical experiments are shown (A) over the protein sequence by blue bars or (B) displayed by blue peptides on the model of human ISCU2 with the active site cysteine residues shown in yellow. Eight unique peptides were identified covering approximately 55% of the protein sequence.

Similarly, the peptides from NFS1 were identified after trypsin digestion of the SD, SDU or SDUF complexes. The rates of modification for the 7 peptides identified (~27 % sequence coverage) were monitored to determine the sites of interaction for ISCU2 in the SDU complex and FXN on the SDUF complex. The sites of interaction for ISD11 could not be determined because NFS1 could not be purified without ISD11. The peptides identified in at least 2 of the three experiments are displayed above the protein sequence by the blue bars (Figure 2-3A) and on the model of human NFS1 dimer generated using the human sequence and the coordinates from the *E. coli* IscS crystal structure (see Methods) by highlighting the peptides in blue (Figure 2-3B). The peptides were mapped onto both subunits of the NFS1 dimer with the unmodified or unidentified peptides displayed in gray. The protein sequence contains the N-terminal histidine tag used for protein purification (the N-terminal ~20 amino acids). The residue numbers are shown at the left of each line.

A.

```
1   MGSSHHHHHH SSGLVPRGSH MLEMLRPLYM DVQATTPLDP RVLDAMLPYL INYYGNPHSR
61  THAYGWESEA AMERARQQVA SLIGADPREI IFTSGATESN NIAIKGVARF YRSRKKHLIT
121 TQTEHKCVLD SCRSLEAEGF QVTYLPVQKS GIIDLKELEA AIQPDTSLVS VMTVNNEIGV
181 KQPIAEIGRI CSSRKVYFHT DAAQAVGKIP LDVNDMKIDL MSISGHKIYG PKGVGAIYIR
241 RRPRVRVEAL QSGGGQERGM RSGTVPTPLV VGLGAACEVA QQEMEYDHKR ISKLSERLIQ
301 NIMKSLPDVV MNGDPKHHYP GCINLSFAYV EGESLLMALK DVALSSGSAC TSASLEPSYV
361 LRAIGTDEDL AHSSIRFGIG RFTTEEEVDY TVEKCIQHVK RLREMSPLWE MVQDGIDLKS
421 IKWTQH426
```

B.

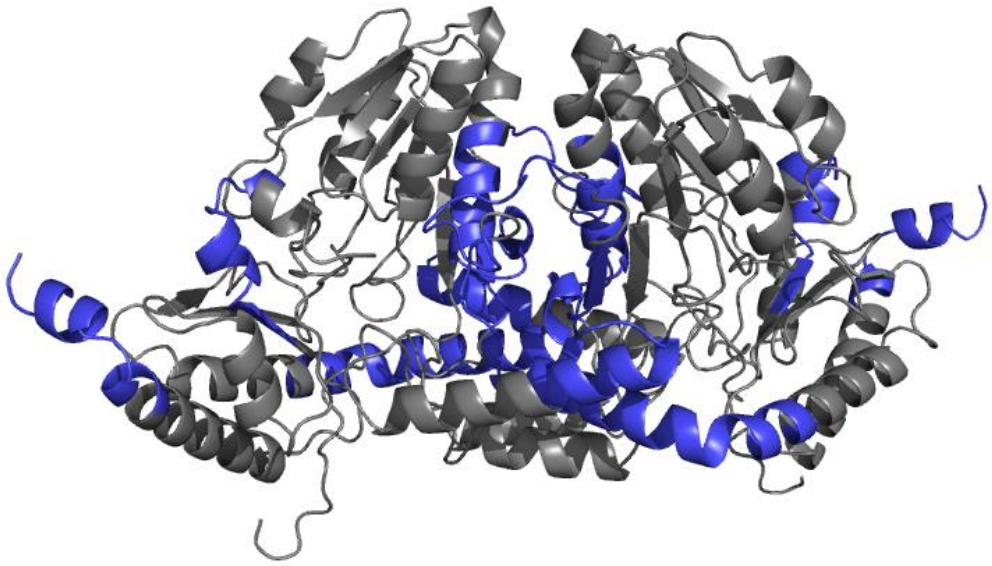

Figure 2-3. Peptides identified from the SD, SDU, and SDUF complexes after trypsin digestion of NFS1 in the 3 independent hydroxyl radical footprinting experiments are shown (A) above the protein sequence by blue bars or (B) mapped onto the model of human NFS1 dimer shown in blue. Seven unique peptides were identified corresponding to approximately 27% sequence coverage.

Finally, the peptides from FXN identified either from FXN or from FXN in the SDUF complex are shown over the protein sequence (Figure 2-4A) in red or on the crystal structure of human FXN (PDB 3SS4M) by red peptides (Figure 2-4B). The regions not observed in the hydroxyl radical footprinting experiments are shown in gray on the structure. Seven unique peptides were identified covering approximately 48% of the FXN sequence.

A.

```
 81 SGTLGHPGSL DETTYERLAE ETLDSLAEFF EDLADKPYTF EDYDVSFGSV
131 LTVKLGGDLG TYVINKQTPN KQIWLSSPSS GPKRYDWTGK NWVYSHDGVS
181 LHELLAAELT KALKTKLDLA SSLAYSGKDA 210
```

B.

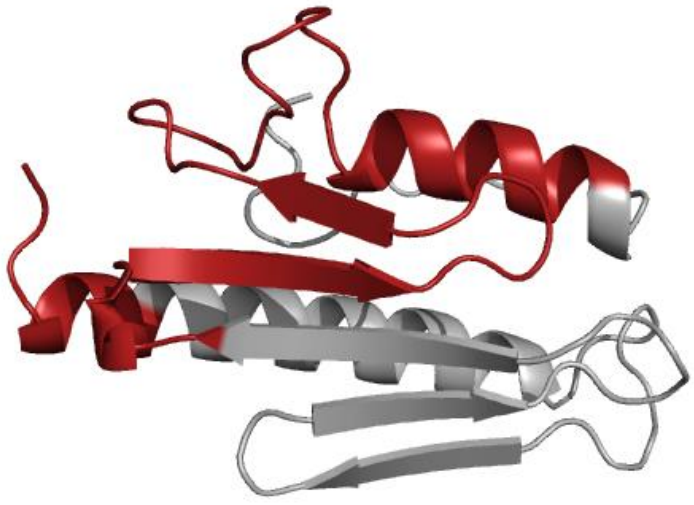

Figure 2-4. The peptides of FXN that were identified by trypsin digests after hydroxyl radical modification for at least two of the three independent experiments are shown (A) over the protein sequence by red bars or (B) as red peptides on the structure of human FXN (PDB 3S4M). Seven unique peptides were identified correlating to approximately 48% sequence coverage.

Changes in Peptide Modification upon the Formation of the SDU Complex. The peptides from ISCU2 and NFS1 mentioned were monitored in the SDU complex as well as in for the individual proteins. The changes in rates of modification upon complex formation indicate the regions involved in protein-protein interactions or protein conformational change protecting the region(s) from solvent exposure to hydroxyl radicals. First, the MALDI TOF mass spectra from ISCU2 either alone or in the SDU complex were analyzed to determine the changes rates of modification for the peptides on ISCU2 (Appendix Figures A1-A52). The relative amount of modification was determined by observing oxidation events for the peptide, where one oxidation event was defined as the appearance of a peak at +16 Da *m/*z spacing from the parent, unmodified peak and two oxidation events were determined by the observation of a peak at $[M+H+32]^+$ Da with the trend continuing in +16 Da increments. The fraction or percent of the peptide that was unmodified was calculated using Equation 2-1 then plotted as a function of exposure time and the resulting data was fit to Equation 2-2 in KaleidaGraph (Figure 2-5). The calculated rates of modification for each peptide from ISCU2 or the SDU complex are shown in Table 2-1. The error associated with each calculated rate reflects the error in the fit. Additionally, the cases in which the amount of modification appears to decrease at longer time points is likely due to low signal intensity of the parent and modified peaks. This led to potentially not observing modified species or relative abundance values that were not reflective of the true amount of modification. The data revealed one peptide on ISCU2 that showed a decrease in modification upon binding the SD complex, specifically residues 5-13 (unmodified *m/z*

1128.5). This peptide underwent 3 oxidation events noted by the appearance of peaks at 1144.5, 1160.5, and 1176.6 *m/z* in ISCU2 and the SDU complex with the relative abundance of the oxidized peaks being lower in the SDU complex. Furthermore, two ISCU2 peptides (residues 56-76, unmodified *m/z* 2190.1 and residues 102-113, unmodified *m/z* 1330.7) were identified in two independent experiments and showed protection in one of those experiments (Figure 2-5, Table 2-1). In experiment 3, the ISCU2 peptide 56-76 at *m/z* 2190.1 had peaks appear at 2206.1, 2222.1, 2238.1, and 2254.0 *m/z* (4 oxidation events) as a function of exposure to hydroxyl radicals but in the SDU complex, only peaks at 2206.1 and 2222.1 *m/z* (2 oxidation events) were observed. Additionally in experiment 3, the ISCU2 peptide 102-113 at *m/z* 1330.7 had peaks appear at 1314.6, 1346.6, and 1362.6 *m/z* upon exposure to hydroxyl radicals. When ISUC2 bound the SD complex to form the SDU complex, this peptide only had a peak at *m/z* 1346.6 appear indicating protection of this peptide in the SDU complex. The appearance of the peak at *m/z* 1314.6 in the sample for ISCU2 corresponding to residues 102-113 relates to a loss of 16 Da, which is one potential modification for cysteine containing peptides.

Interestingly, one peptide on ISCU2 (residues 58-76, *m/z* 1914.8), appeared much more susceptible to oxidation (Table 2-1) upon SDU complex formation for two independent experiments while the peptide was not observed in the third experiment. In experiment 2, for both ISCU2 and ISCU2 in the SDU complex, peaks at 1930.8, 1946.8, and 1962.9 *m/z* (3 oxidation events) appeared upon exposure to hydroxyl radicals but the modified peaks in the SDU complex were more abundant compared to the unmodified peak than for ISCU2 alone. In experiment 3 for the same peptide, only peaks at 1930.9 and 1946.9 *m/z* became more abundant with ISCU2 formed the complex with SD. ISCU2 peptides for other regions of the protein (residues 14-20, 41-48, 77-87, and 114-120 corresponding to 732.4, 972.5, 1188.6, and 751.4 *m/z*, respectively) did not show a change in modification in any of the three independent experiments (Figure 2-5, Table 2-1). The regions on ISCU2 that underwent protection or additional modification upon complex formation with NFS1 have been mapped onto the model of human ISCU2 with the protected peptide shown in blue, the more modified peptide (residues 58-76) shown in orange, and the active site cysteines highlighted in yellow (Figure 2-6).

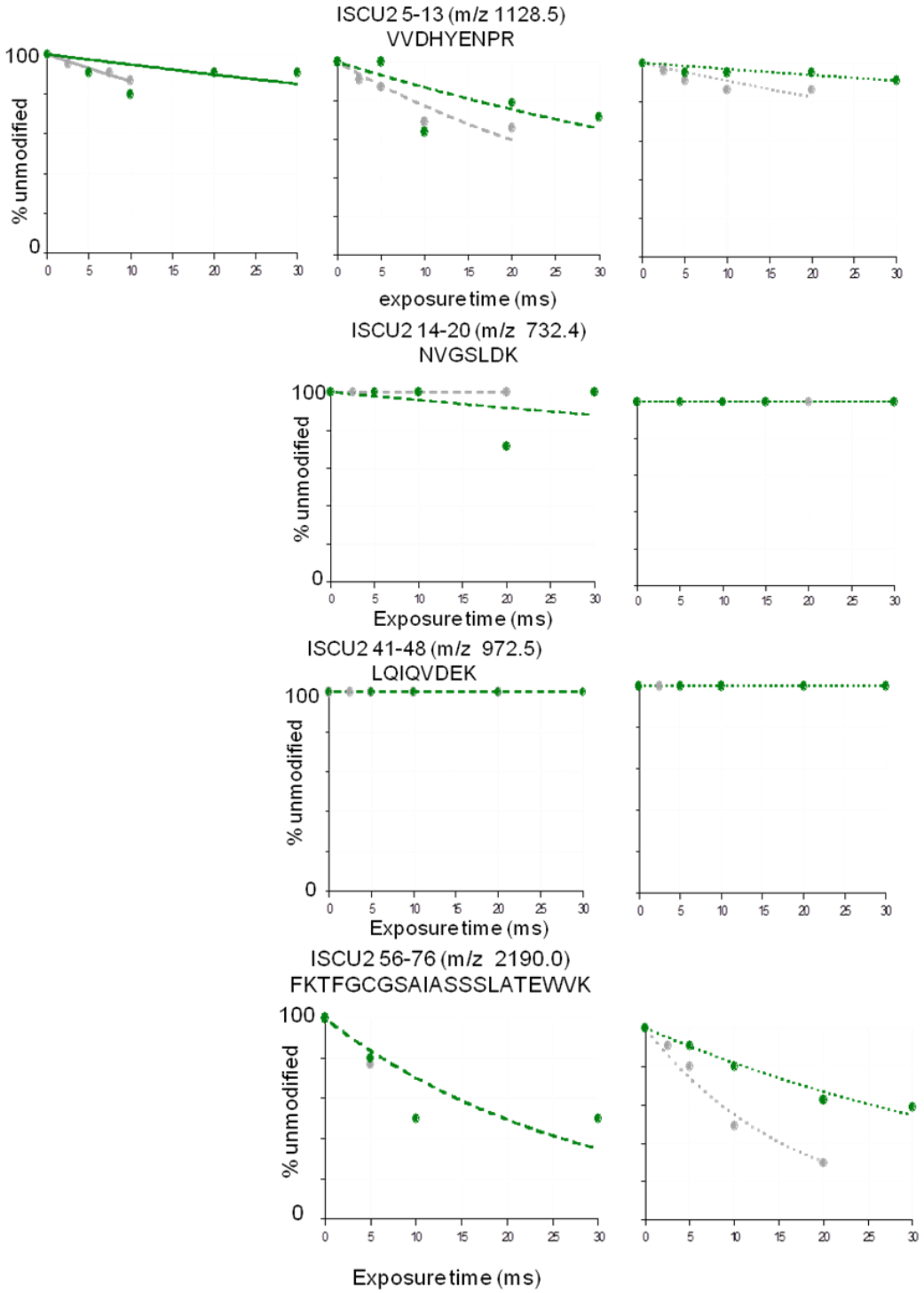

Figure 2-5. The rates of modification are shown for the ISCU2 peptides generated from tryptic digests from: ISCU2 (dark gray) or ISCU2 from SDU (green). The data from experiment 1 (solid lines), experiment 2 (dashed lines), and experiment 3 (dotted lines) are shown.

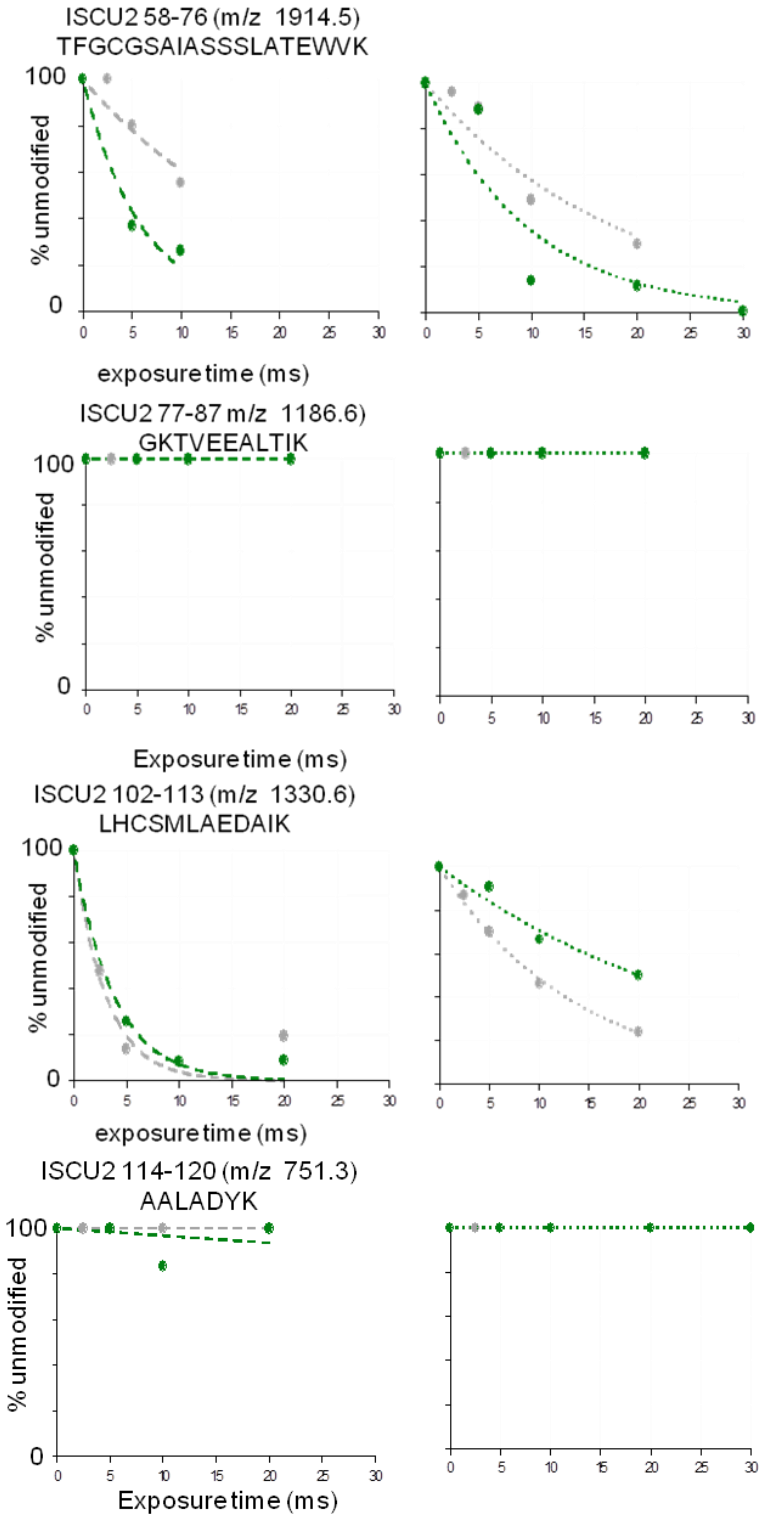

Figure 2-5. Continued.

Table 2-1. The rates of modification for peptides on ISCU2 that were observed in the ISCU2 and SDU samples.

peptide	*m/z*	Experiment 1		Experiment 2		Experiment 3		Overall change from ISCU2 to SDU
		ISCU2 (sec^{-1})	ISCU2 from SDU (sec^{-1})	ISCU2 (sec^{-1})	ISCU2 from SDU (sec^{-1})	ISCU2 (sec^{-1})	ISCU2 from SDU (sec^{-1})	
5-13	1128.5	15 ± 1	5 ± 3	25 ± 4	15 ± 5	9.7 ± 2	3.2 ± 0.6	decrease
14-20	732.4	0	0	4 ± 4	0	0	0	none
41-48	972.5	0	0	0	0	0	0	none
58-76	1914.8	n.d	n.d.	50 ± 10	166 ± 24	55 ± 9	103 ± 33	increase
77-87	1188.6	0	0	0	0	0	0	none
102-113	1330.7	n.d	n.d	324 ± 68	261 ± 32	72 ± 3	35 ± 4	decrease
114-120	751.4	0	0	3 ± 3	0	0	0	none

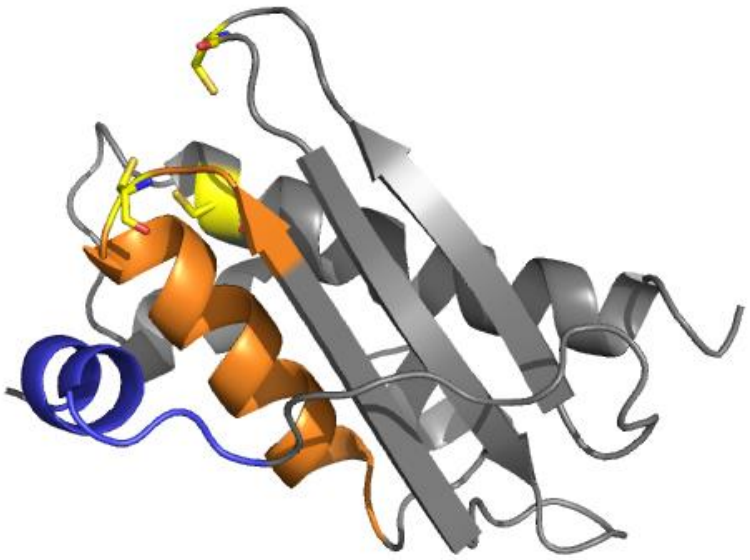

Figure 2-6. The peptides that underwent protection (residues 5-13, blue) or became more modified (residues 58-76, orange) upon complex formation with NFS1 were mapped onto the model of human ISCU2. The regions that were not observed or that did not undergo modification are shown in gray. The active site cysteine residues are shown as yellow sticks.

In a similar manner, the rates of modification for NFS1 in the SD and SDU complexes were compared. The MALDI TOF mass spectra were analyzed to determine rates of modification for NFS1 (Appendix figures A52-A81) and the relative abundance of the parent and modified peaks were monitored to calculate the fraction unmodified by Equation 2-1. The fraction unmodified was plotted against exposure time to determine the rate of oxidation using Equation 2-2 in KaleidaGraph. The rate graphs for the 7 NFS1 peptides corresponding to ~27% sequence coverage are shown (Figure 2-7) with the calculated rates of modification shown in Table 2-2. The error associated with the rate of modification reflects the error in the fit. In the cases where the modification appears to decrease as the exposure time increases is likely due to low peptide abundance in the MS spectra and does not reflect a change in modification due to protein conformational change or changes in protein-protein interactions. Comparison of the data from SD and SDU revealed two NFS1 peptides (residues 262-290, unmodified *m/z* 3085.6 and residues 402-419, unmodified *m/z* 2160.1) that were less susceptible to oxidation upon SDU complex formation (Table 2-2, Figure 2-8). Interestingly, there is significantly more protection to the 262-290 peptide (two independent experiments) than for the C-terminal peptide (residues 402-419) upon forming the SDU complex (Table 2-2).

For residues 262-290 in experiments 1 and 3, a peak at *m/z* 3101.6 appeared corresponding to one oxidation event as SD or SDU was exposed to hydroxyl radicals compared to the parent peak at *m/z* 3085.6. In the SDU complex, the peak at *m/z* 3101.6 was less abundant, relatively, than for the SD complex indicating a protection from hydroxyl radicals or conformational change. The C-terminal peptide (residues 402-416) with a parent peak at *m/z* 2160.1 underwent one or two oxidation events as observed by the appearance of peaks in experiment 1 at *m/z* 2176.1 and in experiment 3 at 2176.1 and 2192.1 *m/z* upon exposure to hydroxyl radicals; the relative abundance of the modified peaks decreased in the SDU complex compared to the SD complex in both experiments. There were 5 additional peptides that were observed in at least 2 of the experiments that were unmodified in either the SD or SDU complexes (residues 75-88, 89-105, 233-240, 245-258, 363-379 corresponding to 1481.8, 1807.9, 848.5, 1485.8, 1484.7 *m/z*, respectively) indicating no change in conformation or interaction with additional complex components (Table 2-2, Figure 2-7).

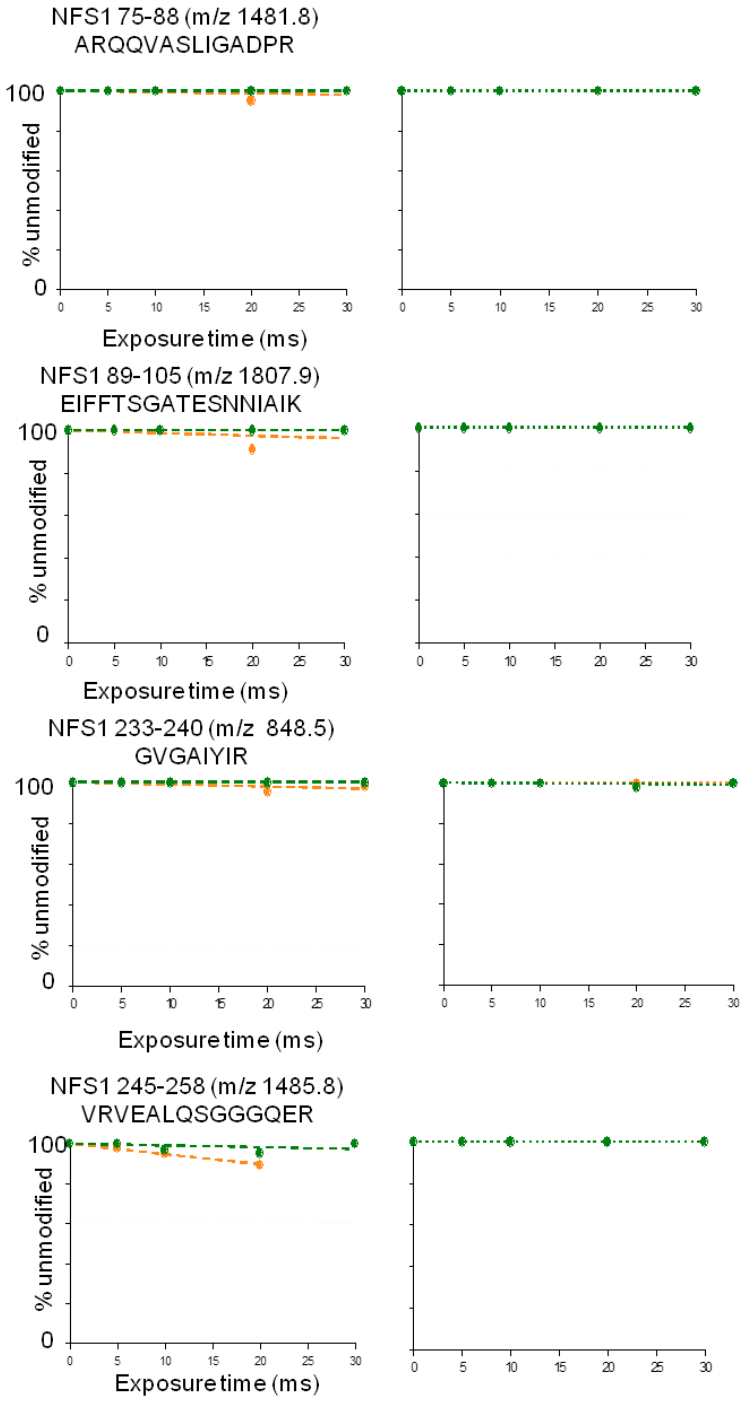

Figure 2-7. The peptides observed in the hydroxyl radical footprinting experiments from NFS1 in the SD and SDU complexes are shown as a function of exposure time to X-ray radiation. The data from three independent experiments are shown with the peptides of NFS1 from SD (orange) and SDU (green).

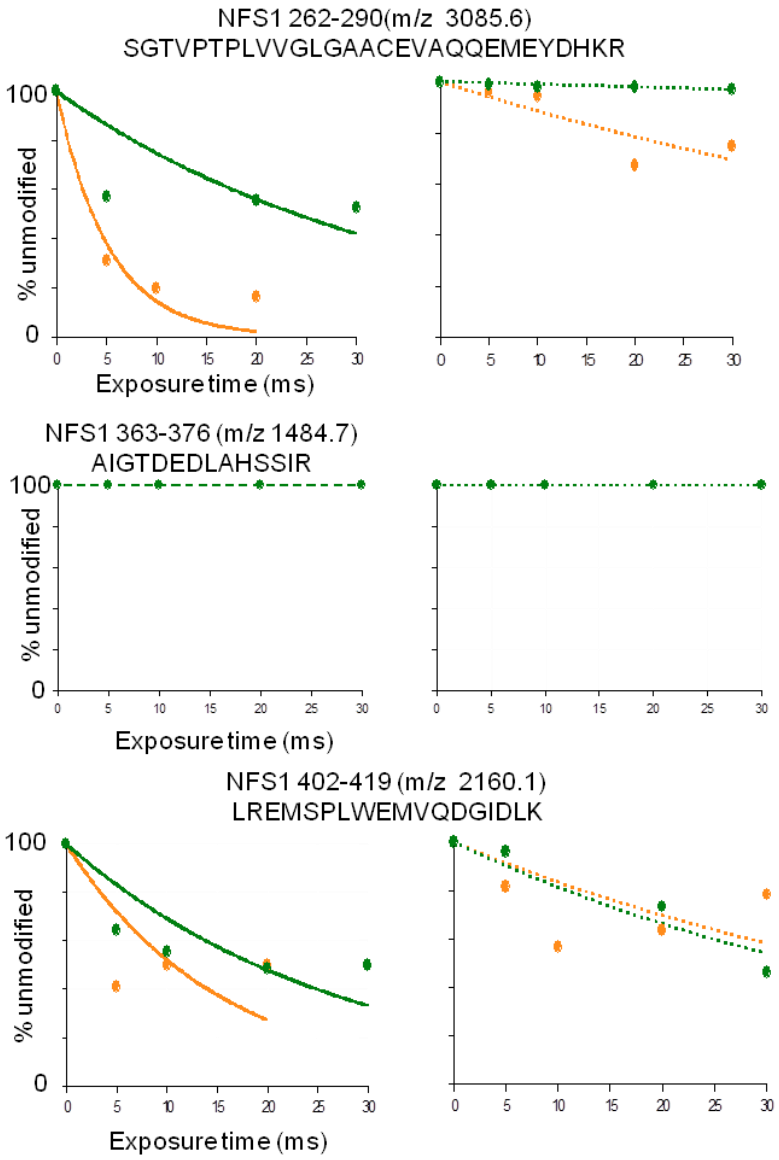

Figure 2-7. Continued.

Table 2-2. The rate of modification was calcualted for peptides from NFS1 from the SD and SDU compelexes. The instances where "0" is shown indicates that no modification was observed.

NFS1 peptide	*m/z*	Experiment 1		Experiment 3		Overall Change from SD to SDU
		NFS1 from SD (sec^{-1})	NFS1 from SDU (sec^{-1})	NFS1 from SD (sec^{-1})	NFS1 from SDU (sec^{-1})	
75-88	1481.8	0	0	0	0	none
89-105	1807.9	1 ± 1	0	0	0	none
233-240	848.5	1.1 ± 0.4	0	0	0	none
245-258	1485.8	5.1 ± 0.3	0.9 ± 0.6	0	0	none
262-290	3085.6	192 ± 40	29 ±10	12 ± 3	1.1 ± 0.1	decrease
363-376	1484.7	0	0	0	0	none
402-419	2160.1	65 ± 27	37 ± 9	33 ± 9	21 ± 3	decrease

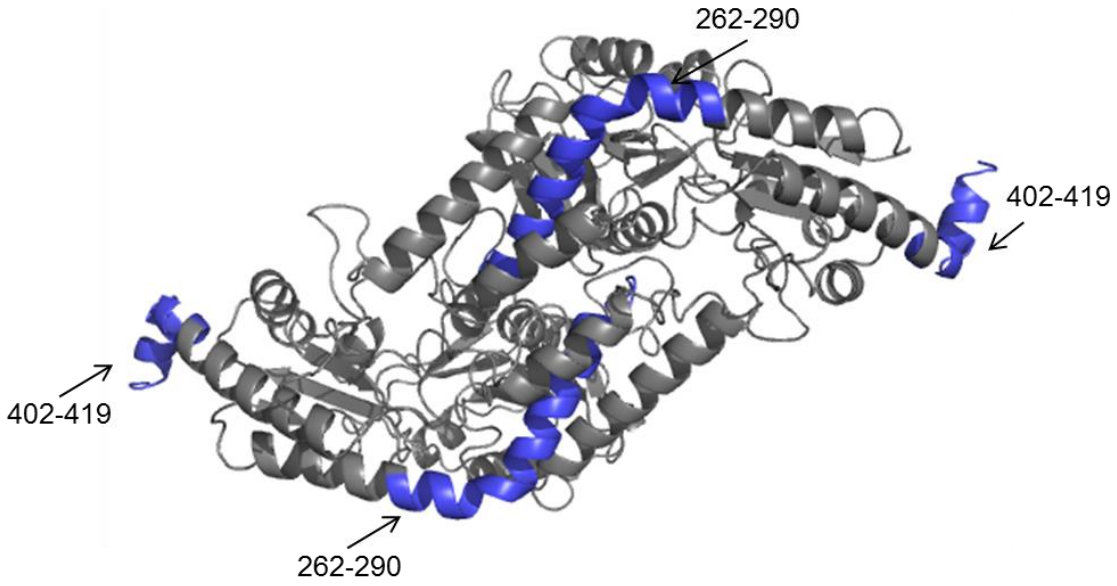

Figure 2-8. The peptides that were protected from modification from NFS1 upon ISCU2 binding to form the SDU complex are shown in blue on the model of human NFS1 dimer. The peptides, which were not observed or were unmodified, are shown in gray.

Changes in Modification for the SDU Complex upon FXN Binding. Currently, there is a lack of structural information for how FXN binds and activates the low activity Fe-S assembly complex SDU. A similar hydroxyl footprinting strategy outlined above was used to examine how FXN alters the kinetics of modification for ISCU2 and NFS1. MALDI TOF mass spectra were analyzed to generate the rate graphs for ISCU2 and NFS1 shown in Figure 2-8 (Appendix figures A1-A81). Evaluation of the data showed there was one peptide on ISCU2 that exhibited protection upon FXN binding the SDU complex, namely residues 102-113 at peak *m/z* 1330.7 (Figure 2-9, Table 2-3). In both the SDU and SDUF complexes, the modified species at peaks 1346.7 and 1362.7 *m/z* corresponding to 2 oxidation events were observed (experiment 2) but the overall abundance of the oxidized peaks decreased in the SDUF complex. In the third experiment for the SDU complex, the single oxidation event peak at *m/z* 1346.7 was apparent but upon FXN binding the complex, the *m/z* 1346.7 peak disappeared indicating that this peptide was protected from modification the SDUF complex (Figure 2-9). The peptide that became protected upon FXN binding the SDU complex has been shown on the model of human ISCU2 in cyan with the active site cysteines highlighted in yellow (Figure 2-11). Additional ISCU2 peptides (residues 5-13 and 56-76, corresponding to unmodified peaks at 1128.5 and 2190.0 *m/z*, respectively) described above had similar or slightly decreased modification rates upon FXN binding (Table 2-3). Unfortunately, no additional peptides on NFS1 were identified with altered modification rates when comparing the SDU and SDUF complexes (Figure 2-10, Table 2-4).

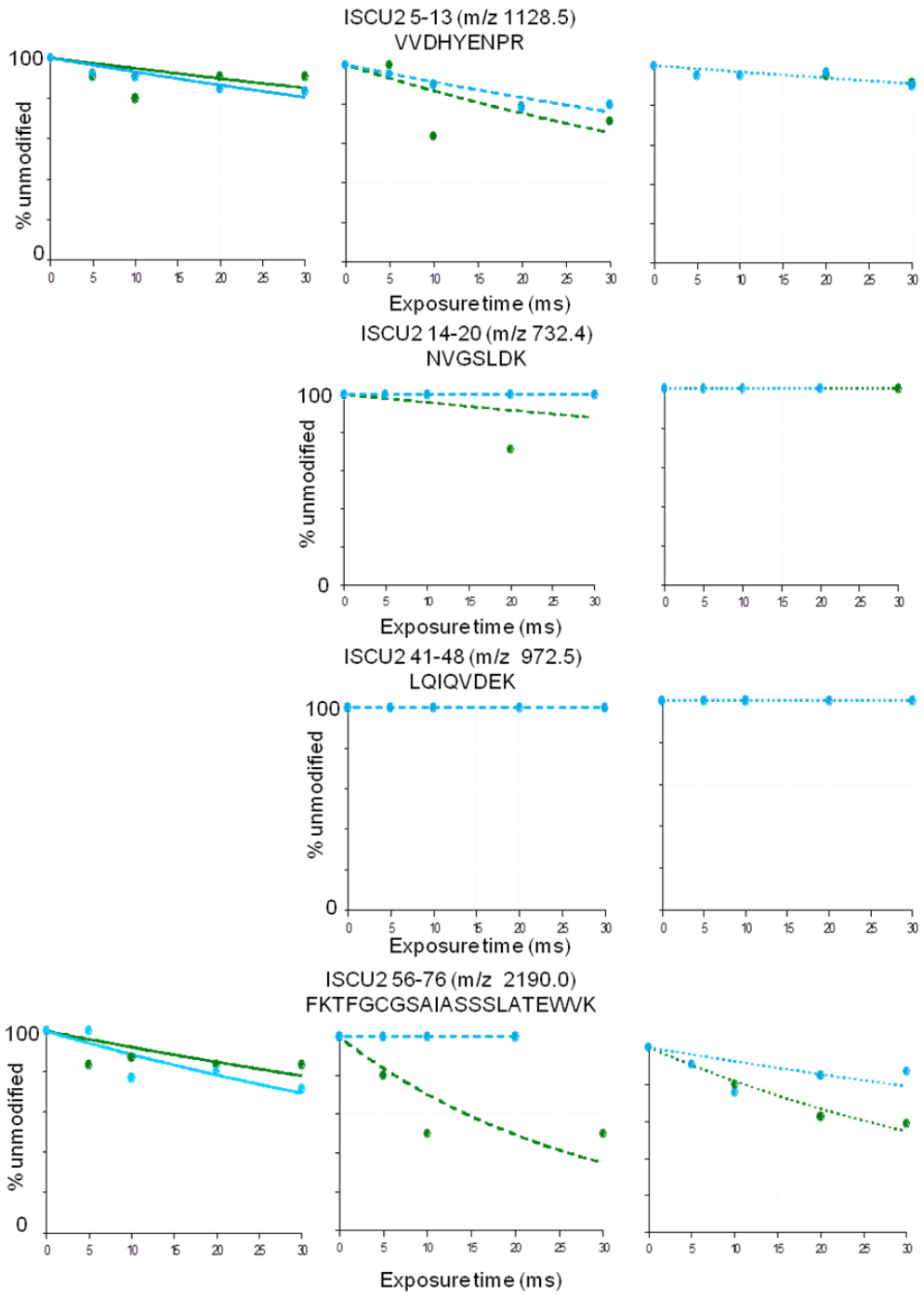

Figure 2-9. The peptides of ISCU2 that were observed in the three experiments from the SDU (green) or SDUF (cyan) complexes as a function of exposure time to hydroxyl radicals.

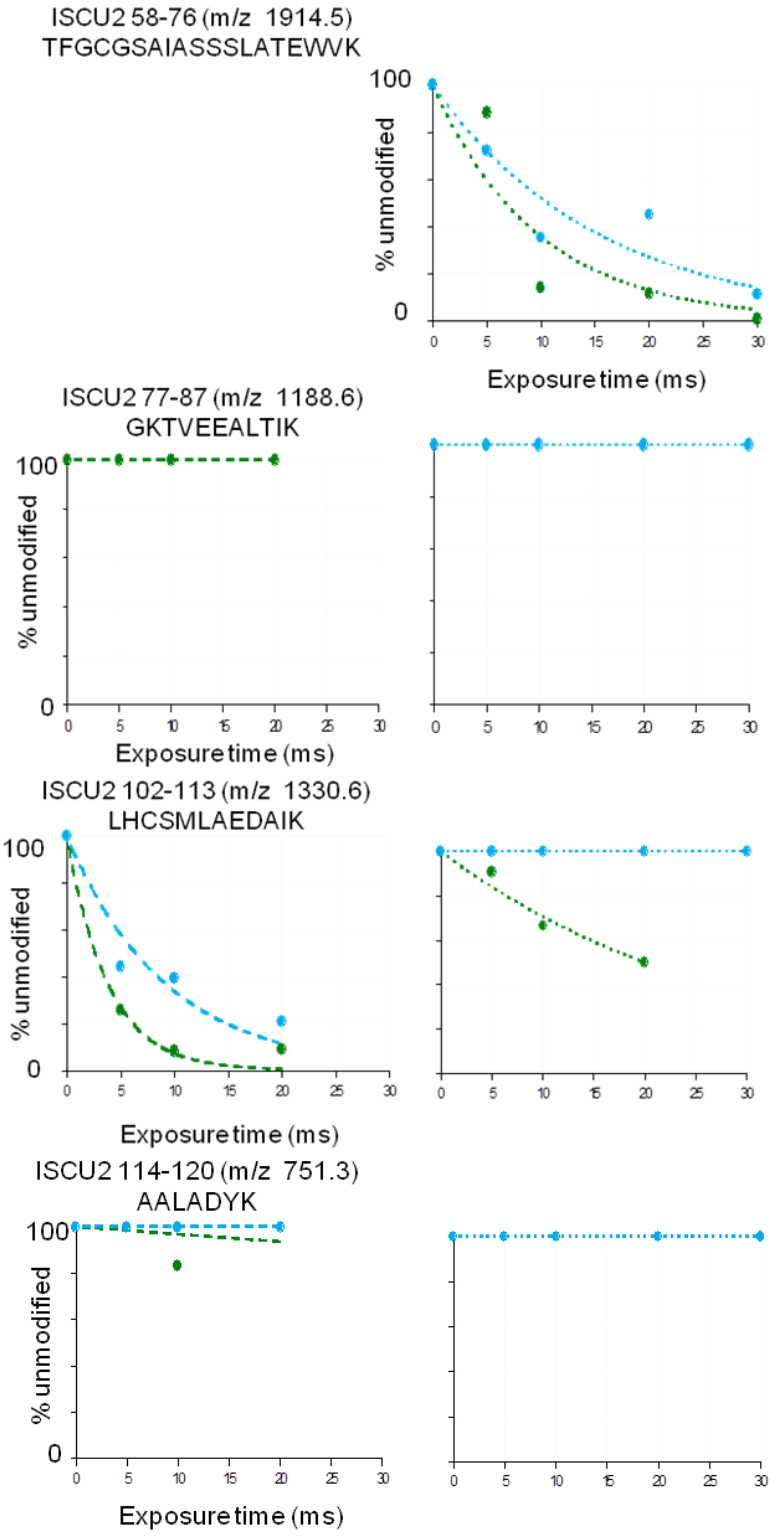

Figure 2-9. Continued

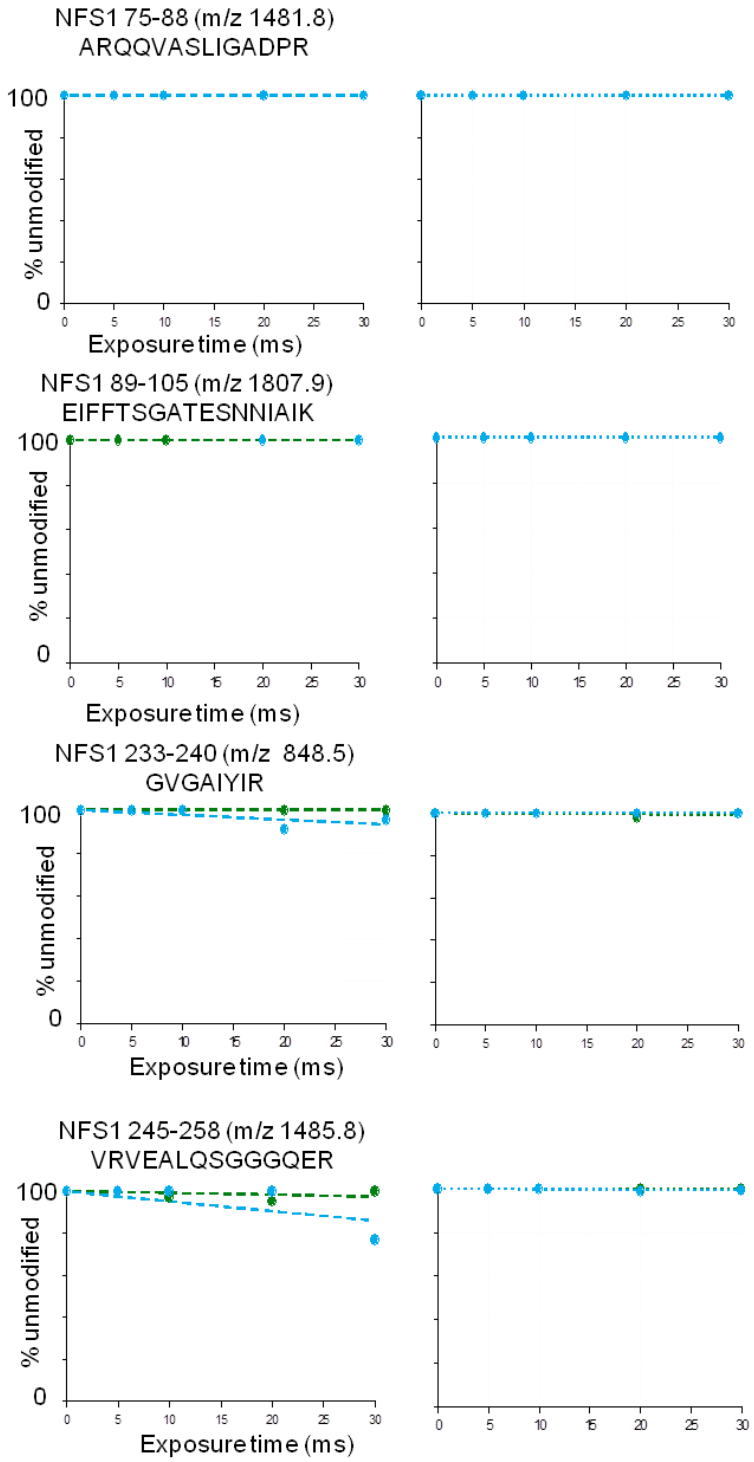

Figure 2-10.The fraction unmodified for the peptides from NFS1 that were observed in the SDU (green) and SDUF (cyan) complexes were plotted as a function of exposure time to hydroxyl radicals.

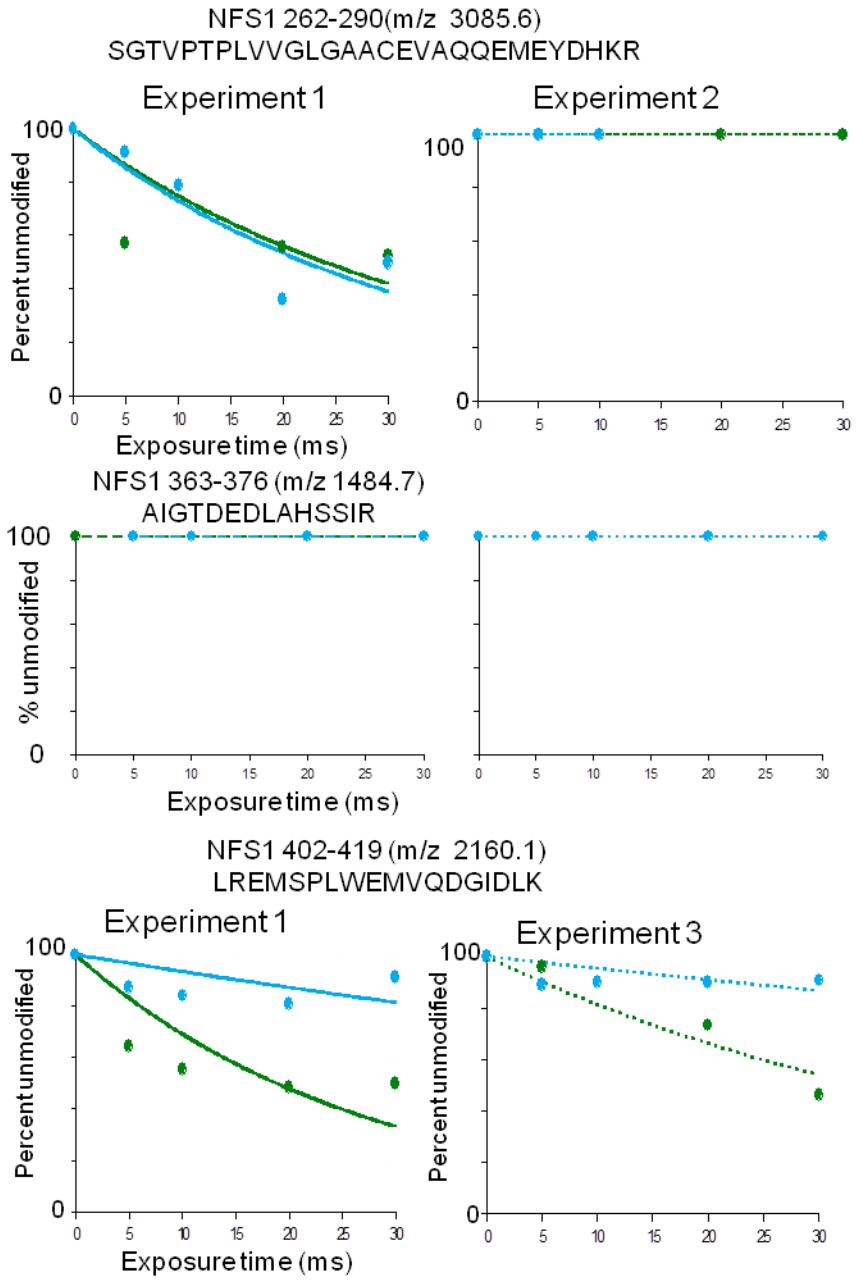

Figure 2-10. Continued

Table 2-3. The rates of modification for peptides from ISCU2 from the SDU and SDUF complexes fit to Equation 2-2 are shown.

peptide	m/z	Experiment 1		Experiment 2		Experiment 3		Overall change in ISCU2 from SDU to SDUF
		ISCU2 from SDU (sec^{-1})	ISCU2 from SDUF (sec^{-1})	ISCU2 from SDU (sec^{-1})	ISCU2 from SDUF (sec^{-1})	ISCU2 from SDU (sec^{-1})	ISCU2 from SDUF (sec^{-1})	
5-13	1128.5	5 ± 3	7.2 ± 0.9	14 ± 5	9 ± 1	3.2 ± 0.6	3.2 ± 0.7	inconclusive
14-20	732.4	0	0	0	0	0	0	none
41-48	972.5	0	0	0	0	0	0	none
56-76	2190.0	8.4 ± 2.4	12.3 ± 2	35 ± 11	0	20.2 ± 1	13 ± 5	inconclusive
77-87	1188.6	0	0	0	0	0	0	none
102-113	1330.7	n.d.	n.d.	261 ± 32	108 ± 20	35 ± 4	0	decrease
114-120	751.4	0	0	0	0	0	0	none

Table 2-4. The rates of modification for peptides from NFS1 from the SDU and SDUF compelexes are shown calculated from Figure 2-10 and fit to equation 2-2.

NFS1 peptide	m/z	Experiment 1		Experiment 3		Overall Change from NFS1 from SDU to SDUF
		NFS1 from SDU (sec^{-1})	NFS1 from SDUF (sec^{-1})	NFS1 from SDU (sec^{-1})	NFS1 from SDUF (sec^{-1})	
75-88	1481.8	0	0	0	0	none
89-105	1807.9	0	0	0	0	none
233-240	848.5	0	2.3 ± 0.8	0	0	none
245-258	1485.8	0.9 ± 0.6	5 ± 2	0	0	none
262-290	3085.6	29 ±10	31 ± 6	1.1 ± 0.1	n.d.	none
363-376	1484.7	0	0	0	0	none
402-419	2160.1	37 ± 9	17 ± 4	21 ± 3	4 ± 2	decrease

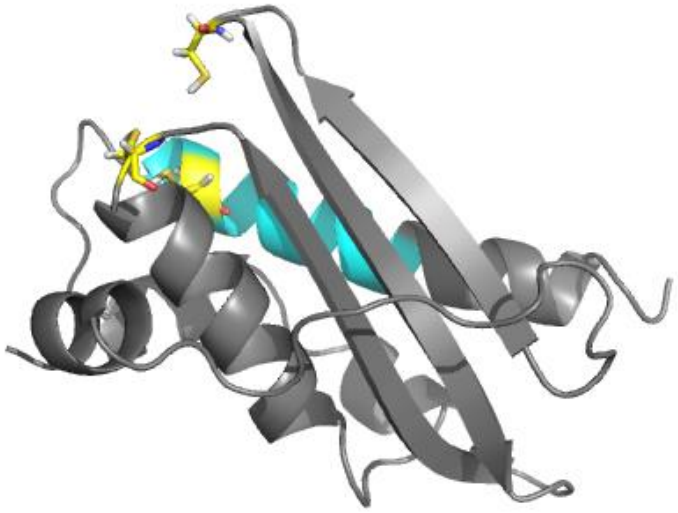

Figure 2-11. The peptide on ISCU2 that showed a decrease in oxidation upon the addition of FXN to the SDU complex to form the SDUF complex is shown in cyan (residues 102-113). The active site cysteines are highlighted as yellow sticks. The peptides that did not have changed modification kinetics or that were unobserved are shown in gray. The molecule is in the same orientation as the molecule in Figure 2-6.

Changes in Modification to FXN upon Binding to the SDU Complex. The changes in FXN peptide oxidation were also monitored between FXN and binding FXN to the SDU complex. The change in FXN modification rates was particularly evident due to the presence of 3 tryptophan residues in the sequence, which are easily modified by hydroxyl radicals in this 130 amino acid protein. Although 7 peptides (~48% of the sequence) were identified for FXN, the residues of the acidic patch were not observed. Each peptide (residues 81-97, 148-164, 148-165, 153-164, 153-165, 165-171, 165-192) had decreased oxidation kinetics in the SDUF complex compared to FXN alone (Figure 2-12, Table 2-5). The error associated with the rate reflects the error in the fit of the data.

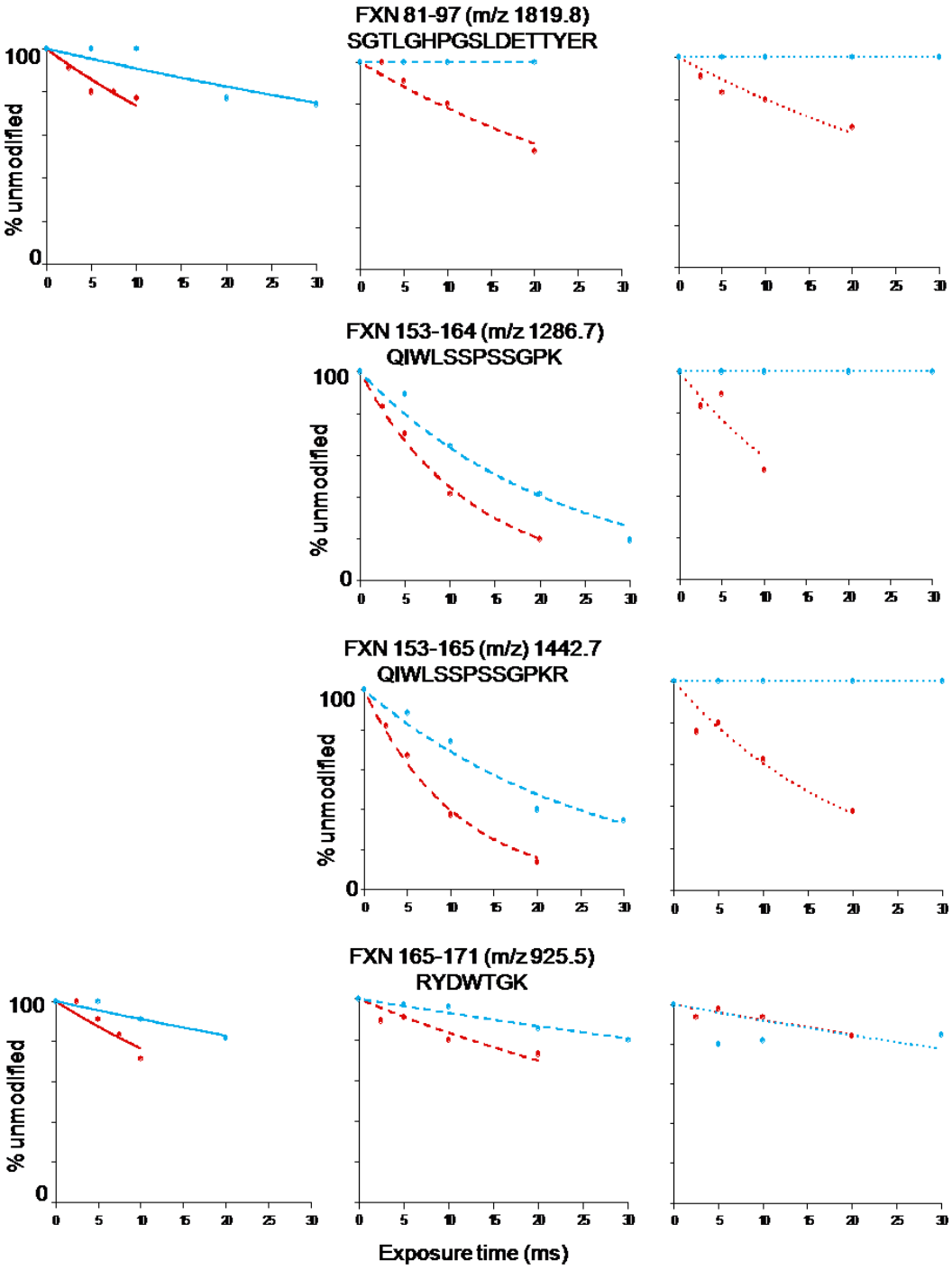

Figure 2-12.Peptides generated by trypsin digestion of FXN that were oxidized by hydroxyl radicals are shown for three independent experiments for FXN alone (red) or in the SDUF complex (cyan). Data was fit in KaleidaGraph to Equation 2-2.

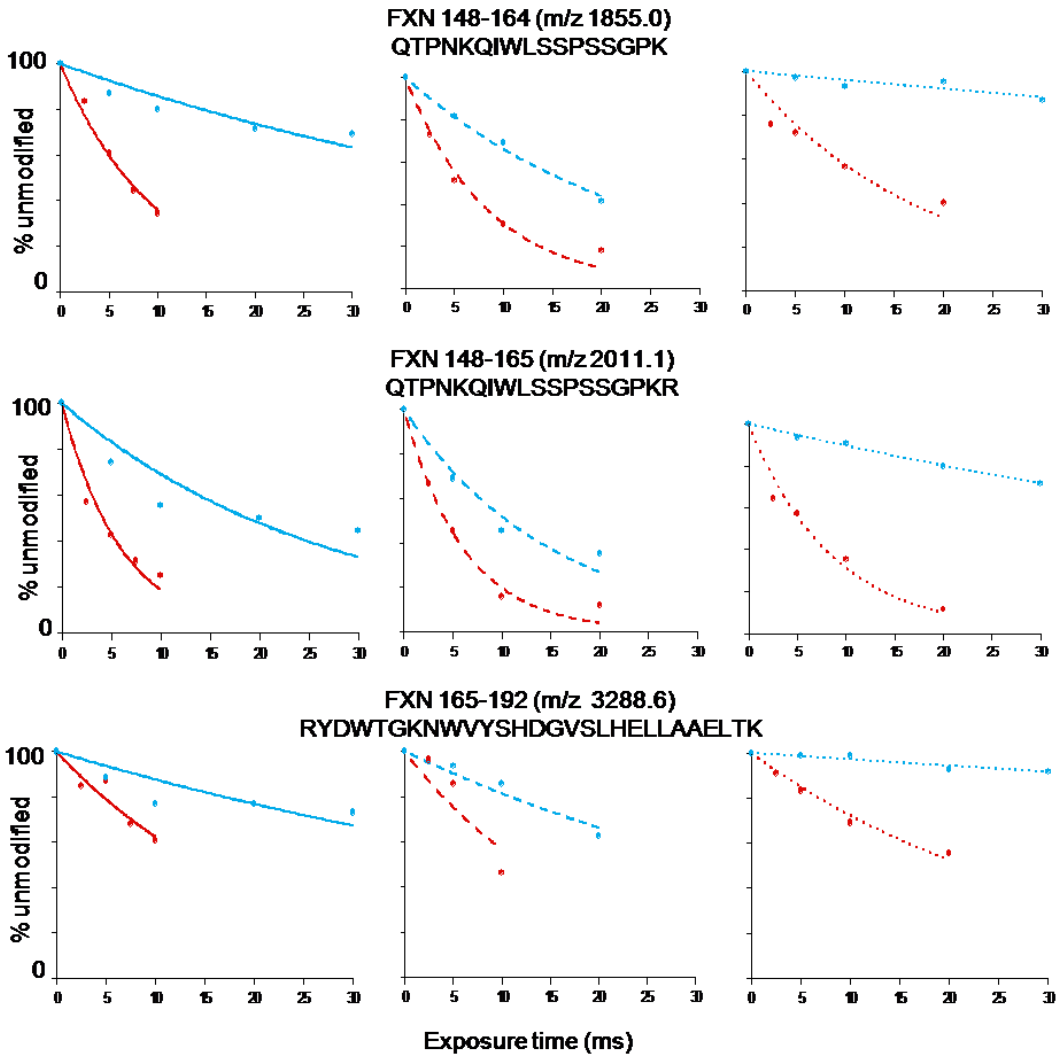

Figure 2-12. Continued.

Table 2-5. The rates of modification are shown for peptides of FXN from FXN or the SDUF complex upon exposure to hydroxyl radicals.

		Experiment 1		Experiment 2		Experiment 3		Overall change from FXN to SDUF
peptide	m/z	FXN (sec $^{-1}$)	FXN from SDUF (sec $^{-1}$)	FXN (sec $^{-1}$)	FXN from SDUF (sec $^{-1}$)	FXN (sec $^{-1}$)	FXN from SDUF (sec $^{-1}$)	
81-97	1819.8	37.6 ± 3.2	9.7 ± 2	25 ± 3	--	22.4 ± 2.4	--	decrease
148-164	1855.0	102 ± 5.2	15.29 ± 2.0	117.2 ± 9.9	41.1 ± 1.8	55.3 ± 7.1	4.2 ± 0.68	decrease
148-165	2011.1	166.2 ± 14	36.8 ± 6.3	161.1 ± 13	65.5 ± 7.6	116.1 ± 11	11.1 ± 0.32	decrease
153-164	1286.7	n.d.	n.d.	80.3 ± 3.4	45.0 ± 4.3	52.6 ± 11.5	0	decrease
153-165	1442.8	n.d.	n.d.	91.9 ± 4.6	37.0 ± 3.4	50.1 ± 6.1	0	decrease
165-171	925.5	26.7 ± 4.1	9.39 ± 1.4	18.1 ± 2.3	7.2 ± 0.5	8.2 ± 1.3	7.3 ± 3.3	decrease
165-192	3288.7	47.2 ± 5	13.2 ± 2.4	56.6 ± 14	20.7 ± 2.3	32.4 ± 1.9	3.0 ± 0.4	decrease

For the N-terminal peptide residues 81-97 a parent peak at *m/z* 1819.8, there appeared peaks at 1835.9 and 1851.9 *m/z* indicating 2 oxidation events of this peptide upon exposure to hydroxyl radicals. Both oxidation events were evident in the SDUF complex for experiment 1 but significantly decreased in relative abundance compared to FXN; no oxidation events were evident in the SDUF complex spectra for experiments 2 and 3.Similarly, the peak at *m/z* 1855.0 corresponding to residues 148-164 on FXN had 3 oxidation event peaks appear with exposure to hydroxyl radicals observed by the appearance of peaks at 1871.0, 1887.0, and 1903.0 *m/z* in experiments 1, 2, and 3 where only 2 oxidation events at 1871.0 and 1887.0 *m/z* at lower abundances were observed when FXN interacted with the SDU complex. The peak at *m/z* 2011.1 corresponding to FXN peptide 148-165 had oxidized peaks appear at 2027.1, 2043.1, 2059.1, and 2075.1 *m/z* for the FXN protein corresponding to 4 oxidation events. When the FXN bound the SDU complex, peaks at *m/z* 2027.1 (experiments 1, 2, and 3), *m/z* 2043.1 (experiments 1

and 2), and *m/z* 2059.1 (experiment 1 only) appeared at lower abundances than for FXN. For the FXN peptide with residues 153-164 (unmodified peak at *m/z* 1286.7), peaks appeared at 1302.6, 1318.7, and 1334.7 *m/z* corresponding to 3 oxidation events when FXN was either unbound or bound to the SDU complex with lower abundances (experiment 2) in the SDUF complex; the peaks at 1302.6, 1318.7, and 1334.7 *m/z* were not observed in experiment 3. The peptide corresponding to FXN residues 153-165 (unmodified peak *m/z* 1442.8) had peaks corresponding to 1, 2, or 3 oxidation events (1458.8, 1474.8, and 1490.8 *m/z*, respectively) appear for experiment 2 for both FXN and FXN in the SDUF complex and peaks corresponding to 1 or 2 oxidation events (1458.8 and 1474.7 *m/z*, respectively) were observed in experiment 3 for FXN but were absent for FXN in the SDUF complex. For the peptide 165-171 with an unmodified peak at *m/z* 925.5, peaks appeared at 941.4 and 957.5 *m/z* upon exposure to hydroxyl radicals in all three experiments for FXN corresponding to 2 oxidation events. When FXN bound the SDU complex, both of the oxidation peaks (941.4 and 957.5 *m/z*) were observed but at a lower abundance than for FXN. The most C-terminal peptide observed for FXN, residues 165-192 with a peak at *m/z* 3288.7, showed oxidation by peaks appearing at 3304.6 and 3320.7 *m/z* corresponding to 1 or 2 oxidation events, respectively. When FXN bound the SDU complex, both of the peaks at *m/z* 3304.6 (experiments 1, 2, and 3) and *m/z* 3320.7 (experiments 1 and 2) were observed at a lower abundance than for FXN.

Analysis of ISD11 in the Hydroxyl Radical Footprinting Experiments. The overall sequence coverage by trypsin digestion for ISD11 is shown on the protein sequence (Figure 2-13). This small, mostly basic protein was not significantly modified through the footprinting experiments and changes in modification were not monitored (data not shown). The peptides identified were highlighted by black bars corresponding to approximately 66% of the protein sequence.

Figure 2-13. The sequence coverage of ISD11 by trypsin digest from the hydroxyl radical footprinting experiments is shown with black bars indicating the fragments identified over the protein sequence.

DISCUSSION

The aims of this chapter were to obtain a better understanding of the interactions of the components of the human Fe-S assembly complex to create a model that correlates structure with function that can be further tested by biochemical assays. These results were then used to compare the interactions of the human system to the homologous complex previously studied from *E. coli* by protein crystallography. Previous attempts at protein crystallography of the NFS1-ISD11, SDU, or SDUF complexes has been unsuccessful and techniques such as NMR are inappropriate due to the size of the

complex, the amount of material required, and the challenges of producing labeled protein. Therefore, a technique which requires significantly less material, is not size limited, and is applicable to proteins in buffered solutions was employed, namely hydroxyl radical footprinting. This technique covalently modifies amino acid side chains that are exposed to the bulk solution by oxidation from radical species. The covalent modification allows for the proteins or complexes to be digested and analyzed further by techniques such as mass spectrometry.

Hydroxyl radicals can be generated by various chemical means, most commonly through Fenton chemistry, in which Fe^{2+} is oxidized to Fe^{3+} and radicals are generated from H_2O_2 to produce hydroxide and a hydroxyl radical which can modify protein side chains (Figure 2-14, top panel).[119-121] This reaction requires high concentrations of H_2O_2 (mM), is relatively slow (minutes to modify), and is also not appropriate for metal binding proteins such as the SDUF complex because modification would be localized to the region around the metal binding site. A second approach is to generate radicals by the laser photolysis of H_2O_2 by a KrF laser at 254nm.[122-125] This approach is attractive because the exposure time is on the microsecond time scale and the concentrations of H_2O_2 are much lower (μM) than required for Fenton chemistry but was not used in this application due to the laser requirement. Lastly, radicals can be generated from water molecules in buffered solutions by exposure to synchrotron radiation (Figure 2-14, lower panel).[113, 119, 126]

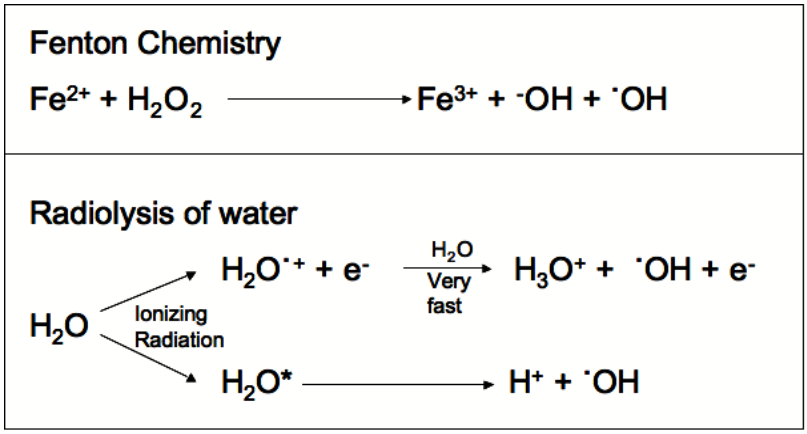

Figure 2-14. The generation of hydroxyl radicals is shown by various methods including Fenton chemistry (top) or the radiolysis of water by a synchrotron source (bottom).

Solvent accessible side chains are susceptible to modification by hydroxyl radicals whereas those involved in protein tertiary structure or protein-protein interactions are protected from oxidation. The general reactivity of the solvent exposed side chains from most reactive to least reactive are as follows: Cys> Met >Trp> Tyr >Phe> His >Leu ~ Ile >Arg ~ Lys ~ Val >Ser ~Thr ~ Pro >Gln ~ Glu> Asp ~ Asn>Ala>Gly.[119, 127] The oxidation reaction is quenched by the addition of a radical scavenger, such as methionine.[112, 128] After labeling and quenching, the level of modification can be determined as a function of exposure time by monitoring the shift in peptide molecular weight by mass spectrometry after proteolytic digestion to determine the side chain accessibility to modification. To determine the interfaces important for protein-protein interactions, the proteins were labeled both individually (Figure 2-15, top panel) and after the assembly of the complexes (Figure 2-15, bottom panel) and the changes in rates of modification of a particular peptide or peptides after binding its

protein partner(s) were observed.[113, 115, 119, 129] The application of hydroxyl radical footprinting monitored by MALDI TOF mass spectrometry to understand interactions of a multiple protein complex, such as the SDU or SDUF complexes, which build upon a core protein, NFS1, is a unique application of the hydroxyl radical footprinting technique.

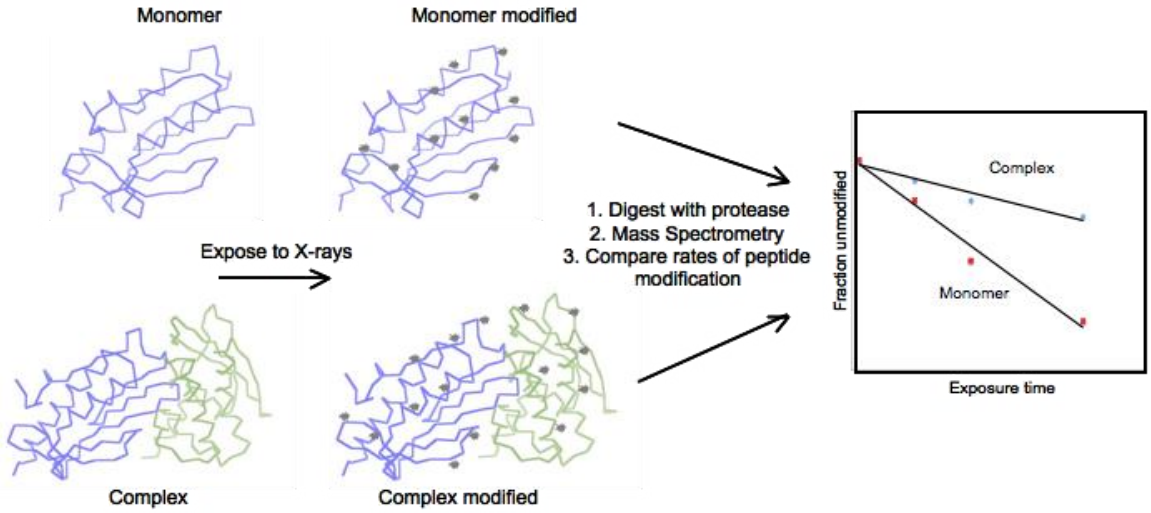

Figure 2-15. Experimental design of hydroxyl radical footprinting showing the comparison between modification for the monomer (top panel) and the complex (bottom panel to identify the regions of protein-protein interaction.

Many of the components of the human Fe-S cluster assembly complex have relatively little structural information known. Of the four proteins, only one component has been crystallized, namely FXN. In addition to structural data from NMR, the interactions between FXN and the SDU complex have been studied by kinetic binding assays indicating regions on FXN that likely interact with the SDU complex. [33, 66, 75] The

human system has functional differences from the homologous bacterial system, namely that ISD11 is required for the stability and activity of the cysteine desulfurase NFS1[61, 78] and that the addition of frataxin to the SDU core activates the complex for sulfur transfer and enhances Fe-S cluster synthesis.[33, 78] In contrast, the bacterial system does not contain a protein homologous to ISD11 and the cysteine desulfurase-scaffold complex has high cysteine desulfurase and Fe-S cluster activity that becomes diminished upon the addition of frataxin.[78, 130]Additional differences exist between the human and bacterial systems, such as the calculated pI of the scaffold proteins is vastly different between *E. coli* (pI 4.9) and human (pI 8.6) leading to a difference of overall charge at the pH at which most experiments are performed (pH ~7-7.5). Furthermore, there exists two bacterial co-crystal structures of the cysteine desulfurase-scaffold complex, one from *E. coli*[31] and one from *A. fulgidus,* which contains one [2Fe-2S] cluster bound at the dimer interface.[32] Despite the differences in functional activity between the human and bacterial systems, a strong sequence conservation exists between the components (*E. coli* IscU to human ISCU2 73%, *E. coli* IscS to human NFS1 59%, *E. coli* frataxin to human frataxin 24%). The results from the hydroxyl radical footprinting experiments indicate that there are some structural components conserved between the bacterial and human systems.

The change in oxidative modification kinetics for the N-terminus of ISCU2 (residues 5-13) suggests that this region is protected upon forming the SDU complex (Figure 2-6). Consistent with this hypothesis, an equivalent region on bacterial IscU is located near the protein-protein interface in crystal structures of the IscS-IscU complex

from *E. coli* and *A. fulgidus*.[31, 32] More specifically, *E. coli* IscU residues Y3, Y11, G38, V40, K42, K59-G64, and K103 interact with IscS residues R379-K391. Some of the corresponding residues (M1, Y9, G36, V38, K40, K57-62, and K101) are found in the N-terminal peptide 5-13 of human ISCU2, and with exception of M1 and K40, are highly conserved in eukaryotes. These interactions may play a role in the disease ISCU myopathy with exercise intolerance if the N-terminus of ISCU2 is unable to interact with NFS1 based on the location of the point mutation on ISCU2 (G16E).[79]

The slight protection of residues near the C-terminus of NFS1 (residues 402-419; two independent experiments) is consistent with the interaction of the cysteine desulfurase in the bacterial crystal structure of IscS-IscU (corresponding residues 379-391 in *E. coli*).[33, 34] The peptide residues 262-290 is not near the expected NFS1-ISCU2 interface (Figure 2-8), suggesting this region of NFS1 may be protected due to a conformational change that occurs upon ISCU2 binding either on NFS1 or interactions with ISD11. Together, these hydroxyl radical footprinting results may indicate interaction surfaces between the cysteine desulfurase to the scaffold proteins which may be diagnostic of conformational changes induced by complex formation.

A model of the human NFS1 and ISCU2 interactions was generated based on the *E. coli* crystal structure and the human protein sequences by the SWISS-MODEL software. The generated human model has an overall structure that is similar to its bacterial homologs and the interactions between NFS1 and ISCU2 as determined by the regions of protection from hydroxyl radical labeling are in good agreement with a conserved interaction (Figure 2-16A). Furthermore, when electrostatic potential maps were generated by the CHARMM-GUI PBEQ Solver for the human NFS1 and ISCU2 model proteins and the regions of interaction were compared from the results of the hydroxyl radical footprinting experiments and were determined to be complimentary in charge (Figure 2-16B). The N-terminus of ISCU2 is positively charged, displayed by the blue color whereas the C-terminus of NFS1 has overall negative charge, as shown by the red color. This model further supports the probability that NFS1 and ISCU2 interact in a semi-conserved manner to the bacterial system.

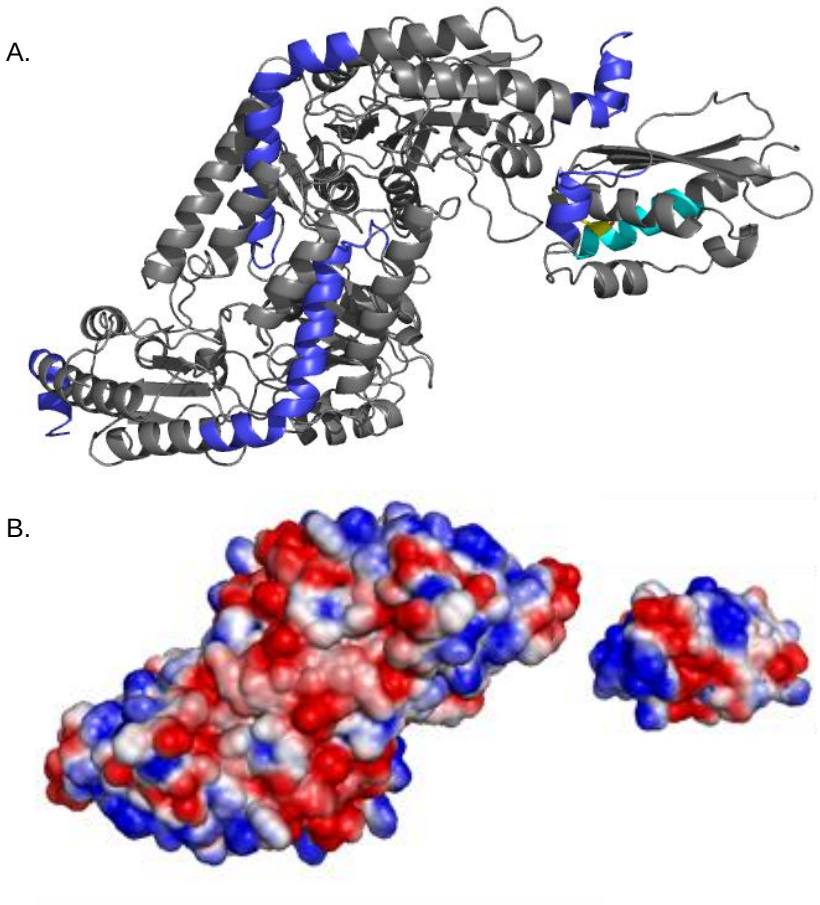

Figure 2-16. A.) A ribbon diagram of the human model of the interactions between NFS1 and ISCU2 is shown highlighting the peptides that were protected in the SDU (blue) or SDUF (cyan) complex. The active site cysteines on ISCU2 are shown as yellow sticks. B.) Electrostatic potential maps of NFS1 and ISCU2 in the same orientation as the ribbon diagram showing the complementary nature of the charge of the C-terminus of NFS1 and N-terminus of ISCU2.

Interestingly, there was one peptide on ISCU2 that appeared to be more susceptible to oxidation in two of the three experiments (residues 58-76, Table 2-1) in the SDU complex compared to ISCU2 alone in solution. This peptide is located near the core of ISCU2 and the increased modification in the SDU complex indicates that this region became more exposed to hydroxyl radicals potentially as a result of becoming more unstructured upon binding NFS1-ISD11 (Figure 2-6). The equivalent residues in bacterial IscU are located in the core of the αβ structure, suggesting ISCU2 has conformation and/or dynamic differences that expose core residues when it binds the SD complex. This supposition is supported by previous NMR results by the Markley group in which bacterial IscU was shown to exist as in equilibrium between structured and disordered states with the disordered state being favored to form the IscU-IscS complex.[35] The ISCU2 peptide 58-76 was not observed in the SDUF complex, but a peptide corresponding to a similar region, residues 56-76 (Table 2-3, unmodified peak at *m/z* 2190.0), was observed. This peptide became slightly more modified in one experiment (Experiment 1) but was more protected in Experiments 2 and 3 compared to SDU indicating that this peptide on ISCU2 may become more structured upon formation of the SDUF complex, also in good agreement with the NMR results from the Markley lab in which they hypothesize that the disordered form of the scaffold will bind the cysteine desulfurase but the structured conformation is the active form for Fe-S cluster assembly[35] and also supports a conservation of interaction between the bacterial and human systems.

In the SDUF complex, the NFS1 peptides did not show additional modification or protection compared to the NFS1 peptides from the SDU complex. This void is probably due to the low sequence coverage (~27%) of NFS1 by peptides seen in two or more experiments from the hydroxyl radical footprinting experiments. Previous studies in *E. coli* have shown that mutations at residues R116, R220, R223, R225/E227, G234, R237/M239, A327, or R340 on IscS (*E. coli* numbering) diminish or prevent the ability of the cysteine desulfurase to pull down bacterial frataxin, CyaY.[31] SAXS studies also showed that IscS residues R220, R223, R225 were important for CyaY binding.[34] Unfortunately, additional peptides that would provide information about the SDU complex activation upon FXN binding, specifically the mobile loop on NFS1 residues 330-360 (based on the bacterial IscS-IscU structure) could not be evaluated because the peptide by trypsin digestion for residues 330-360 was not observed by the hydroxyl radical footprinting experiment (Figure 2-10, Table 2-4). If the interaction between NFS1 and FXN was conserved between the human and *E. coli* systems, we would have expected to see protection of NFS1 in corresponding regions to the IscS protein.

The one peptide was identified on ISCU2 (residues 102-113) that became protected upon FXN binding to the SDU complex indicating an interaction between FXN and ISCU2. The interaction to ISCU2 through this region of the protein is highly likely due to the accessibility for FXN based on the model generated (Figure 2-16A). Additionally, this peptide is near the highly conserved LPPVK motif (residues 97-101, human numbering) on ISCU2 which has implications in chaperone protein interactions for cluster transfer,[52, 53] contains the highly conserved histidine (H103) which has been

implicated as being important for protein-protein interactions and possibly cluster ligation,[36] a hypothesized active site cysteine (C104), and a methionine residue (M106) that, when mutated to isoleucine, has shown the ability to stimulate the cysteine desulfurase and Fe-S assembly activities of the SDU complex in the absence of frataxin.[67, 68] The interaction between FXN and this region of ISCU2 has been further interrogated by mutational studies in which residues on ISCU2, K101, H103,[67] and L107, have been mutated and showed a 10-600 fold decrease in FXN binding to the SDU complex (Chapter IV). Interestingly, the ability to stimulate the cysteine desulfurase activity was diminished for only the H103D mutation whereas K101A, K101H, H103A, H103K, and L107Q were able stimulate the cysteine desulfurase activity to wild-type levels when the binding deficiency was overcome (Chapters IV and V). Mutations were also incorporated on the FXN molecule to attempt to overcome the binding deficiency seen with the ISCU2 mutation. Only one complimentary mutation set was able to overcome the decrease in binding affinity for FXN (H103K ISCU2 with R165H FXN) indicating a specific interaction between histidine 103 on ISCU2 and arginine 165 on FXN.[67] Although binding was able to be partially recovered, the ability to stimulate cysteine desulfurase activity was completely destroyed indicating that the interaction between the binding region on ISCU2 identified by hydroxyl radical footprinting and FXN is vital for binding and complex activation.

The regions on FXN that were protected in the SDUF complex determined in the hydroxyl radical footprinting experiments corresponded to the N-terminus (residues 81-97) and the β-sheet region (residues 148~165) (Figure 2-4). The region of protection

determined by the hydroxyl radical footprinting experiments also contain many of the FRDA mutants which showed significantly decreased binding to the SDU complex by kinetic assays, specifically residues N146K, Q153A, W155R, and R165C.[66, 131] Additionally, the binding constant of wild-type FXN to the SDU complex was determined using fluorescence anisotropy and was used to compare to the binding constant of the W155R FXN to the SDU complex, which was approximately 140 times weaker (Chapter III). Furthermore, mutations to the following FXN residues: E108K, E111K, D124K, N146K, W155R diminished or dissolved the ability of FXN to pull-down NFS1, ISD11, and ISCU2 indicating a potential surface for protein-protein interactions as determined by Schmucker *etal.* This region corresponds to the residues spanning from the acidic ridge to the β-sheet on FXN.[64] Taking these results taken in combination indicate that it is probable that FXN interacts with ISCU2 through the β-sheet region on FXN to the helix on ISCU2 (residues 102-113). The electrostatic potential of the β-sheet region of FXN is overall neutral, with a positively charged pocket due to R165 (Figure 2-17) that is complimentary to the region on ISCU2 that showed protection (residues 102-113), which has an overall negative charge (Figure 2-16B). As mentioned above, the binding of FXN to the SDU complex can be recovered by making complimentary mutations on both FXN (R165H) and ISCU2 (H103K) but their specific interaction and the importance of either of these two residues to stimulate the cysteine desulfurase activity of the NFS1 remains to be fully understood.

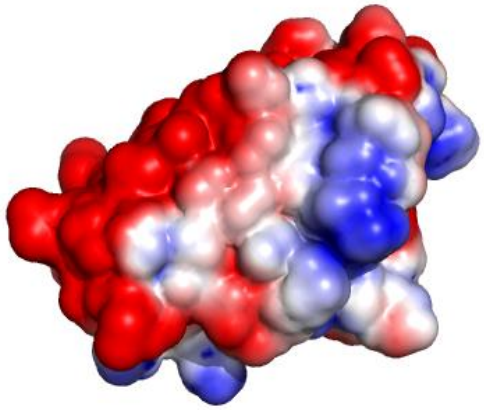

Figure 2-17. Electrostatic potential map of FXN is shown with the acidic patch at the top portion of the molecule (overall negative charge, red). The β-sheet region is shown on in the center of the molecule with residue arginine 165 shown (positive charge, blue). The region that was protected in the hydroxyl radical footprinting experiments is neutral (white) to positively charged (blue) which would complement the area on ISCU2 that was protected in the SDUF complex (residues 102-113) which had an overall negative charge.

FXN has also been shown to interact specifically with ISD11 *in vivo* by co-localization experiments and *in vitro* by pull-down studies using FXN as the anchor protein.[72] When the I154F mutation was incorporated on FXN, the ability of FXN to bind ISD11 was demolished, where the W155R FXN mutation only decreased the interactions of FXN to ISD11.[72] This tryptophan residue that is implicated in binding to the SDU complex by biochemical assays[75, 93] is shown as being near a positively charged patch of the electrostatic map (Figure 2-17).

The peptides that were not identified on FXN corresponded to the acidic patch, which has previously been hypothesized to interact with the cysteine desulfurase in *E coli*.[64] Although it cannot be ruled out based on the data presented here alone that there

is no interaction between the acidic patch on FXN and the SDU complex, the data does indicate that there is an interaction between the β-sheet region of FXN to NFS1.

Lastly, the regions of NFS1 that were unmodified in the hydroxyl radical footprinting experiments were mapped onto the model of human NFS1 to better understand if these peptides were involved in the dimer interface or determine potential binding sites for ISD11. NFS1 was not exposed to hydroxyl radicals in the absence of ISD11 because NFS1 is inherently unstable in solution without its binding partner.[61, 132] The peptides on NFS1 that were identified after trypsin digestion are shown in Figure 2-3 and 5 of the 7 peptides did not show modification in the SD, SDU, or SDUF complex (Figure 2-6, 2-9, Tables 2-2, 2-4). These peptides were mapped onto the human model of the NFS1 dimer and this revealed that most of the region that was protected in the SD complex was in the dimer interface (Figure 2-18, cyan) although an additional possibility is that these regions were involved in interactions with ISD11 consistent with that region being inexcessible to hydroxyl radicals in buffer solution. These peptides contain residues that have a high susceptibility to become modified, specifically leucine (L), tyrosine (Y), proline (P), histdine (H), phenylalanine (F), and methionine (M) indicating protection rather than slower reaction conditions.[133] Further, some of these regions appear to be highly negatively charged (red) region (Figure 2-18B), which is in good support of a potential surface of interaction for ISD11 due to the overall positive charge of ISD11 (pI ~10).

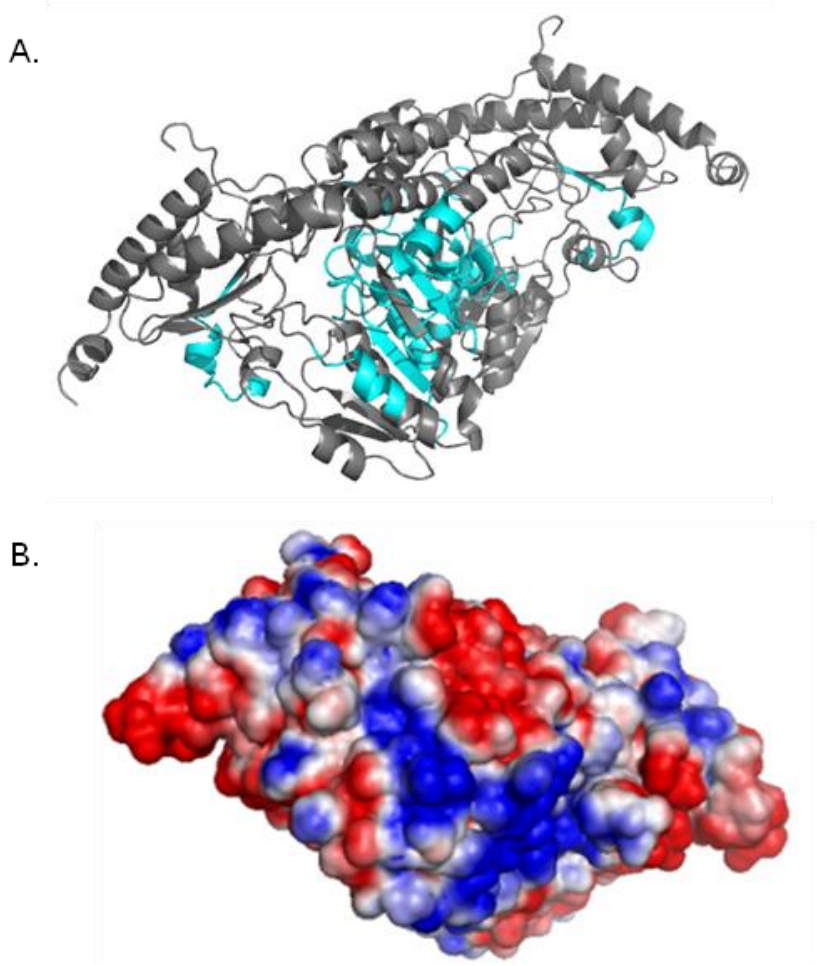

Figure 2-18. The regions protected on NFS1 during hydroxyl radical footprinting. A.) The peptides, which were not modified in the footprinting experiments, are shown in cyan on the NFS1 dimer (gray). B.) Electrostatic map of the NFS1 dimer is shown in the same orientation as the ribbon diagram in A.

The results presented herein show that hydroxyl radical footprinting monitored by mass spectrometry was successful in identifying regions of interaction between NFS1, ISCU2 and FXN in the SDU and SDUF complexes. The region of protection on NFS1, namely the C-terminus, is consistent with interactions observed in the bacterial crystal structure of the IscS-IscU complex as well as the protection of the N-terminus of ISCU2 indicating a conservation of interaction through evolution from bacteria to humans. These experiments also identified a region on ISCU2 that has been implicated as being important for interactions with the cysteine desulfurase (N-terminus), corroborated NMR results that indicate that ISCU2 becomes more unstructured upon binding NFS1, and the chaperone proteins as being important for interactions with human FXN as well. Although a specific interaction of FXN to the SDU complex was not identified, the hydroxyl radical footprinting results did correctly identify the β-sheet region as being important for interactions as previously seen by kinetic bioassays. The binding interactions of FXN to the SDU complex will be further analyzed by fluorescence anisotropy and the interactions of the β-sheet residue W155 will specifically be tested (Chapter III).

The results also indicate that a further structural arrangement of ISCU2 or the SDUF complex after cluster formation, a dissociation of the cluster bound ISCU2 from the SDUF complex, or a dissociation of FXN after cluster formation to allow the chaperone proteins access to the LPPVK motif for cluster transfer would be required if the interaction is conserved between bacteria and humans. The region of ISCU2 that is involved in these interactions (residues 102-113 by hydroxyl radical footprinting) will be

further analyzed by incorporating point mutations (K101, L107) to better understand the importance of this region for FXN binding and complex activation (Chapters IV and V). The importance of the N-terminus interactions of ISCU2 to NFS1 will be tested by incorporating the clinical mutant G16E on ISCU2 or the residues around the active site (D37) will be observed by monitoring the changes in binding and complex activation (Chapter V).

CHAPTER III

DETERMINING THE BINDING CONSTANT OF NATIVE AND MUTANT FRATAXIN TO THE SDU COMPLEX BY USING FLUORESCENCE ANISOTROPY

INTRODUCTION

Iron-sulfur clusters are assembled by a multi-protein complex which has been conserved in all branches of organisms.[9, 13, 16, 134] In eukaryotes, specifically humans, it has been discovered that four, conserved components are required for the assembly of Fe-S clusters.[33, 64] The four required proteins for cluster assembly are a cysteine desulfurase (NFS1) along with its co-protein ISD11 that is responsible for the conversion of cysteine to alanine through a persulfide bound cysteine on NFS1.[84] This persulfide can then be transferred to an active site cysteine on the scaffold protein named ISCU2 in humans.[37] Frataxin (FXN) is the fourth required component and acts as an allosteric activator in the human system to switch the complex from an "off" state to an "on" state.[33] The interactions of the four components of this complex are still being elucidated with the best model for protein-protein interactions coming from the bacterial system.[31, 32]

Currently, the interactions of the subunits from both bacterial and human systems have been studied multiple biophysical techniques such as protein crystallography where the crystal structure of the bacterial IscS-IscU shows a C-terminal interaction of the cysteine desulfurase to the N-terminus of the scaffold,[31, 32] and SAXS, where the interactions of the bacterial IscS-IscU complex formed an elongated S-shaped molecular

envelope.[34, 64] These interactions appear to be conserved in the human system where the C-terminal peptide on NFS1 (residues 402-419) and the N-terminal peptide on ISCU2 (residues 5-13) were protected from hydroxyl radicals upon SDU complex formation (Chapter II). Furthermore, the hydroxyl radical footprinting experiments uncovered a potential interaction between FXN and ISCU2 which was previously unknown (Chapter II) although information about protein binding kinetics were unable to be determined from these experiments.

In the bacterial system, which has been studied in more detail than the human system, some of the binding phenomena have been elucidated. Previously, the binding of IscU to IscS in *E. coli* was determined by surface plasmon resonance (SPR) and isothermal titration calorimetry (ITC) and determined the K_d to be 2.0 μM and 2.2 μM, respectively, approximating a 1:1 ratio.[135] In good agreement with the values presented by Urbina *et al.*, Prischi *et al.* calculated the K_d of IscS:IscU to be 1.3 ± 0.2 μM, again fitting the ITC data to a 1:1 binding model.[34] Additionally, using a 1:1 binding model for the interaction between IscS:CyaY the K_d was calculated to be 18.5 ± 2.4μM.[34] Interestingly, a direct interaction between IscU and CyaY was not observed.

In addition to the ITC data, Prischi *et al.* wanted to determine if the binding of one component of the Fe-S cluster assembly could affect the binding of the other components.[34] To answer these questions, the complex interactions were measured by biolayer interferometry (BLI) which is sensitive molecular interactions to give on and off interaction rates.[34] When CyaY was immobilized to the surface, the binding constant for IscS:CyaY was determined to be 23 ± 3 μM but when IscU was added to the

reaction, the interaction strength increased by ~650X and the K_d decreased to 0.035 ± 0.006 μM.[34] In a similar experiment, IscS was immobilized and the K_d for IscS:IscU was determined to be 1.5 ± 0.3 μM but when CyaY was added to the reaction the K_d decreased almost four fold to 0.400 ± 0.03 μM indicating a much tighter interaction.[34]

Previously, binding constants have been determined for pair-wise combinations of the four components of the Fe-S cluster assembly complex.[136-138] Specifically, the binding constant for NFS1 to ISD11 in humans using surface plasmon resonance with ISD11 immobilized was determined to be 100 nM when fit to a 1:1 binding model.[136] The interaction of FXN to ISCU2 has been determined as a result in the change in heat by ITC in which Yoon *et al.* utilized the D37A ISCU2 variant (human numbering), which is known to bind a Fe-S cluster tighter as the titrant into full length or truncated, mature, holo human frataxin to give a K_d of 5.4 μM and 0.15μM, respectively.[37, 137, 138] The binding constant for wild-type ISCU2 using tryptophan fluorescence quenching titrated with holo frataxin gave a K_d of 0.67 μM or 0.45 μM for D37A ISCU2 with holo frataxin.[137]

The first instance of determining the binding constant of frataxin to the human SDU complex was determined by Bridwell-Rabb *et al.* using the kinetic rate constants. In these experiments, the K_d was calculated based on the ability of varying concentrations of FXN to stimulate the cysteine desulfurase in the SDUF complex.[66, 75] The K_d determined for native FXN to the SDU complex was determined to be 0.07 ± 0.04 μM.[67] The binding constant of many of the FRDA mutants were also determined using the kinetic rate constant, approach, which in all cases, the mutation to FXN caused a

decrease in the ability of FXN to bind the SDU complex. Many of these mutations are found on the β-sheet region of FXN (N146, Q153, W155, R165) and their decreased binding affinity upon mutation further supports the interactions determined by the hydroxyl radical footprinting results (Chapter II). This binding constant of native FXN to SDU is similar to the binding constant determined for IscS:IscU:CyaY from *E. coli*.[34] The kinetic binding assays were unable to determine the conditions in which the proteins formed the tightest complex due to the nature of the experiments. Therefore, it was the goal of this work to better understand the reaction conditions required for the interactions of the SDUF proteins using fluorescently labeled frataxin and observing the changes in fluorescence anisotropy indicating protein complex formation.

Fluorescence anisotropy, as a technique, has been used to calculate binding constants between protein-DNA and protein-protein complex interactions.[139-141] Briefly, fluorescence anisotropy is a measure the emission of a fluorophore that has been excited by horizontally and vertically polarized light. The ability of the fluorescently labeled subunit to freely "tumble" in solution is measured as the anisotropy.[139] The change in anisotropy is related to the change in the ability of the molecule to emit polarized light, which changes when the labeled molecule interacts with unlabeled molecules to form larger complexes. The formation of a larger complex changes the ability of the fluorescently labeled protein to tumble in solution, thereby creating a difference in anisotropy values. These changes in anisotropy values as a function of complex formation can be fit to determine the binding constant of the labeled protein. In the experiments described below, the reaction conditions were modified for the SDUF

complex and the binding constants calculated from the anisotropy experiments were compared to both the previously published values calculated from kinetic rate constants and the rate constants determined for homologous systems in bacteria.

EXPERIMENTAL PROCEDURES

Preparation of Frataxin. Site-directed mutagenesis (Stratagene) of the codon-optimized frataxin gene (Δ1-55) in a pET11a vector was used to introduce a S202C mutation or the double mutation W155R S202C and the mutation was confirmed by DNA sequencing (Gene Technologies Laboratory, Texas A&M University). Each vector was transformed into BL21 (DE3) cells and was grown at 37 ^{o}C until an OD_{600} of 0.6. Protein expression was induced with the addition of 0.5 mM IPTG and expression progressed at 16 ^{o}C for 16 hours with shaking. The recombinantly expressed protein was purified as previously described for wild-type.[33] Native NFS1-ISD11 and ISCU2 were expressed recombinantly and purified as previously described.[33, 131]

Incorporation of Fluorophore on FXN. Purified S202C FXN or W155R S202C FXN was brought into an anaerobic glovebox (Mbraun, <2ppm O_2) and allowed to exchange with nitrogen overnight. Texas Red® C_2maleimide (Invitrogen) was resuspended in DMSO to a final concentration of 20 mM. The fluorophore was brought into the glovebox and excess fluorophore was added to the FXN in 50 mM HEPES pH 7.5, 150 mM NaCl. The labeling was allowed to proceed for approximately 6 hours in the dark at ~16 ^{o}C prior to dialysis aerobically against 2L of 50 mM Tris pH 7.5, 250 mM NaCl to remove excess fluorophore. Protein and fluorophore concentrations were calculated

using UV-absorbance at Abs_{280nm} and Abs_{590nm}(native FXN ε_{280}= 26,030 $M^{-1}cm^{-1}$, W155R FXN ε_{280}= 20,430 $M^{-1}cm^{-1}$and Texas Red ε_{590}=85,000 $M^{-1}cm^{-1}$). The labeling efficiency was estimated at 80% using the ratio of protein to fluorophore concentration.

Measurement of Cysteine Desulfurase and Fe-S Cluster Activity. The Texas Red labeled FXN (FXN_{TX}) was used to stimulate the cysteine desulfurase activity of the SDU complex to generate sulfide which is reacted with 20 mM *N, N'*-diphenyl-*p*-phenylenediamine (DPD) and 30 mM $FeCl_3$ as previously described.[33, 66, 75] Briefly, 0.5 µM SD, 2 mM DTT, 1.5 µM ISCU2, 5 µM $Fe(NH_4)_2(SO_4)_2$ and 1.5 µM FXN or FXN_{TX} in 50 mM Tris pH 8.0 and 250 mM NaCl was incubated for 30 minutes in an anaerobic glovebox. The reaction was initiated with the addition of 100 µM cysteine and incubated for 10 minutes at 37 ^oC before quenching the reaction with DPD and $FeCl_3$. The amount methylene blue generated was determined by measuring at absorbance of the reaction at 670nm and the amount of sulfide was quantitated using a standard curve generated using Na_2S.

The ability of FXN_{TX} to stimulate Fe-S assembly on the SDU complex was assayed and compared to wild-type as previously described using an Infintite M200 Pro microplate reader (Tecan) in an anaerobic glovebox.[33, 66, 75, 78] Briefly, 8µM SD, 24µM ISCU2, 24 µM FXN_{TX}, 3 mM DTT, and 200 µM $Fe(NH_4)_2(SO_4)_2$ was incubated for 30 minutes in the glovebox before initiating the reaction by the addition of 100 µM cysteine and shaking for 10 seconds. The absorbance was monitored at 456 nm every 30 seconds at 18 ^oC and the first 2000 seconds were used to fit the data in KaleidaGraph as

previously described.[33, 66, 75] The reported error is the error in the fit as opposed to error associated with technical replicate analysis.

Fluorescence Anisotropy Measurements. The labeled FXN, ISCU2, and SD were brought into the anaerobic glovebox ~12 hours prior to being used to allow them to exchange with nitrogen. To initiate the experiment, 10 nM FXN_{TX}, 10 μM ISCU2, 2 mM DTT, and additional reagents such as Fe^{2+}or cysteine in 50 mM Tris pH 7.5, 250 mM NaCl were added to an anaerobic cuvette and was sealed in the glovebox prior to titrations outside of the glovebox. In a separate vial, SD with 2 mM DTT was diluted in the same buffer as above and was sealed with a rubber septum in the anaerobic glovebox prior to titration. SD was titrated to FXN_{TX} with ISCU2 using a gas tight syringe to prevent oxygen contamination. Titrations with DTT alone, Fe^{2+}, and cysteine for native FXN_{TX} to the SDU complex were performed by Mr. Andrew Winn. Fluorescence anisotropy experiments were performed on a Fluoromax4 instrument (Horiba Jovin-Yvon) in a 1-ml anaerobic fluorescence cuvette. Anisotropy measurements were collected at an emission wavelength of 610 nm after excitation at 580 nm. The signal was integrated for 1 s with slits set at 5 nm each while the temperature of the cuvette was kept constant at 22 ^{o}C. Fluorescence anisotropy is based on the ratio between the detected sensitivities of the horizontally and vertically polarized light and can be accounted for by calculating the *G* factor.[139] The *G* factor can be calculated by the Equation 3-1:

$$G = \frac{I_{HV}}{I_{HH}} \tag{3-1}$$

where I_{HV} and I_{HH} are the signals from fluorophore when excited with horizontally polarized light, *H*, and emission observed with either vertically, *V*, or horizontally, *H*, aligned polarizers. The observed signals must be corrected by the *G* factor for the calculated anisotropy to be accurate.[139]

As the labeled protein interacts with complex components, the fluorophore rotation becomes more restricted and is reflected by the change in anisotropy, which is measured. The anisotropy, *r*, is calculated by Equation 3-2:

$$r = \frac{I_{VV} - G I_{VH}}{I_{VV} + 2G I_{VH}} \tag{3-2}$$

where I_{VV} and I_{VH} are the signals observed when excited with vertically polarized light and emission is observed with the polarizers in the vertical or horizontal position, respectively. [139] The anisotropy of the labeled protein not interacting with its protein partners was observed and the anisotropy is monitored as complex components were titrated until there was no longer a change in signal. The binding constant was then calculated by fitting the curve to the binding equation shown in Equation 3-3 in the KaleidaGraph software.

$$y = A_0 + (A - A_0)\left(\frac{[SD]}{[SD] + K_d}\right) \tag{3-3}$$

where A_0 and A are the anisotropy of the unbound protein and the anisotropy at a given titrant concentration, respectively, and the K_d is the calculated binding constant. In the case of a weakly bound complex, Equation 3-3 was fit making the assumption that the final complex anisotropy would be the same as wild-type SDUF complex which was tightly bound since the mutant W155R FXN_{TX} did not reach saturation anisotropy. The error associated with the anisotropy values for wild-type and W155R FXN binding to the SDU complex reflects the variability in the fit as opposed to error in the data for technical replicate analysis.

RESULTS

Fluorescence anisotropy was used to calculate the binding constant of FXN to the SDU complex under different experimental conditions by incorporating a cysteine mutation (S202C) into native FXN, allowing for the conjugation of a maleimide-derivative of the Texas Red® fluorophore. This fluorophore was chosen because its excitation (590 nm) and emission (610 nm) wavelengths do not overlap with the spectral properties of the PLP cofactor, and the lifetime of the fluorophore (4.2 ns) is appropriate for anisotropy experiments. Prior to the initiating binding measurements, the activity of the SDUF complex was measured to determine the effect of the placement of the fluorophore on the ability of FXN_{TX} to stimulate the cysteine desulfurase and Fe-S cluster assembly activities. When FXN_{TX} was substituted for wild-type FXN in the cysteine desulfurase reaction, the activity of the SDU complex was not compromised (Figure 3-1A) indicating the location fluorophore was not inhibiting the activity of the

complex. The relatively low cysteine desulfurase activity seen for the reaction with both the native and labeled FXN are due to batch variations in the SD protein. Additionally, the ability of FXN_{TX} to stimulate the Fe-S cluster assembly was also measured using a plate reader in an anaerobic glovebox (Figure 3-1B). The rate of Fe-S cluster assembly for SDUF complex was 0.18 ± 0.01 min^{-1} whereas the rate for the $SDUF_{TX}$ complex was 0.31 ± 0.02 min^{-1}.

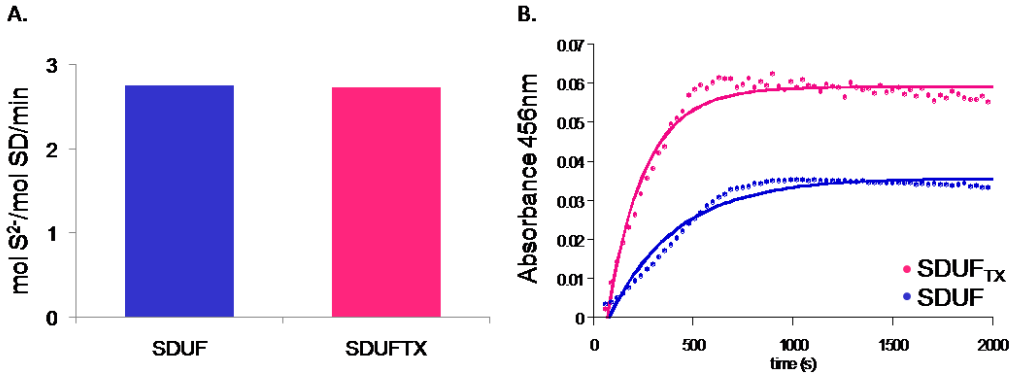

Figure 3-1. The activation of the SDUF complex with fluorescently labeled FXN was determined and compared to the SDUF complex with native FXN. A. The activity of the cysteine desulfurase was monitored for wild-type SDUF (blue) and $SDUF_{TX}$ (magenta). B. Rates of Fe-S assembly were determined for SDUF (blue) and $SDUF_{TX}$ (magenta).

Measuring the Binding Constant of FXN to SDU Complex. The binding constant of FXN to SDU was determined under the varying conditions using the fluorescently labeled material. The observed anisotropy was plotted as a function of SD titrated (Figure 3-2 A-D) and K_d values calculated using Equation 3-3 are shown in Table 3-1. All of the reactions contained 2 mM DTT in the fluorescence cuvette and also the titrant vial containing dilute SD to prevent protein precipitation and scattering of the fluorescence signal. The binding of FXN_{TX} to SDU with DTT in the absence of cysteine or $Fe^{2+}$was determined to be 0.55 ± 0.09 μM (Figure 5-2A, red). Upon the addition of either cysteine or Fe^{2+} along with DTT the binding was increased another 3 to 7 fold, respectively (Figures 5-2B, green and 5-2C, cyan). Lastly, with the addition of both cysteine and $Fe^{2+}$to the fluorescence cuvette prior to the SD titration, the binding increased approximately 11 fold compared to the binding constant with determined with just DTT (0.05 ± 0.01 μM, Figure 3-2D, magenta).

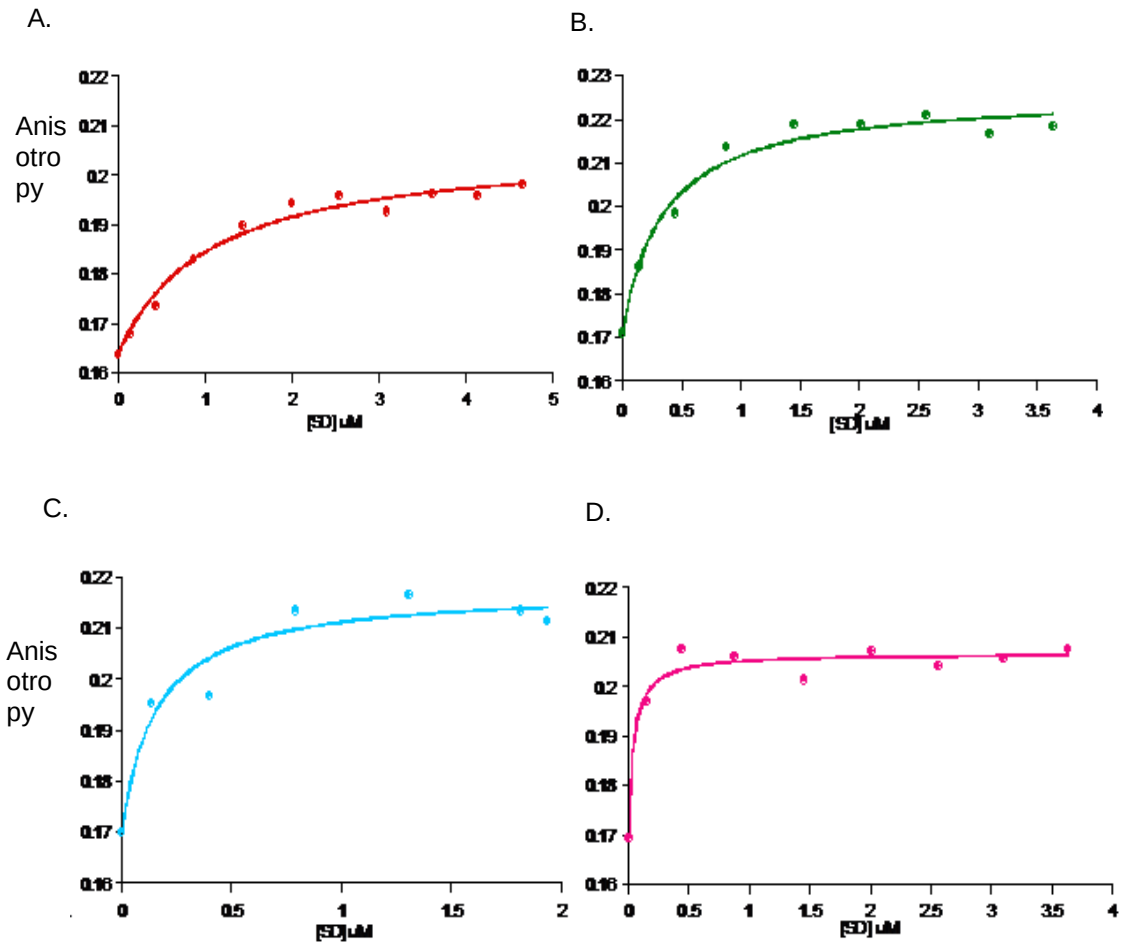

Figure 3-2. The binding graphs of FXN_{TX} and ISCU2 titrated with SD under varying conditions are shown with: A). 2 mM DTT (red), B).DTT and cysteine (green), C.)DTT and Fe^{2+} (cyan), and D.)DTT, cysteine, and Fe^{2+}(magenta).

Table 3-1. The calculated binding constants of native and W155R FXN_{TX} to the SDU complex determined by fluorescence anisotropy and fit to equation 3-3. **Previously determined binding constants by kinetic bioassays.[67]

Complex	Native FXNTX K_d (μM)	W155R FXNTX K_d (μM)
SD, ISCU2, FXN_{TX}, 2 mM DTT	0.55 ± 0.09	5.4 ± 0.4
SD, ISCU2, FXN_{TX}, 2 mM DTT, Fe^{2+}	0.08 ± 0.03	4.6 ± 0.5
SD, ISCU2, FXN_{TX}, 2 mM DTT, cysteine	0.20 ± 0.05	3.6 ± 0.3
SD, ISCU2, FXN_{TX}, 2 mM DTT, Fe^{2+}, cysteine	0.05 ± 0.01	5.6 ± 0.3
SDUF ($k_{cat}K_d$)**	0.07 ± 0.04	5.5 ± 13

Binding of Mutant W155R FXN to SDU. Previously, the FRDA clinical mutant W155R FXN located on the β-sheet region of FXN was shown to have compromised binding determined by kinetic rate constants.[66, 67, 75]To further test the accuracy of the fluorescence anisotropy method, W155R FXN was also labeled with the Texas Red® fluorophore and binding was determined in a similar manner to native FXN_{TX} (see Methods). The binding of the W155R FXN_{TX} mutant to SDU with DTT and either Fe^{2+}or cysteine, or both was measured and fit to Equation 3-3 (Figure 3-3, Table 3-1). The anisotropy data, even at 5-10 μM SD did not reach saturation, so the data was forced through the maximum anisotropy value determined for the complex with native FXN. The results indicate that the binding of W155R FXN_{TX} was slightly improved with the addition of Fe^{2+} or cysteine 1.2 to 1.5 fold, respectively but the addition of Fe^{2+} and cysteine did not improve the binding to the same degree as the native complex (Table 3-1).

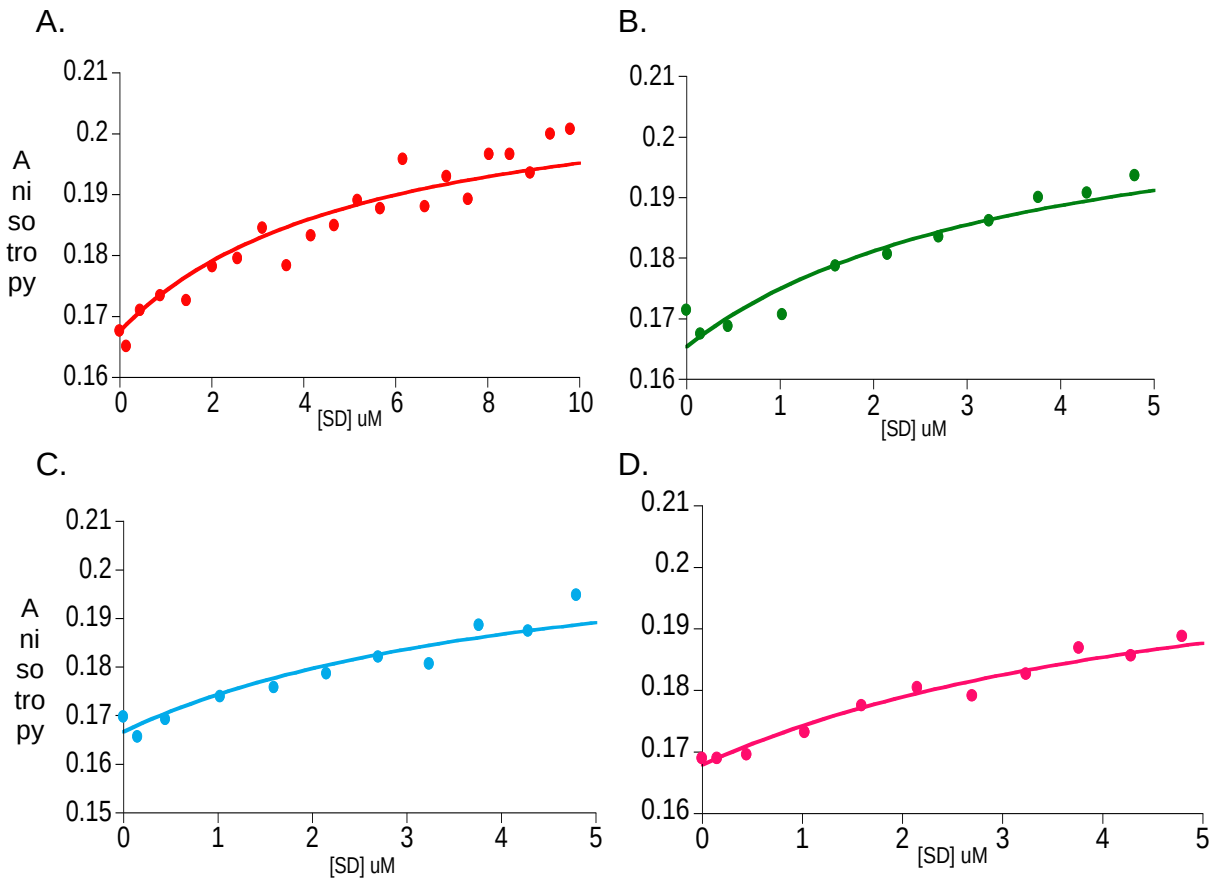

Figure 3-3. The binding of W155R FXN_{TX} to the SDU complex was measured under varying conditions containing: A.) 2 mM DTT (red), B.) 2 mM DTT and cysteine (green), C.) 2 mM DTT and Fe^{2+} (cyan), or D.)2 mM DTT, cysteine, and Fe^{2+} (magenta). The data was fit to equation 3-3.

DISCUSSION

The interaction of FXN to the SDU complex was identified by the hydroxyl radical footprinting experiments. The results of these experiments indicate that residues 102-113 on ISCU2 likely interact with the β-sheet region of FXN due to the observed decrease in oxidation upon SDUF complex formation (Chapter II). These experiments were performed in the absence of Fe^{2+} or cysteine and although these experiments were important to better understand the regions in which the proteins interact, they gave little information about the binding affinity of FXN to the SDU complex under different experimental conditions (Chapter II). Therefore, the goal of this work was to better understand the conditions in which the SDUF complex was the tightest bound using fluorescence anisotropy. A single-site mutation was incorporated on FXN at position S202 to incorporate a cysteine residue to covalently attach the Texas Red® fluorophore.

Initially, FXN_{TX} was titrated with either ISCU2 or SD to determine whether human FXN would form a complex with either component in the absence of the other and these results indicate that FXN_{TX} did not form a complex due to a lack in change of anisotropy (data not shown). These results are in good agreement with ITC data obtained from *E. coli* in which no interaction between IscU and CyaY, the frataxin homolog was observed,[34] but are in contrast to previously reported eukaryotic interactions, in which frataxin has been shown to coimmunoprecipitate with Isu2 in yeast,[74] interact with a mutant ISCU2 protein in humans by ITC titrations,[137, 138] and interact through chemical crosslinking.[142] In *E. coli*, an interaction between IscS and CyaY was observed by ITC with a binding constant of 18.5 ± 2.4 μM and BLI binding constant of 23 ± 3 μM.[34]

Taken together, these results strengthen the postulation that all four of components of the Fe-S assembly complex are required to form a stable complex.[33, 64] Furthermore, the inability of FXN to interact with SD further supports the hypothesis that there has been a change in the function of FXN from the simpler *E.coli* systems.[34, 78]The anisotropy data is in good agreement with the K_d determined by BLI in *E. coli* in which the binding strengthens approximately 660 times in the presence of IscS, IscU, and CyaY are bound (0.035 ± 0.006 μM) or was approximately an order of magnitude tighter by ITC than for the proteins in a pair-wise fashion.[34]

An additional strength of using fluorescence anisotropy to determine binding compared to using the bioassay kinetics is the ability to test different experimental conditions, such as the isolated use of cysteine or Fe^{2+}. Initial experiments determined that DTT was required both in the fluorescence cuvette and in the titrant to prevent protein precipitation and scattering of the fluorescence signal (data not shown). The strength of the interaction of SDUF complex was increased with the addition of cysteine < Fe^{2+}< cysteine and Fe^{2+} indicating that the tightest complex was formed when all of the components required to assemble Fe-S clusters were present (Figure 3-2D, magenta; Table 3-1). The calculated binding constant of the fluorescence anisotropy based on Equation 3-3 for the SDUF complex with Fe^{2+} and cysteine, 50 nM, was in good agreement with previously published data obtained using the k_{cat} values in which the calculated binding constant was70 nM.[67]

To further investigate the ability of fluorescence anisotropy to measure the binding of FXN to the SDU complex, a clinical FRDA mutant, W155R FXN was fluorescently

labeled. The binding constants obtained by the fluorescence anisotropy experiments for the W155R FXN were calculated using the maximum anisotropy for the wild-type FXN. This approach was taken because the anisotropy had not reached saturation. By estimating that the final anisotropy value would be the same as for the wild-type FXN binding to the SDU complex, the data could be fit to equation 3-3. The W155R FXN mutation in humans is known to be deficient in complex binding,[67, 75] activity,[66] and have decreased stability.[143-145] Furthermore, the equivalent mutation in yeast showed growth deficiencies[74] and the ability of FXN to pull down ISD11[72] or IscS and IscU was diminished.[64] Additionally, the peptide containing the residue W155 was significantly protected in the SDUF complex compared to FXN as seen by hydroxyl radical footprinting (Chapter II) indicating that this region becomes protected from solvent in the SDUF complex indicating a protein interface.

The experiments performed for wild-type FXN were repeated with W155R FXN_{TX} and the K_d values are shown in Table 3-1. The binding constant for W155R FXN_{TX} was approximately 110 times weaker than native FXN to the SDU complex with DTT, cysteine and Fe^{2+}. This result is similar to the K_d determined by kinetic activity in which the $SDUF_{W155R}$ complex bound approximately bound 78 times weaker than the SDUF complex.[67] It was interesting to note that the binding was not altered significantly upon the addition of cysteine, Fe^{2+} or both cysteine and Fe^{2+}as observed for the native complex. The $SDUF_{W155R}$ complex is also deficient in the ability to stimulate cysteine desulfurase and Fe-S activity,[66, 67] indicating that the SDUF complex must form prior to being able to generate sulfide and Fe-S clusters and that the binding and activity occur

sequentially as opposed to concurrently. Additionally, it was previously postulated the W155R may adopt a different conformation than native FXN in which interactions are not favorable to interact with the SDU complex[66] in support of the binding not being recovered by the addition of Fe^{2+} or cysteine as observed in the fluorescence anisotropy experiments. The decreased binding along with the inability of the complex interactions to be strengthened with the addition of cysteine or Fe^{2+} may be one explanation for the severe phenotype observed in patients with this point mutation.[73] The fluorescence anisotropy results also support the claims that FXN interacts with SDU through the β-sheet region as previously published[34, 64, 75, 144, 146] and is further supported by the hydroxyl radical footprinting experiments that show a significant protection of this region upon SDUF complex formation (Chapter II). The results from this chapter along with data from Chapter II will be used to design future experiments to test the SDUF complex formation.

Overall, the development of an approach that utilizes fluorescently labeled proteins to determine the binding of subunits to form the SDUF complex can be highly useful in further understanding the conditions necessary for the interactions of the individual components of this complex. This approach is highly flexible to different experimental conditions and the ability of FXN to interact with mutants of ISCU2, NFS1, or ISD11 in future studies. This approach is not dependent on the ability of the activity of the SDUF complex, which may be useful in determining binding constants mutant proteins that have diminished activity.

CHAPTER IV

INVESTIGATING THE IMPORTANCE OF THE FRATAXIN BINDING INTERACTIONS TO ISCU2 ON THE ACTIVITY OF THE FE-S ASSEMBLY COMPLEX

INTRODUCTION

Iron-sulfur (Fe-S) clusters are important biological cofactors involved in many cellular processes from DNA repair to electron transport.[147, 148] A complex of conserved proteins is responsible for sequestering and assembling Fe-S clusters *in vivo*. In humans, the complex is composed of a cysteine desulfurase and its co-protein, NFS1 and ISD11, which is responsible for the catalytic conversion of cysteine to alanine through a persulfide bound cysteine on NFS1,[149] a scaffold protein ISCU2, and frataxin (FXN) which acts as an allosteric activator.[33]

The human ISCU2 protein serves as a scaffold for the assembly of Fe-S clusters prior to their delivery to biological targets and both the structure and function have been remarkably conserved throughout evolution (Figure 4-1). The highly conserved LPPVK motif on ISCU2 (residues 97-101 using human numbering) has been implicated in being critical for interactions with the chaperone proteins, HscA/HscB in bacteria,[52, 53] Ssq1/Jac1 in yeast,[150, 151] and human mortalin (Hsp70),[152, 153] for cluster transfer to apo-proteins *in vivo*. The lysine in this motif, K101 ISCU2 also appears to be important for interactions with a conserved glutamate on the cysteine desulfurase (Figure 4-2A) which is also as observed in the co-crystal structure of the *E. coli* IscS-IscU complex[31] (Figure

4-2B), where the IscS subunit is shown in yellow, IscU is shown in blue, and the salt bridge between K103 IscU and E311 IscS (*E. coli* numbering) has been highlighted in magenta. Additionally, the importance of this interaction was observed when, in yeast, mutagenesis of the lysine on Isu to glutamate or alanine followed by pull-down studies decreased the ability to pull-down Nfs1 compared to wild-type Isu.[154] The three highly conserved cysteine residues (C35, C61, and C104 in human numbering) are universally agreed to be critical for Fe-S cluster biosynthesis (Figure 4-1, blue triangles). These cysteines have been proposed to be Fe-S ligands along with either H103,[155, 156] C96,[157] or conserved cysteines from a second ISCU2 molecule in a dimeric assembly.[158, 159]

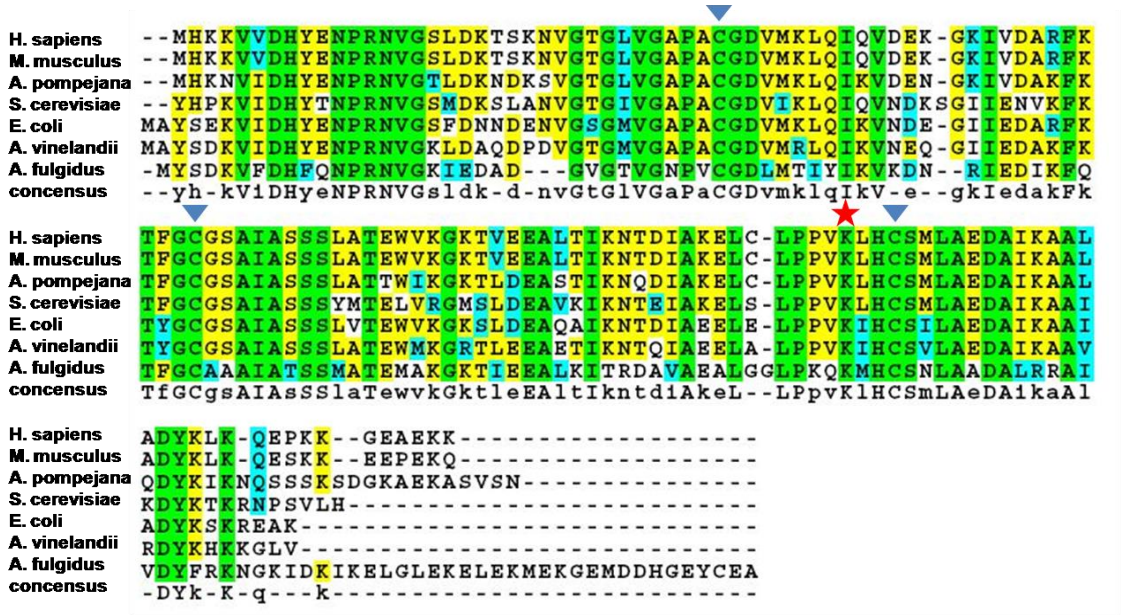

Figure 4-1. The sequence alignment of ISCU2 homologues is shown highlighting the conserved cysteines with blue triangles and the conserved lysine in the LPPVK motif with the red star.

A.

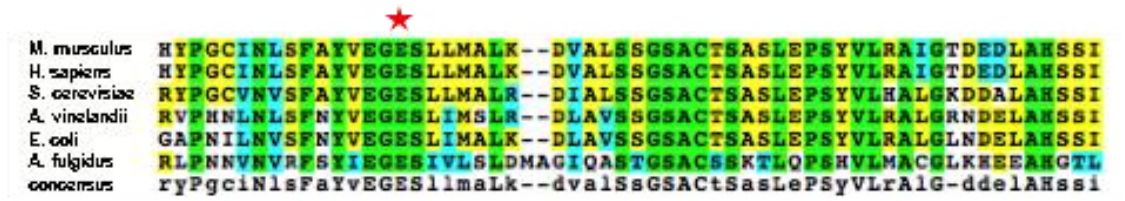

B.

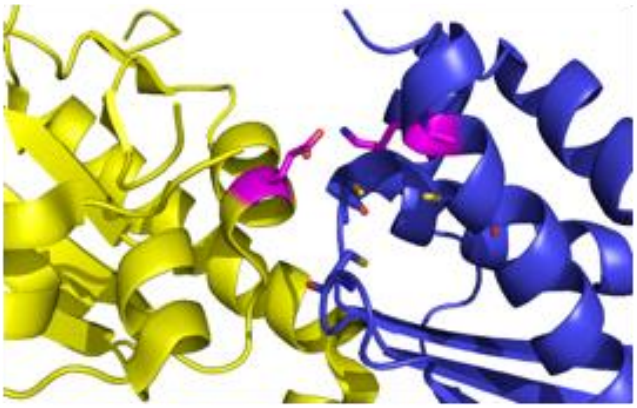

Figure 4-2. A.) A portion of the cysteine desulfurase sequence alignments is shown highlighting the conserved glutamate that interacts with lysine of the scaffold protein by the red star. B.) Crystal structure of IscS-IscU from *E. coli* (PDB 3LVL) with one IscS monomer shown in yellow and IscU shown in blue with the interaction between E311 on IscS and K103 on IscU shown in magenta. The active site cysteines are also shown as sticks with the sulfur atoms displayed in yellow on IscU.

We hypothesize that the loop on which this lysine residue, K101 is located undergoes a helix-to-coil transition upon complex formation to activate Fe-S cluster assembly similar to the conformation observed in the crystal structure of IscU from *Aquifex aeolicus*.[91] We suspect that this conformational change positions the active site cysteine residues on ISCU2 to accept the sulfide from the cysteine on the mobile loop on NFS1. Studies to determine the initial cysteine acceptor on ISCU2 have been performed by individually mutating the cysteine residues on ISCU2 and monitoring the transfer of

radiolabeled cysteine resulting in the observation that that C104 is the initial sulfur acceptor in the human Fe-S cluster assembly complex.[67] The effect of the helix-to-coil transition initiated by frataxin binding to the complex has not been previously determined although interactions between ISCU2 and FXN were observed in the hydroxyl radical footprinting experiments in this region of ISCU2 (Chapter II).

Frataxin is a conserved mitochondrial protein that interacts with the core components of the Fe-S cluster biosynthetic machinery and forms a multi-subunit complex, SDUF.[64, 160, 161] Previous data indicated that FXN binding to the SDU complex dramatically changed the catalytic efficiency (k_{cat} /K_M) of the cysteine desulfurase from 25 to 7900 $M^{-1}sec^{-1}$ and resulted in a 25-fold increase in the rate of Fe-S cluster biosynthesis.[33, 160] Subsequent studies investigating the impact of substituting Friedreich's ataxia (FRDA) clinical variants for the native FXN on the rates of the cysteine desulfurase and Fe-S cluster assembly reactions revealed that these variants were compromised in their binding affinity for the SDU complex and also in their abilities to facilitate sulfur transfer from NFS1 to ISCU2.[162, 163] In the native FXN crystal structure, W155 is stacked above the positive charge contributed by residue R165.[162] Consistent with this hypothesis, the crystal structure of the FRDA clinical R165C FXN variant revealed W155 in the proposed rotated conformation and while the mutant bound the SDU complex ~50 times weaker than native FXN, the k_{cat}/K_M for the cysteine desulfurase was nearly equivalent to that of the wild-type SDUF complex.[162]

We previously hypothesized that an important component for FXN interactions with the SDU complex is the rotated W155 conformation.[162, 163] Additionally, the β-

sheet region on FXN was shown to be important for protein-protein interactions to the SDU complex (Chapter II) and the W155R mutation was unable to bind the SDU complex by fluorescence anisotropy (Chapter III). We identified ISCU2 residue K101 as a candidate for interactions with this rotated conformation of FXN due to its conservation, proximity to the active site and residue C104 that is implicated as the primary sulfur acceptor residue during catalysis.[67]

Therefore, it was the goal of this study to better understand the interactions between the ISCU2 and FXN in the SDUF complex by using site directed mutagenesis followed by kinetic bioassays. The peptide encompassing the LPPVK motif was not observed in the hydroxyl radical footprinting experiments although the peptide adjacent to K101 did become protected upon FXN binding indicating a potential binding site for FXN in the SDUF complex. The results herein showed that if K101 was mutated to alanine or histidine the binding was significantly decreased but the ability of these mutants to stimulate the cysteine desulfurase activity of the $SDU_{K101X}F$ complex to wild type levels was observed suggesting that once the binding deficiency of FXN to the SDU complex was overcome, the activity of the complex was not affected. In an attempt to better understand the interactions of two FRDA mutants to the SDU complex, the ability to stimulate the activity of the complex with mutations to both ISCU2 and FRDA mutants was observed. It was determined that the binding of FXN to the SDU_{K101X} complex could not be recovered by making a complimentary mutation on FXN by mutating N146 to lysine. The binding of N146K FXN was ~10 fold weaker than wild-type and activity was also significantly impaired. Further, the interactions of the W155R

FXN mutation were examined in the complex with the K101H ISCU2 mutantand the results showed that there was no stimulation of cysteine desulfurase activity upon the substitution of W155R FXN for WT in the SDU_{K101H} complex further showing the importance of the W155 residue on FXN binding to the SDU complex. The results presented in this chapter give further evidence of the importance of the interactions of ISCU2 and FXN and will serve to aid in the generation of a model to test with future experiments.

EXPERIMENTAL PROCEDURES

Protein Preparation and Purification. The QuikChange method (Stratagene) was used to introduce point mutants (K101A, K101H) into a pET11a vector containing the human ISCU2 gene or the point mutant (N146K, W155R) into a pET11a vector containing human FXN (Δ1-55). After DNA sequencing confirmed the mutation sites, K101A ISCU2, K101H ISCU2, N146K FXN, and W155R FXN were individually transformed into *E. coli* strain BL21 (DE3) cells and grown at 37°C until an OD_{600} of 0.6. Expression was induced with 0.5 mM IPTG and expressed for 16°C for 16 hours with shaking. NFS1-ISD11, ISCU2, FXN and variants were purified as previously described for wild-type.[33]

Cysteine Desulfurase Activity of ISCU2 Variants. A previously described assay to detect methylene blue formation was used to determine the rate of sulfide production of the SDU complex as a function of ISCU2 variant concentration.[33] For the titration reactions, assay mixtures contained 0.5 μM SD, 2 mM DTT, 50 mM Tris pH 8.0, and

250 mM NaCl. ISCU2 variants were titrated to SD to determine the number of equivalents that saturated the cysteine desulfurase activity. Titrations of native FXN were then performed using the maximum amount of variant ISCU2 to determine maximize the activity of the SDU_{K101A} and $SDU_{K101H,}$complexes.Briefly, the standard assay mixture composed of 0.5 μM SD, 2 mM DTT, 50 mM Tris pH 8.0, 250 mM NaCl, and 5 μM $Fe(NH_4)_2(SO_4)_2$, maximally stimulating amounts of ISCU2 or ISCU2 variants determined above, and was incubated for 30 minutes with various concentrations of FXN in an anaerobic glovebox prior to the addition of 100 μM cysteine to initiate the reaction. Similarly, the number of equivalents of mutant FXN required to maximally stimulate the SDU, SDU_{K101A} or SDU_{K101H} complexes with was determined by titrating N146K FXN or W155R FXN to each complex instead of native FXN.

Determination of Michaelis-Menten Kinetics. The Michaelis-Menten kinetic bioassays were performed as previously described.[33] Briefly, the standard assay mixture contained 0.5 μM SD, 2 mM DTT, 50 mM Tris pH 8.0, 250 mM NaCl, and 5 μM $Fe(NH_4)_2(SO_4)_2$ with maximally stimulating amounts of ISCU2 and FXN determined above and was incubated for 30 minutes in the anaerobic glovebox. The reaction was initiated by the addition of cysteine and incubated anaerobically at 37 ^oC for prior to being quenched by the addition of 100 μL of each 20 mM DPD and 30 mM $FeCl_3$. The formation of methylene blue was monitored by UV absorbance at 670 nm to determine the amount of sulfide produced by each complex. Reaction rates as a function of cysteine concentration (0.0125-1.0 mM) were fit to the Michaelis-Menten equation using KaleidaGraph (Synergy Software).

Binding Constant Determination of FXN Variants. The binding constant of native or mutant FXN to the SDU complexes with native ISCU2 or mutant ISCU2 was determined as previously described.[67, 75] Briefly, the k_{cat} was determined for the SDU or SDU_{K101X} complexes at various FXN or mutant FXN concentrations. The curve was fit to Equation 4-1 using KaleidaGraph software (Synergy Software) to solve for K_d.

$$[SDUF] = \frac{[SDU]_t+[FXN]_t+ K_d-\sqrt{([SDU]_t+[FXN]_t+K_d)^2-4[SDU]_t[FXN]_t}}{2} \quad (4\text{-}1)$$

In the above concentration, $[SDU]_t$ is the total SDU concentrationin the assay and $[FXN]_t$ is the total FXN concentration.[67]

RESULTS

Protein Complex Stoichiometries to Stimulate Maximum Activity. The cysteine desulfurase activity of the NFS1-ISD11 complex (SD) was measured as a function of added native ISCU2, K101A ISCU2, or K101H ISCU2variants. The cysteine desulfurase activity of SD was minimized with the addition of 3 equivalents of wild-type ISCU2 (Figure 4-3A), consistent with published results.[33] Similar to ISCU2, the cysteine desulfurase activity decreased with the addition of K101A with a minimization of activity at 100 equivalents (Figure 4-3B). Unlike native ISCU2, the cysteine desulfurase activity increased as a function of added K101H ISCU2 variants and maximized with the addition of approximately 100 equivalents of K101H (Figure 4-3C). These data show that the K101 ISCU2 variants bind much weaker than wild-type ISCU2by the requirement of additional equivalents implying that the salt bridge formed

between K101 on ISCU2 and the glutamate on NFS1 is important for complex formation.

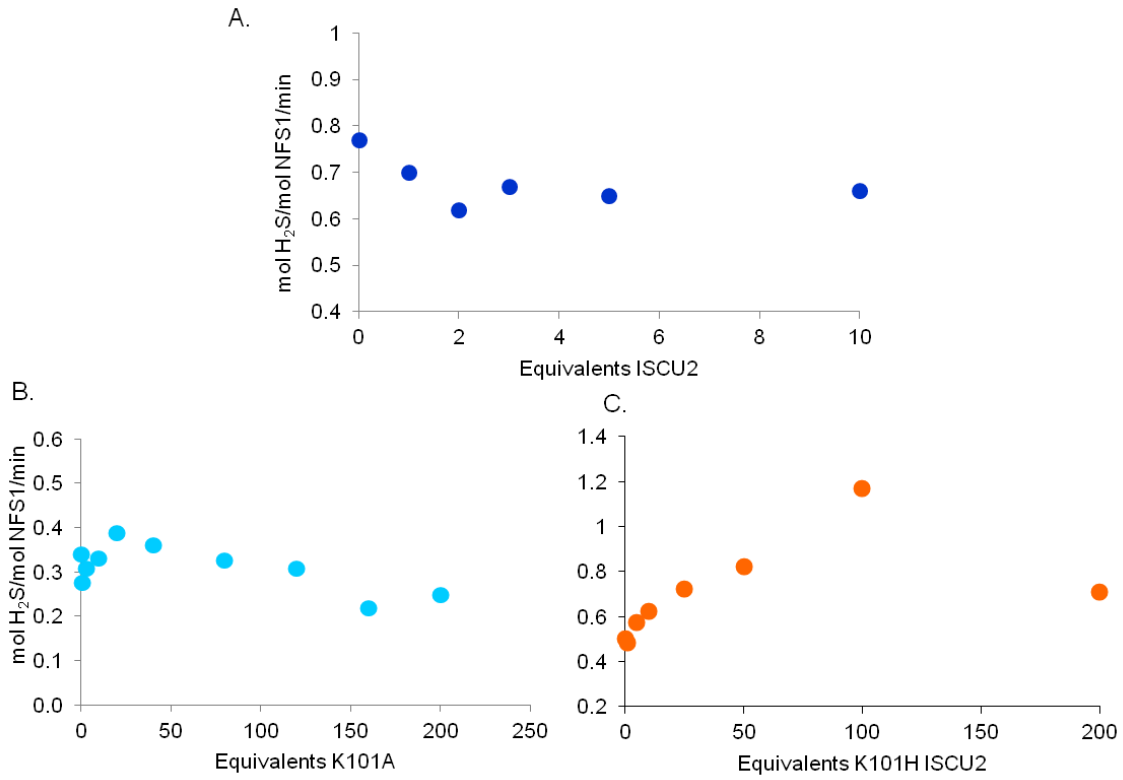

Figure 4-3. The cysteine desulfurase activity of SD was measure to determine the number of equivalents of native or variant ISCU2 required for further experiments. A.) Cysteine desulfurase activity of SD titrated with wild-type ISCU2. B.) Cysteine desulfurase activity of SD titrated with K101A ISCU2. C.) SD titrated with K101H ISCU2.

In a similar manner, FXN was titrated to the SDU_{K101A} or SDU_{K101H} complexes to determine the concentration of FXN that maximally stimulated each complex. The titrations revealed that the SDU_{K101A} and SDU_{K101H} complexes required 40 or 50 equivalents, respectively, to achieve maximum stimulation compared to three

equivalents for FXN to the native SDU complex (Figure 4-4, Table 4-1).Cysteine desulfurase activity levels similar to wild type (k_{cat}9.4 ±0.9 min^{-1}) were achieved when saturating amounts of FXN were added to SDU_{K101A} or SDU_{K101H} (Table 4-1).

Table 4-1. Kinetic parameters determined for variant ISCU2 with native and mutant FXN variants. *Previously reported kinetic parameters.[75] ** Previously reported kinetic parameters. [93]

		equivalents				
ISCU2	FXN	ISCU2	FXN	k_{cat} (min^{-1})	K_M (mM)	k_{cat}/K_M ($M^{-1}s^{-1}$)
WT	WT	3	3	9.4 ± 0.9	0.022 ± 0.01	7200 ± 3000
K101A	WT	75	40	10.4 ± 0.8	0.022 ± 0.008	7800 ± 2800
K101H	WT	100	50	7.4 ± 0.6	0.008 ± 0.002	15900 ± 4800
K101A	N146K	100	50	0.70 ± 0.02	0.007 ± 0.002	530 ± 300
K101H	N146K	100	50	3.09 ± 0.06	0.0057 ± 0.0008	9000 ± 1200
K101H	W155R	100	100	n.d.	n.d.	n.d.
WT	N146K*	3	50	4.0 ± 0.1	0.019 ± 0.004	3500 ± 700
WT	W155R**	3	40	1.8 ± 0.1	0.013 ± 0.003	2300 ± 500

In an effort to determine if the charge of the lysine was also required for FXN binding, we used FRDA variants that have a point mutation FXN at positions N146K or W155R to compliment the loss of lysine on ISCU2and also determine if either of these residues was involved in direct interactions with K101 on ISCU2. Titrations of N146K FXN to either K101A or K101H ISCU2 revealed that 50 equivalents of N146K were required to maximally stimulate SDU_{K101A} or SDU_{K101H} (Figures 4-5A and B). Titration of W155R FXN to the SDU_{K101H} complex was unable to stimulate the activity above SD alone even at 100 equivalents (Figure 4-5C). The ability to stimulate the cysteine desulfurase to wild-type levels was impaired as well, where the $SDU_{K101A}F_{N146K}$ complex had a k_{cat} approximately 13 times lower than wild-type and the $SDU_{K101H}F_{N146K}$ had a k_{cat} ~2.5 times lower than SDUF (Table 4-1). The primary implication is that the mutation of K101A or K101H on ISCU2 affects the ability to form a complex with SD and that the K101H ISCU2 stimulates activity more similarly to wild-type ISCU2 than K101A ISCU2.

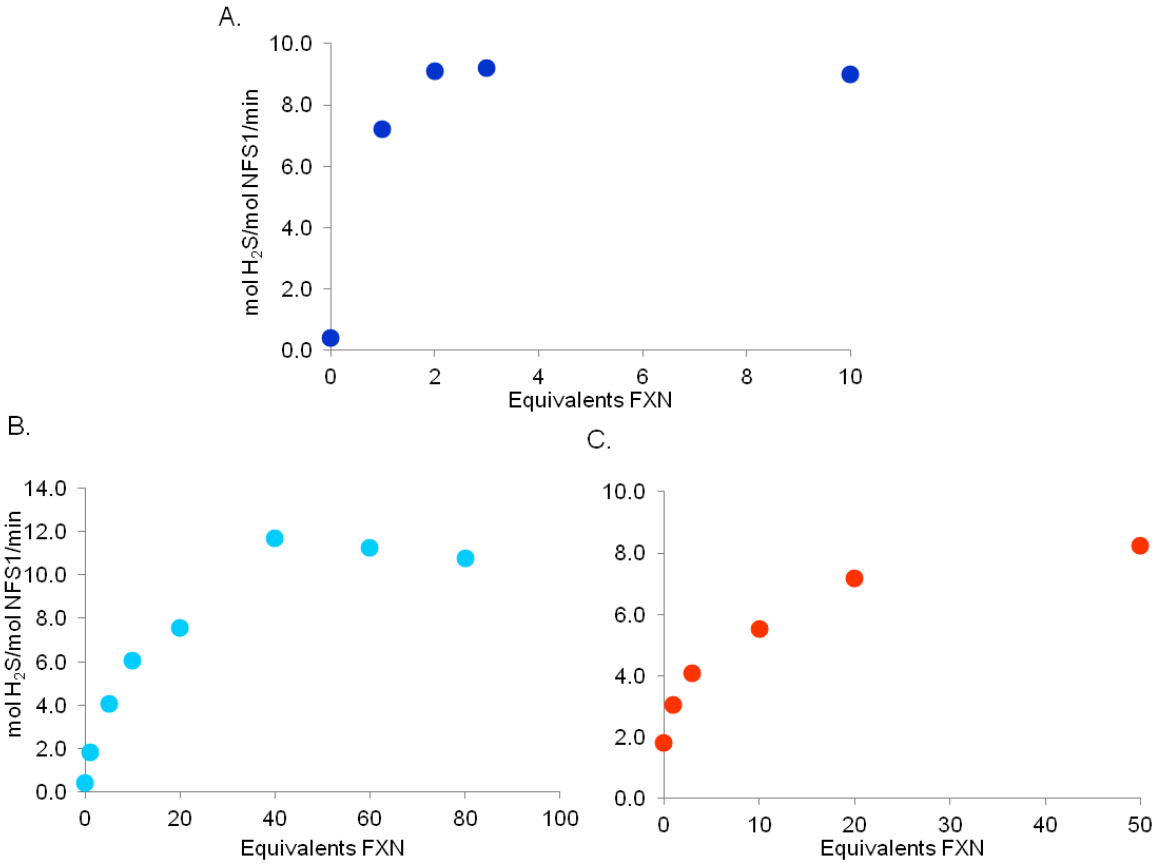

Figure 4-4. The number of equivalents of wild-type FXN required to maximally stimulate the cysteine desulfurase activity of the SDU_{K101X} complexes was determined and compared to the wild-type SDU complex. A.) Wild-type SDU titrated with FXN. B.) SDU_{K101A} titrated with FXN. C.) SDU_{K101H} titrated with FXN.

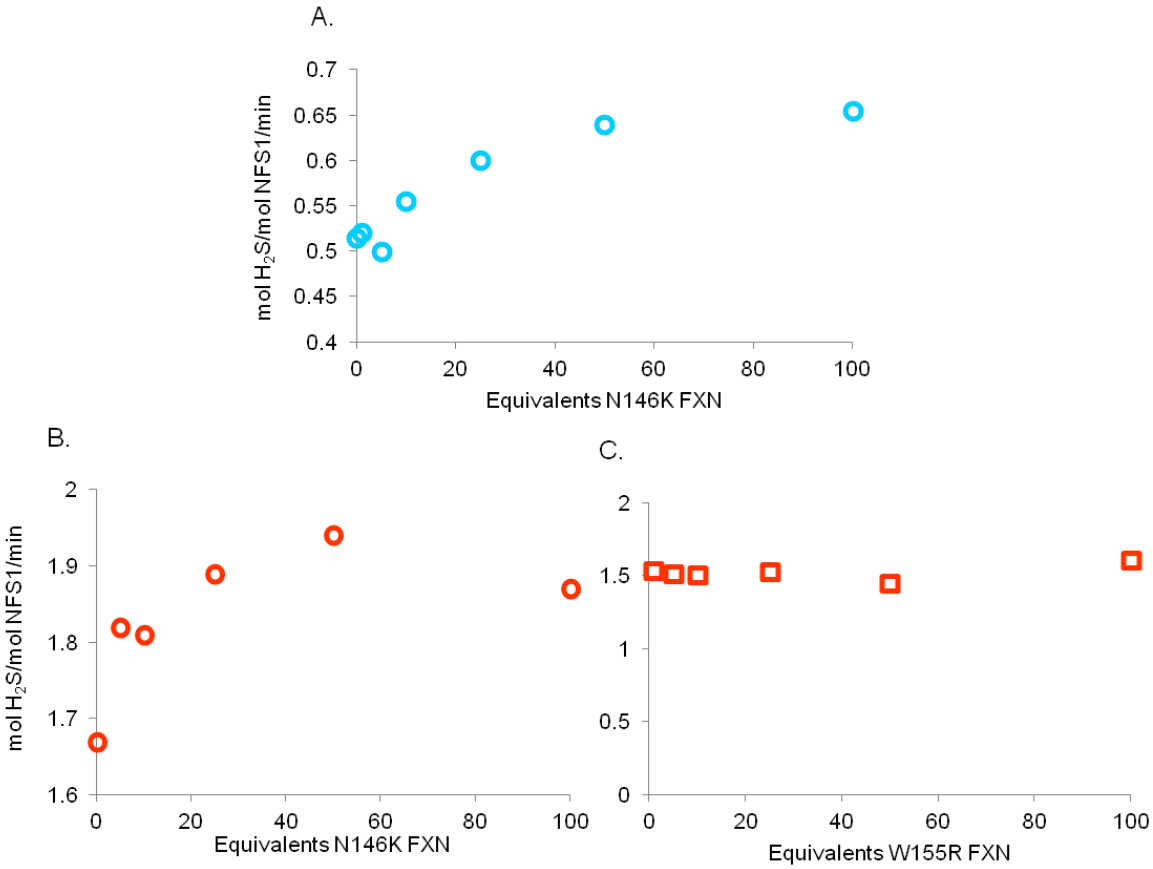

Figure 4-5. The number of equivalents of mutant FXN required to maximally stimulate the cysteine desulfurase activity of the SDU_{K101A} and SDU_{K101H} complexes was determined. A.) SDU_{K101A} titrated with N146K FXN. B.) SDU_{K101H} titrated with N146K FXN. C.) SDU_{K101H} titrated with W155R FXN.

Kinetic Parameters for Assembly Complexes Substituted with K101X-ISCU2 Variants and/or N146K FXN. Michaelis-Menten kinetics were determined for the native SDU, SDUF, $SDU_{K101A}F$, $SDU_{K101H}F$, $SDU_{K101A}F_{N146K}$, $SDU_{K101H}F_{N146K}$ complexes under the conditions described above. The k_{cat}/K_M of K101A or K101H ISCU2 with native FXN did not decrease upon these substitutions but rather was the same as SDUF or increased by ~2 fold respectively (Table 4-1). The substitution of wild-type FXN for

N146K FXN in the SDU_{K101A} complex decreased the k_{cat}/K_M by ~13 fold whereas using N146K FXN with SDU_{K101H} complex recovered the k_{cat}/K_M to wild-type SDUF levels (Table 4-1). The kinetic parameters were not determined for the $SDU_{K101A}F_{W155R}$ or $SDU_{K101H}F_{W155R}$ complexes because no change in cysteine desulfurase activity was determined during the titration experiments.

Binding Constant Determination for FXN Variants Binding to Native SDU and ISCU2 Variant Complexes. The binding constants were calculated by measuring the complex kinetics (k_{cat}) at varying concentrations of FXN and the data were fit to equation 4-1. These results show that the binding constant for FXN to SDU_{K101A} is decreased ~49 fold to 3.4 ± 0.7μMcompared to wild type and FXN binding to SDU_{K101H} is decreased ~9 fold to 0.6 ± 0.2 μM (Figure 4-6, Table 4-2). We further speculated that K101 on ISCU2 interacts with residues on FXN upon binding the SDU complex. We show that the decreased W155R FXN binding cannot be recovered by SDU_{K101H} (Figure 4-5C). The N146K FXN variant did not show a significant recovery in binding to the SDU_{K101A} complex, which had a binding constant of 2.3 ± 1.9 μM (Figure 4-6C, Table 4-2). The binding constant of N146K FXN to the SDU_{K101H} complex was decreased an additional 15 fold to 9.2 ± 4.8 μM (Figure 4-6D, Table 4-2).

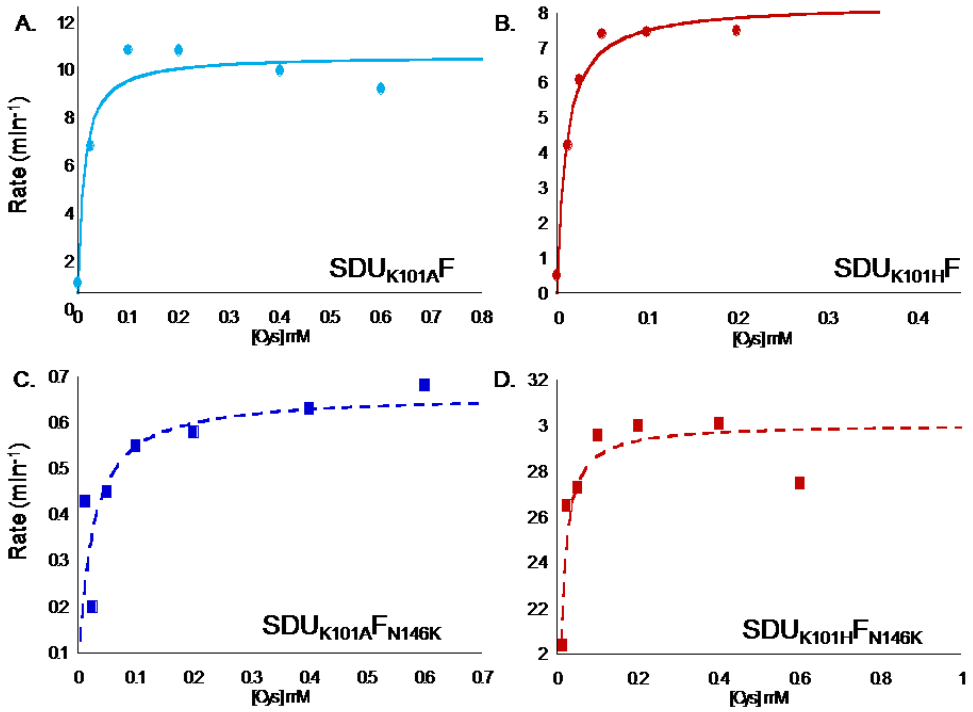

Figure 4-6. The binding constants for FXN and FXN variants to mutant ISCU2 in the complex were measured kinetically by the ability to stimulate the cysteine desulfurase activity at varying concentrations of native or mutant FXN. A.) FXN binding to SDU_{K101A}. B.) FXN binding curve to SDU_{K101H}. C.) N146K FXN binding to SDU_{K101A}. D.) N146K FXN binding to the SDU_{K101H} complex.

Table 4-2. Binding constant of FXN variants to ISCU2 variants in the SDUF complexes was determined kinetically. *Previously reported binding constant.[67] **Previously reported binding constant.[75]

Variant		FXN K_d (μM)
ISCU2 WT	FXN WT	0.07 ± 0.04*
K101A	WT	3.4 ± 0.7
K101A	N146K	2.3 ± 1.9
K101H	WT	0.6 ± 0.2
K101H	N146K	9.21 ± 4.8
WT	N146K	6.25 ± 1.40 **

DISCUSSION

There currently exists no structural model of the human interaction of between NFS1 and ISCU2. The closest related results are from bacteria in which the protein interactions of the cysteine desulfurase and the scaffold in the Fe-S cluster assembly pathway have been shown crystallographically in *E. coli* and *A. fulgidus*.[31, 32] It appears that the interaction between a conserved glutamate on IscS (E311) and lysine on IscU (K103, both *E. coli* numbering) is required for complex formation as observed was in the crystal structure.[31] In yeast, the importance of the conserved lysine in the LPPVK motif on Isu was studied by mutation to an alanine or glutamate and the ability of mutated Isu to pull down the NFS1 was abolished.[154] The results presented from the hydroxyl radical footprinting (Chapter II) indicate that the region on ISCU2 (residues 102-113) near residue K101 was protected upon FXN binding SDU to form the SDUF complex. Furthermore, the results of the fluorescence anisotropy experiments (Chapter III) indicate the importance of β-sheet residue W155R to interact with the SDU complex for binding. Therefore it was our intention to further probe the implications of disrupting the interactions between ISCU2 and FXN by designing point mutations on both ISCU2 (K101) and the β-sheet region on FXN (N146K) to better understand the effects on cysteine desulfurase activity and FXN binding.

First, we investigated a conserved ISCU2 protein residue K101 to understand its role in complex formation with SD. Mutation of residue lysine 101 to either alanine or histidine and subsequent titrations of K101A or K101H ISCU2 to SD revealed that 100 equivalents of ISCU2 were required to minimally or maximally stimulate the cysteine

desulfurase activity, respectively. Thus, the substitution of K101 with either alanine or histidine severely disrupted the ability of ISCU2 to bind SD as expected from interactions observed from the crystal structure from *E. coli*.[31] The titrations of FXN to the SDU_{K101X} complexes with maximally stimulating amounts of variant ISCU2 revealed that 50 equivalents of FXN were required to maximally stimulate the rate of the cysteine desulfurase in each reaction; this value is~17 fold higher than that required for the native SDU complex suggesting a perturbation of the native FXN interaction to the SDU complex. The decreased interaction was validated by measuring the binding constant of FXN to the SDU_{K101X} complexes kinetically. FXN binding to the SDU_{K101A} complex was decreased by ~49 fold compared to wild-type, whereas the binding of FXN to the SDU_{K101H} complex was only decreased by ~9 fold (Table 4-2). This result indicates that the imidazole ring of K101H ISCU2 may be able to partially compensate for the loss of lysine in the interaction between SDU_{K101H} and FXN. The K101A and K101H mutations potentially cause a shift in conformation from the helix, as seen in the crystal structure without frataxin, to the coil conformation preventing the tight binding of FXN to the SDU complex.

We have previously identified the primary sulfur acceptor from NFS1 to ISCU2 as residue C104 which, is on a surface exposed C-terminal alpha helix close to the chaperone binding LPPVK motif.[67] Based on the results presented here, we propose a model in which ISCU2 binds NFS1 through the salt bridge formed between the lysine on ISCU2 and glutamate (E333) on NFS1 and proceeds to undergo a conformation change to allow for FXN to bind and stimulate the cysteine desulfurase activity. NMR data from

the Markley lab suggests two distinct conformations of the *E. coli* scaffold protein that interconvert on the millisecond time scale; we suggest these two states correspond to one in which the C-terminal helix housing C104 is helical and one that is coiled. We hypothesize that in order for C104 to accept the persulfide sulfur from NFS1, ISCU2 must be in the coiled conformation. When FXN binds to the SDU complex, it stabilizes the coiled ISCU2 conformation and stimulates the rate of the cysteine desulfurase by exposing C104 to participate in the sulfur transfer reaction.

FXN binding is accomplished by interactions of β-sheet region (residues 136-175) to SD in the human system as observed by changes in rates of modification in the hydroxyl radical footprinting experiments (Chapter II) and kinetic binding experiments using FRDA variants.[67, 93, 162] It was previously shown that the N146K mutation on FXN binds to the SDU complex approximately 28 times weaker than wild-type FXN.[75] We hypothesize that this could be due to charge repulsion between the lysine on ISCU2 and the mutated residue on FXN. To better address this question, we analyzed the activity of N146K FXN with the ISCU2 variants discussed above. We show that the $SDU_{K101A}F_{N146K}$ complex is unable to stimulate the cysteine desulfurase and is severely impaired kinetically with a k_{cat}/K_M that is 14 times lower than native SDUF (Table 4-1). The N146K FXN binding to SDU_{K101A} is approximately 10 times weaker than the SDUF complex but is nearly equal to that of the $SDU_{K101A}F$ complex. The $SDU_{K101H}F_{N146K}$ had decreased cysteine desulfurase activity by about half to SDUF but was similar to the $SDUF_{N146K}$ complex. The kinetic activity of $SDU_{K101H}F_{N146K}$ was not affected indicated by the fact that the k_{cat}/K_M was unaffected. The binding of N146K FXN to the SDU_{K101H}

complex was ~42 times weaker than SDUF. These results taken together indicate that both the ability of FXN to bind and stimulate the SDU complex are integral components of this complex and also that the mutation at position N146K on FXN cannot be compensated for by making complimentary mutations on ISCU2 at position K101.

Additional mutational studies of the hypothesized ISCU2-FXN binding region (residues 102-113 on ISCU2 by hydroxyl radical footprinting, Chapter II) in which ISCU2 was mutated at residue H103 showed that the interactions between ISCU2 and NFS1 were likely uninterrupted but to a lesser degree than those observed for the K101 mutant. Mutations at residue H103 ISCU2 caused a more severe FXN binding phenomenon than the K101 ISCU2 mutation but the activity of complexes was unaffected compared to native ISCU2 in the SDUF complex. Interestingly, the binding of FXN to H103K ISCU2 could be partially recovered as determined by kinetic binding assays by incorporating a complimentary mutation on FXN at residue arginine 165 to histidine although the activity of the $SDU_{H103K}F_{R165H}$ was unable to be recovered.[67] Specifically, the implication is that residue K101 is more affected in binding NFS1 than H103 and H103 is likely involved in interactions with FXN and also in complex activation possibly due to a conformational change due to its proximity to the primary sulfur acceptor C104.[67]

The complexity of the choreography of this complex is highlighted by the ability of a single point mutation on ISCU2 to decrease the ability to bind NFS1 (K101) but also have an effect on FXN binding and complex activation. These results in this chapter implicate the importance of the conformation state of ISCU2 to interact with NFS1, bind

FXN and become activated to receive sulfur from NFS1 for cluster assembly and subsequent transfer to apo proteins. It will be interesting to gain a better understanding of the effect on transferring intact Fe-S clusters from the K101 ISC2 variants in future experiments. The interactions between ISCU2 and FXN in the context of the SDUF complex can be further tested by using the fluorescence anisotropy experiments outlined in Chapter III and doing additional mutation studies to both ISCU2 and FXN.

CHAPTER V

IMPLICATIONS OF POINT MUTATIONS ON HUMAN ISCU2 TO THE IRON-SULFUR CLUSTER BIOSYNTHESIS COMPLEX

INTRODUCTION

The synthesis of Fe-S clusters in humans is achieved by a four protein complex composed of NFS1, ISD11, ISCU2, and FXN.[33] The cysteine desulfurase, NFS1 and its co-protein ISD11 convert cysteine to alanine through the formation of a transient persulfide on a mobile loop cysteine on NFS1. The sulfur can then be transferred to the scaffold protein, ISCU2, which will assemble Fe-S clusters with the addition of Fe^{2+} and electrons. Frataxin (FXN) functions as an allosteric activator for the Fe-S cluster assembly complex.[33] Since Fe-S cofactors are critical for many biological processes, it is not surprising that there are human diseases associated with mutations in the Fe-S cluster biosynthetic process, including the ISCU2 and FXN components of the assembly complex.

Mutations to FXN lead to the human disease Friedreich's ataxia (FRDA), which is an autosomal recessive neurodegenerative disease brought on by an expanded GAA repeat on both *FXN* alleles or an expanded GAA repeat on one allele and a missense or nonsense mutation on the other allele.[75, 164] *In vitro* experiments revealed that FXN missense mutations have decreased stability, an inability to stimulate cysteine desulfurase activity, and loss of Fe-S cluster assembly activity.[66, 75, 143, 144] Interestingly,

the decreased binding and activation of FRDA variants appears to correlate to age of onset and severity of disease progression.[75]

Mutations in the ISCU2 gene lead to a human disease known as ISCU myopathy that is characterized by exercise intolerance in which even trivial exercise can cause tachycardia and palpitations, muscle fatigue, and lactic acidosis.[81] As early as 1995, 19 patients in northern Sweden were identified with a phenotype that included decreased succinate dehydrogenase and aconitase activities and an overload in mitochondrial iron.[80, 165] This phenotype has been linked to a homozygous point mutation in intron 4 of the ISCU gene that results in the retention of a 100 base pair fragment of intron sequence between exons 4 and 5 in the ISCU2 mRNA; additionally, it also includes a premature translational stop codon in the open reading frame (Figure 5-1).[81] Consequently, the mRNA levels in muscle tissue were reduced and there appeared to be a decrease in translated mitochondrial ISCU2 as determined by western blot analysis.[80] This splicing defect in ISCU2 results in the disease known as myopathy with exercise intolerance, Swedish type.[79, 81] Subsequently, a more severe disease progression was identified that was linked to a specific point mutation on ISCU2.[79, 81]

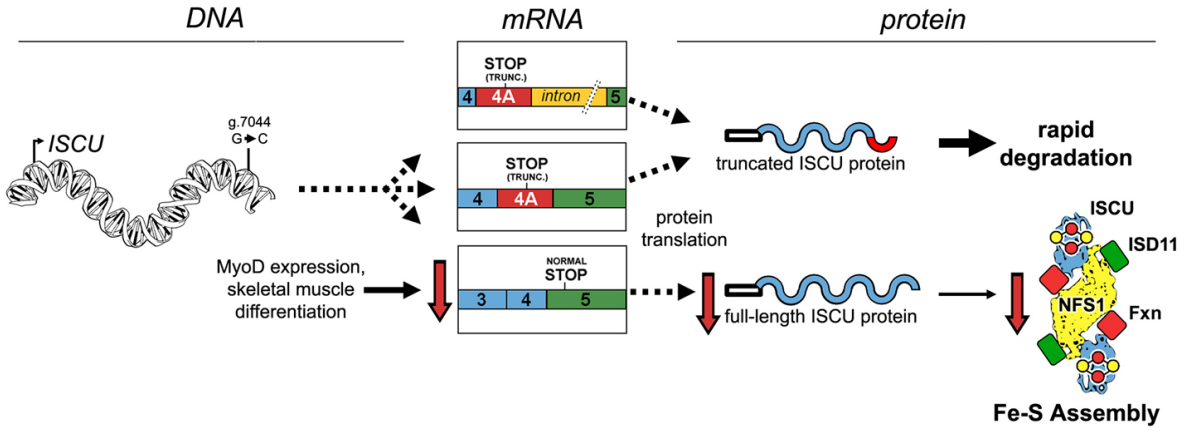

Figure 5-1. A schematic of the disease pathway for the ISCU2 gene that causes the disease myopathy with exercise intolerance is shown from the point mutation in the DNA to protein expression. Adapted with permission from *Journal of Biol. Chem.*, 287:40119-40130. Copyright 2012 American Society for Biochemistry and Molecular Biology.[81]

Kollberg*et al.* determined that such individuals contain a G>C mutation on one allele along with a newly identified heterozygous missense mutation on exon 3 of their second allele, which resulted in the conversion of a highly conserved glycine to glutamate (G16E) near the N-terminus of ISCU2.[79] Since residues near the N-terminus are critical for IscU binding to IscS in bacterial systems,[31] and the N-terminal residues were involved in protein-protein interactions as determined by hydroxyl radical footprinting (Chapter II, Figure 2-6), the G16E clinical variant may impact formation of the Fe-S assembly complex. Together, their results indicate lower ISCU2 expression is responsible for the ISCU2 myopathy with exercise intolerance phenotype for the homozygous patients but the effect of the missense mutation for the heterozygous patients has not been biochemically evaluated. Recently, these results were validated in

which the cellular effects of the G16E mutation (G50E in the publication) were determined in human and yeast cells for protein expression and activity.[166]

NMR studies by the Markley group revealed that bacterial IscU exists as a mixture of structured and dynamically disordered.[35, 40] Interestingly, the D37A mutation favors the structured state, binds IscS tighter, and contains a more tightly bound Fe-S cluster that evidently has slower transfer kinetics to apo targets.[26, 29, 37-39] Mutational studies coupled to enzyme kinetics and radiolabeling experiments suggests a similar equilibrium between functional and non-functional states of the human SDU complex, and that FXN binds and stabilizes the functional form to activate the complex (Figure 5-2).[78]

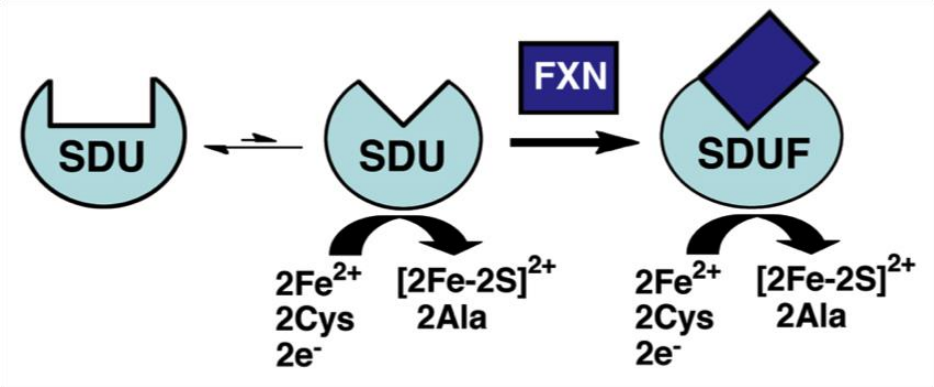

Figure 5-2. A model of the FXN based activation of a pre-equilibrium binding model of the SDUF complex is shown in which FXN binds an inactive form of the SDU complex stabilizing the complex and activating Fe-S assembly. Reprinted with permission *Biochemistry*, 51:2506-2514. Copyright 2012 American Chemical Society.[78]

Consistent with this hypothesis, mutants of ISCU2 such as M106I were identified,[68] and biochemically verified[67] that when bound to SD no longer require FXN for activation of the Fe-S assembly complex. Here, we test mutants predicted to stabilize the

structured state of ISCU2 such as D37A and L107Q (Figure 3-3, magenta), which was designed to hydrogen bond to the native D37 side chain, along with the G16E clinical mutant (Figure 5-3, cyan) in functional and binding assays. In addition, if the initial hypotheses that the G16E weakens and the D37A variant strengthens binding to the SD complex, these variants could be useful in evaluating different super complex vs dissociative models for cluster transfer (Figure 1-15).

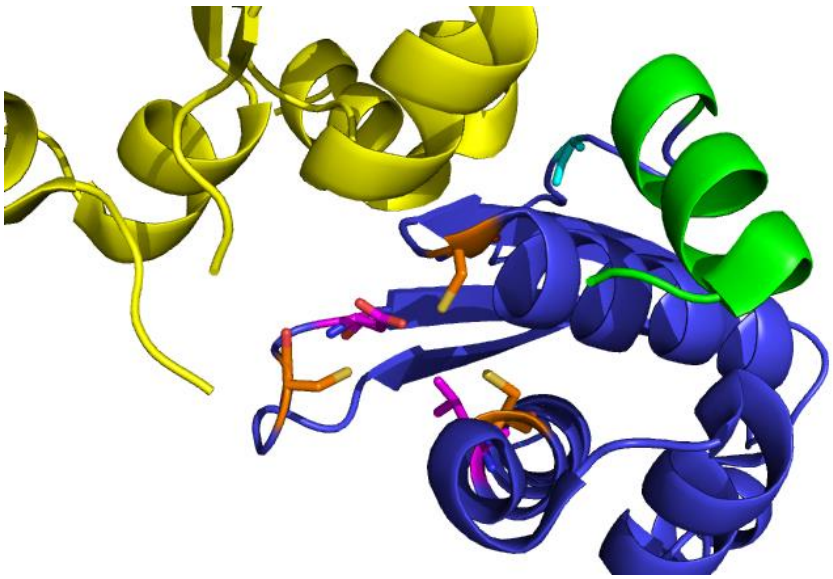

Figure 5-3. IscU structure overlaid with a portion of the IscS structure. The IscU molecule is shown in blue with the G16E residue in cyan and the N-terminal α-helix in green. The active site cysteine residues are shown in orange and the D37 and L107 are shown in magenta. Part of the IscS molecule is shown in yellow.

EXPERIMENTAL PROCEDURES

Protein Preparation. The QuikChange method (Stratagene) was used to introduce the point mutations G16E, D37A, and L107Q into the human ISCU2 gene in the pET11a

vector. The successful mutation was verified by DNA sequencing (Gene Technology Laboratory, TAMU). The resulting plasmids were individually transformed into BL21 (DE3) *E. coli* competent cells. Cells were grown at 37 ^{o}C until protein expression was induced at an OD_{600} of 0.6 with 0.5 mM IPTG and expression continued at 16 ^{o}C overnight. The mutant ISCU2 proteins were purified using the established protocol for wild-type human ISCU2.[33] Human proteins wild-type ISCU2, FXN and NFS1/ISD11 were purified as previous described.[33]

Measurement of Cysteine Desulfurase Activity. The cysteine desulfurase activity of SD was measured as a function of mutant ISCU2 concentration using a previously described assay.[33, 66, 75] Briefly, SD (0.5 μM), mutant ISCU2, and 2 mM DTT in 50 mM Tris pH 7.5, 250 mM NaCl reaction buffer were incubated in an anaerobic glovebox (<2 ppm O_2) for ~30 minutes, which was maintained at 12-16 ^{o}C before the initiation of the reaction with 100 μM L-cysteine. The reactions were incubated anaerobically for 20 minutes at 37 ^{o}C before being quenched with the addition of 100 μL of 20 mM DPD in 7.2 M HCl and 100 μl of 30 mM $FeCl_3$ in 1.2 M HCl. The formation of methylene blue was quantitated by monitoring absorbance at 670 nm. Rates were calculated using a standard curve of sulfide produced from Na_2S. FXN was titrated to determine the amount required to maximally stimulate the cysteine desulfurase activity. In each 800 μl reaction, FXN was incubated with 0.5 μM SD, mutant ISCU2, 2 mM DTT, 5 μM $Fe(NH_4)_2(SO_4)_2$ in reaction buffer for 30 minutes in an anaerobic glovebox. The reaction was initiated with the addition of 100 μM L-cysteine and was incubated at 37 ^{o}C

in a sealed flask for 10 minutes. The reaction was quenched, monitored at 670nm, and the amount of sulfide quantified as described above.

Determination of Michaelis-Menten Kinetics. A reaction mixture of 0.5 μM SD, 2 mM DTT, 5 μM $Fe(NH_4)_2(SO_4)_2$, and saturating amounts of mutant ISCU2 and FXN determined above was incubated for 30 minutes in the anaerobic glovebox. The reaction was initiated with the addition of 12.5-1000 μM L- cysteine and allowed to react for 10 minutes at 37 ^oC. The reaction rates, as a function of cysteine concentration, were fit to the Michaelis-Menten equation using KaleidaGraph (Synergy Software).

Binding Constant Determination of FXN with Mutant ISCU2 to the Complex. The binding constant of FXN to the $SDU_{G16E,}$ SDU_{D37A}, or SDU_{L107Q} complex was performed as previously described.[66, 75] The k_{cat} of each reaction as a function of [FXN] was fit to a modified quadratic interpretation of the Michaelis-Menten equation in KaleidaGraph to calculate the K_d of FXN binding using equation 4-1 previously described.[67]

Iron-Sulfur Cluster Assembly Assay. The ability of the mutant ISCU2 to assemble Fe-S clusters was assayed and compared to wild-type as previously described using maximally stimulating amounts of mutant ISCU2 and FXN anaerobically either in a sealed UV-Vis cuvette or on a Tecan microplate reader which was in an anaerobic glovebox.[33, 66, 75, 78]

RESULTS

The Effect of G16E ISCU2 to the SDU and SDUF Complexes. The effect of G16E ISCU2 binding to SD was monitored by the change in cysteine desulfurase activity upon G16E ISCU2 titration. The activity of the SD complex is minimized upon the addition of 3 equivalents of wild type ISCU2 (Figure 5-4A). The cysteine desulfurase activity upon G16E ISCU2 titration did not decrease as significantly as for wild-type even at 100 equivalents (Figure 5-4B). The error bars represent the average activity of three independent titrations. Therefore, for further experimentation, 80 equivalents of G16E ISCU2 were used to determine the maximum cysteine desulfurase activity upon the titration of native FXN. The maximum stimulation of the SDU_{G16E} activity was achieved at approximately 60 equivalents of FXN (5-4C). The titration, with additional equivalents of $ISCU2_{G16E}$ and FXN, did not affect the rate cysteine desulfurase activity.

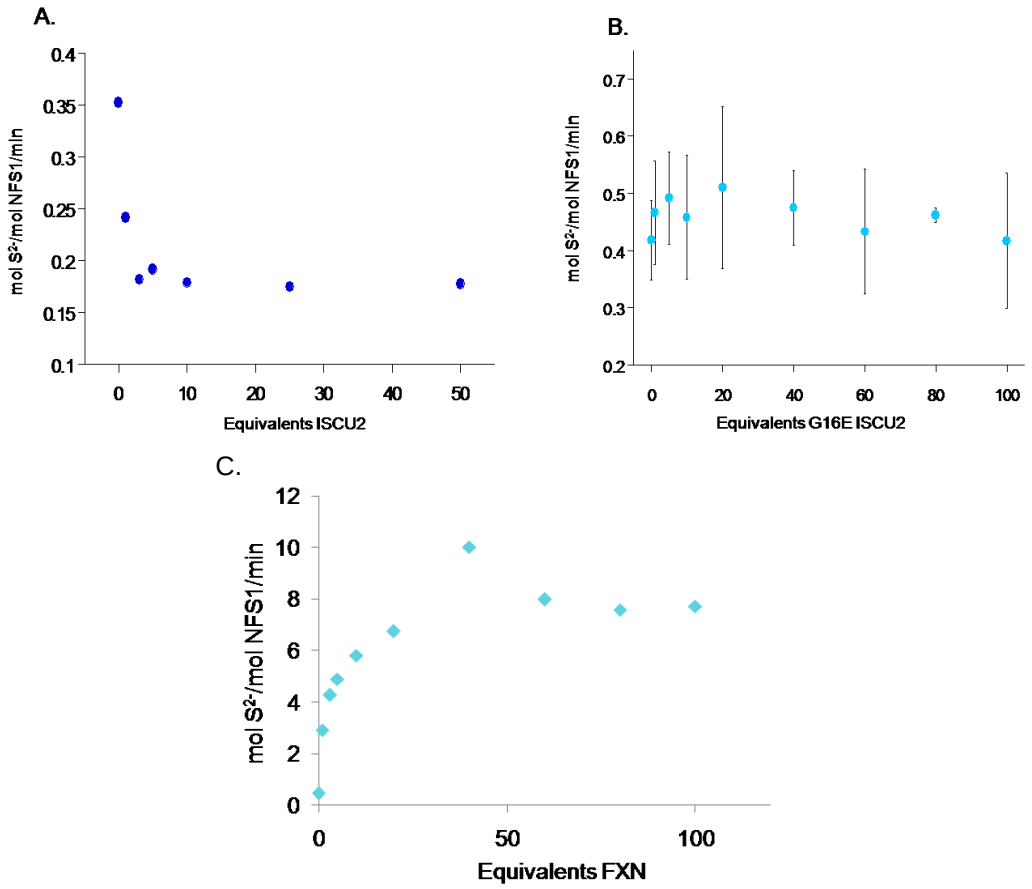

Figure 5-4. Cysteine desulfurase activity of SD with G16E ISCU2 monitored as a function of methylene blue formation at 670 nm. A.) Cysteine desulfurase activity of SD as a function of equivalents of native ISCU2. B.) The clinical mutant G16E ISCU2 titrated into SD to determine the effect on cysteine desulfurase activity with SD alone. C). Titration of FXN to SDU_{G16E} to determine maximum stimulation of cysteine desulfurase activity.

Cysteine Desulfurase Activity of the $SDU_{G16E}F$ Complex. The maximally stimulating amounts of G16E ISCU2 and FXN determined above were used to measure the Michaelis-Menten kinetics of the $SDU_{G16E}F$ complex (Figure 5-5). Upon comparison to the wild-type SDUF complex, the activity of the mutant $SDU_{G16E}F$ complex was not compromised (Table 5-1).

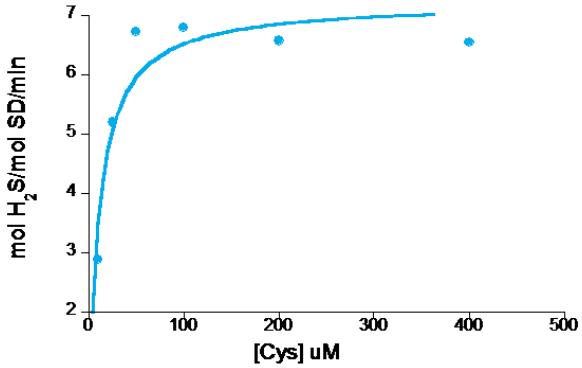

Figure 5-5. Michaelis-Menten kinetics were determined for the $SDU_{G16E}F$ complex using 80 equivalents of G16E ISCU2 and 60 equivalents of FXN. The rate was fit in KaleidaGraph.

Table 5-1. Kinetic parameters for determined the clinical mutant $ISCU2_{G16E}$ complex. *Previously published binding constant for the native SDUF complex.[67]

Complex	k_{cat} (min^{-1})	K_M^{Cys} (mM)	k_{cat}/K_M ($M^{-1}s^{-1}$)	K_d (μM)
SDUF	11.0 ± 1	0.021 ± 0.009	8,700 ± 3,800	0.07 ± 0.04*
$SDU_{G16E}F$	7.2 ± 0.4	0.011 ±0.003	10,900 ± 3,000	2.7 ± 0.6

Determining the Binding Constant of FXN to SDU_{G16E}. The effect of FXN binding to the SDU complex with the clinical mutant G16E ISCU2 was determined using the cysteine desulfurase activity assay where the rate was plotted as a function of the concentration of FXN and the K_d was calculated (Figure 5-6) and compared to wild-type SDUF based on Equation 4-1.[66, 75] Frataxin binds the SDU_{G16E} complex approximately 40 times weaker than the native SDU complex (Table 5-1).

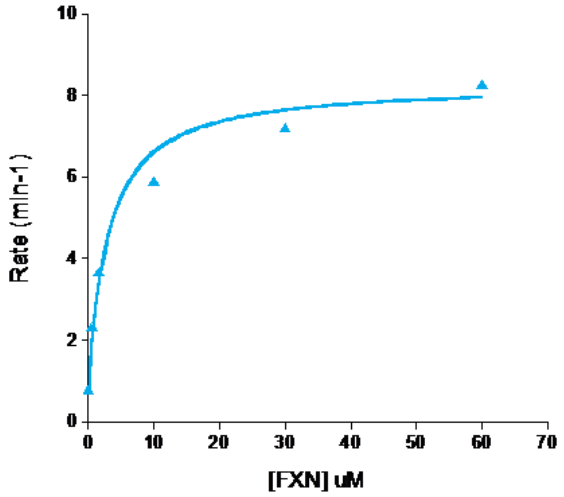

Figure 5-6. The binding constant was measured for FXN to SDU_{G16E} as a function of [FXN] and measured k_{cat} values. The K_d was fit to Equation 4-1 in KaleidaGraph.

Iron- Sulfur Cluster Assembly Assay. The ability of the $SDU_{G16E}F$ complex to turn over Fe-S clusters was determined by monitoring the absorbance at 456 nm, typical for [2Fe-2S], as a function of time and the curve was fit to first order kinetics. Maximally stimulating amounts of G16E ISCU2 and FXN were used and the rate was compared to the wild-type SDUF complex (Figure 5-7).The rate of Fe-S cluster

assembly for the native SDUF complex was 0.45 ± 0.02 min^{-1} (Figure 5-7, blue) compared to the $SDU_{G16E}F$ complex which was slightly compromised in activity at a rate of 0.35 ± 0.04 min^{-1} (Figure 5-7, cyan).

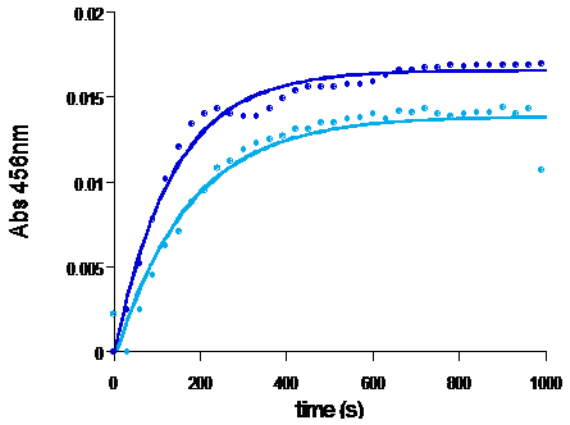

Figure 5-7. Iron sulfur cluster assembly of SDUF and $SDU_{G16E}F$. The rate of Fe-S cluster assembly was monitored as a function of time at 456 nm for SDUF (blue, 0.45 ± 0.02 min^{-1}), and$SDU_{G16E}F$ (cyan, 0.35 ± 0.04 min^{-1}).

Effects of the Stability of Mutant ISCU2 to Stimulate Cysteine Desulfurase Activity. The ability of the D37A or L107Q ISCU2 to decrease the cysteine desulfurase activity of SD was determined (Figure 5-8A) and compared to wild-type (Figure 5-1A). There was no noticeable change in the cysteine desulfurase activity when D37A ISCU2 was titrated (Figure 5-8A, orange) to SD. When L107Q ISCU2 was titrated, a similar trend to wild type, a decrease in SD activity, was observed (Figure 5-8 A, green). From these curves, further experiments were performed with 30 equivalents $ISCU2_{D37A}$ and 20 equivalents $ISCU2_{L107Q}$.

The amount of FXN required to maximally stimulate the SDUF complex with the mutant ISCU2 was determined by titrating FXN to the mutant SDU complex using the amount of ISCU2 determined above (Figure 5-8B). Both mutants were able to fully stimulate the cysteine desulfurase activity to wild type levels with the addition of either 10X FXN or 20X FXN for SDU_{D37A} or SDU_{L107Q}, respectively. Additional equivalents of D37A ISCU, L107Q ISCU2, or FXN did not further affect the rate of cysteine desulfurase activity.

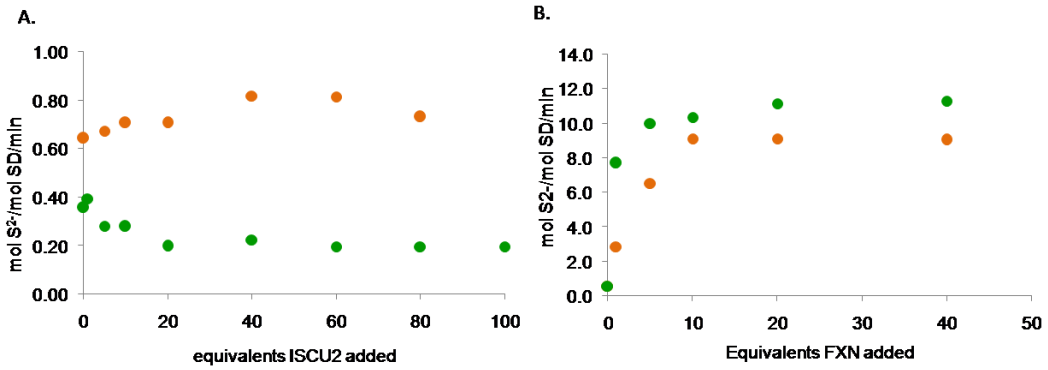

Figure 5-8. The cysteine desulfurase activity stimulated with ISCU2 mutants D37A and L107Q. A.) Cysteine desulfurase activity of SD with mutant ISCU2 titrated (orange D37A; green L107Q). B.) Cysteine desulfurase activity of SDU_{mutant} with FXN titrated (colors the same as in A).

Determination of Michaelis-Menten Kinetics for the $SDU_{mutant}F$ Complexes. The Michaelis-Menten kinetics were determined for the maximally stimulating amounts of D37A ISCU2 or L107Q ISCU2 and FXN determined above as above and the rate of

cysteine desulfurase activity as a function of cysteine concentration was plotted to determine the k_{cat} (min^{-1}) and K_M (mM) for each complex (Figure 5-9). The $SDU_{D37A}F$ or $SDU_{L107Q}F$ complex was not compromised it its cysteine desulfurase activity compared to wild type when maximally stimulating amounts of either D37A ISCU2 or L107Q ISCU and FXN were used (Table 5-2).

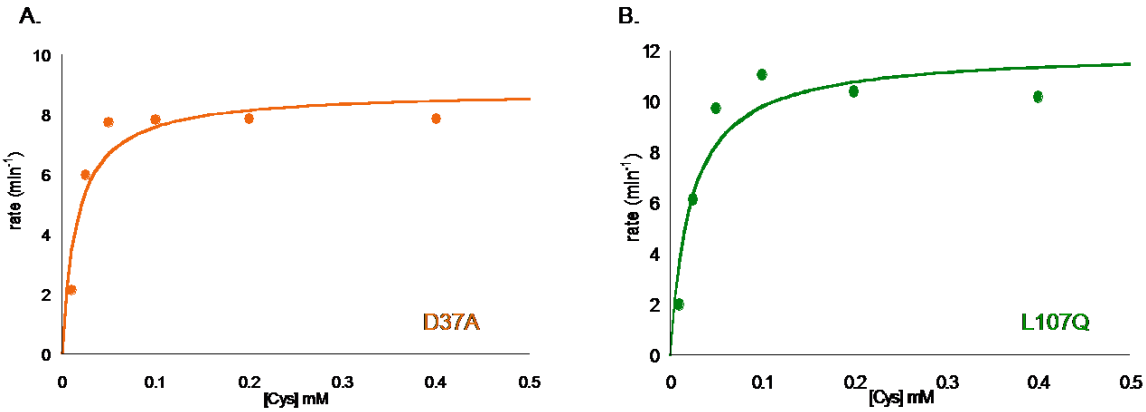

Figure 5-9. The Michaelis-Menten kinetics of $SDU_{mutant}F$ complex with ISCU2 mutants A.) D37A and B.) L107Q were measured using maximally stimulating amounts of mutant ISCU2 and FXN.

Table 5-2. Kinetic parameters determined for the $SDU_{D37A}F$ and $SDU_{L107Q}F$ complexes.

Complex	k_{cat} (min^{-1})	K_M^{Cys} (mM)	k_{cat}/K_M ($M^{-1}s^{-1}$)	Fe-S assembly rate (min^{-1})
SDUF	11.0 ± 1	0.021 ± 0.009	8,700 ± 3,800	0.168 ± 0.008
$SDU_{D37A}F$	8.7 ± 0.7	0.016 ±0.006	9,300 ± 3,000	0.38 ± 0.05
$SDU_{L107Q}F$	12.0 ± 1	0.022 ± 0.009	9,000 ± 4,000	0.19 ± 0.02

Iron Sulfur Cluster Assembly with Mutant ISCU2 Protein. The ability of the mutant ISCU2 proteins in the SDUF complex to assemble Fe-S clusters was interrogated by monitoring the increase in absorbance at 456nm which is typical for 2Fe-2S clustersas a function of time. The cluster assembly was determined using 30X D37A ISCU2 and 10X FXN or 20X L107Q ISCU2 and 20X FXN (Figure 5-10). The Fe-S cluster assembly rates for wild type SDUF, $SDU_{D37A}F$ and $SDU_{L107Q}F$ were fit to first order kinetics and compared to native SDUF (Table 5-3). These results show that the rate of Fe-S cluster assembly with the L107Q ISCU2 is similar to wild-type whereas the rate is almost twice that of the SDUF complex.

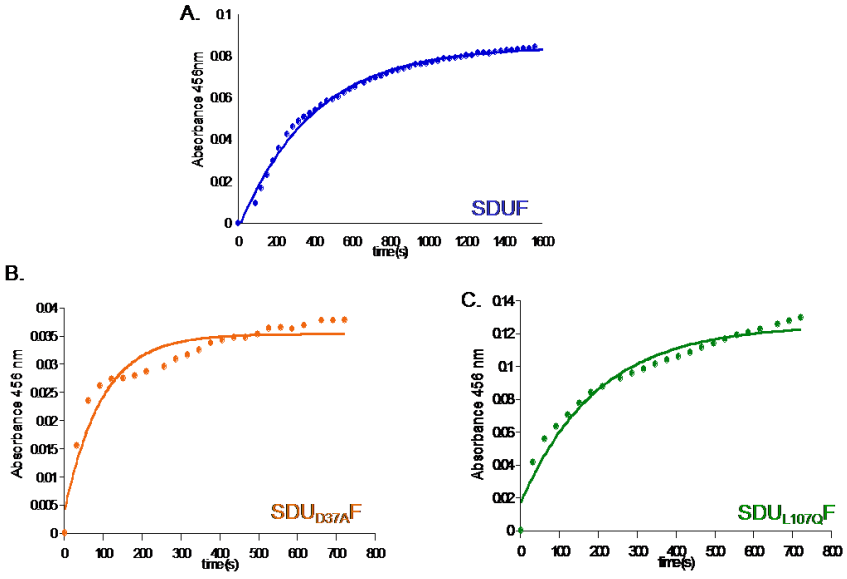

Figure 5-10. Fe-S assembly kinetics measured of the ISCU2 mutants D37A and L107Q in the A.) wild-type SDUF, B.) $SDU_{D37A}F$, or C.) $SDU_{L107Q}F$ complexes.

DISCUSSION

The clinical mutation of the highly conserved glycine at residue 16 (human numbering) to glutamate on the scaffold protein ISCU2 has been identified as being the cause of myopathy with exercise intolerance, Swedish type. The location of the glycine in the native peptide is on a flexible linker between the N-terminal α-helix (residues 1-11) and the first β- sheet and mutation may cause a decrease the binding to the NFS1/ISD11 (SD) complex.[31] The unpublished NMR structure of ISCU2 from *Mus musculus* (PDB 1WFZ) indicates this region of the protein is highly flexible and unstructured loop. Examination of the human ISCU2 homolog structure from *E. coli* revealed the native glycine residue at position 16 (human numbering) is in a forbidden region of the Ramachandran plot, and suggests that the G16E mutation may adopt a different main-chain conformation and perturb the N-terminal region of ISCU2. The N-terminal region of the *E. coli* IscU structure is known to interact with IscS as determined by deletion mutagenesis coupled to pull-down studies, which indicated IscU residues 1-6 have minor contribution in binding IscS, whereas deletion of residues 1-12 or 1-17 completely abolished binding.[31] Although we suspect that the G16E ISCU2 mutation may weaken its binding to the SD complex, its functional properties have not been evaluated. Additionally, frataxin binding to the IscS-IscU complex in *E. coli* has been shown to increase the binding of IscU to IscS.[34] This trend was also observed in the hydroxyl radical footprinting experiments in which the peptides that were protected in the SDU complex underwent further protection upon the addition of FXN indicating a more tightly bound complex was formed (Chapter II). How the clinical mutation on

human ISCU2 affected FXN binding the SDU complex was also determined using previously established biochemical kinetic assays.[66, 75]

First, we aimed to determine if the binding of G16E ISCU2 to the NFS1/ISD11 complex was affected by monitoring the change in cysteine desulfurase activity upon mutant ISCU2 titration. The results presented are in good agreement with the hypothesis that the glutamate is unable to adopt the same conformation as the native protein with glycine at this position by the requirement of 80 equivalents of G16E ISCU2. This mutation, in turn, likely affects the ability of the N-terminus of G16E ISCU2 to adopt the correct conformation to make important interactions with SD, which were also observed from the hydroxyl radical footprinting experiments. Furthermore, the binding of FXN to the SDUG16E complex was approximately 40 times weaker than FXN to the native SDU complex (Table 5-1). The weaker binding of FXN could be due to the flexible N-terminus of G16E ISCU2 adopting a conformation that is not preferential to FXN binding. The importance of the N-terminus of ISCU2 to interact with NFS1 has been previously determined by pull-down studies in which truncation of the N-terminus loses the ability to pull down IscS.[31] Furthermore, the G16E ISCU2 mutation in yeast loses the ability to interact with human NFS1 or yeast Nfs1.[166]

Furthermore, the combination of the lower expression of G16E ISCU2 protein in patients with myopathy with exercise intolerance[80, 166] and compromised binding of FXN to the SDU_{G16E} complex can be used to correlate the phenotypes observed with the biochemical results presented here. The slight decrease in Fe-S clusters assembly could lead to an iron overload, which was is consistent with the increase in iron by

histochemical staining and electron microscopy.[79] The combination of decreased expression levels G16E ISCU2 protein and decreased FXN binding might be able to explain the decrease in aconitase, succinate dehydrogenase and cytochrome oxidate activities seen previously[79, 80, 165] by lower amounts of Fe-S clusters being synthesized..*In vivo* human and yeast cell studies showed that the activity of aconitase, a down-stream acceptor of Fe-S clusters, was compromised, the cell viability decreased, and there was an increase in iron content and reactive oxygen species for the cells containing the G16E mutation (G50E in the manuscript) compared to cells containing native ISCU2.[166] In contrast to that work, the wild-type activity levels were obtained using the $SDU_{G16E}F$ complex once the binding deficiencies were overcome (Table 5-1) indicating that the activity of the G16E ISCU2 mutant does not compromise the cysteine desulfurase activity (Figure 5-5) and only slightly affects Fe-S assembly activity (Figure 5-7). This result would presume that the mutation does not affect the active site of the scaffold protein but that deficiencies observed *in vivo* are likely due to a decrease in mutant scaffold protein expression, decreased interactions with the cysteine desulfurase, and the diminished ability of FXN to bind and stimulate the SDUF complex.

Additionally, a D37A (human numbering) point mutation on ISCU2 was discovered in NifU, a bacterial homolog to ISCU2, in which the Fe-S cluster is more stably bound than in the native protein and exhibits inhibited cluster transfer kinetics.[26, 29, 37-39] UV-Vis and Mössbauer spectroscopy of the human ISCU2 D37A variant revealed a $[2Fe\text{-}2S]^{2+}$.[37] The role of this aspartate has been hypothesized: (1) to function as a cluster binding ligand; and (2) in charge destabilization of this region of the protein

structure to labilize the cluster for transfer to apo-target proteins.[37] NMR spectroscopy and thermal stability assays indicate the D39A IscU (*E. coli* numbering) is more structured than wild-type and binds IscS tighter.[32, 35, 40] The effects of the D37A and also L107Q point mutation on ISCU2 on the cysteine desulfurase and Fe-S cluster assembly were determined using previously described biochemical kinetic assays.[66, 75]

Introducing the D37A or L107Q point mutation on ISCU2 did not have as pronounced of an effect upon binding SD as the G16E mutation as they only required 30 or 20 equivalents, respectively (Figure 5-8A). Additionally, both required fewer equivalents of FXN than the G16E ISCU2 protein to fully stimulate the cysteine desulfurase (Figure 5-8B). Taken together, these results indicate that there was a larger structural perturbation upon introducing the G16E mutation than either the D37A or L107Q mutation which affected not only interactions with SD but also interactions with FXN. The $SDU_{D37A}F$ and $SDU_{L107Q}F$ complexes were not compromised in their ability to stimulate the cysteine desulfurase if additional equivalents of both mutant ISCU2 and FXN compared to wild-type were added to the assay. Furthermore, the $SDU_{L107Q}F$ complex was not compromised in its ability to assemble Fe-S clusters.

Interestingly, there was a difference in Fe-S cluster assembly rate from wild-type for the $SDU_{D37A}F$ complex. The $SDU_{D37A}F$ complex assembled Fe-S clusters at twice the rate of the wild-type SDUF complex. The overall change in absorbance was only approximately half indicating that although the cluster may assemble faster, the total number of Fe-S clusters assembled was less than wild-type potentially implying that the cluster is retained on the complex and is not lost in solution, allowing fewer turnovers.

Therefore, it will be important to determine if, once the cluster is assembled, there is a difference in rate of transfer to apo target proteins. The functional biochemical studies show that once binding is overcome, the SDU_{D37A} and SDU_{L107Q} complexes can be stabilized by FXN and the cysteine desulfurase activity is not affected and the Fe-S cluster assembly is not compromised for the $SDU_{L107Q}F$ complex.

The amino acid leucine 107 was included on a peptide on ISCU2 that was protected in the SDUF complex by hydroxyl radical footprinting (Chapter II) in the SDUF complex and is adjacent to residue M106 which has been shown to be able to recover activity due to FXN deficiency in both humans and yeast.[67, 68] It was interesting to note by the results in this chapter that substitutions at L107 that the cysteine desulfurase and Fe-S assembly activities were not affected and it appears that the FXN binding is only minimally decreased although the cysteine desulfurase activity in the absence of FXN was not recovered by this particular mutation indicating that single amino acid exchange from methionine to isoleucine at position 106 has some functional as well as potentially structural effect in stimulating the cysteine desulfurase protein.

Future studies to better understand the binding phenomena of FXN to the SDU complex with ISCU2 active site variants, similar to the fluorescence anisotropy experiments described in Chapter III, would be necessary to fully understand the implications of making active site mutation to ISCU2 in the SDUF complex. In addition to deeper understanding of binding phenomena, the ability of these mutant ISCU2 proteins to interact with the chaperone proteins and transfer the cluster to apo proteins

will be useful to fully understand the importance of these mutations to the active site of ISCU2.

CHAPTER VI

CONCLUSIONS

The studies presented here give insight into the protein-protein interactions of the four proteins involved in iron sulfur cluster assembly in humans. The data collected and analyzed in this dissertation was then compared to the available data from the highly homologous bacterial system, which is much more thoroughly studied than the human system to date. A multidimensional approach that was applied allowed for the complex to be studied structurally in solution by hydroxyl radical footprinting and fluorescence anisotropy but also kinetically by introducing point mutations and observing the changes in the ability of the complex to stimulate the cysteine desulfurase and Fe-S cluster assembly assays and determine binding constants. The data taken in combination leads toward a better understanding of the interactions of this complex and their implications in the diseases associated with mutations to their components, namely Friedreich's Ataxia and ISCU myopathy with exercise intolerance.

Initially, hydroxyl radical footprinting experiments were designed to understand how the proteins interacted since more popularized techniques such as protein crystallography and NMR analysis were not successful. The results presented in Chapter II uncovered a region on NFS1 (C-terminus, residues 402-419) that interacted with ISCU2 (N-terminus, residues 5-13) in the SDU complex and a region on ISCU2 that was protected in the SDUF complex (residues 102-113). The C-terminal to N-terminal interaction of the NFS1 protein to ISCU2 has been previously observed in the bacterial

systems[31, 32] and leads to the hypothesis that this particular interaction is conserved through evolution. Additionally, a region on ISCU2 was identified as becoming protected upon FXN binding the SDU complex, residues 102-113 as well as protection of FXN on the β-sheet region of the protein. The results indicated a potential site of interaction for ISCU2 and FXN in the SDUF complex and further supported the hypothesis the FXN interacts with the SDU complex through the β-sheet region.[66, 75]

The interactions of FXN to the SDU complex were further studied by fluorescence anisotropy to measure the binding constant of native and W155R FXN, a mutation seen in some instances of FRDA. These results showed that the binding constants determined by biochemical kinetic assays were consistent with the values determined using fluorescence anisotropy, that the binding of FXN could be determined under various conditions and that the tightest binding complex was obtained when all of the components required for Fe-S cluster assembly were present (Chapter III). Further, the inability of the W155R FXN mutation to form a stable complex was highlighted by the inability to increase binding upon the addition of Fe^{2+} or cysteine indicating the importance of this residue in protein-protein interactions.

The results presented in chapters 2 and 3 were further studied by incorporating a point mutation on ISCU2 (K101) near the hypothesized FXN binding region uncovered by the hydroxyl radical footprinting to determine the effects kinetically (Chapter IV). The K101 mutation on ISCU2 had a decreased affinity to bind NFS1 and subsequently FXN but the activity was not compromised after the binding was compensated for indicating that perturbations to this region of the protein have a larger impact on binding.

A point mutation on FXN was designed (N146K) to attempt to compensate for the decreased binding of native FXN to the SDU_{K101X} complexes but was unsuccessful in recovering binding and furthermore, showed a decrease in activity for the $SDU_{K101A}F_{N146K}$ complex. Therefore, it has been hypothesized that the combination of the K101A ISCU2 and N146K FXN mutation changes the environment on the SDUF complex that is required for sulfide transfer and that conformational state of the complex is vital for activity.

Lastly, to test effects of the ISCU2 clinical mutant on the activity of the SDUF complex, the G16E ISCU2 mutation was introduced and the ability of this mutant to stimulate cysteine desulfurase and Fe-S assembly activities was determined (Chapter V). Additionally, the ability of FXN to bind the SDU_{G16E} complex was determined. The results of these experiments indicate that the G16E ISCU2 protein likely binds less tightly with NFS1 and therefore FXN does not bind as tightly. These results are consistent with the results of the hydroxyl radical footprinting experiments (Chapter II), which determined that the N-terminus of ISCU2 interacts with NFS1. The glutamate substitution at position 16 on ISCU2 likely prevents the N-terminus from adopting the correct conformation to interact with NFS1 similar to the native protein. The activity of the $SDU_{G16E}F$ complex was slightly decreased in Fe-S assembly activity likely due to the decreased binding of FXN. We determined that the activity of the complex was not compromised with the introduction of mutations near the active site.

Future studies are required to determine the effects of FXN binding when active site mutations are introduced on ISCU2 and the conditions in which Fe-S cluster transfer

occurs to apo target proteins and determine the stability of the SDUF complex upon Fe-S cluster transfer. The rate of transfer for intact Fe-S clusters in both the wild-type SDUF and also the $SDU_{D37A}F$ complexes will give further insight to the effect of structure/disorder of ISCU2 and the role of this conserved aspartate in cluster assembly and transfer. Additionally, a newly determined regions of interest on NFS1 (residues 262-290) and ISCU2 (residues 102-113) were observed the implications of additional mutations to these regions can be tested. The results presented in this dissertation show the utility of previously unused techniques to uncover protein-protein interactions of large heteroprotein complexes. Furthermore, fluorescence anisotropy experimental protocols were established in which the binding constant of fluorescently labeled protein can quickly be determined using low protein concentrations for subunits to the complex. The regions of interactions determined by the hydroxyl radical footprinting and fluorescence anisotropy experiments were further validated by using the kinetic bioassays previously established in our lab and the results have led to additional testable hypotheses.

REFERENCES

1. Py, B., and Barras, F. (2010) Building Fe-S proteins: bacterial strategies, *Nat Rev Microbiol 8*, 436-446.

2. Bandyopadhyay, S., Chandramouli, K., and Johnson, M. (2008) Iron-sulfur cluster biosynthesis, *Biochem Soc Trans 36*, 1112-1119.

3. Rouault, T. A., and Tong, W.-H. (2008) Iron-sulfur cluster biogenesis and human disease, *Trends Genet 24*, 398-407.

4. Tang, Y., and Guest, J. R. (1999) Direct evidence for mRNA binding and post-transcriptional regulation by *Escherichia coli* aconitases, *Microbiology 145*, 3069-3079.

5. Hidalgo, E., Bollinger, J. M., Jr., Bradley, T. M., Walsh, C. T., and Demple, B. (1995) Binuclear [2Fe-2S] clusters in the *Escherichia coli* SoxR protein and role of the metal centers in transcription, *J Biol Chem 270*, 20908-20914.

6. Tang, Y., Guest, J. R., Artymiuk, P. J., Read, R. C., and Green, J. (2004) Post-transcriptional regulation of bacterial motility by aconitase proteins, *Mol Microbiol 51*, 1817-1826.

7. Taylor, A. M., Stoll, S., Britt, R. D., and Jarrett, J. T. (2011) Reduction of the [2Fe-2S] cluster accompanies formation of the intermediate 9-mercaptodethiobiotin in *Escherichia coli* biotin synthase, *Biochemistry 50*, 7953-7963.

8. Beinert, H., and Kiley, P. J. (1996) Redox control of gene expression involving iron-sulfur proteins. Change of oxidation-state or assembly/disassembly of Fe-S clusters?, *FEBS Lett 382*, 218-221.

9. Johnson, D. C., Dean, D. R., Smith, A. D., and Johnson, M. (2005) Structure, function, and formation of biological iron-sulfur clusters, *Annu Rev Biochem 74*, 247-281.

10. Huber, C., Eisenreich, W., Hecht, S., and Wachtershauser, G. (2003) A possible primordial peptide cycle, *Science 301*, 938-940.

11. Sheftel, A., Stehling, O., and Lill, R. (2010) Iron-sulfur proteins in health and disease, *Trends Endocrinol Metab 21*, 302-314.

12. Lill, R., Diekert, K., Kaut, A., Lange, H., Pelzer, W., Prohl, C., and Kispal, G. (1999) The essential role of mitochondria in the biogenesis of cellular iron-sulfur proteins, *Biol Chem 380*, 1157-1166.

13. Lill, R., Hoffmann, B., Molik, S., Pierik, A. J., Rietzschel, N., Stehling, O., Uzarska, M. A., Webert, H., Wilbrecht, C., and Muhlenhoff, U. (2012) The role of mitochondria in cellular iron-sulfur protein biogenesis and iron metabolism, *Biochim Biophys Acta 1823*, 1491-1508.

14. Lill, R., and Kispal, G. (2000) Maturation of cellular Fe-S proteins: an essential function of mitochondria, *Trends Biochem Sci 25*, 352-356.

15. Rouault, T. A. (2006) The role of iron regulatory proteins in mammalian iron homeostasis and disease, *Nat Chem Biol 2*, 406-414.

16. Rouault, T. A. (2012) Biogenesis of iron-sulfur clusters in mammalian cells: new insights and relevance to human disease, *Dis Model Mech 5*, 155-164.

17. Averill, B. A., Herskovitz, T., Holm, R. H., and Ibers, J. A. (1973) Synthetic analogs of the active sites of iron-sulfur proteins. II. Synthesis and structure of the tetra(mercapto-m 3 -sulfido-iron) clusters, (Fe 4 S 4 (SR) 4) 2, *J Am Chem Soc 95*, 3523-3534.

18. Jacobson, M. R., Cash, V. L., Weiss, M. C., Laird, N. F., Newton, W. E., and Dean, D. R. (1989) Biochemical and genetic analysis of the nifUSVWZM cluster from *Azotobacter vinelandii*, *Mol Gen Genet 219*, 49-57.

19. Takahashi, Y., and Nakamura, M. (1999) Functional assignment of the ORF2-iscS-iscU-iscA-hscB-hscA-fdx-ORF3 gene cluster involved in the assembly of Fe-S clusters in *Escherichia coli*, *J Biochem 126*, 917-926.

20. Zheng, L., Cash, V. L., Flint, D. H., and Dean, D. R. (1998) Assembly of iron-sulfur clusters. Identification of an iscSUA-hscBA-fdx gene cluster from *Azotobacter vinelandii*, *J Biol Chem 273*, 13264-13272.

21. Ayala-Castro, C. N., Saini, A., and Outten, F. W. (2008) Fe-s cluster assembly pathways in bacteria, *Microbiol Mol Biol Rev 72*, 110-125.

22. Lill, R., and Muhlenhoff, U. (2006) Iron-sulfur protein biogenesis in eukaryotes: components and mechanisms, *Annu Rev Cell Dev Biol 22*, 457-486.

23. Muhlenhoff, U., and Lill, R. (2000) Biogenesis of iron-sulfur proteins in eukaryotes: a novel task of mitochondria that is inherited from bacteria, *Biochim Biophys Acta 1459*, 370-382.

24. Frazzon, J., and Dean, D. R. (2003) Formation of iron-sulfur clusters in bacteria: an emerging field in bioinorganic chemistry, *Curr Opin Chem Biol 7*, 166-173.

25. Smith, A. D., Agar, J., Johnson, K. A., Frazzon, J., Amster, I. J., Dean, D. R., and Johnson, M. (2001) Sulfur transfer from IscS to IscU: the first step in iron-sulfur cluster biosynthesis, *J Am Chem Soc 123*, 11103-11104.

26. Smith, A. D., Jameson, G. N. L., Dos Santos, P. C., Agar, J., Naik, S., Krebs, C., Frazzon, J., Dean, D. R., Huynh, B. H., and Johnson, M. (2005) NifS-mediated assembly of [4Fe-4S] clusters in the N- and C-terminal domains of the NifU scaffold protein, *Biochemistry 44*, 12955-12969.

27. Agar, J., Krebs, C., Frazzon, J., Huynh, B. H., Dean, D. R., and Johnson, M. (2000) IscU as a scaffold for iron-sulfur cluster biosynthesis: sequential assembly of [2Fe-2S] and [4Fe-4S] clusters in IscU, *Biochemistry 39*, 7856-7862.

28. Chandramouli, K., Unciuleac, M.-C., Naik, S., Dean, D. R., Huynh, B. H., and Johnson, M. (2007) Formation and properties of [4Fe-4S] clusters on the IscU scaffold protein, *Biochemistry 46*, 6804-6811.

29. Yuvaniyama, P., Agar, J., Cash, V. L., Johnson, M., and Dean, D. R. (2000) NifS-directed assembly of a transient [2Fe-2S] cluster within the NifU protein, *Proc Natl Acad Sci USA 97*, 599-604.

30. Cupp-Vickery, J., Urbina, H. D., and Vickery, L. (2003) Crystal structure of IscS, a cysteine desulfurase from *Escherichia coli*, *J Mol Biol 330*, 1049-1059.

31. Shi, R., Proteau, A., Villarroya, M., Moukadiri, I., Zhang, L., Trempe, J.-F., Matte, A., Armengod, M. E., and Cygler, M. (2010) Structural basis for Fe-S cluster assembly and tRNA thiolation mediated by IscS protein-protein interactions, *PLoS Biol 8*, e1000354.

32. Marinoni, E. N., de Oliveira, J. S., Nicolet, Y., Raulfs, E. C., Amara, P., Dean, D. R., and Fontecilla-Camps, J. C. (2012) (IscS-IscU)2 complex structures provide insights into Fe2S2 biogenesis and transfer, *Angew Chem Int Ed Engl 51*, 5439-5442.

33. Tsai, C. L., and Barondeau, D. P. (2010) Human frataxin is an allosteric switch that activates the Fe-S cluster biosynthetic complex, *Biochemistry 49*, 9132-9139.

34. Prischi, F., Konarev, P. V., Iannuzzi, C., Pastore, C., Adinolfi, S., Martin, S. R., Svergun, D. I., and Pastore, A. (2010) Structural bases for the interaction of frataxin with the central components of iron-sulphur cluster assembly, *Nat Commun 1*, 95.

35. Kim, J. H., Tonelli, M., and Markley, J. L. (2011) Disordered form of the scaffold protein IscU is the substrate for iron-sulfur cluster assembly on cysteine desulfurase, *Proc Natl Acad Sci USA 109*, 454-459.

36. Ramelot, T. A., Cort, J. R., Goldsmith-Fischman, S., Kornhaber, G. J., Xiao, R., Shastry, R., Acton, T. B., Honig, B., Montelione, G. T., and Kennedy, M. A. (2004) Solution NMR structure of the iron-sulfur cluster assembly protein U (IscU) with zinc bound at the active site, *J Mol Biol 344*, 567-583.

37. Foster, M. W., Mansy, S. S., Hwang, J., Penner-Hahn, J. E., Surerus, K. K., and Cowan, J. A. (2000) A mutant human IscU protein contains a stable [2Fe2S]2+ center of possible functional significance, *J Am Chem Soc 122*, 6805-6806.

38. Unciuleac, M.-C., Chandramouli, K., Naik, S., Mayer, S., Huynh, B. H., Johnson, M., and Dean, D. R. (2007) In vitro activation of apo-aconitase using a [4Fe-4S]

cluster-loaded form of the IscU [Fe-S] cluster scaffolding protein, *Biochemistry 46*, 6812-6821.

39. Wu, G., Mansy, S. S., Wu, S.-p., Surerus, K. K., Foster, M. W., and Cowan, J. A. (2002) Characterization of an iron-sulfur cluster assembly protein (ISU1) from *Schizosaccharomyces pombe*, *Biochemistry 41*, 5024-5032.

40. Kim, J. H., Tonelli, M., Kim, T., and Markley, J. L. (2012) Three-dimensional structure and determinants of stability of the iron-sulfur cluster scaffold protein IscU from *Escherichia coli*, *Biochemistry 51*, 5557-5563.

41. Krebs, C., Agar, J., Smith, A. D., Frazzon, J., Dean, D. R., Huynh, B. H., and Johnson, M. (2001) IscA, an alternate scaffold for Fe-S cluster biosynthesis, *Biochemistry 40*, 14069-14080.

42. Ollagnier de Choudens, S., Mattioli, T., Takahashi, Y., and Fontecave, M. (2001) Iron-sulfur cluster assembly: characterization of IscA and evidence for a specific and functional complex with ferredoxin, *J Biol Chem 276*, 22604-22607.

43. Ding, H., Clark, R. J., and Ding, B. (2004) IscA mediates iron delivery for assembly of iron-sulfur clusters in IscU under the limited accessible free iron conditions, *J Biol Chem 279*, 37499-37504.

44. Ding, H., Yang, J., Coleman, L. C., and Yeung, S. (2007) Distinct iron binding property of two putative iron donors for the iron-sulfur cluster assembly: IscA and the bacterial frataxin ortholog CyaY under physiological and oxidative stress conditions, *J Biol Chem 282*, 7997-8004.

45. Ding, H., and Clark, R. J. (2004) Characterization of iron binding in IscA, an ancient iron-sulphur cluster assembly protein, *Biochem J 379*, 433-440.

46. Yoon, T., and Cowan, J. A. (2004) Frataxin-mediated iron delivery to ferrochelatase in the final step of heme biosynthesis, *J Biol Chem 279*, 25943-25946.

47. Lill, R. (2009) Function and biogenesis of iron-sulphur proteins, *Nature 460*, 831-838.

48. Bonomi, F., Iametti, S., Morleo, A., Ta, D., and Vickery, L. (2008) Studies on the mechanism of catalysis of iron-sulfur cluster transfer from IscU[2Fe2S] by HscA/HscB chaperones, *Biochemistry 47*, 12795-12801.

49. F ry, A., Tonelli, M., Ta, D., Cornilescu, G., Vickery, L., and Markley, . (2008) Solution structure of the iron-sulfur cluster cochaperone HscB and its binding surface for the iron-sulfur assembly scaffold protein IscU, *Biochemistry 47*, 9394-9404.

50. Kim, J., Füzéry, A., Tonelli, M., Ta, D., Westler, W., Vickery, L., and Markley, J. (2009) Structure and dynamics of the iron-sulfur cluster assembly scaffold protein IscU and its interaction with the cochaperone HscB, *Biochemistry 48*, 6062-6071.

51. Cupp-Vickery, J., Peterson, J. C., Ta, D. T., and Vickery, L. (2004) Crystal structure of the molecular chaperone HscA substrate binding domain complexed with the IscU recognition peptide ELPPVKIHC, *J Mol Biol 342*, 1265-1278.

52. Hoff, K. G., Cupp-Vickery, J., and Vickery, L. (2003) Contributions of the LPPVK motif of the iron-sulfur template protein IscU to interactions with the Hsc66-Hsc20 chaperone system, *J Biol Chem 278*, 37582-37589.

53. Hoff, K. G., Ta, D. T., Tapley, T. L., Silberg, J. J., and Vickery, L. (2002) Hsc66 substrate specificity is directed toward a discrete region of the iron-sulfur cluster template protein IscU, *J Biol Chem 277*, 27353-27359.

54. Tapley, T. L., Cupp-Vickery, J., and Vickery, L. (2006) Structural determinants of HscA peptide-binding specificity, *Biochemistry 45*, 8058-8066.

55. Pierik, A. J., Netz, D. J. A., and Lill, R. (2009) Analysis of iron-sulfur protein maturation in eukaryotes, *Nat Protoc 4*, 753-766.

56. Stehling, O., Elsässer, H.-P., Brückel, B., Muhlenhoff, U., and Lill, R. (2004) Iron-sulfur protein maturation in human cells: evidence for a function of frataxin, *Hum Mol Genet 13*, 3007-3015.

57. Lill, R., and Mühlenhoff, U. (2008) Maturation of Iron-Sulfur Proteins in Eukaryotes: Mechanisms, Connected Processes, and Diseases, *Annu Rev Biochem 77*, 22.21-22.32.

58. Sharma, A. K., Pallesen, L. J., Spang, R. J., and Walden, W. E. (2010) The cytosolic iron sulfur cluster assembly (CIA) system: factors, mechanism, and relevance to cellular iron regulation, *J Biol Chem 285*, 26745-26751.

59. Stehling, O., Netz, D. J. A., Niggemeyer, B., Rösser, R., Eisenstein, R., Puccio, H., Pierik, A. J., and Lill, R. (2008) The human CIA component huNbp35 is essential for both cytosolic iron-sulfur protein assembly and iron homeostasis, *Mol Cell Biol 28*, 5517-5528.

60. Pandey, A., Yoon, H., Lyver, E. R., Dancis, A., and Pain, D. (2011) Isd11p protein activates the mitochondrial cysteine desulfurase nfs1p protein, *J Biol Chem 286*, 38242-38252.

61. Adam, A. C., Bornhövd, C., Prokisch, H., Neupert, W., and Hell, K. (2006) The Nfs1 interacting protein Isd11 has an essential role in Fe/S cluster biogenesis in mitochondria, *EMBO J 25*, 174-183.

62. Wiedemann, N., Urzica, E., Guiard, B., Muller, H., Lohaus, C., Meyer, H. E., Ryan, M. T., Meisinger, C., Muhlenhoff, U., Lill, R., and Pfanner, N. (2006) Essential role of Isd11 in mitochondrial iron-sulfur cluster synthesis on Isu scaffold proteins, *EMBO J 25*, 184-195.

63. Schmucker, S., and Puccio, H. (2010) Understanding the molecular mechanisms of Friedreich Ataxia to develop therapeutic approaches, *Hum Mol Genet 19*, R103-R110.

64. Schmucker, S., Martelli, A., Colin, F., Page, A., Wattenhofer-Donzé, M., Reutenauer, L., and Puccio, H. (2011) Mammalian frataxin: an essential function for cellular viability through an interaction with a preformed ISCU/NFS1/ISD11 iron-sulfur assembly complex, *PLoS ONE 6*, e16199.

65. Siegel, L. M. (1965) A direct microdetermination for sulfide, *Anal Biochem 11*, 126-132.

66. Tsai, C. L., Bridwell-Rabb, J., and Barondeau, D. P. (2011) Friedreich's Ataxia variants I154F and W155R diminish frataxin-based activation of the iron-sulfur cluster assembly complex, *Biochemistry 50*, 6478-6487.

67. Bridwell-Rabb, J., Barondeau, David P. (2012) Frataxin based regulation of the iron-sulfur cluster assembly complex. PhD dissertation. Texas A&M University.

68. Yoon, H., Golla, R., Lesuisse, E., Pain, J., Donald, J., Lyver, E. R., Pain, D., and Dancis, A. (2011) Mutation in Fe-S scaffold Isu bypasses frataxin deletion, *Biochem J 441*, 473-480.

69. Tsai, C.-L. (2011) Structural and functional studies on human mitochondrial iron-sulfur cluster assembly biogenesis. PhD dissertation. Texas A&M University.

70. Adinolfi, S., Iannuzzi, C., Prischi, F., Pastore, C., Iametti, S., Martin, S., Bonomi, F., and Pastore, A. (2009) Bacterial frataxin CyaY is the gatekeeper of iron-sulfur cluster formation catalyzed by IscS, *Nat Struct Mol Biol 16*, 390-396.

71. Uhrigshardt, H., Singh, A., Kovtunovych, G., Ghosh, M., and Rouault, T. A. (2010) Characterization of the human HSC20, an unusual DnaJ type III protein, involved in iron-sulfur cluster biogenesis, *Hum Mol Genet 19*, 3816-3834.

72. Shan, Y., Napoli, E., and Cortopassi, G. A. (2007) Mitochondrial frataxin interacts with ISD11 of the NFS1/ISCU complex and multiple mitochondrial chaperones, *Hum Mol Genet 16*, 929-941.

73. Santos, R., Lefevre, S., Sliwa, D., Seguin, A., Camadro, J.-M., and Lesuisse, E. (2010) Friedreich's Ataxia: molecular mechanisms, redox considerations and therapeutic opportunities, *Antioxid Redox Signal 13*, 651-690.

74. Leidgens, S., De Smet, S., and Foury, F. (2010) Frataxin interacts with Isu1 through a conserved tryptophan in its beta-sheet, *Hum Mol Genet 19*, 276-286.

75. Bridwell-Rabb, J., Winn, A. M., and Barondeau, D. P. (2011) Structure-function analysis of Friedreich’s ataxia mutants reveals determinants for frataxin binding and activation of the Fe-S assembly complex, *Biochemistry 50*, 7265-7274.

76. Richardson, D. R., Lane, D. J. R., Becker, E. M., Huang, M. L.-H., Whitnall, M., Rahmanto, Y. S., Sheftel, A. D., and Ponka, P. (2010) Mitochondrial iron trafficking and the integration of iron metabolism between the mitochondrion and cytosol, *Proc Natl Acad Sci USA 107*, 1-8.

77. Tsai, C.-L., and Barondeau, D. P. (2010) Human frataxin is an allosteric switch that activates the Fe-S cluster biosynthetic complex, *Biochemistry 49*, 9132-9139.

78. Bridwell-Rabb, J., Iannuzzi, C., Pastore, A., and Barondeau, D. P. (2012) Effector role reversal during evolution: the case of frataxin in Fe-S cluster biosynthesis, *Biochemistry 51*, 2506-2514.

79. Kollberg, G., Tulinius, M., Melberg, A., Darin, N., Andersen, O., Holmgren, D., Oldfors, A., and Holme, E. (2009) Clinical manifestation and a new ISCU mutation in iron-sulphur cluster deficiency myopathy, *Brain 132*, 2170-2179.

80. Mochel, F., Knight, M. A., Tong, W.-H., Hernandez, D., Ayyad, K., Taivassalo, T., Andersen, P. M., Singleton, A., Rouault, T. A., Fischbeck, K. H., and Haller, R. G. (2008) Splice mutation in the iron-sulfur cluster scaffold protein ISCU causes myopathy with exercise intolerance, *Am J Hum Genet 82*, 652-660.

81. Crooks, D. R., Jeong, S. Y., Tong, W. H., Ghosh, M. C., Olivierre, H., Haller, R. G., and Rouault, T. A. (2012) Tissue specificity of a human mitochondrial disease: differntiation-enhanced mis-splicing of the Fe-S scaffold gene ISCU renders patient cells more sensitive to oxidative stress in ISCU myopathy, *J Biol Chem 287*, 40119-40130.

82. Fontecave, M., and Ollagnier de Choudens, S. (2008) Iron-sulfur cluster biosynthesis in bacteria: mechanisms of cluster assembly and transfer, *Arch Biochem Biophys 474*, 226-237.

83. Zheng, L., White, R. H., Cash, V. L., and Dean, D. R. (1994) Mechanism for the desulfurization of L-cysteine catalyzed by the nifS gene product, *Biochemistry 33*, 4714-4720.

84. Zheng, L., White, R. H., Cash, V. L., Jack, R. F., and Dean, D. R. (1993) Cysteine desulfurase activity indicates a role for NIFS in metallocluster biosynthesis, *Proc Natl Acad Sci USA 90*, 2754-2758.

85. Hoff, K. G., Silberg, J. J., and Vickery, L. (2000) Interaction of the iron-sulfur cluster assembly protein IscU with the Hsc66/Hsc20 molecular chaperone system of *Escherichia coli*, *Proc Natl Acad Sci USA 97*, 7790-7795.

86. Kaiser, J. T., Clausen, T., Bourenkow, G., Bartunik, H., Steinbacher, S., and Huber, R. (2000) Crystal structure of a NifS-like protein from Thermotoga maritima: implications for iron sulphur cluster assembly, *J Mol Biol 297*, 451-464.

87. Paris, Z., Changmai, P., Rubio, M. A. T., Zikova, A., Stuart, K. D., Alfonzo, J. D., and Lukes, J. (2010) The Fe/S cluster assembly protein Isd11 is essential for tRNA thiolation in *Trypanosoma brucei*, *J Biol Chem 285,* 22394-22402.

88. Richards, T. A., and van der Giezen, M. (2006) Evolution of the Isd11-IscS complex reveals a single alpha-proteobacterial endosymbiosis for all eukaryotes, *Mol Biol Evol 23*, 1341-1344.

89. Adinolfi, S., Rizzo, F., Masino, L., Nair, M., Martin, S. R., Pastore, A., and Temussi, P. A. (2004) Bacterial IscU is a well folded and functional single domain protein, *Eur J Biochem 271*, 2093-2100.

90. Liu, J., Oganesyan, N., Shin, D.-H., Jancarik, J., Yokota, H., Kim, R., and Kim, S.-H. (2005) Structural characterization of an iron-sulfur cluster assembly protein IscU in a zinc-bound form, *Proteins 59*, 875-881.

91. Shimomura, Y., Wada, K., Fukuyama, K., and Takahashi, Y. (2008) The asymmetric trimeric architecture of [2Fe-2S] IscU: implications for its scaffolding during iron-sulfur cluster biosynthesis, *J Mol Biol 383*, 133-143.

92. Iannuzzi, C., Adinolfi, S., Howes, B. D., Garcia-Serres, R., Clémancey, M., Latour, J.-M., Smulevich, G., and Pastore, A. (2011) The role of CyaY in iron sulfur cluster assembly on the *E. coli* IscU scaffold protein, *PLoS ONE 6*, e21992.

93. Tsai, C.-L., Bridwell-Rabb, J., and Barondeau, D. P. (2011) Friedreich's ataxia variants I154F and W155R diminish frataxin-based activation of the iron-sulfur cluster assembly complex, *Biochemistry 50*, 6478-6487.

94. Nair, M., Adinolfi, S., Kelly, G., Frenkiel, T. A., and Pastore, A. (2003) NMR assignment of the 1H, 15N and 13C resonances of the *E. coli* frataxin orthologue, CyaY, *J Biomol NMR 27*, 403-404.

95. He, Y., Alam, S., Proteasa, S. V., Zhang, Y., Lesuisse, E., Dancis, A., and Stemmler, T. L. (2004) Yeast frataxin solution structure, iron binding, and ferrochelatase interaction, *Biochemistry 43*, 16254-16262.

96. Karlberg, T., Schagerlöf, U., Gakh, O., Park, S., Ryde, U., Lindahl, M., Leath, K., Garman, E., Isaya, G., and Al-Karadaghi, S. (2006) The structures of frataxin oligomers reveal the mechanism for the delivery and detoxification of iron, *Structure 14*, 1535-1546.

97. Lee, M., Cho, S., Yang, J., Song, H., and Suh, S. (2000) Crystallization and preliminary X-ray crystallographic analysis of *Escherichia coli* CyaY, a structural homologue of human frataxin, *Acta Crystallogr D Biol Crystallogr 56*, 920-921.

98. Pastore, C., Franzese, M., Sica, F., Temussi, P., and Pastore, A. (2007) Understanding the binding properties of an unusual metal-binding protein - a study of bacterial frataxin, *FEBS J 274*, 4199-4210.

99. Cho, S., Lee, M., Yang, J., Lee, J., Song, H., and Suh, S. (2000) Crystal structure of *Escherichia coli* CyaY protein reveals a previously unidentified fold for the evolutionarily conserved frataxin family, *Proc Natl Acad Sci USA 97*, 8932-8937.

100. Dhe-Paganon, S., Shigeta, R., Chi, Y. I., Ristow, M., and Shoelson, S. E. (2000) Crystal structure of human frataxin, *J Biol Chem 275*, 30753-30756.

101. Fang, J., Rand, K. D., Silva, M. C., Wales, T. E., Engen, J. R., and Beuning, P. J. (2010) Conformational dynamics of the *Escherichia coli* DNA polymerase manager proteins UmuD and UmuD', *J Mol Biol 398*, 40-53.

102. Wales, T. E., and Engen, J. R. (2006) Partial unfolding of diverse SH3 domains on a wide timescale, *J Mol Biol 357*, 1592-1604.

103. Houde, D., Arndt, J., Domeier, W., Berkowitz, S., and Engen, J. R. (2009) Characterization of IgG1 conformation and conformational dynamics by hydrogen/deuterium exchange mass spectrometry, *Anal Chem 81*, 5966.

104. Houde, D., Peng, Y., Berkowitz, S. A., and Engen, J. R. (2010) Post-translational modifications differentially affect IgG1 conformation and receptor binding, *Mol Cell Proteomics 9*, 1716-1728.

105. Chalmers, M. J., Busby, S. A., Pascal, B. D., He, Y., Hendrickson, C. L., Marshall, A. G., and Griffin, P. R. (2006) Probing protein ligand interactions by automated hydrogen/deuterium exchange mass spectrometry, *Anal Chem 78*, 1005-1014.

106. Zhang, J., Chalmers, M. J., Stayrook, K. R., Burris, L. L., Garcia-Ordonez, R. D., Pascal, B. D., Burris, T. P., Dodge, J. A., and Griffin, P. R. (2010) Hydrogen/deuterium exchange reveals distinct agonist/partial agonist receptor dynamics within vitamin D receptor/retinoid X receptor heterodimer, *Structure 18*, 1332-1341.

107. Akashi, S., and Takio, K. (2000) Characterization of the interface structure of enzyme-inhibitor complex by using hydrogen-deuterium exchange and electrospray ionization Fourier transform ion cyclotron resonance mass spectrometry, *Protein Sci 9*, 2497-2505.

108. Kiselar, J. G., Datt, M., Chance, M. R., and Weiss, M. A. (2011) Structural analysis of proinsulin hexamer assembly by hydroxyl radical footprinting and computational modeling, *J Biol Chem 286*, 43710-43716.

109. Oztug Durer, Z. A., Kamal, J. K., Benchaar, S., Chance, M. R., and Reisler, E. (2011) Myosin binding surface on actin probed by hydroxyl radical footprinting and site-directed labels, *J Mol Biol 414*, 204-216.

110. Orban, T., Jastrzebska, B., Gupta, S., Wang, B., Miyagi, M., Chance, M. R., and Palczewski, K. (2012) Conformational dynamics of activation for the pentameric

complex of dimeric G protein-coupled receptor and heterotrimeric G protein, *Structure 20*, 826-840.

111. Padayatti, P. S., Wang, L., Gupta, S., Orban, T., Sun, W., Salom, D., Jordan, S. R., Palczewski, K., and Chance, M. R. (2013) A hybrid structural approach to analyze ligand binding by the serotonin type 4 receptor (5-HT4), *Mol Cell Proteomics 12*, 1259-1271.

112. Gupta, S., Sullivan, M., Toomey, J., Kiselar, J., and Chance, M. R. (2007) The beamline X28C of the Center for Synchrotron Biosciences: a national resource for biomolecular structure and dynamics experiments using synchrotron footprinting, *J Synchrotron Radiat 14*, 233-243.

113. Kiselar, J. G., Maleknia, S. D., Sullivan, M., Downard, K. M., and Chance, M. R. (2002) Hydroxyl radical probe of protein surfaces using synchrotron X-ray radiolysis and mass spectrometry, *Int J Radiat Biol 78*, 101-114.

114. Wang, L., and Chance, M. R. Structural mass spectrometry of proteins using hydroxyl radical based protein footprinting, *Anal Chem 83*, 7234-7241.

115. Kiselar, J. G., and Chance, M. R. Future directions of structural mass spectrometry using hydroxyl radical footprinting, *J Mass Spectrom 45*, 1373-1382.

116. Kiefer, F., Arnold, K., Kunzli, M., Bordoli, L., and Schwede, T. (2009) The SWISS-MODEL Repository and associated resources, *Nuc Acids Res 37*, D387-392.

117. Arnold, K., Bordoli, L., Kopp, J., and Schwede, T. (2006) The SWISS-MODEL workspace: a web-based environment for protein structure homology modelling, *Bioinformatics 22*, 195-201.

118. Peitsch, M. C., Wells, T. N., Stampf, D. R., and Sussman, J. L. (1995) The Swiss-3DImage collection and PDB-Browser on the world-wide web, *Trends Biochem Sci 20*, 82-84.

119. Takamoto, K., and Chance, M. R. (2006) Radiolytic protein footprinting with mass spectrometry to probe the structure of macromolecular complexes, *Annu Rev Biophys Biomol Struct 35*, 251-276.

120. Dubinina, E. E., Gavrovskaya, S. V., Kuzmich, E. V., Leonova, N. V., Morozova, M. G., Kovrugina, S. V., and Smirnova, T. A. (2002) Oxidative modification of proteins: oxidation of tryptophan and production of dityrosine in purified proteins using Fenton's system, *Biochemistry. Biokhimiia 67*, 343-350.

121. Shcherbakova, I., Mitra, S., Beer, R. H., and Brenowitz, M. (2006) Fast fenton footprinting: a laboratory-based method for the time-resolved analysis of DNA, RNA and proteins, *Nuc Acids Res 34*, e48.

122. Hambly, D. M., and Gross, M. L. (2005) Laser flash photolysis of hydrogen peroxide to oxidize protein solvent-accessible residues on the microsecond timescale, *J Am Soc Mass Spectrom 16*, 2057-2063.

123. Konermann, L., Stocks, B. B., Pan, Y., and Tong, X. (2010) Mass spectrometry combined with oxidative labeling for exploring protein structure and folding, *Mass Spectrom Rev 29*, 651-667.

124. Stocks, B. B., and Konermann, L. (2009) Structural characterization of short-lived protein unfolding intermediates by laser-induced oxidative labeling and mass spectrometry, *Anal Chem 81*, 20-27.

125. Charvatova, O., Foley, B. L., Bern, M. W., Sharp, J. S., Orlando, R., and Woods, R. J. (2008) Quantifying protein interface footprinting by hydroxyl radical oxidation and molecular dynamics simulation: application to galectin-1, *J Am Soc Mass Spectrom 19*, 1692-1705.

126. Maleknia, S. D., Brenowitz, M., and Chance, M. R. (1999) Millisecond radiolytic modification of peptides by synchrotron X-rays identified by mass spectrometry, *Anal Chem 71*, 3965-3973.

127. Xu, G., Takamoto, K., and Chance, M. R. (2003) Radiolytic modification of basic amino acid residues in peptides: probes for examining protein-protein interactions, *Anal Chem 75*, 6995-7007.

128. Gau, B. C., Sharp, J. S., Rempel, D. L., and Gross, M. L. (2009) Fast photochemical oxidation of protein footprints faster than protein unfolding, *Anal Chem 81*, 6563-6571.

129. Kiselar, J. G., Datt, M., Chance, M. R., and Weiss, M. A. Structural analysis of proinsulin hexamer assembly by hydroxyl radical footprinting and computational modeling, *J Biol Chem 286*, 43710-43716.

130. Bedekovics, Gajdos, Kispal, G., and Isaya, G. (2007) Partial conservation of functions between eukaryotic frataxin and the *Escherichia coli* frataxin homolog CyaY, *FEMS Yeast Res 7*, 1276-1284.

131. Bridwell-Rabb, J., Winn, A. M., and Barondeau, D. P. (2011) Structure-function analysis of Friedreich's ataxia mutants reveals determinants for frataxin binding and activation of the Fe-S assembly complex, *Biochemistry 50*, 7265-7274.

132. Shi, Y., Ghosh, M. C., Tong, W. H., and Rouault, T. A. (2009) Human ISD11 is essential for both iron-sulfur cluster assembly and maintenance of normal cellular iron homeostasis, *Hum Mol Genet 18*, 3014-3025.

133. Xu, G., and Chance, M. R. (2005) Radiolytic modification and reactivity of amino acid residues serving as structural probes for protein footprinting, *Anal Chem 77*, 4549-4555.

134. Stemmler, T. L., Lesuisse, E., Pain, D., and Dancis, A. (2010) Frataxin and mitochondrial Fe-S cluster biogenesis, *J Biol Chem 285*, 26737-26743.

135. Urbina, H. D., Silberg, J. J., Hoff, K. G., and Vickery, L. (2001) Transfer of sulfur from IscS to IscU during Fe/S cluster assembly, *J Biol Chem 276*, 44521-44526.

136. Marelja, Z., Stöcklein, W., Nimtz, M., and Leimkühler, S. (2008) A novel role for human Nfs1 in the cytoplasm: Nfs1 acts as a sulfur donor for MOCS3, a protein involved in molybdenum cofactor biosynthesis, *J Biol Chem 283*, 25178-25185.

137. Yoon, T., and Cowan, J. A. (2003) Iron-sulfur cluster biosynthesis. Characterization of frataxin as an iron donor for assembly of [2Fe-2S] clusters in ISU-type proteins, *J Am Chem Soc 125*, 6078-6084.

138. Yoon, T., Dizin, E., and Cowan, J. A. (2007) N-terminal iron-mediated self-cleavage of human frataxin: regulation of iron binding and complex formation with target proteins, *J Biol Inorg Chem 12*, 535-542.

139. Lakowicz, J. R. (2006) Fluorescence Anisotropy, In *Principles of Fluorescence Spectroscopy, 3rd edition*, pp 353-382, Springer Science+Business Media, LLC, New York, NY.

140. Brownbridge, G. G., Lowe, P. N., Moore, K. J., Skinner, R. H., and Webb, M. R. (1993) Interaction of GTPase activating proteins (GAPs) with p21ras measured by a novel fluorescence anisotropy method. Essential role of Arg-903 of GAP in activation of GTP hydrolysis on p21ras, *J Biol Chem 268*, 10914-10919.

141. Titolo, S., Brault, K., Majewski, J., White, P. W., and Archambault, J. (2003) Characterization of the minimal DNA binding domain of the human papillomavirus e1 helicase: fluorescence anisotropy studies and characterization of a dimerization-defective mutant protein, *J Virol 77*, 5178-5191.

142. Watson, H. M., Gentry, L. E., Asuru, A. P., Wang, Y., Marcus, S., and Busenlehner, L. S. (2012) Heterotrifunctional chemical cross-linking mass spectrometry confirms physical interaction between human frataxin and ISU, *Biochemistry 51*, 6889-6891.

143. Correia, A., Pastore, C., Adinolfi, S., Pastore, A., and Gomes, C. (2008) Dynamics, stability and iron-binding activity of frataxin clinical mutants, *FEBS J 275*, 3680-3690.

144. Correia, A. R., Adinolfi, S., Pastore, A., and Gomes, C. M. (2006) Conformational stability of human frataxin and effect of Friedreich's ataxia-related mutations on protein folding, *Biochem J 398*, 605-611.

145. Musco, G., Stier, G., Kolmerer, B., Adinolfi, S., Martin, S., Frenkiel, T., Gibson, T., and Pastore, A. (2000) Towards a structural understanding of Friedreich's ataxia: the solution structure of frataxin, *Structure 8*, 695-707.

146. Correia, A., Ow, S., Wright, P., and Gomes, C. (2009) The conserved Trp155 in human frataxin as a hotspot for oxidative stress related chemical modifications, *Biochem Biophys Res Commun 390*, 1007-1011.

147. Beinert, H., Holm, R. H., and Münck, E. (1997) Iron-sulfur clusters: nature's modular, multipurpose structures, *Science 277*, 653-659.

148. Rouault, T. A. (2012) Biogenesis of iron-sulfur clusters in mammalian cells: new insights and relevance to human disease, *Dis Model Mech 5*, 155-164.

149. Biederbick, A., Stehling, O., Rösser, R., Niggemeyer, B., Nakai, Y., Elsässer, H.-P., and Lill, R. (2006) Role of human mitochondrial Nfs1 in cytosolic iron-sulfur protein biogenesis and iron regulation, *Mol Cell Biol 26*, 5675-5687.

150. Knieszner, H., Schilke, B., Dutkiewicz, R., D'Silva, P., Cheng, S., Ohlson, M., Craig, E. A., and Marszalek, J. (2005) Compensation for a defective interaction of the hsp70 ssq1 with the mitochondrial Fe-S cluster scaffold isu, *J Biol Chem 280*, 28966-28972.

151. Dutkiewicz, R., Schilke, B., Cheng, S., Knieszner, H., Craig, E. A., and Marszalek, J. (2004) Sequence-specific interaction between mitochondrial Fe-S scaffold protein Isu and Hsp70 Ssq1 is essential for their in vivo function, *J Biol Chem 279*, 29167-29174.

152. Luo, W.-I., Dizin, E., Yoon, T., and Cowan, J. A. (2010) Kinetic and structural characterization of human mortalin, *Protein Expr Purif 72*, 75-81.

153. Vickery, L., and Cupp-Vickery, J. (2007) Molecular chaperones HscA/Ssq1 and HscB/Jac1 and their roles in iron-sulfur protein maturation, *Crit Rev Biochem Mol Biol 42*, 95-111.

154. Song, J. Y., Marszalek, J., and Craig, E. A. (2012) Cysteine desulfurase Nfs1 and Pim1 protease control levels of Isu, the Fe-S cluster biogenesis scaffold, *Proc Natl Acad Sci U S A 109*, 10370-10375.

155. Huang, J., and Cowan, J. A. (2009) Iron-sulfur cluster biosynthesis: role of a semi-conserved histidine, *Chem Commun (Camb) 21*, 3071-3073.

156. Shimomura, Y., Wada, K., Fukuyama, K., and Takahashi, Y. (2008) The asymmetric trimeric architecture of [2Fe-2S] IscU: implications for its scaffolding during iron-sulfur cluster biosynthesis, *J Mol Biol 383*, 133-143.

157. Foster, M. W., Mansy, S. S., Hwang, J., Penner-Hahn, J. E., Surerus, K. K., and Cowan, J. A. (2000) A mutant human IscU protein contains a stable [2Fe-2S](2+) center of possible functional significance, *J Am Chem Soc 122*, 6805-6806.

158. Agar, J. N., Krebs, C., Frazzon, J., Huynh, B. H., Dean, D. R., and Johnson, M. K. (2000) IscU as a scaffold for iron-sulfur cluster biosynthesis: sequential assembly of [2Fe-2S] and [4Fe-4S] clusters in IscU, *Biochemistry 39*, 7856-7862.

159. Bonomi, F., Iametti, S., Morleo, A., Ta, D., and Vickery, L. E. (2011) Facilitated transfer of IscU-[2Fe2S] clusters by chaperone-mediated ligand exchange, *Biochemistry 50*, 9641-9650.

160. Tsai, C.-L., and Barondeau, D. P. (2010) Human frataxin is an allosteric switch that activates the Fe-S cluster biosynthetic complex, *Biochemistry 49*, 9132-9139.

161. Wang, T., and Craig, E. A. (2008) Binding of yeast frataxin to the scaffold for Fe-S cluster biogenesis, Isu, *J Biol Chem 283*, 12674-12679.

162. Bridwell-Rabb, J., Winn, A. M., and Barondeau, D. P. (2011) Structure-function analysis of Friedreich's ataxia mutants reveals determinants of frataxin binding and activation of the Fe-S assembly complex, *Biochemistry 50*, 7265-7274.

163. Tsai, C. L., Bridwell-Rabb, J., and Barondeau, D. P. (2011) Friedreich's ataxia variants I154F and W155R diminish frataxin-based activation of the iron-sulfur cluster assembly complex, *Biochemistry 50*, 6478-6487.

164. Cossee, M., Dürr, A., Schmitt, M., Dahl, N., Trouillas, P., Allinson, P., Kostrzewa, M., Nivelon-Chevallier, A., Gustavson, K. H., Kohlschütter, A., Müller, U., Mandel, J. L., Brice, A., Koenig, M., Cavalcanti, F., Tammaro, A., De Michele, G., Filla, A., Cocozza, S., Labuda, M., Montermini, L., Poirier, J., and Pandolfo, M. (1999) Friedreich's ataxia: point mutations and clinical presentation of compound heterozygotes, *Ann Neurol 45*, 200-206.

165. Drugge, U., Holmberg, M., Holmgren, G., Almay, B. G. L., Linderholm, H. (1995) Heredity myopathy with lactic acidosis, succinate dehydrogenase and aconitase deficiency in northern Sweden: a genealogical study, *J Med Genet 32*, 344-347.

166. Saha, P. P., Kumar, S. K. P., Srivastava, S., Sinha, D., Pareek, G., and D'Silva, P. (2014) Multiple cellular defects associated with a novel G50E ISCU mutation leads to development of mitochondrial myopathy, *J Biol Chem 289*, 10359-10377.

APPENDIX A

MASS SPECTRA USED TO GENERATE RATE CURVES TO DETERMINE PROTEIN-PROTEIN INTERACTIONS

The figures contained within in this appendix are the mass spectra used to generate the rate curves in Figure 2-5, Figure 2-6, Figure 2-8, Figure 2-9, and Figure 2-10. The mass spectra were collected on an Applied Biosystems 4800 MALDI TOF/TOF mass spectrometer and analyzed using Data Analysis software. The relative abundance of the peaks shown was used to calculate the percent unmodified (Equation 2-1), which was then used to determine the rate of modification for a particular peptide (Equation 2-2).

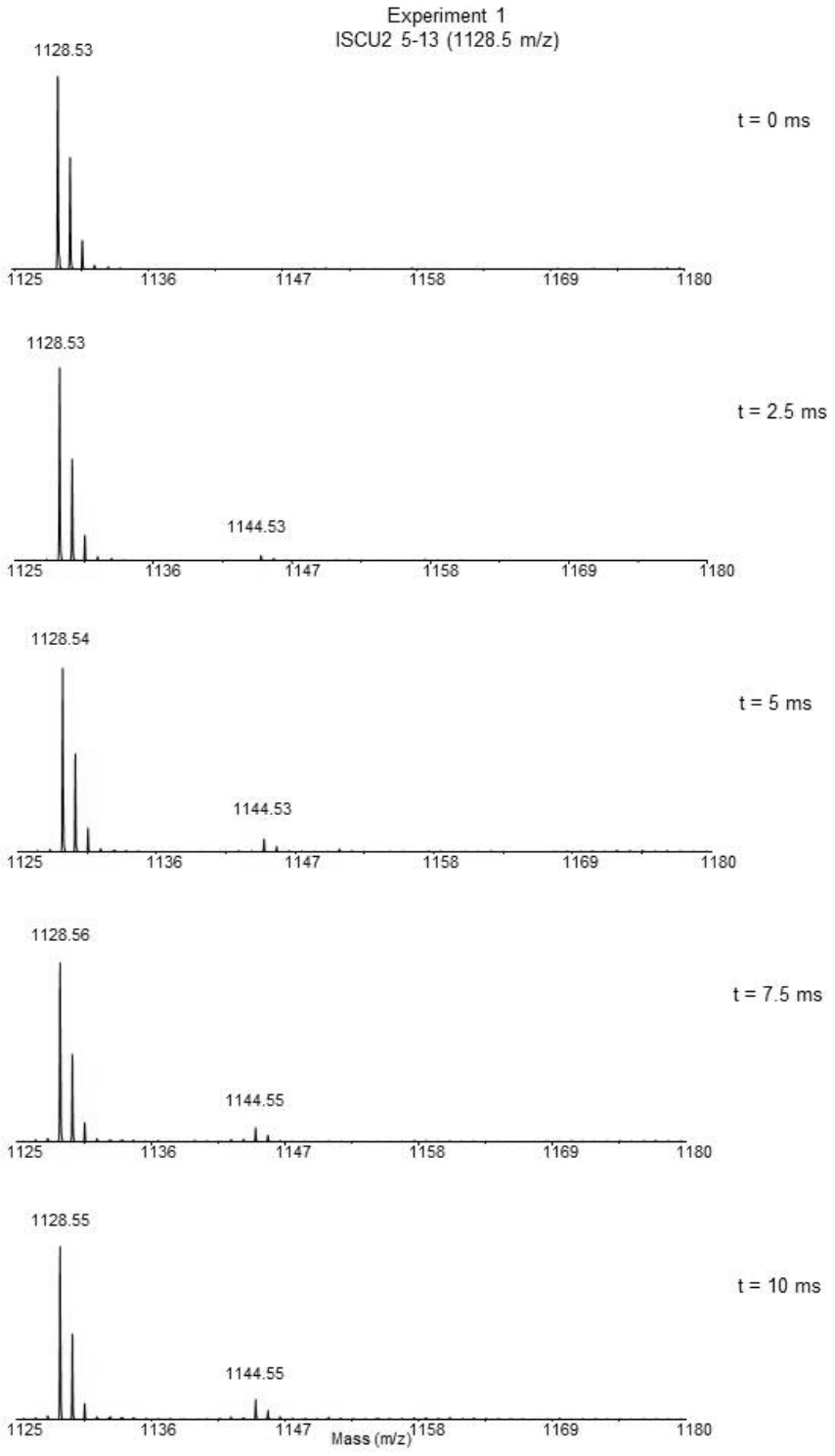

A-1. Mass spectra from ISCU2, Experiment 1 at various exposure time to hydroxyl radicals.

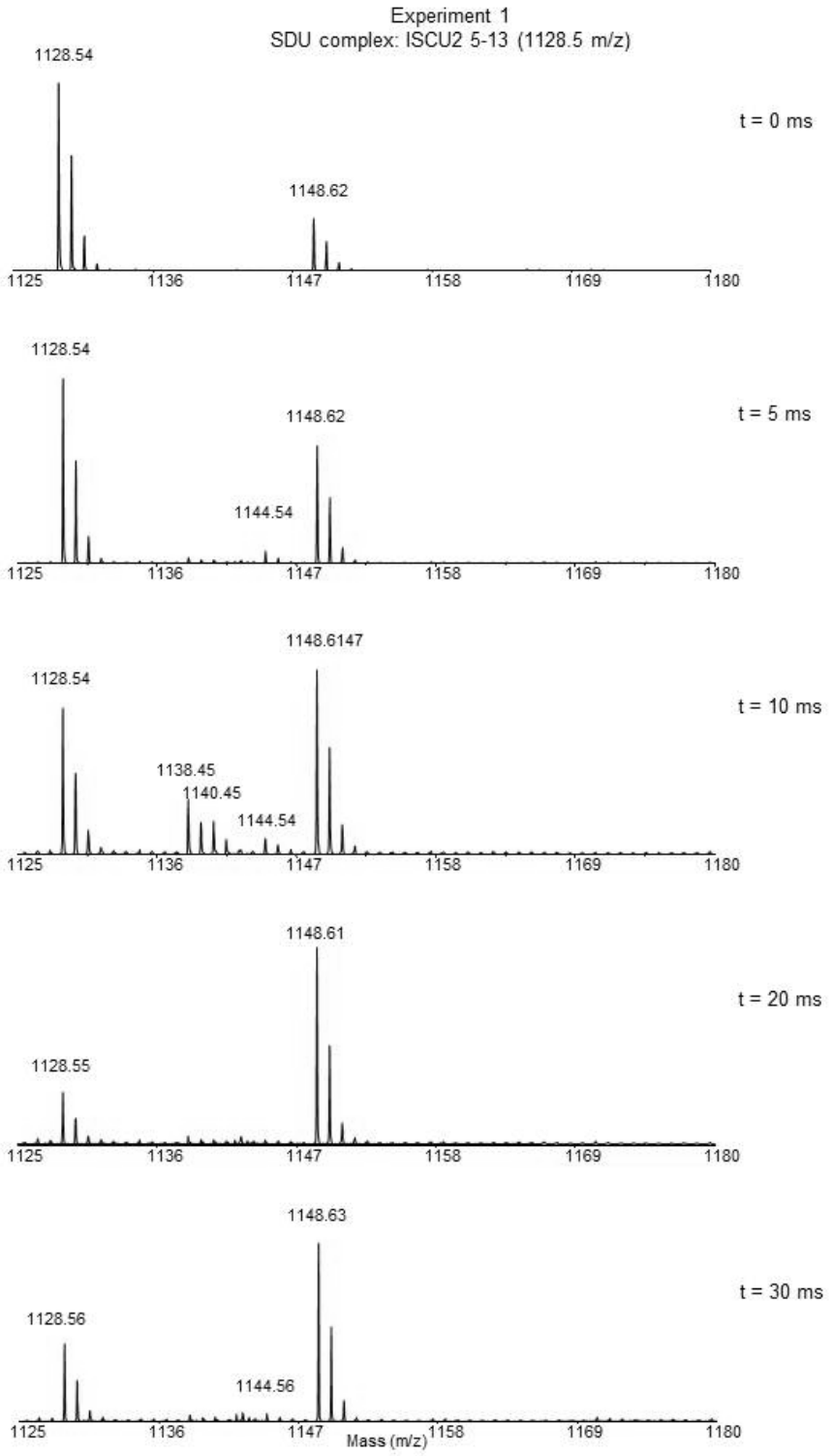

A-2. Mass spectra from SDU, Experiment 1 at various exposure time to hydroxyl radicals.

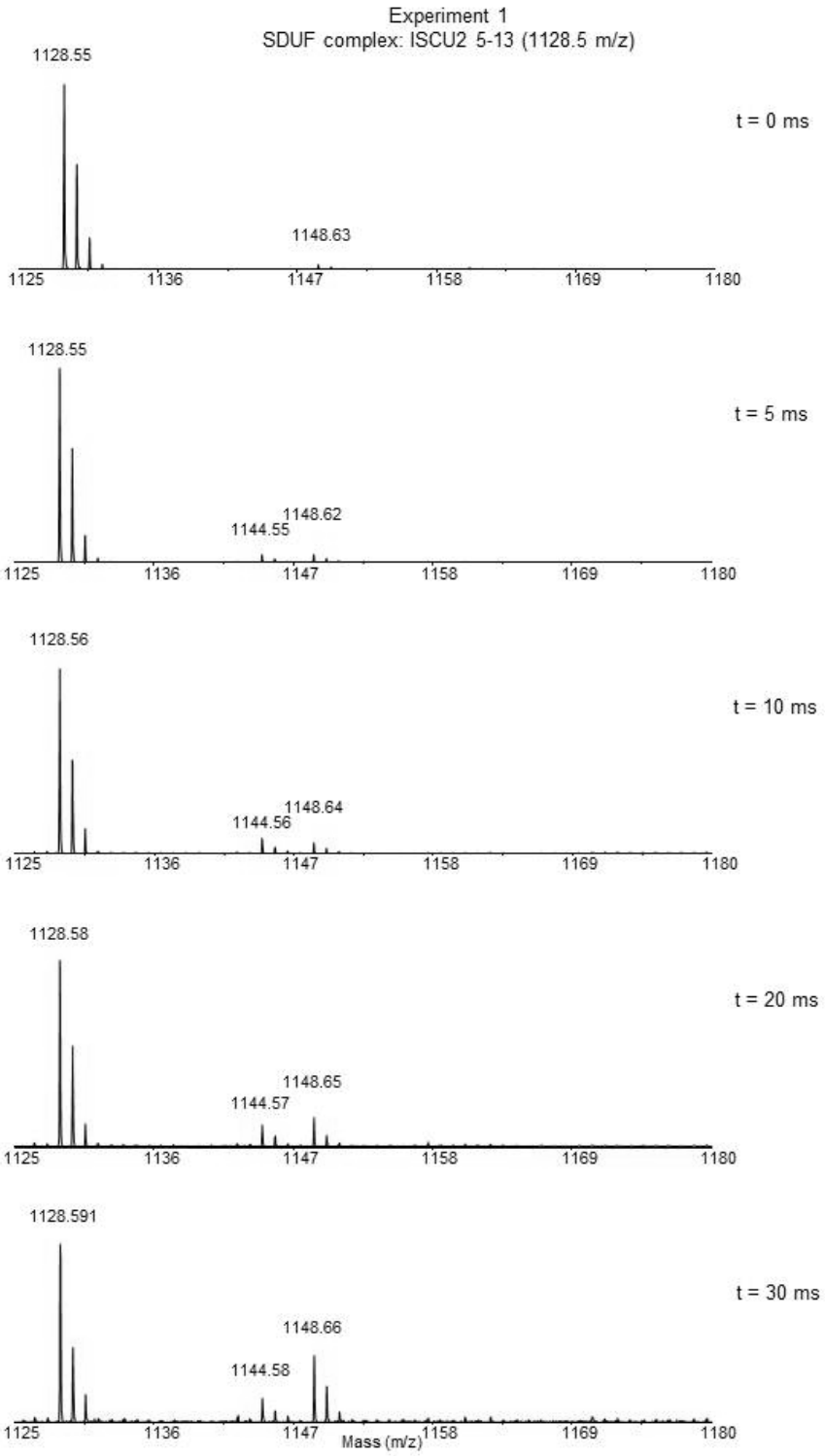

A-3. Mass spectra from SDUF, Experiment 1 at various exposure time to hydroxyl radicals.

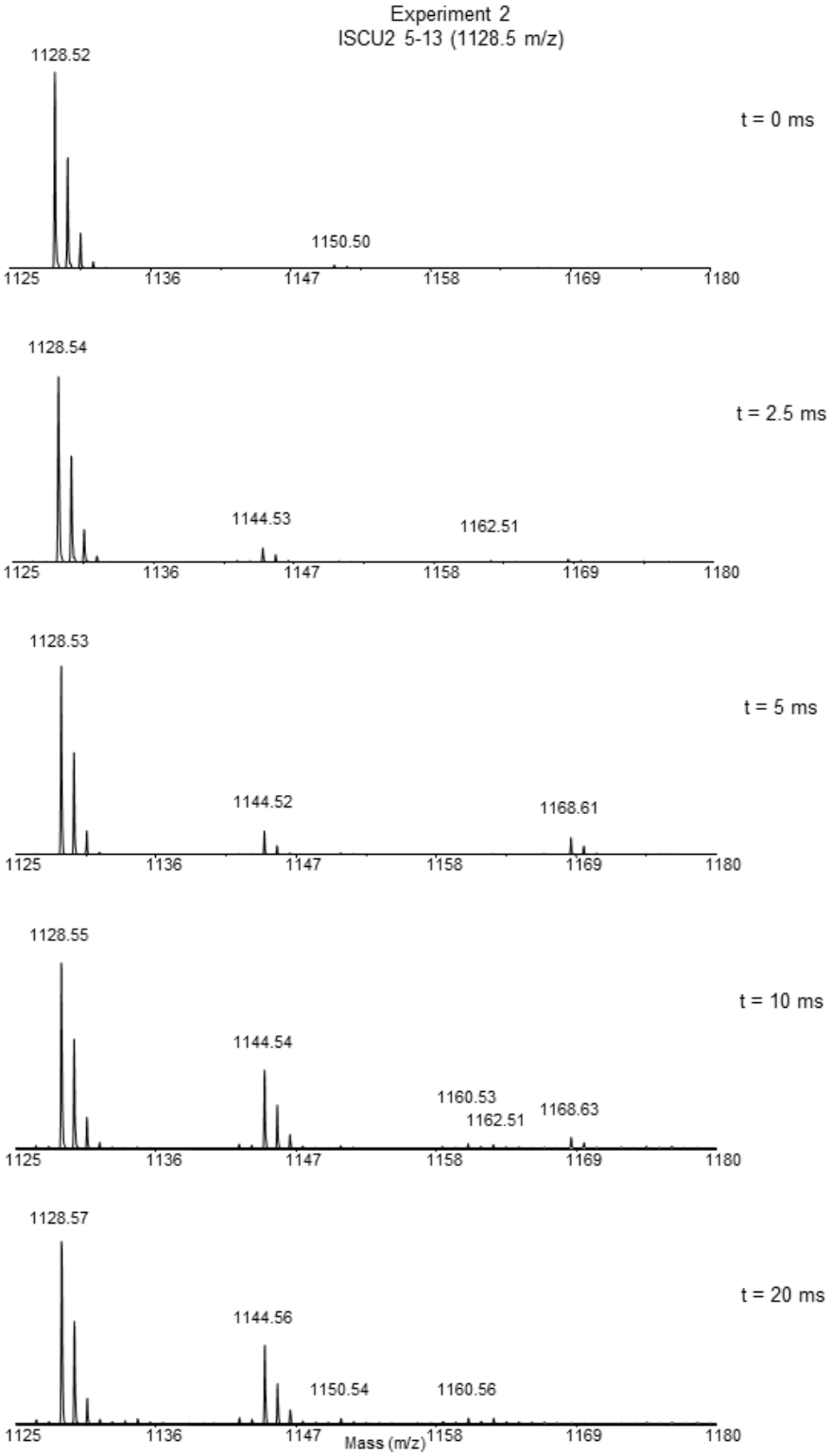

A-4. Mass spectra from ISCU2, Experiment 2 at various exposure time to hydroxyl radicals.

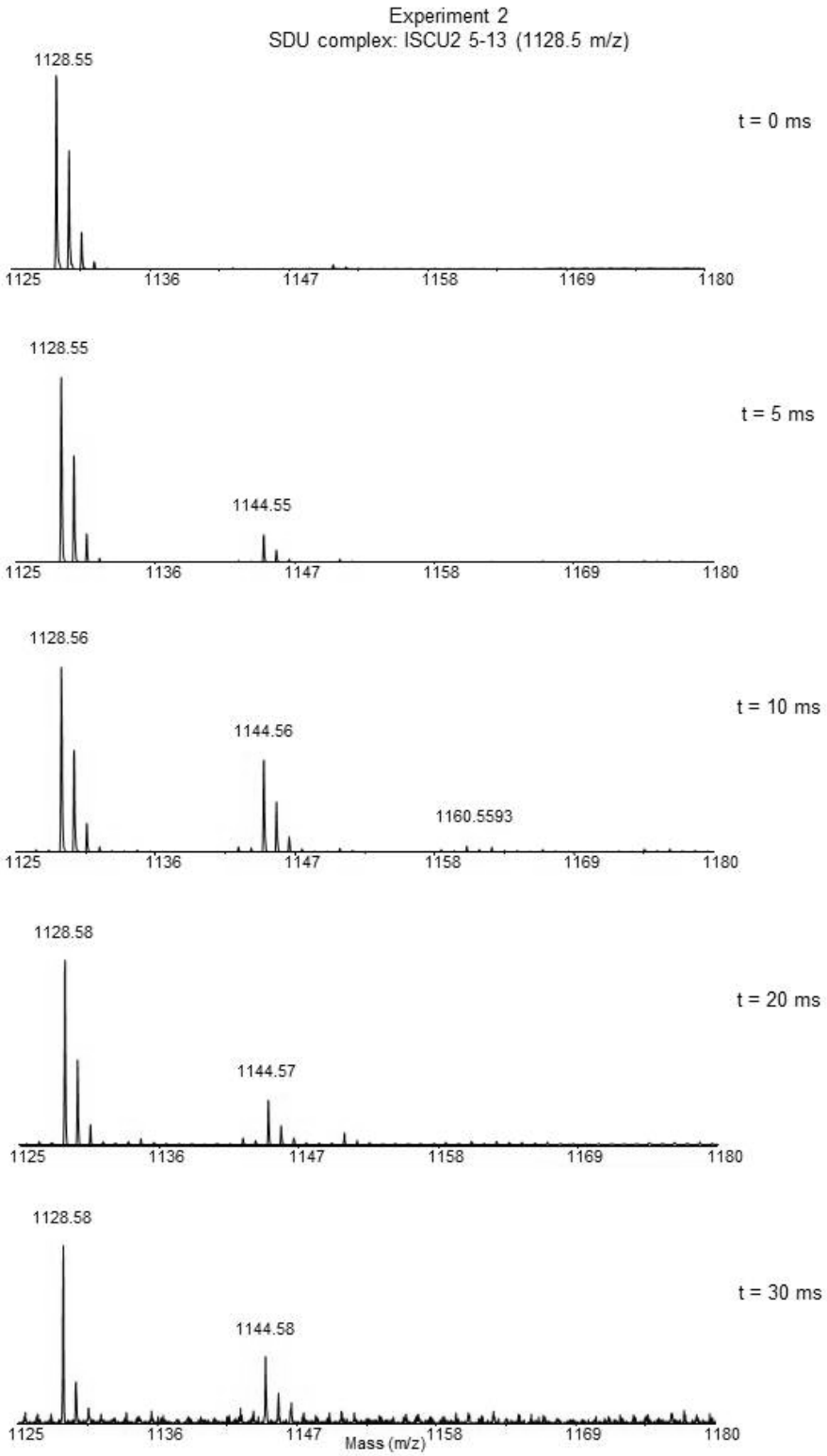

A-5. Mass spectra from SDU, Experiment 2 at various exposure time to hydroxyl radicals.

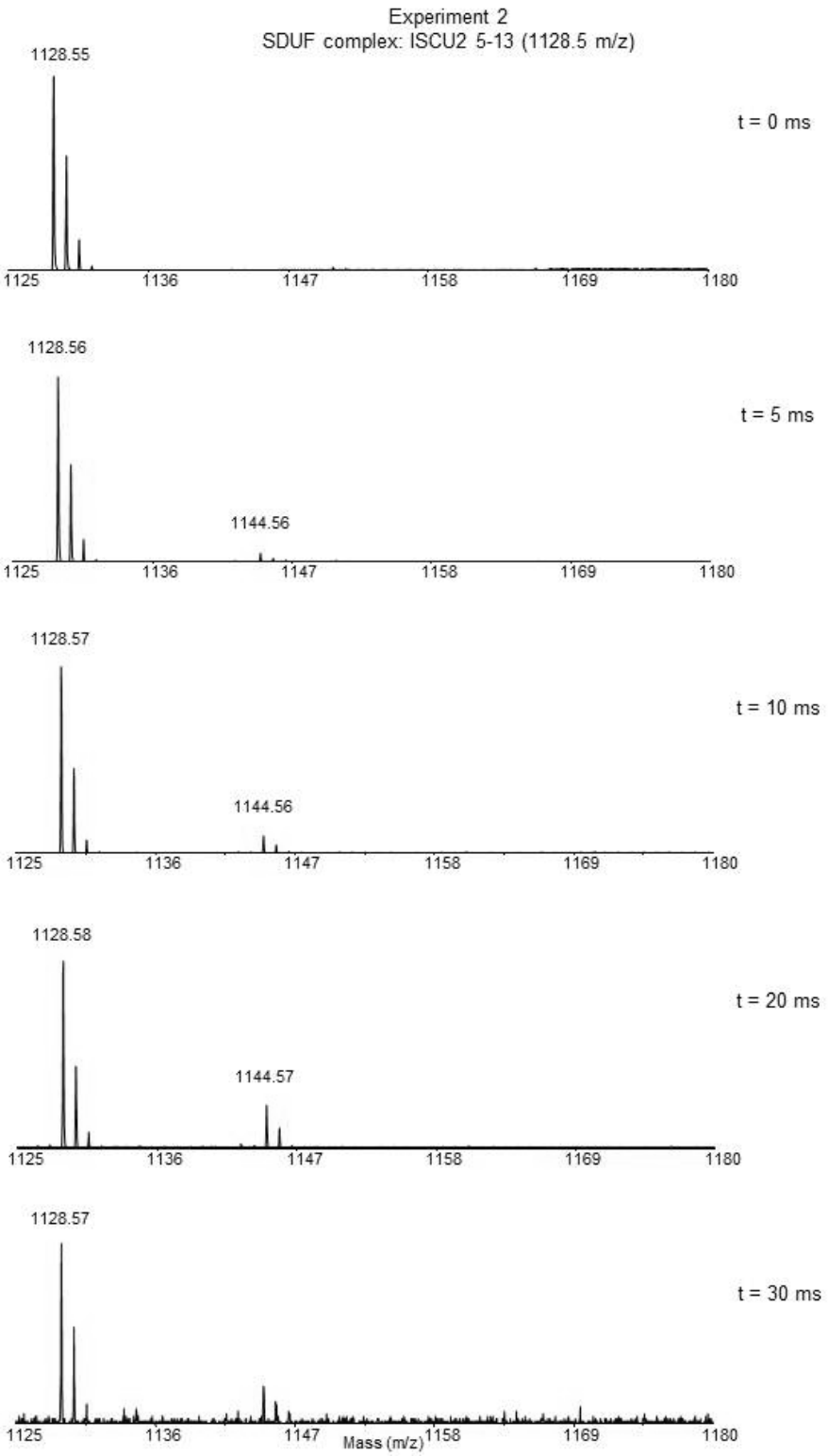

A-6. Mass spectra from SDUF, Experiment 2 at various exposure time to hydroxyl radicals.

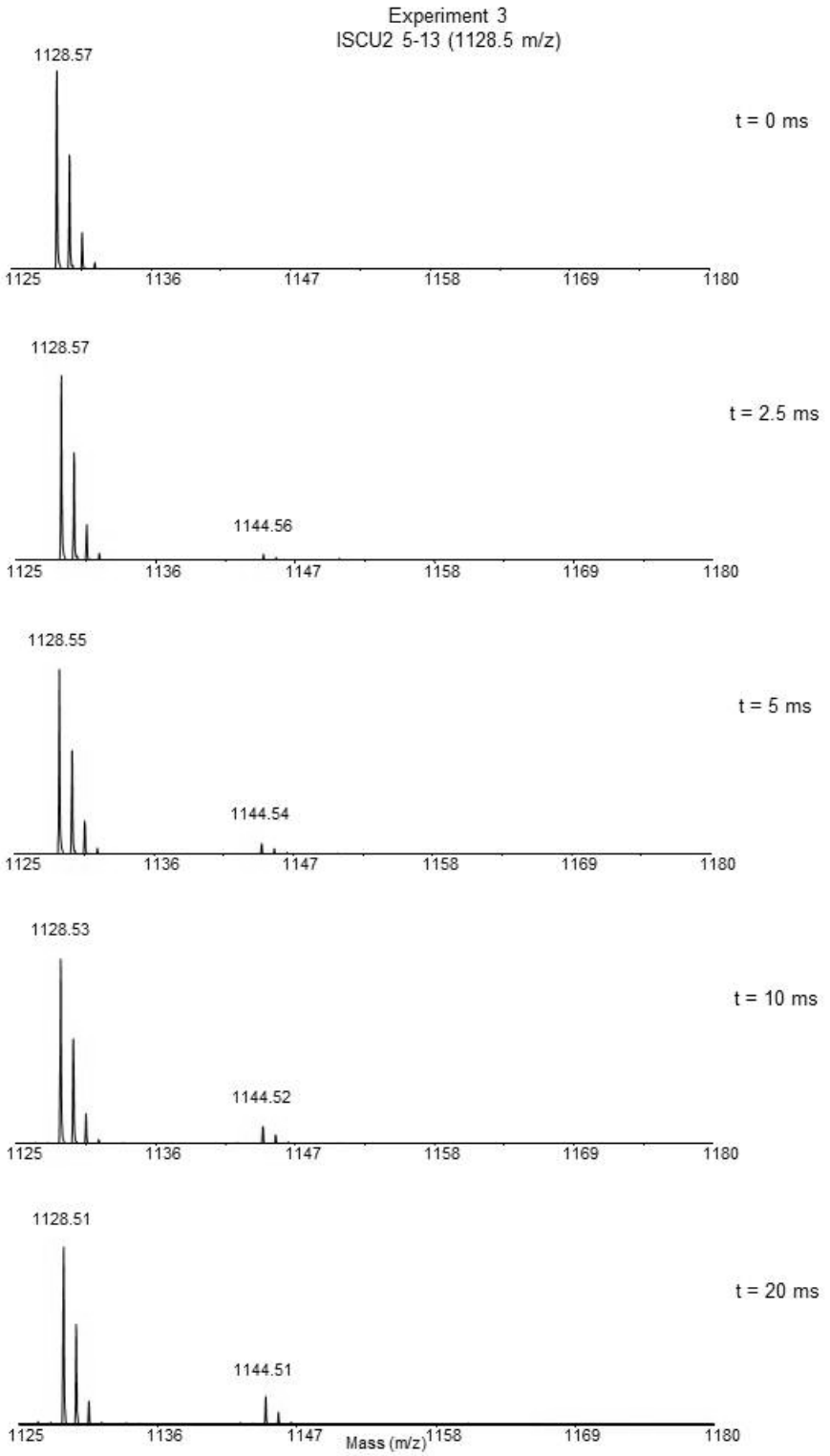

A-7. Mass spectra from ISCU2, Experiment 3 at various exposure time to hydroxyl radicals.

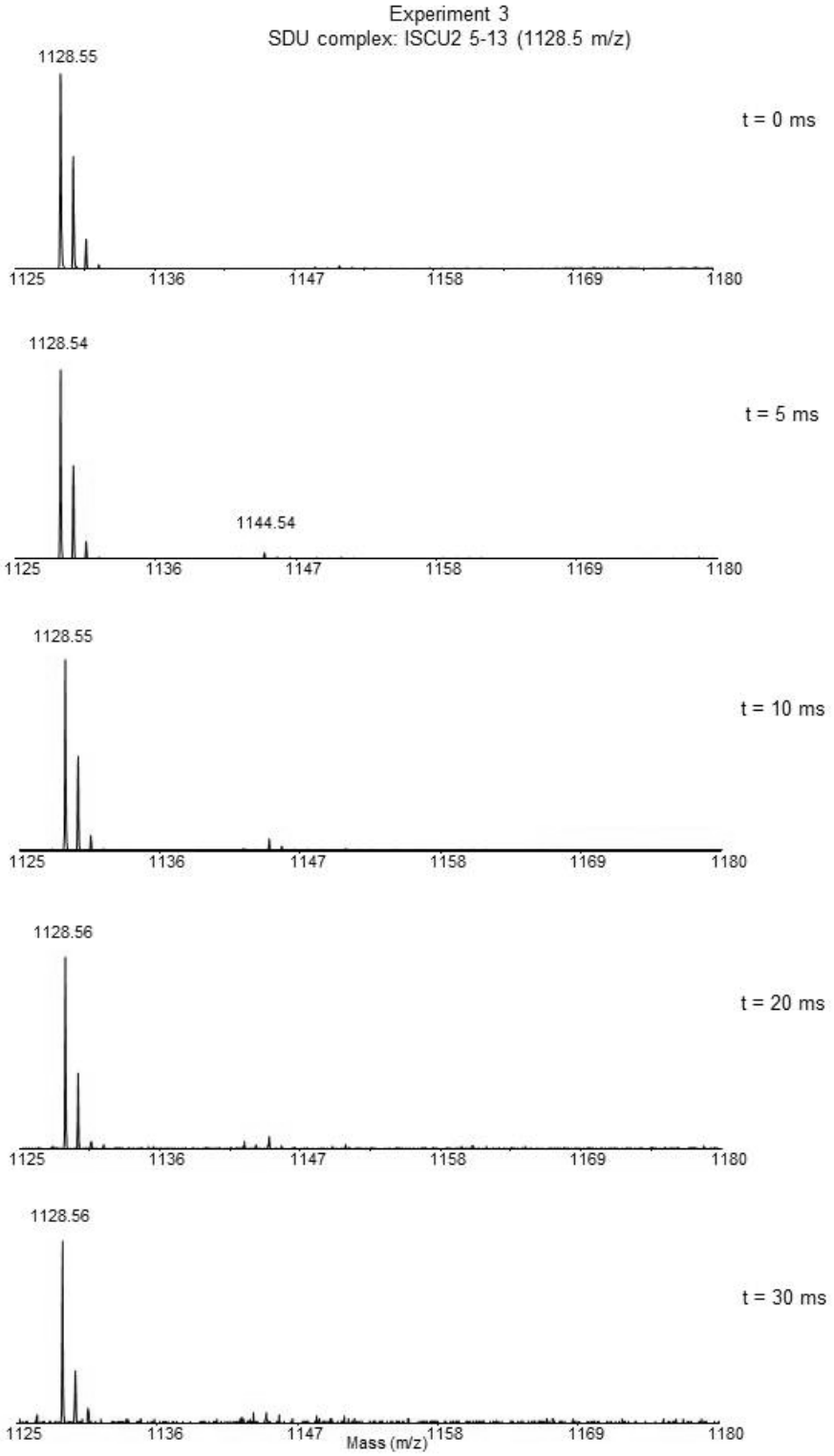

A-8. Mass spectra from SDU, Experiment 3 at various exposure time to hydroxyl radicals.

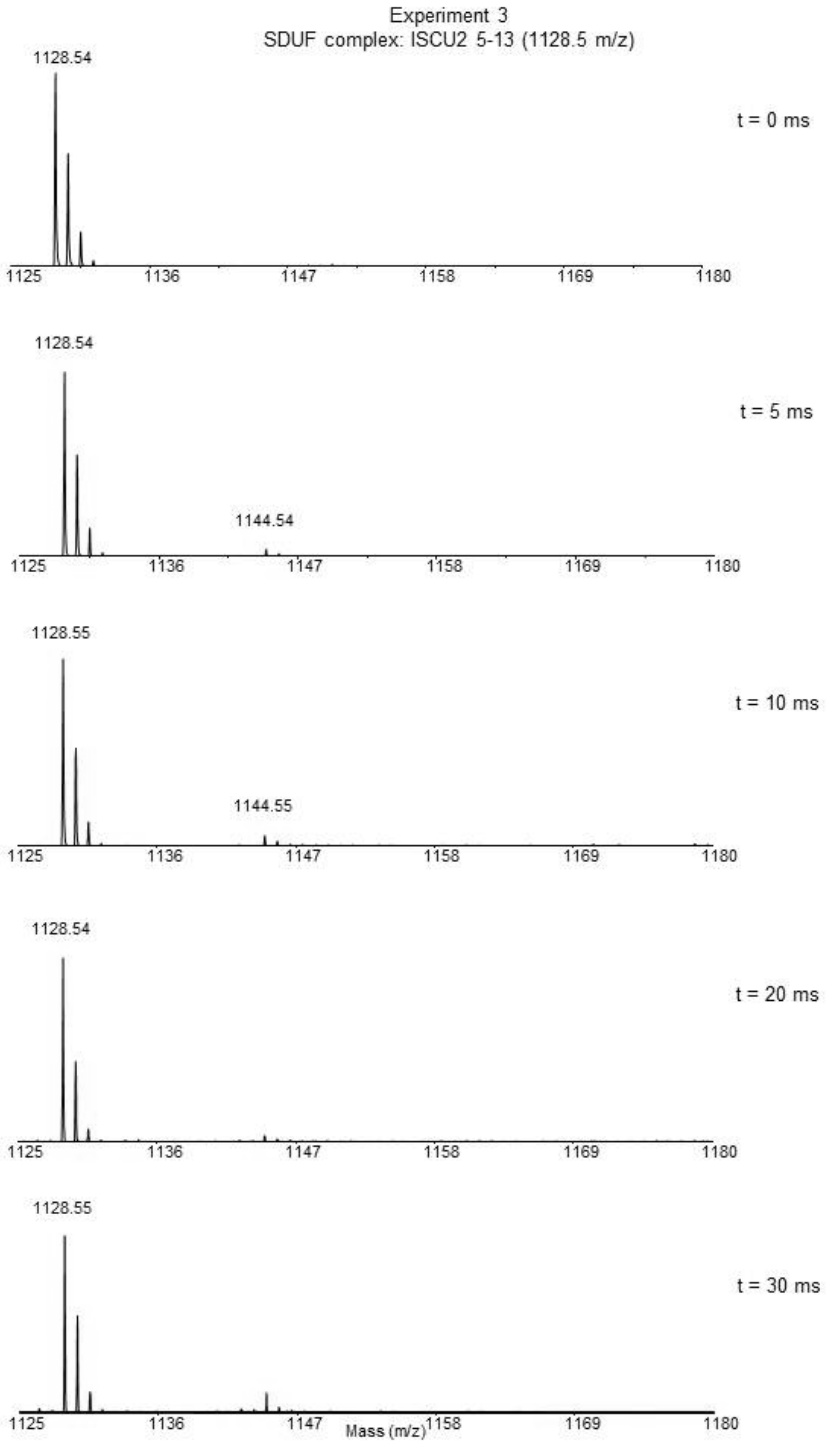

A-9. Mass spectra from SDUF, Experiment 3 at various exposure time to hydroxyl radicals.

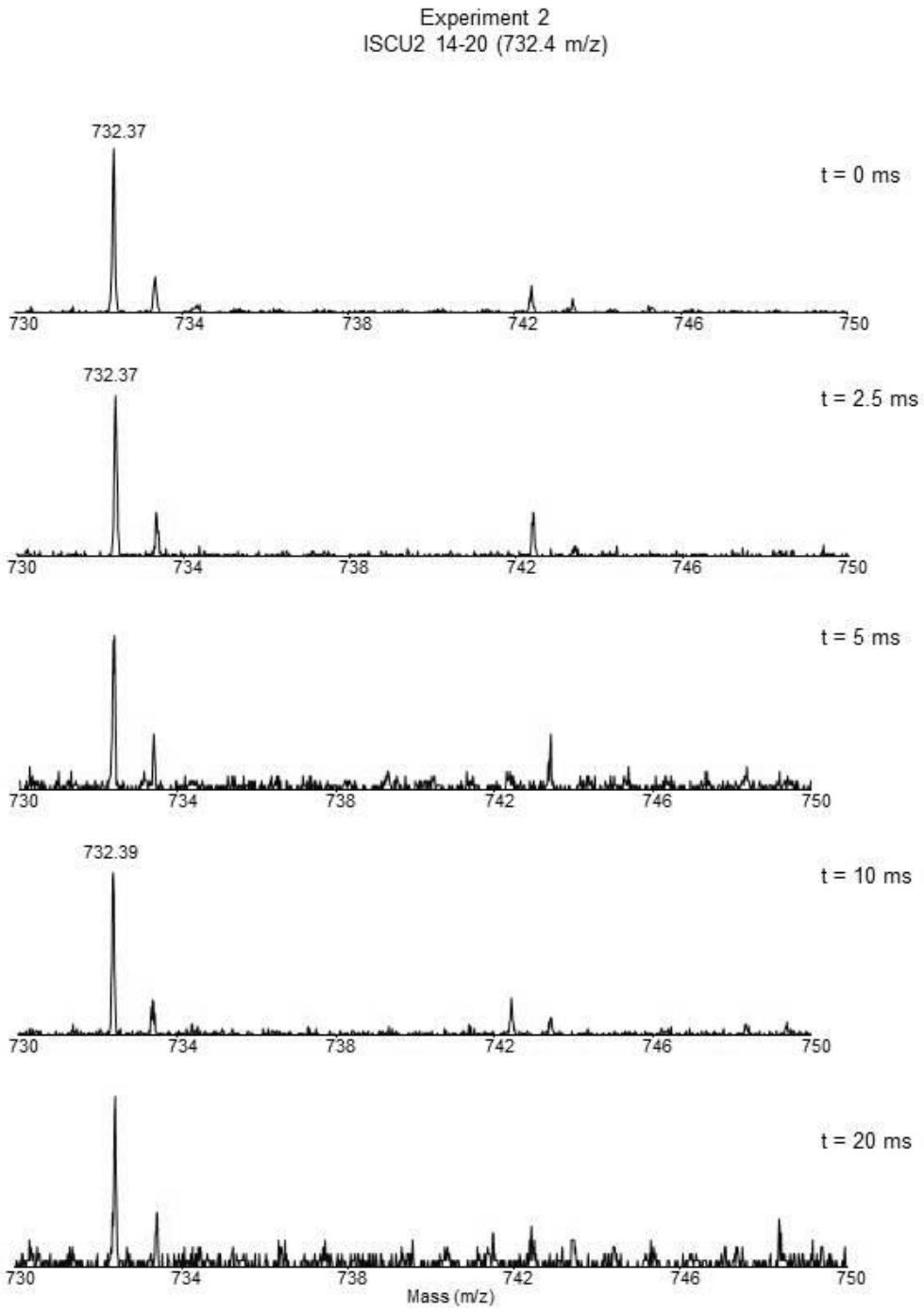

A-10. Mass spectra from ISCU2, Experiment 2 at various exposure time to hydroxyl radicals.

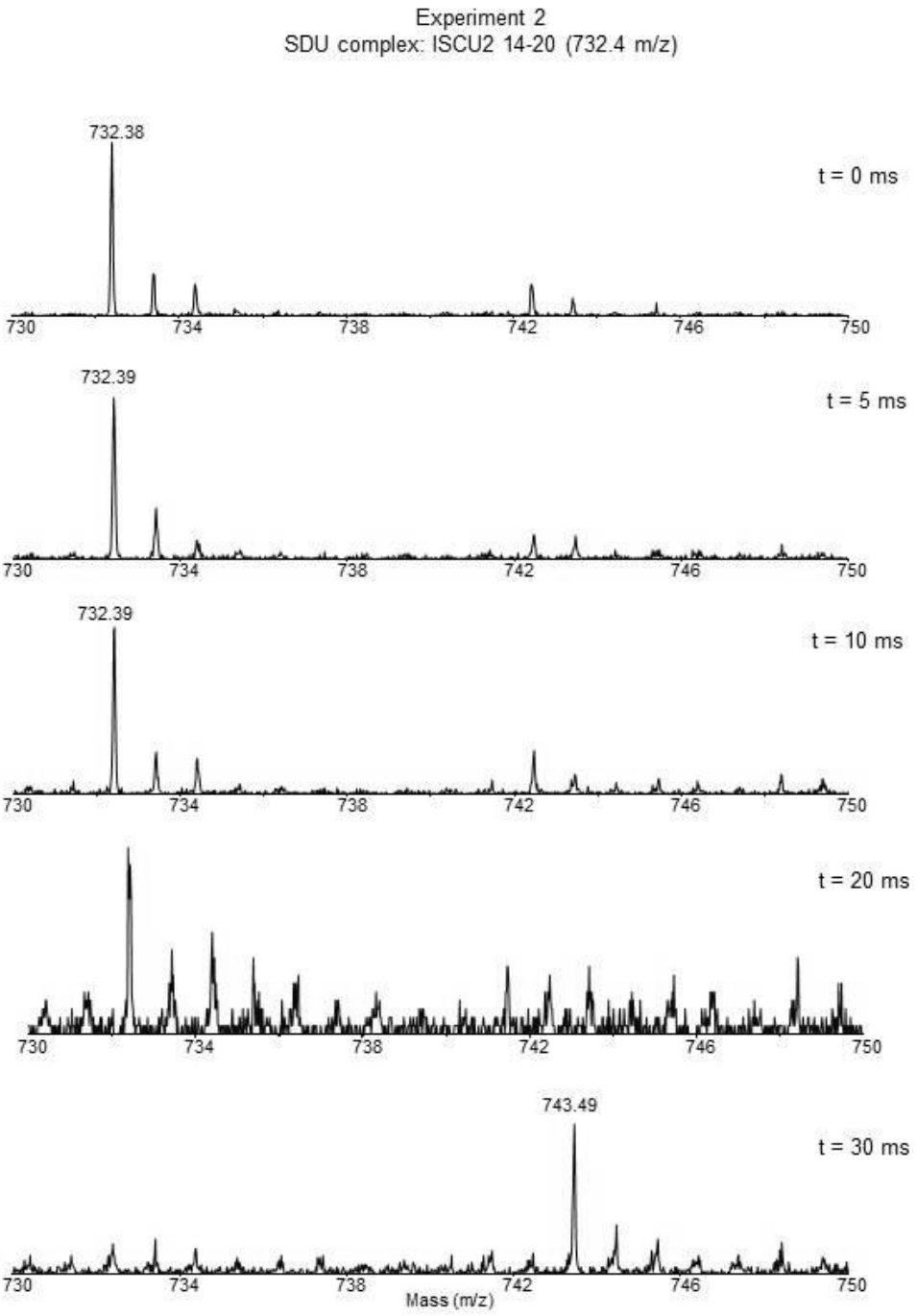

A-11. Mass spectra from SDU, Experiment 2 at various exposure time to hydroxyl radicals.

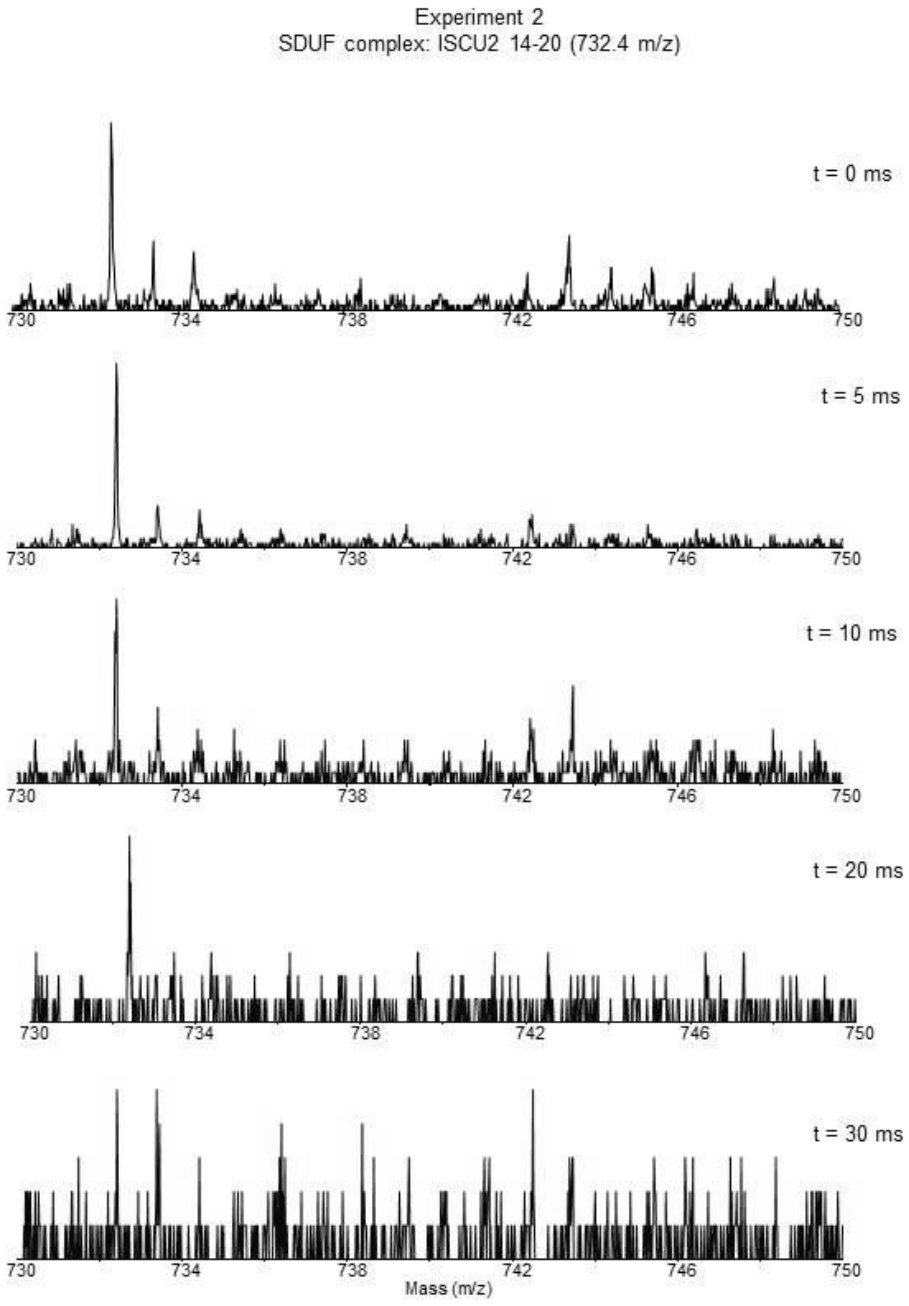

A-12. Mass spectra from SDUF, Experiment 2 at various exposure time to hydroxyl radicals.

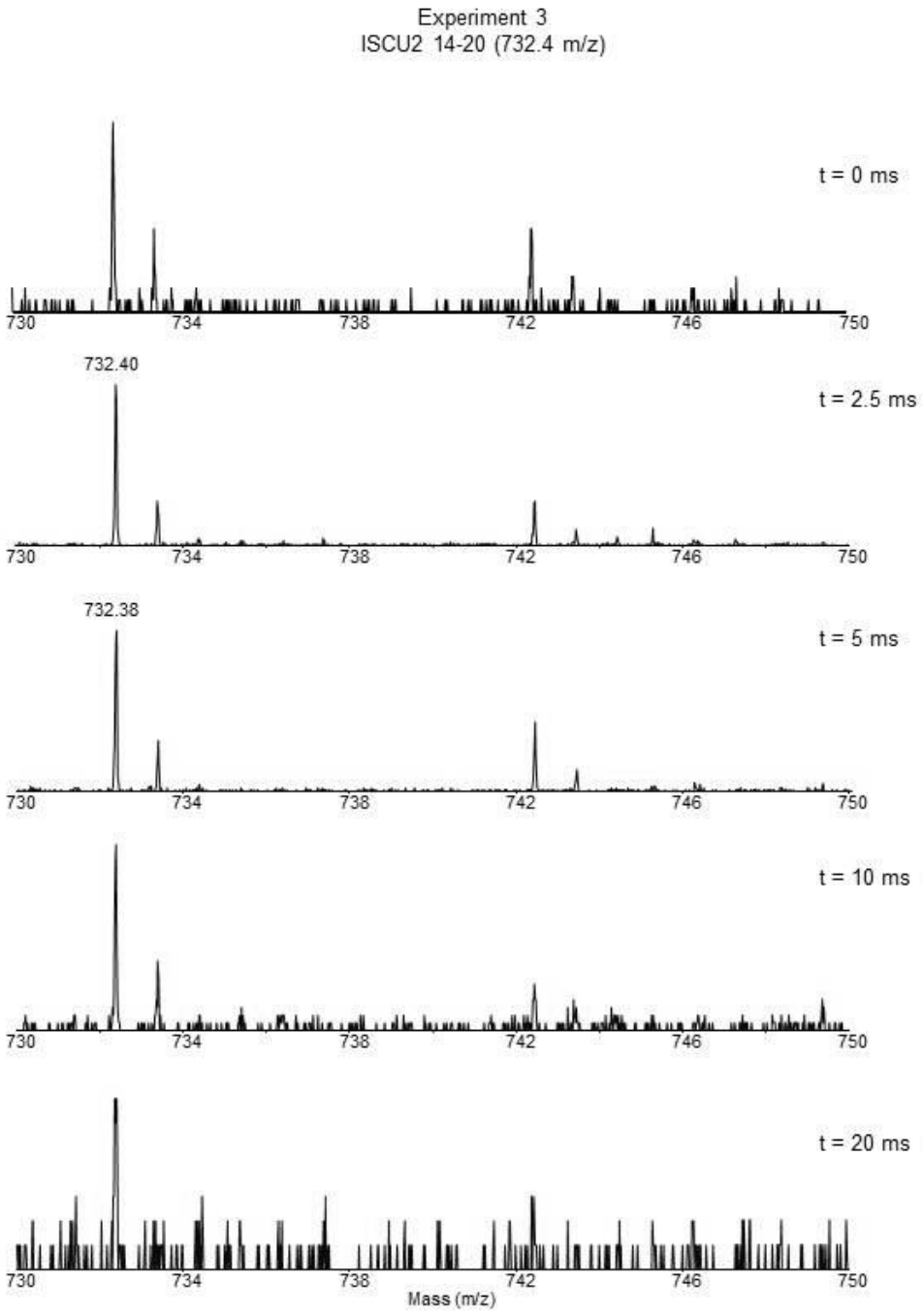

A-13. Mass spectra from ISCU2, Experiment 3 at various exposure time to hydroxyl radicals.

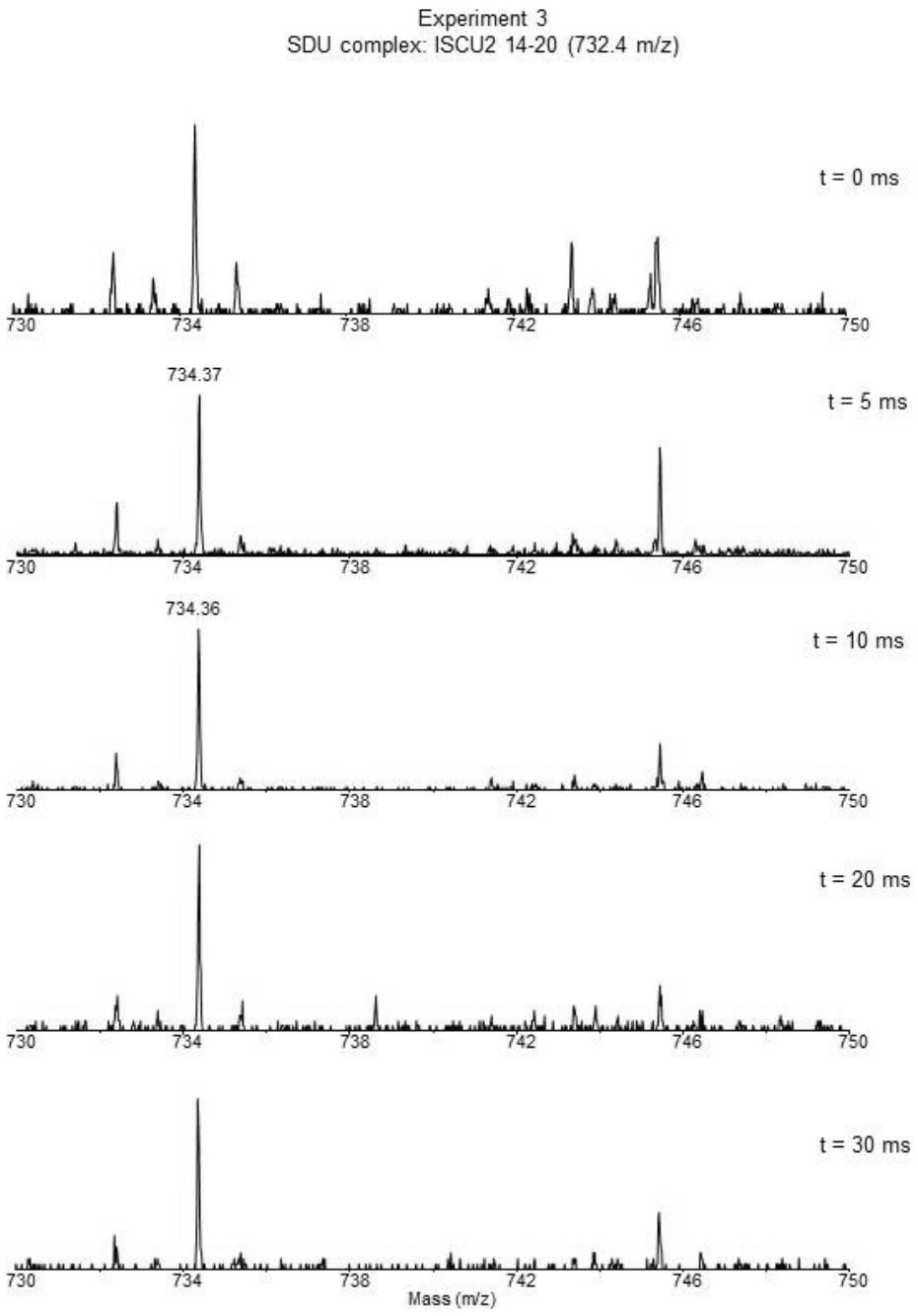

A-14. Mass spectra from SDU, Experiment 3 at various exposure time to hydroxyl radicals.

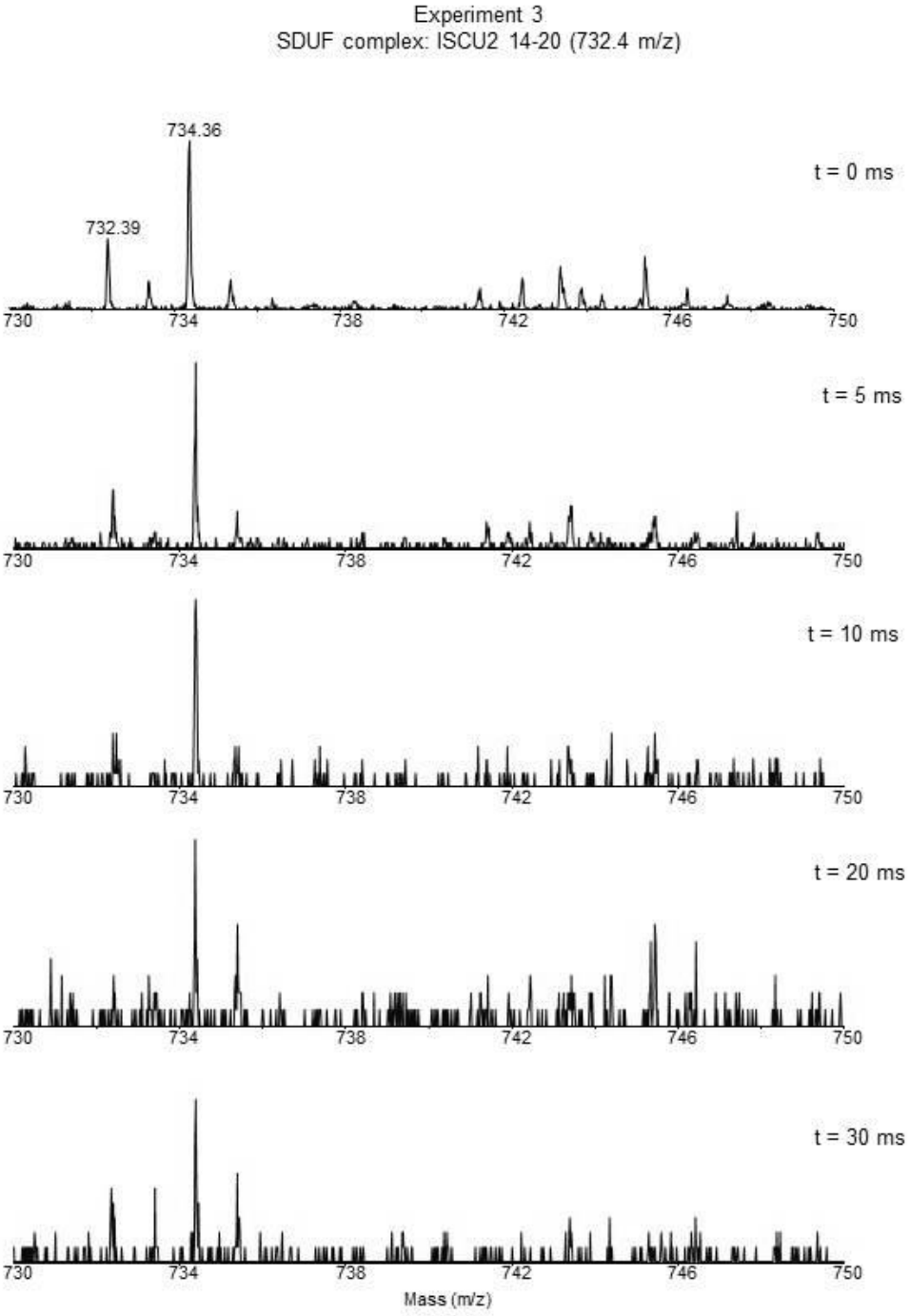

A-15. Mass spectra from SDUF, Experiment 3 at various exposure time to hydroxyl radicals.

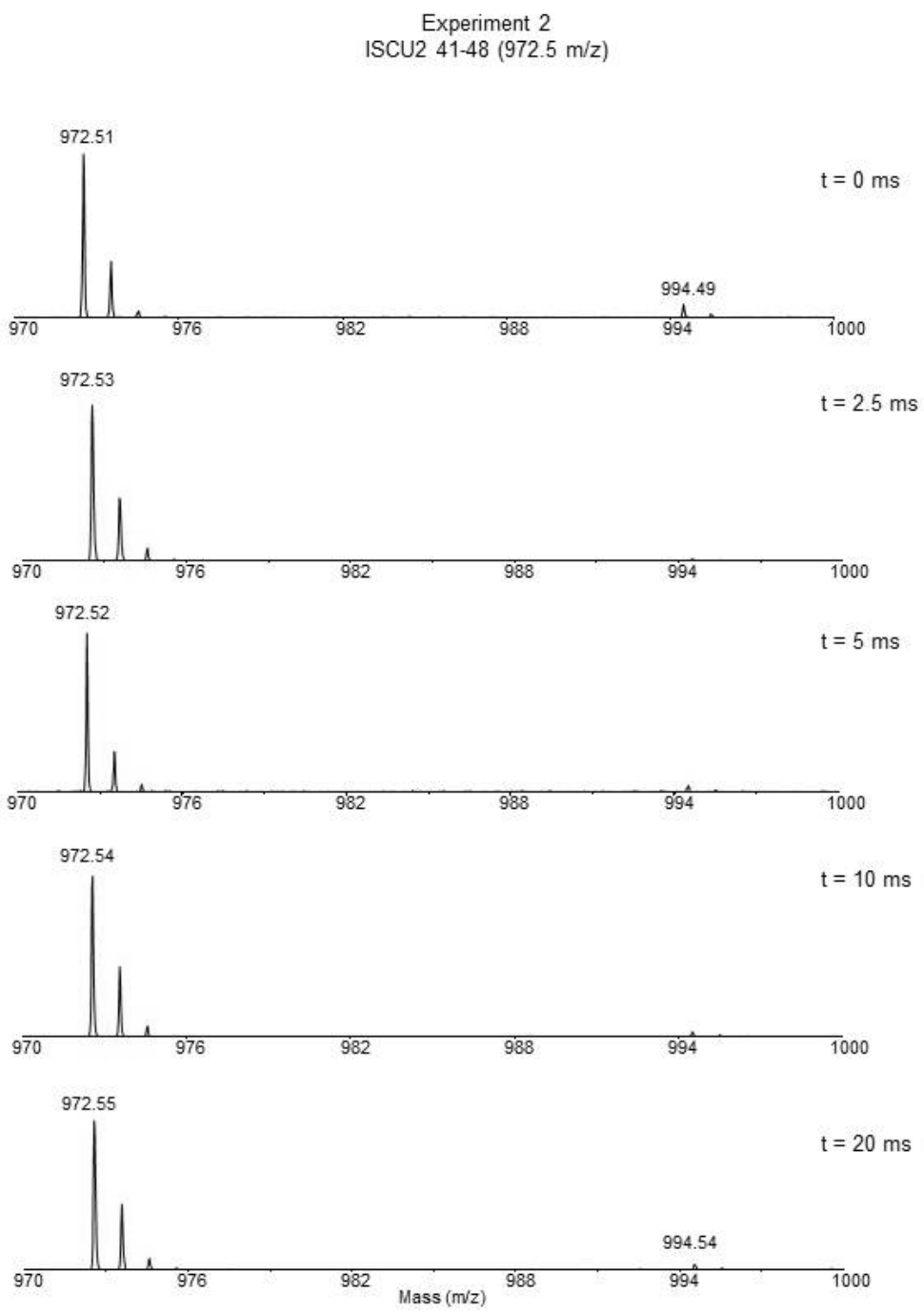

A-16. Mass spectra from ISCU2, Experiment 2 at various exposure time to hydroxyl radicals.

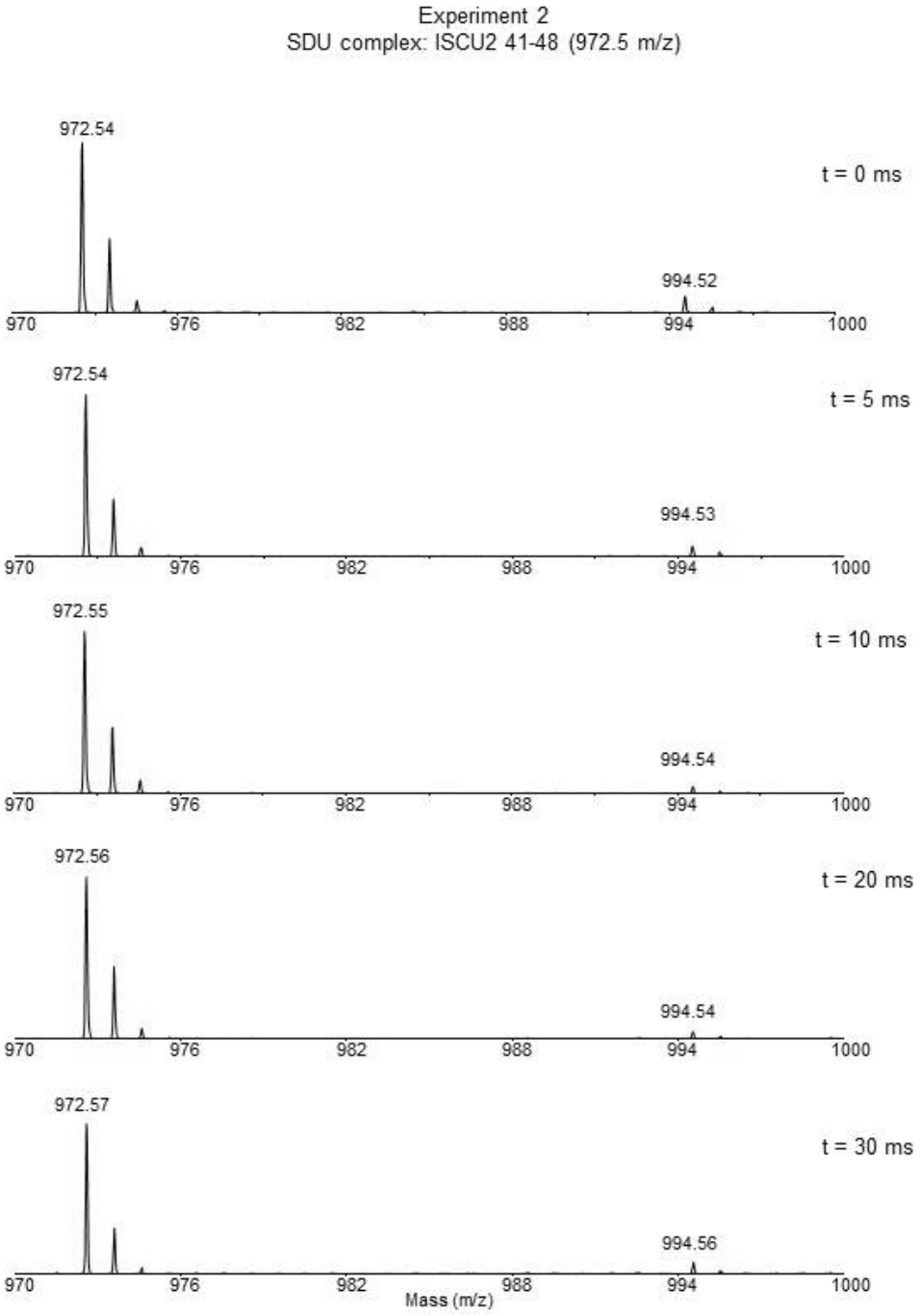

A-17. Mass spectra from SDU, Experiment 2 at various exposure time to hydroxyl radicals.

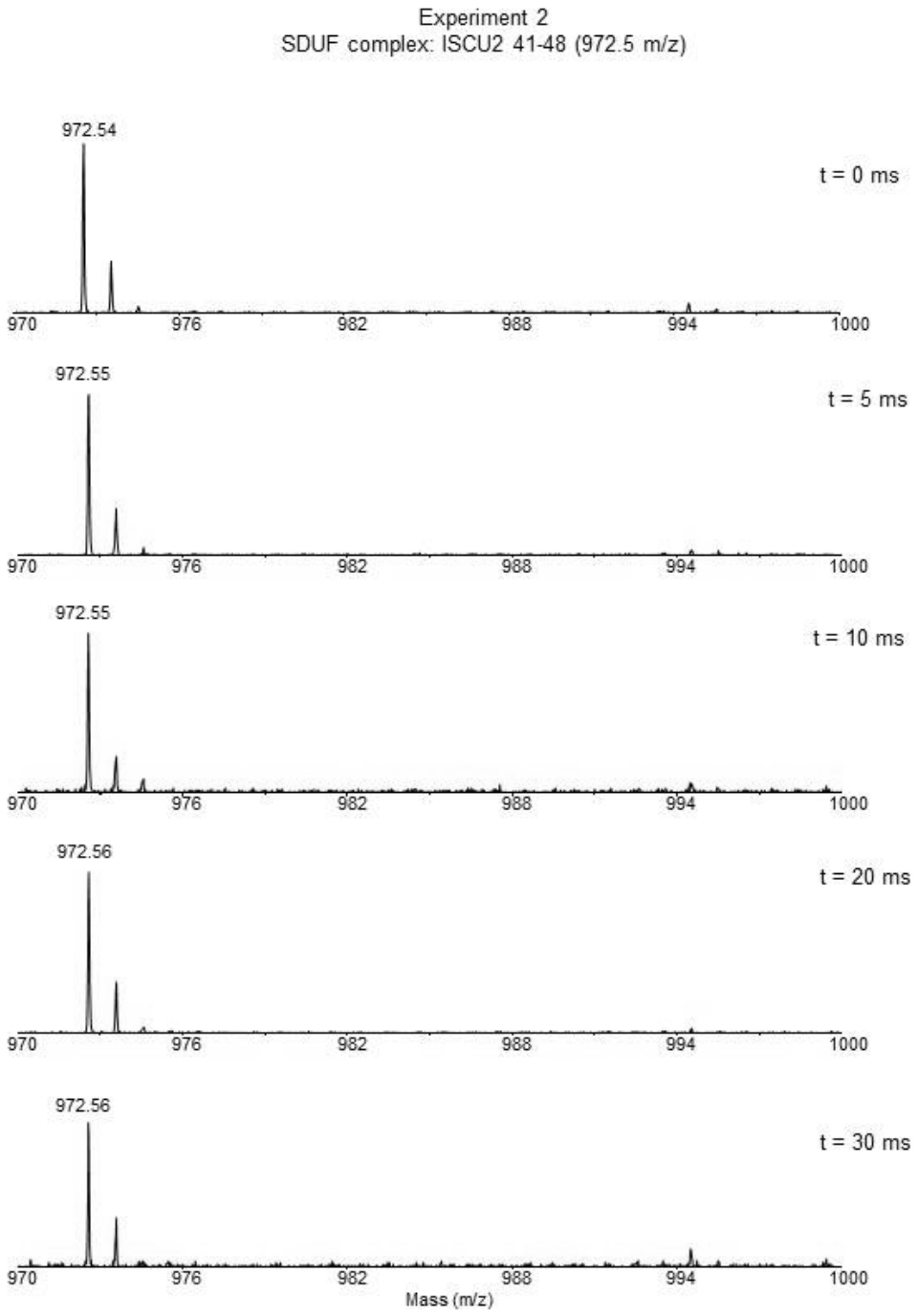

A-18. Mass spectra from SDUF, Experiment 2 at various exposure time to hydroxyl radicals.

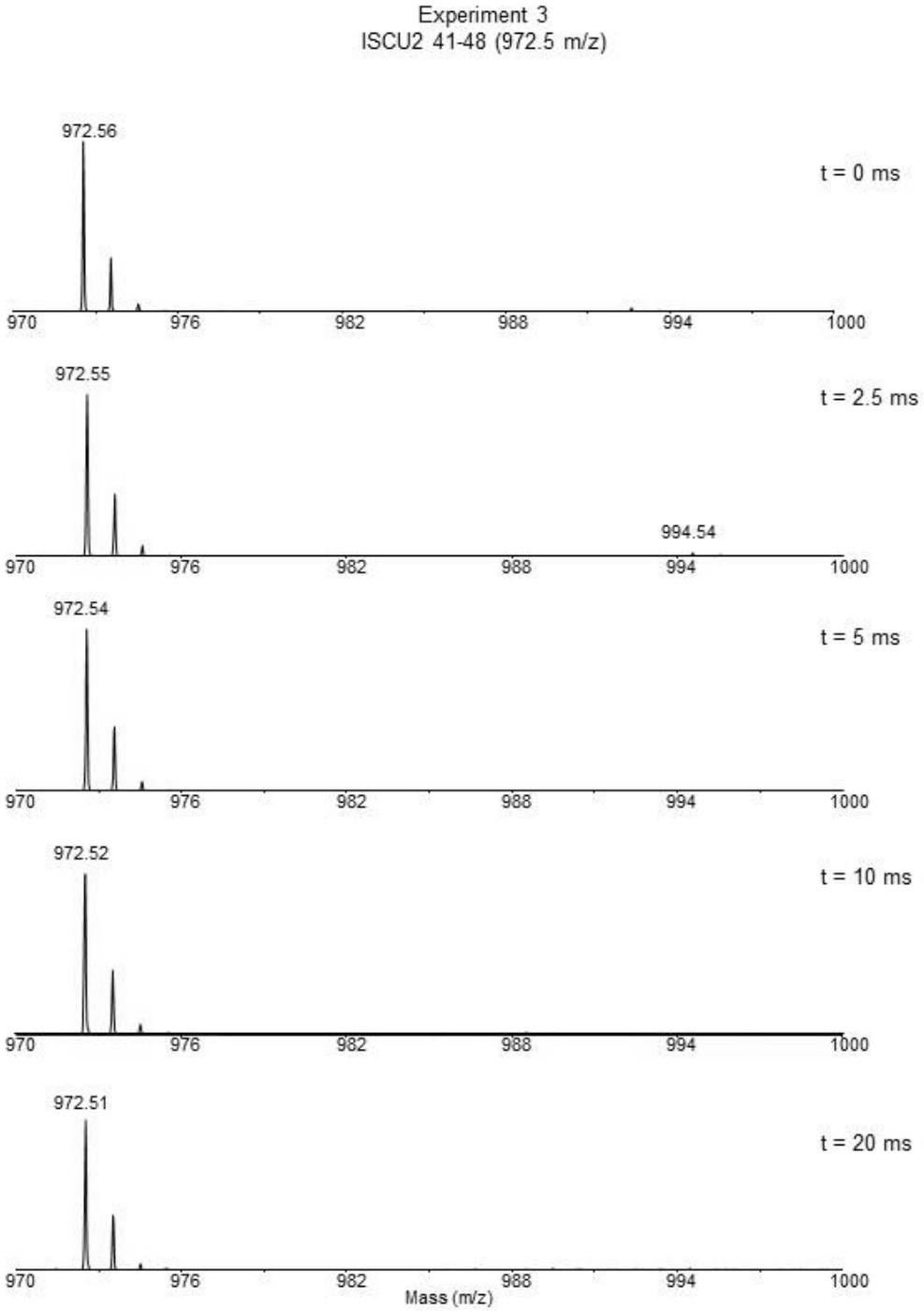

A-19. Mass spectra from ISCU2, Experiment 3 at various exposure time to hydroxyl radicals.

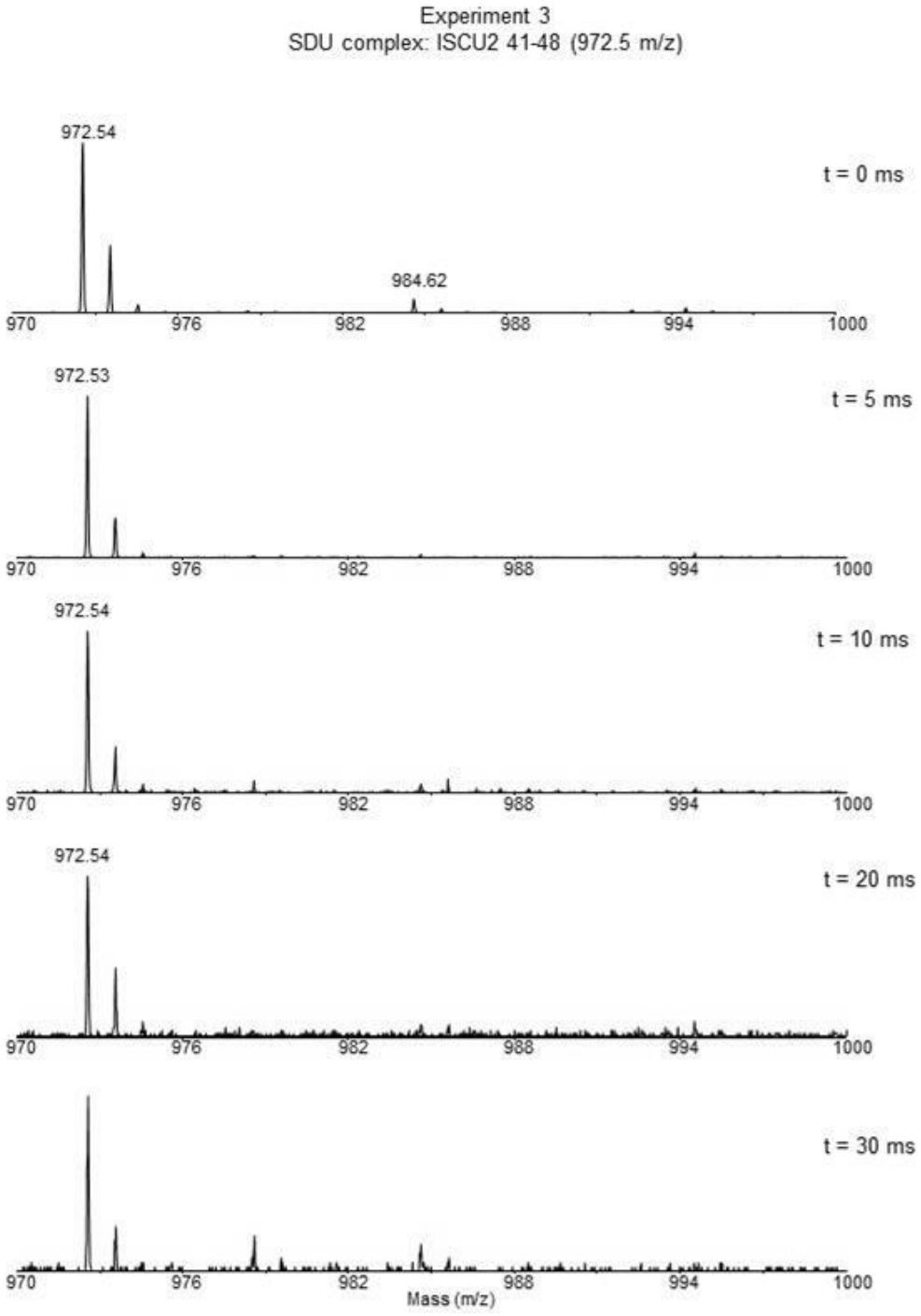

A-20. Mass spectra from SDU, Experiment 3 at various exposure time to hydroxyl radicals.

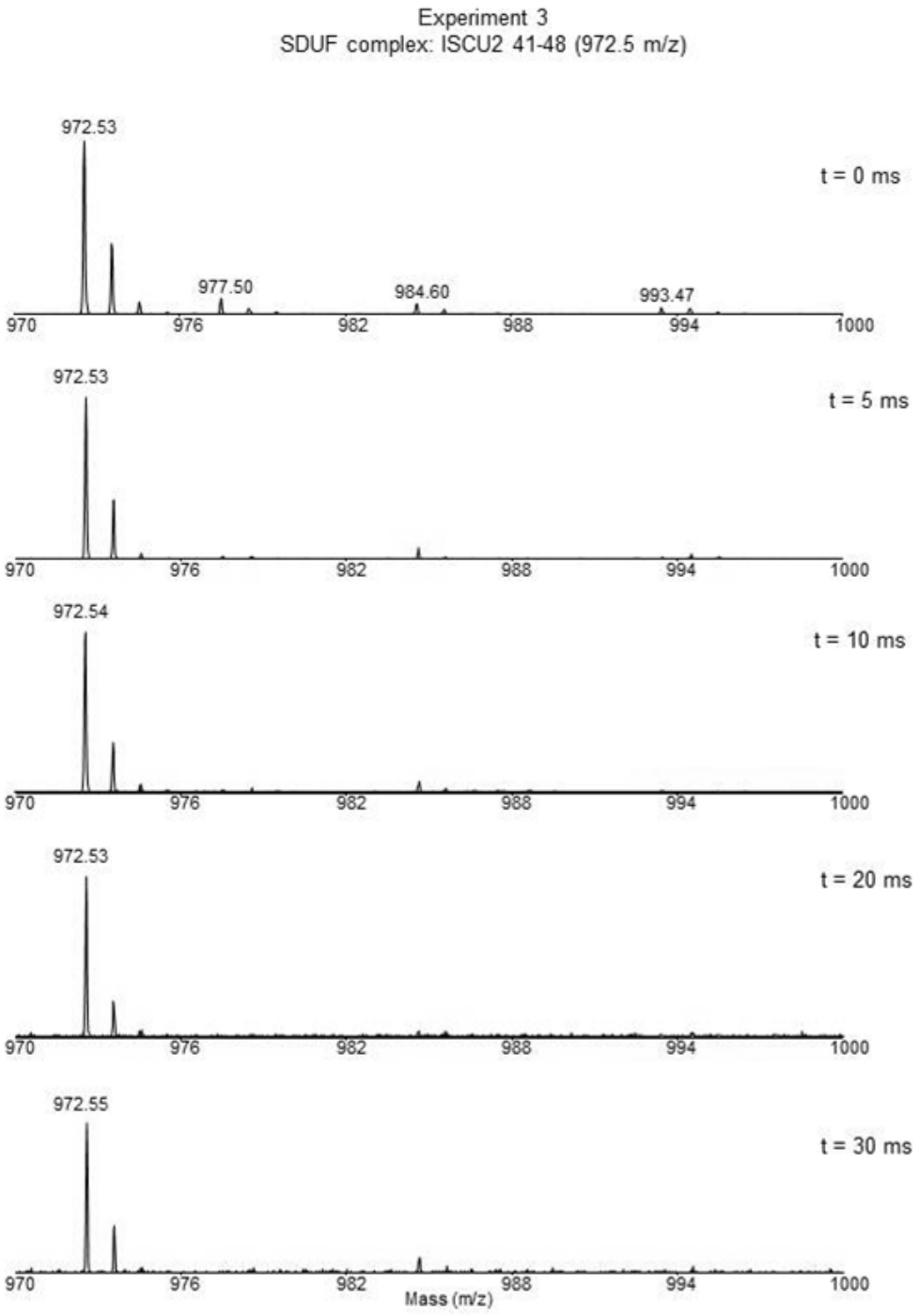

A-21. Mass spectra from SDUF, Experiment 3 at various exposure time to hydroxyl radicals.

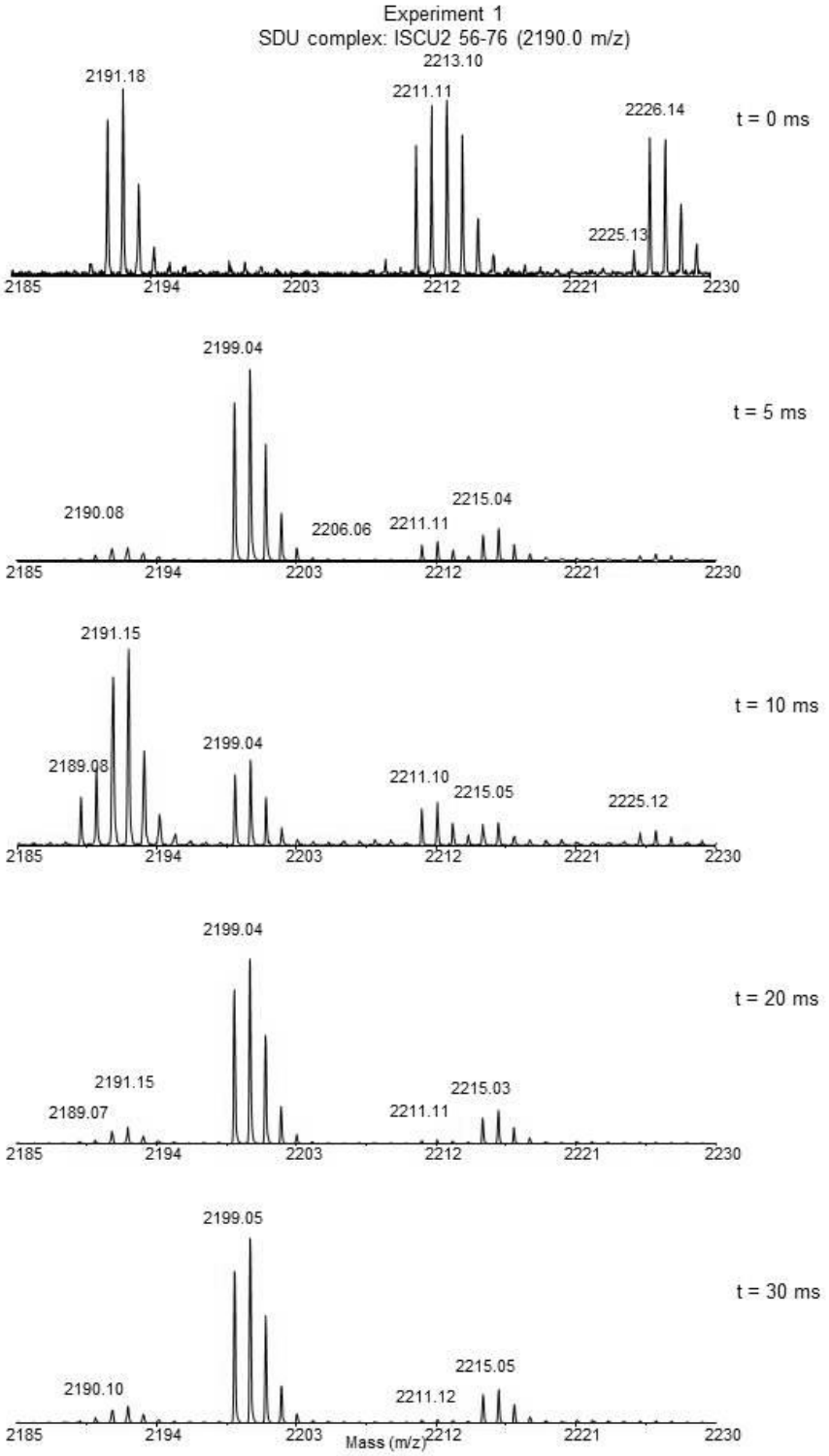

A-22. Mass spectra from SDU, Experiment 1 at various exposure time to hydroxyl radicals.

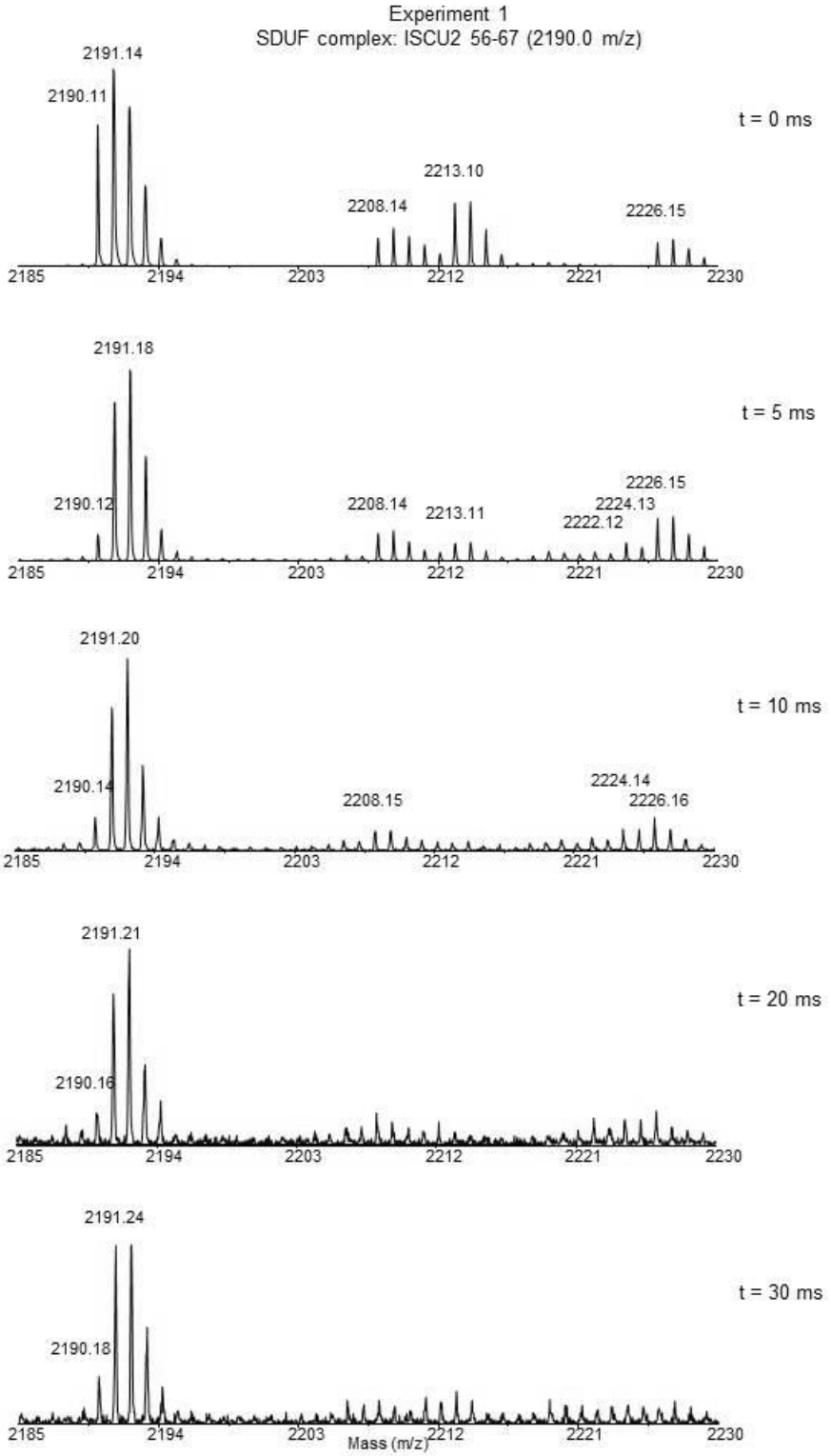

A-23. Mass spectra from SDUF, Experiment 1 at various exposure time to hydroxyl radicals.

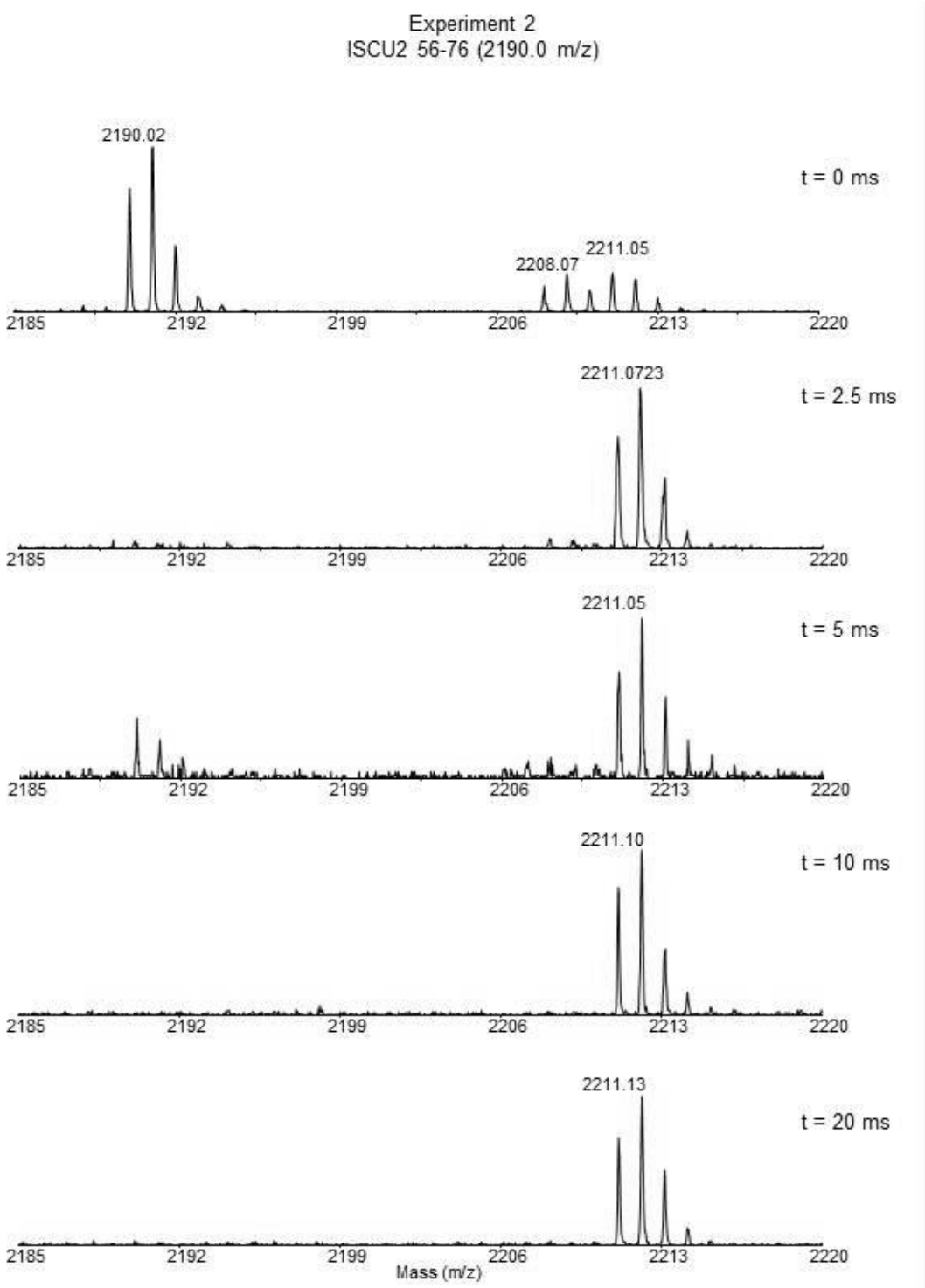

A-24. Mass spectra from ISCU2, Experiment 2 at various exposure time to hydroxyl radicals.

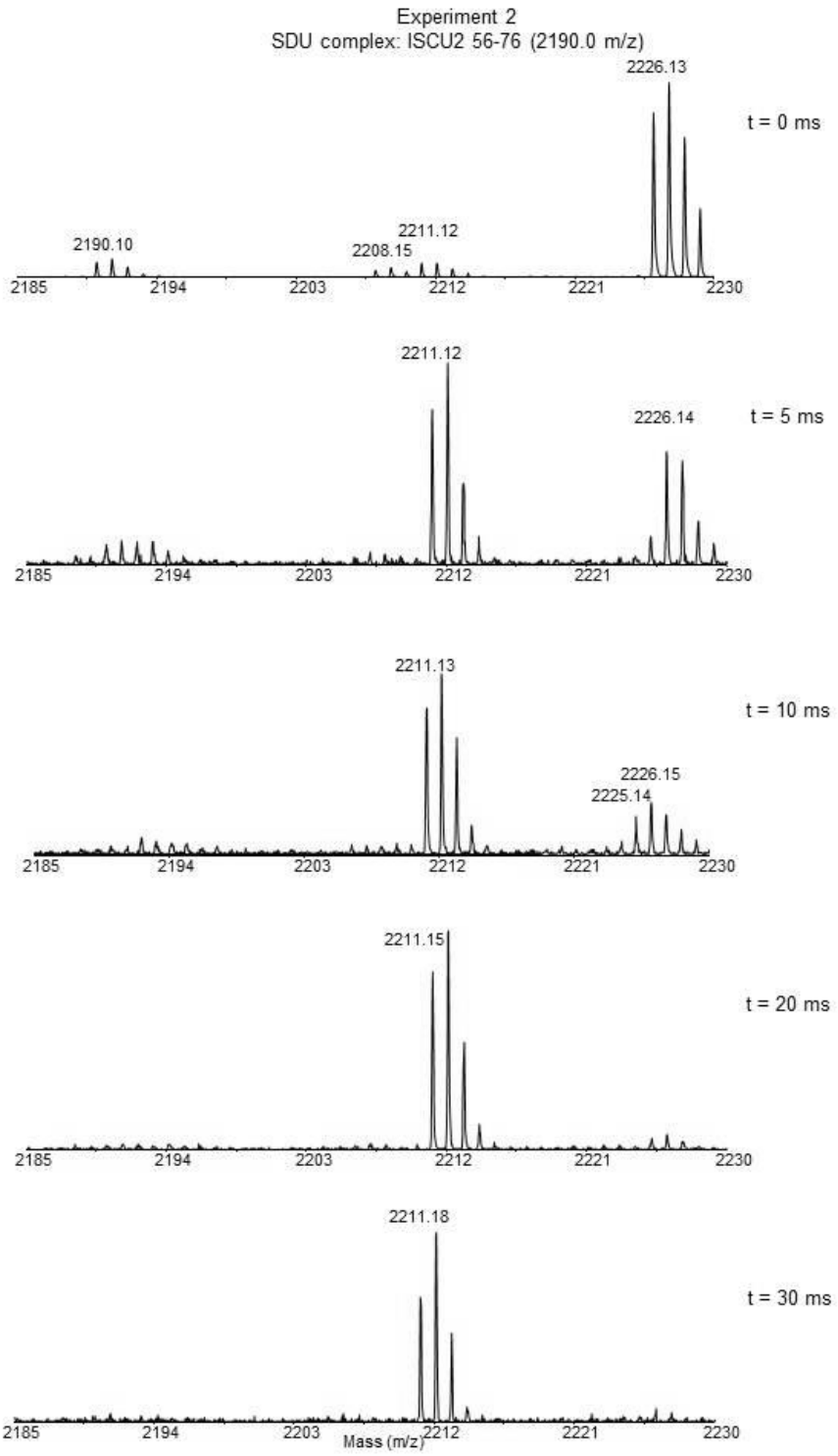

A-25. Mass spectra from SDU, Experiment 2 at various exposure time to hydroxyl radicals.

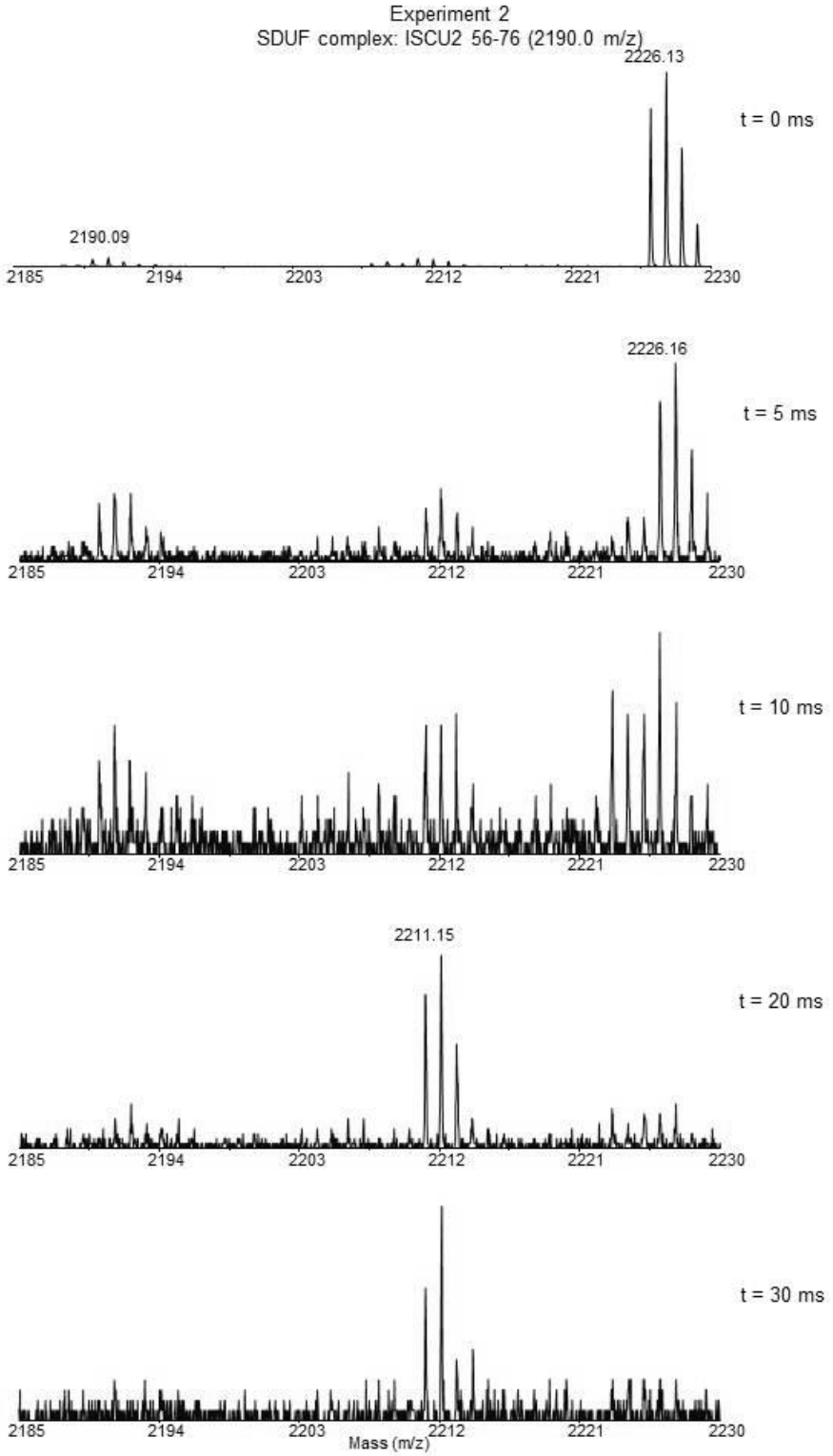

A-26. Mass spectra from SDUF, Experiment 2 at various exposure time to hydroxyl radicals.

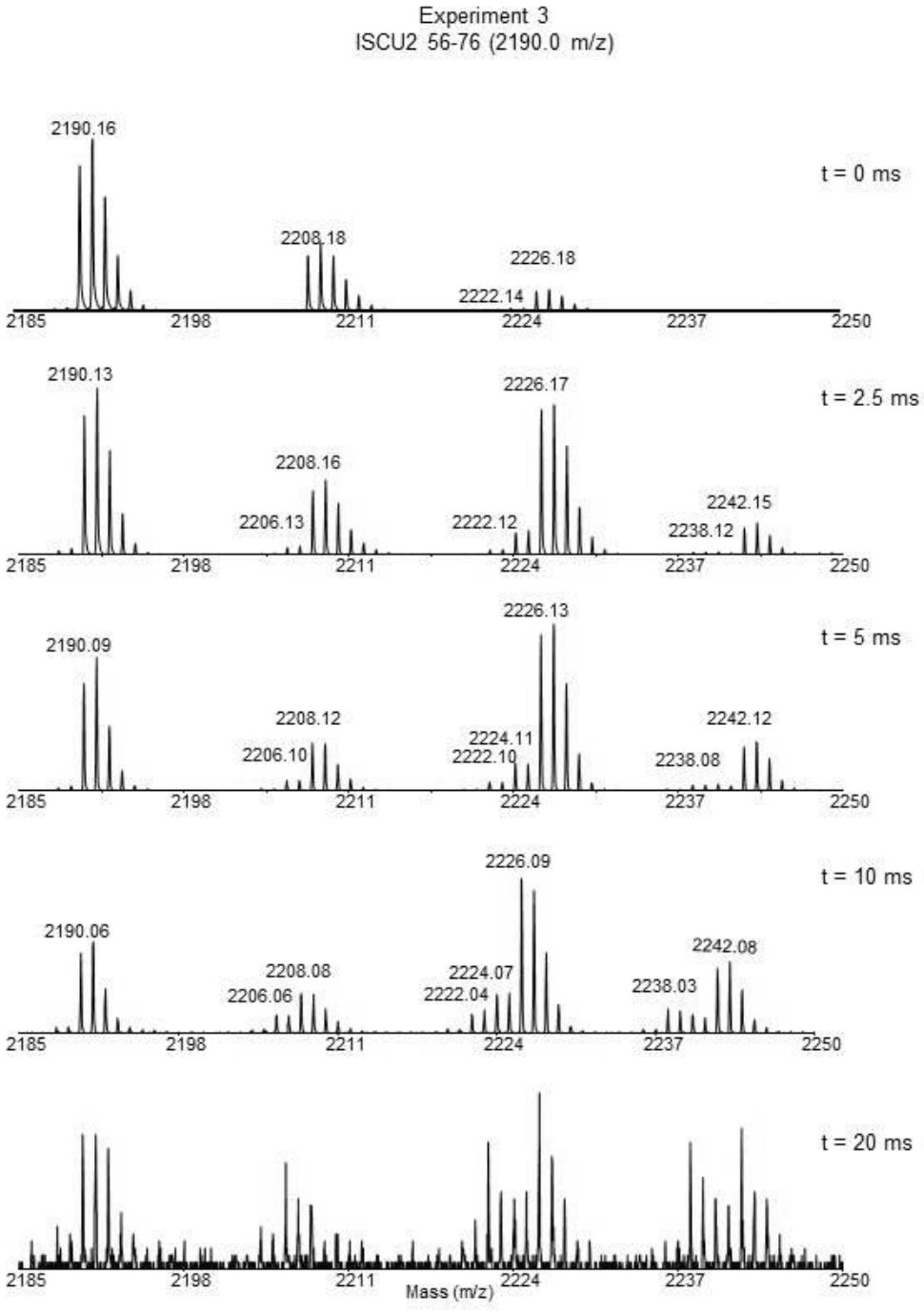

A-27. Mass spectra from ISCU2, Experiment 3 at various exposure time to hydroxyl radicals.

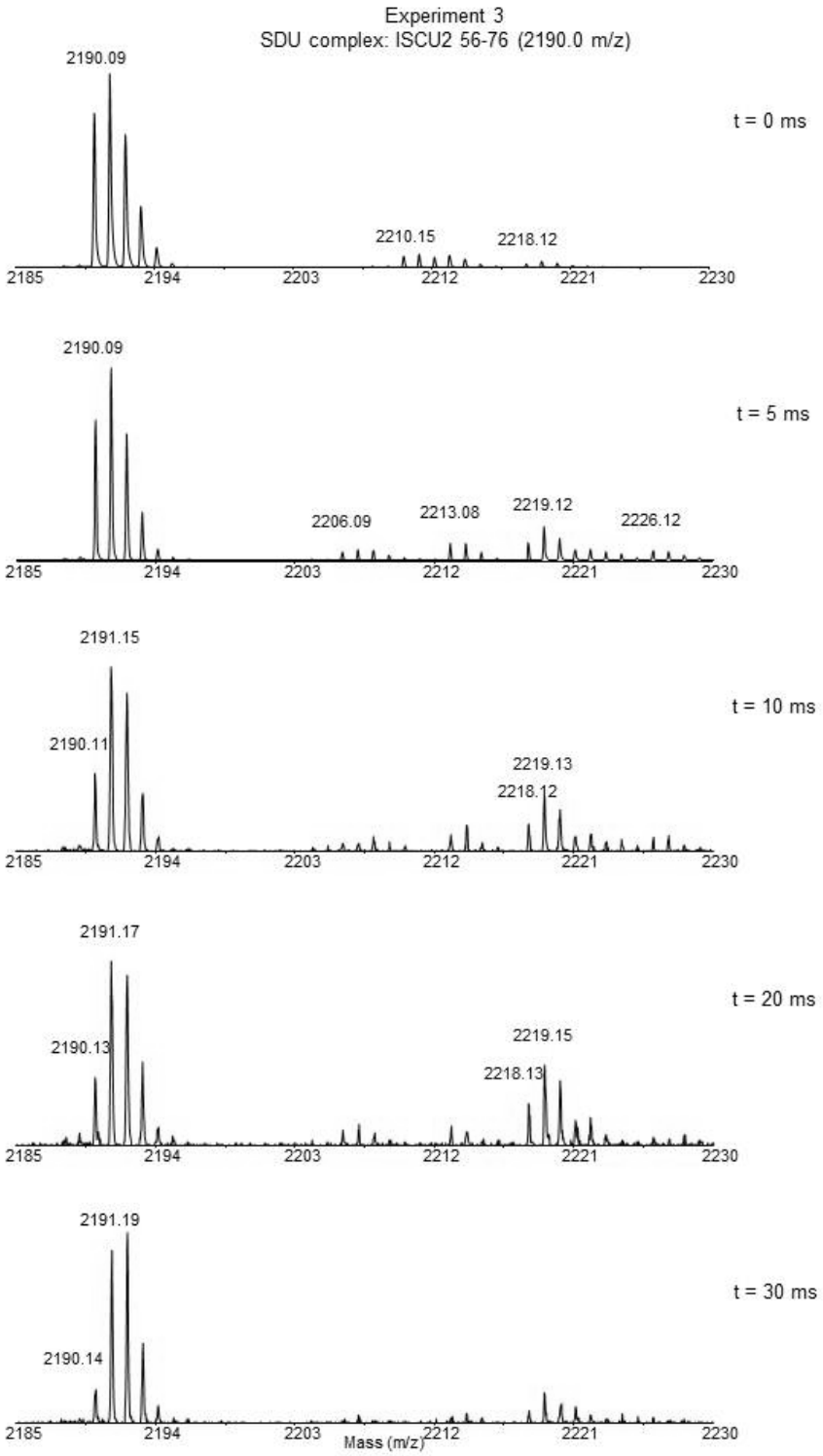

A-28. Mass spectra from SDU, Experiment 3 at various exposure time to hydroxyl radicals.

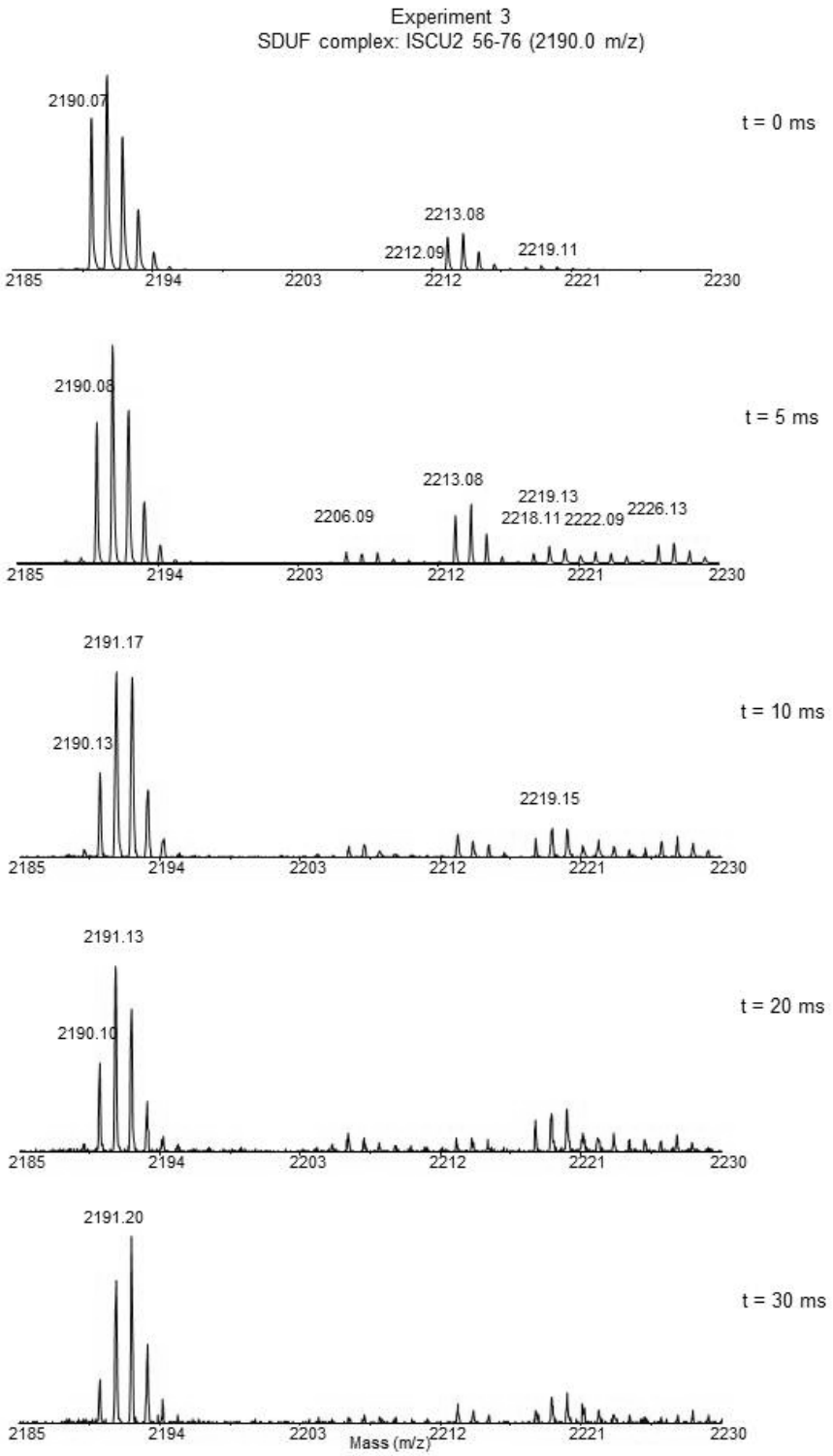

A-29. Mass spectra from SDUF, Experiment 3 at various exposure time to hydroxyl radicals.

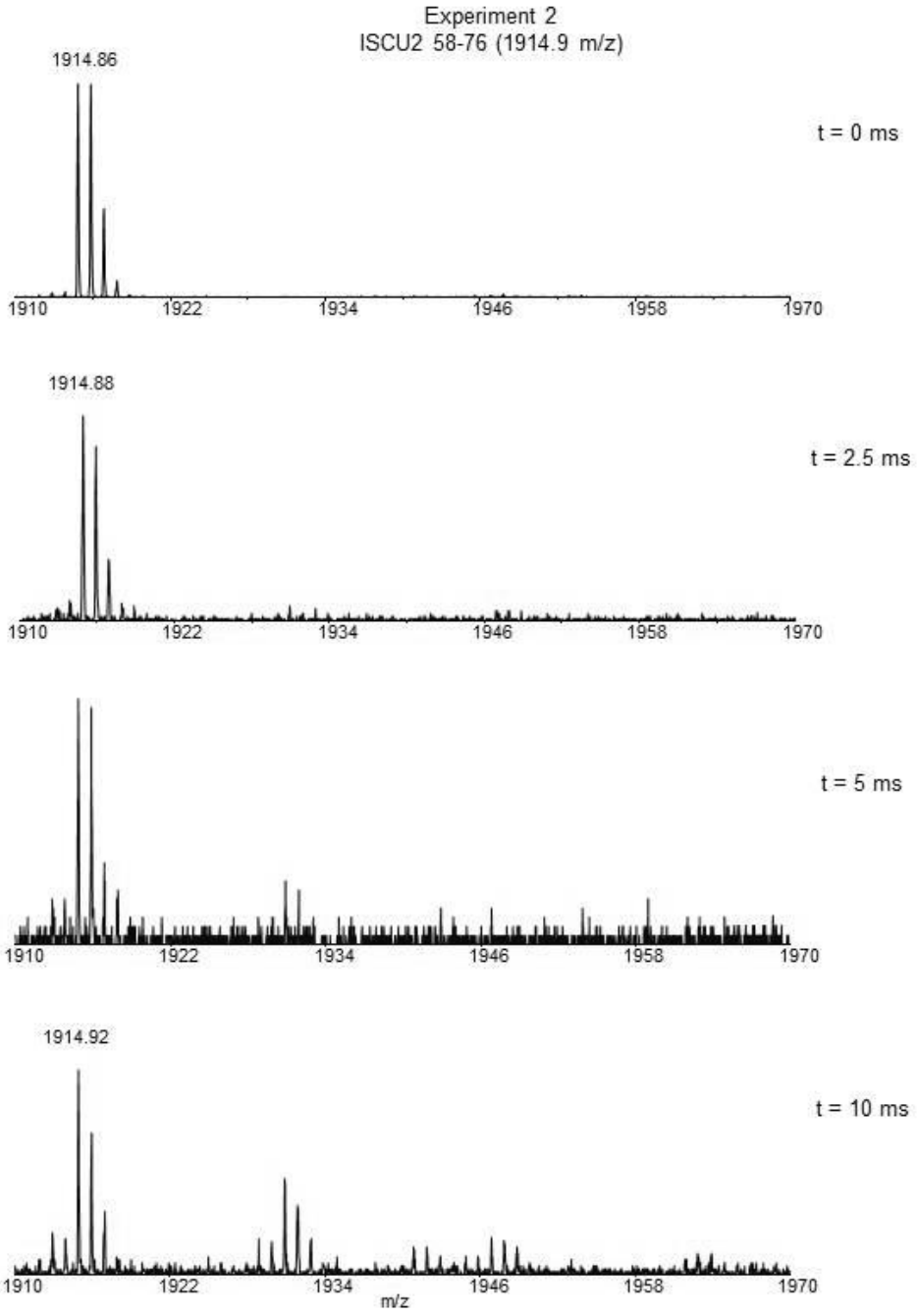

A-30. Mass spectra from ISCU2, Experiment 2 at various exposure time to hydroxyl radicals.

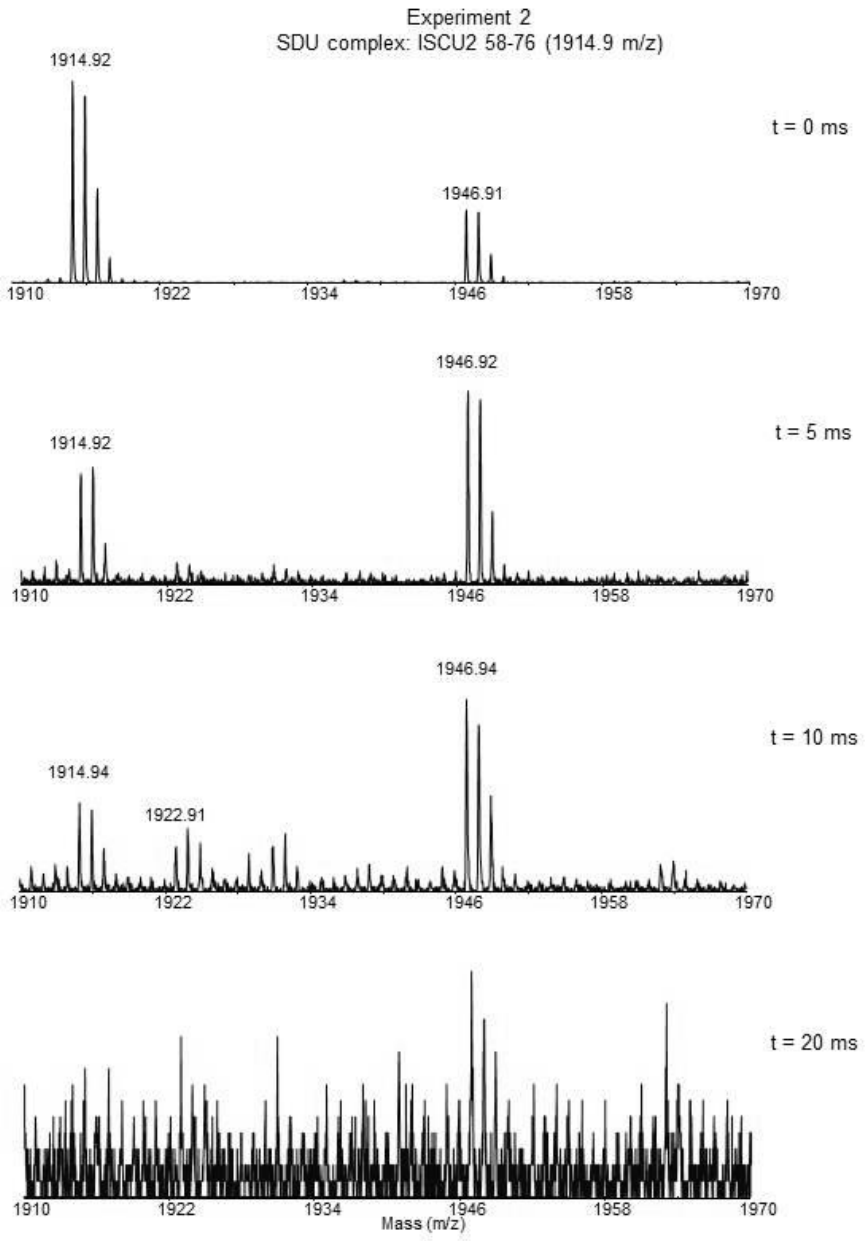

A-31. Mass spectra from SDU, Experiment 2 at various exposure time to hydroxyl radicals.

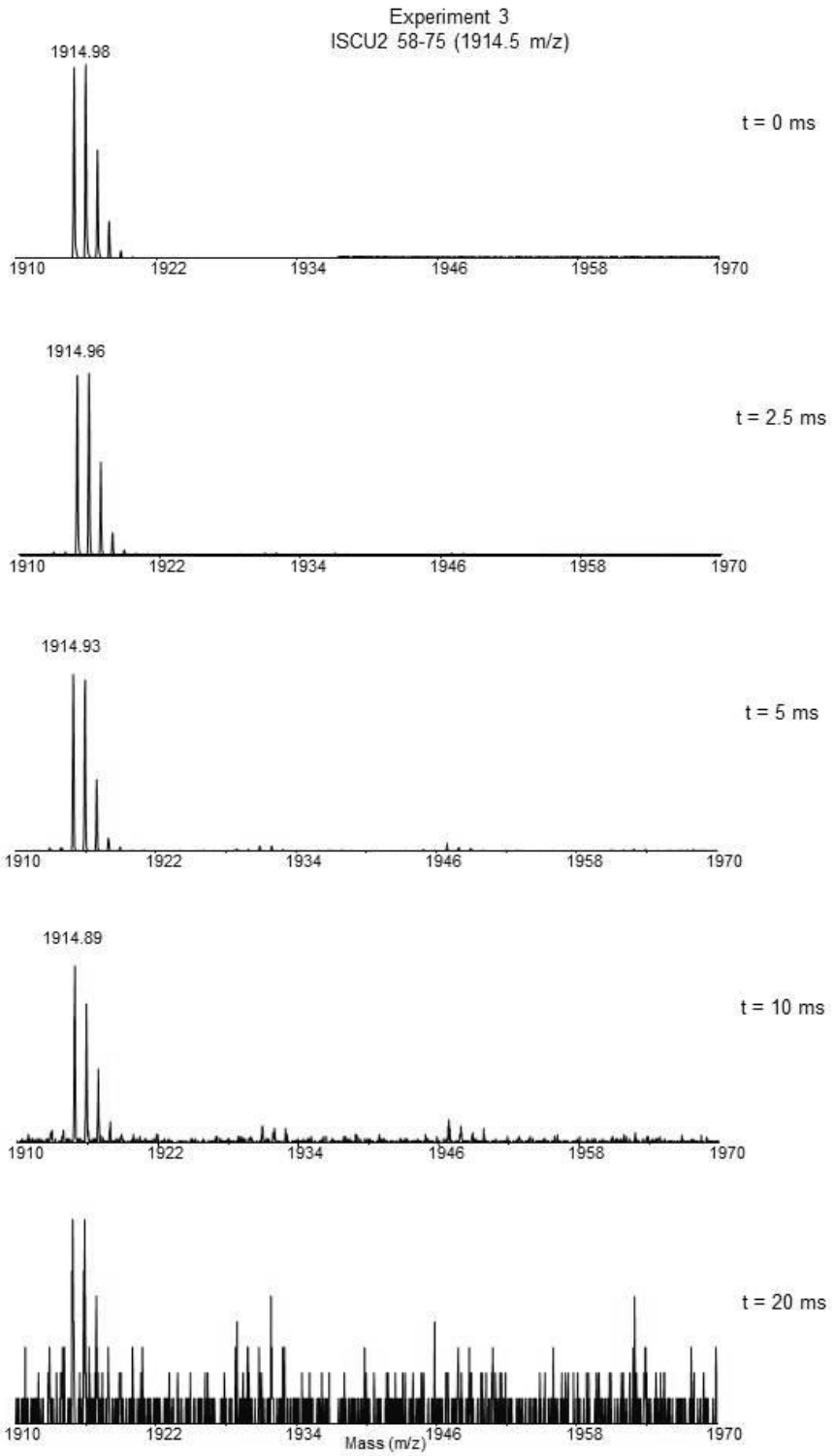

A-32. Mass spectra from ISCU2, Experiment 3 at various exposure time to hydroxyl radicals.

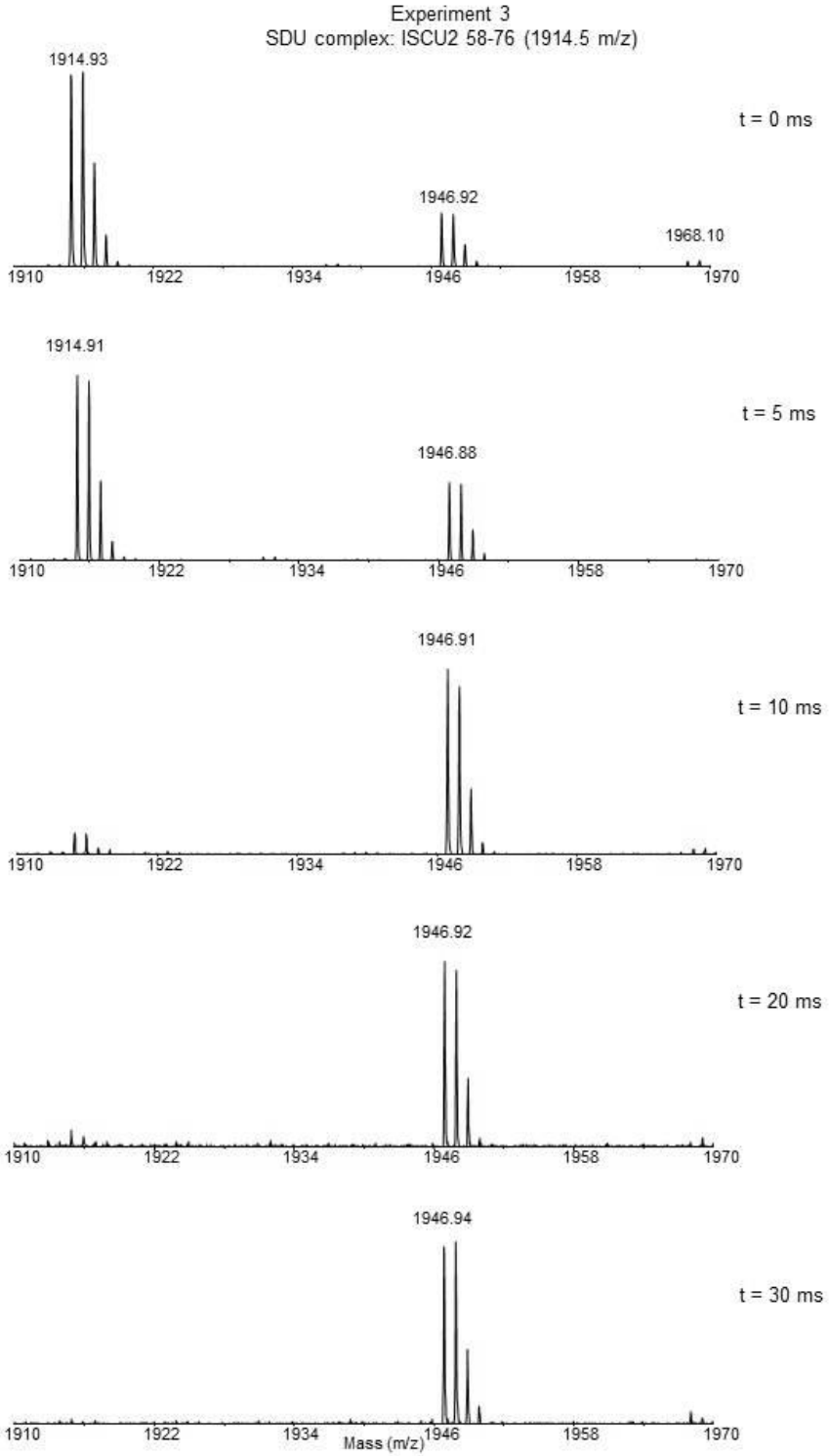

A-33. Mass spectra from SDU, Experiment 3 at various exposure time to hydroxyl radicals.

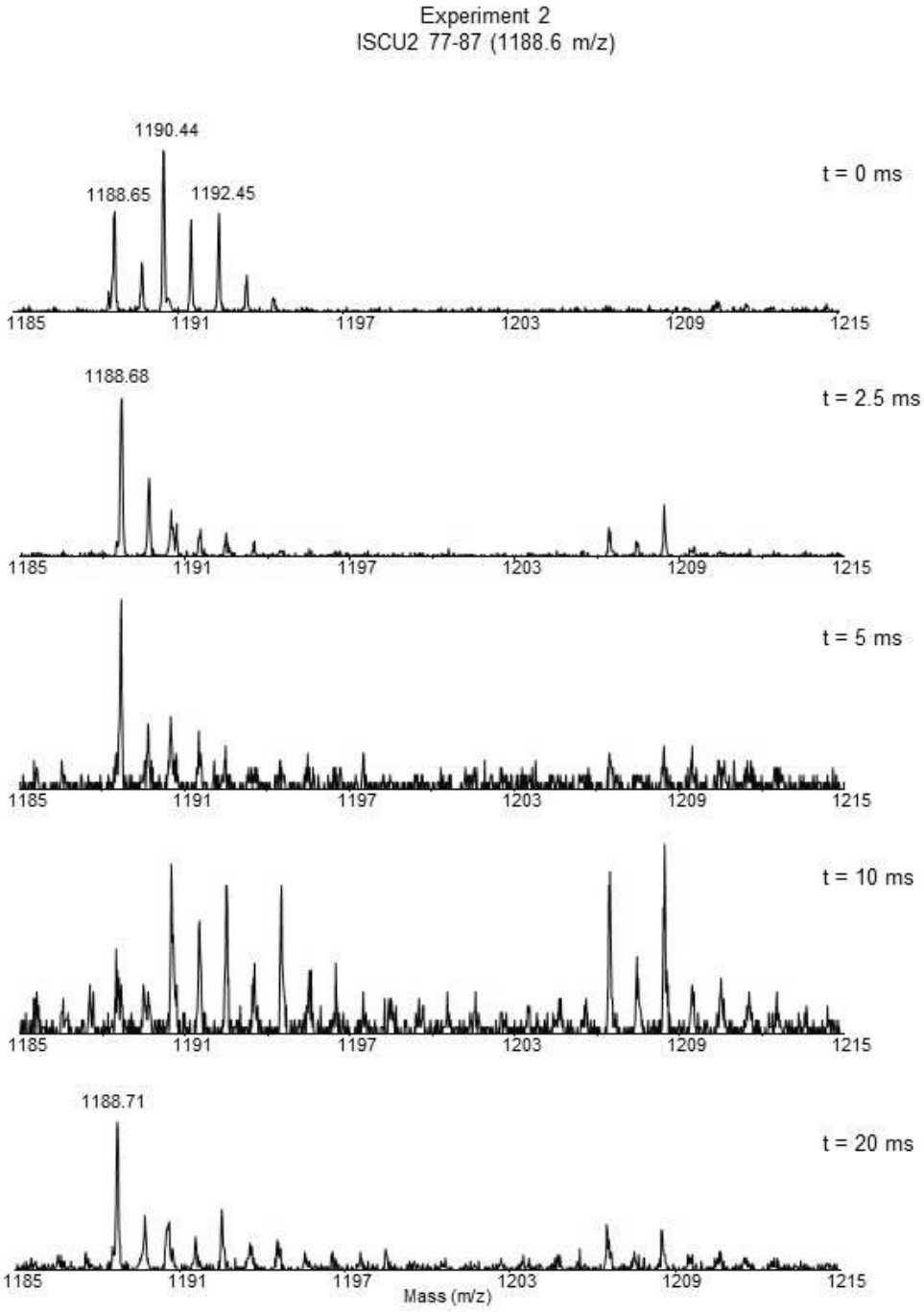

A-34. Mass spectra from ISCU2, Experiment 2 at various exposure time to hydroxyl radicals.

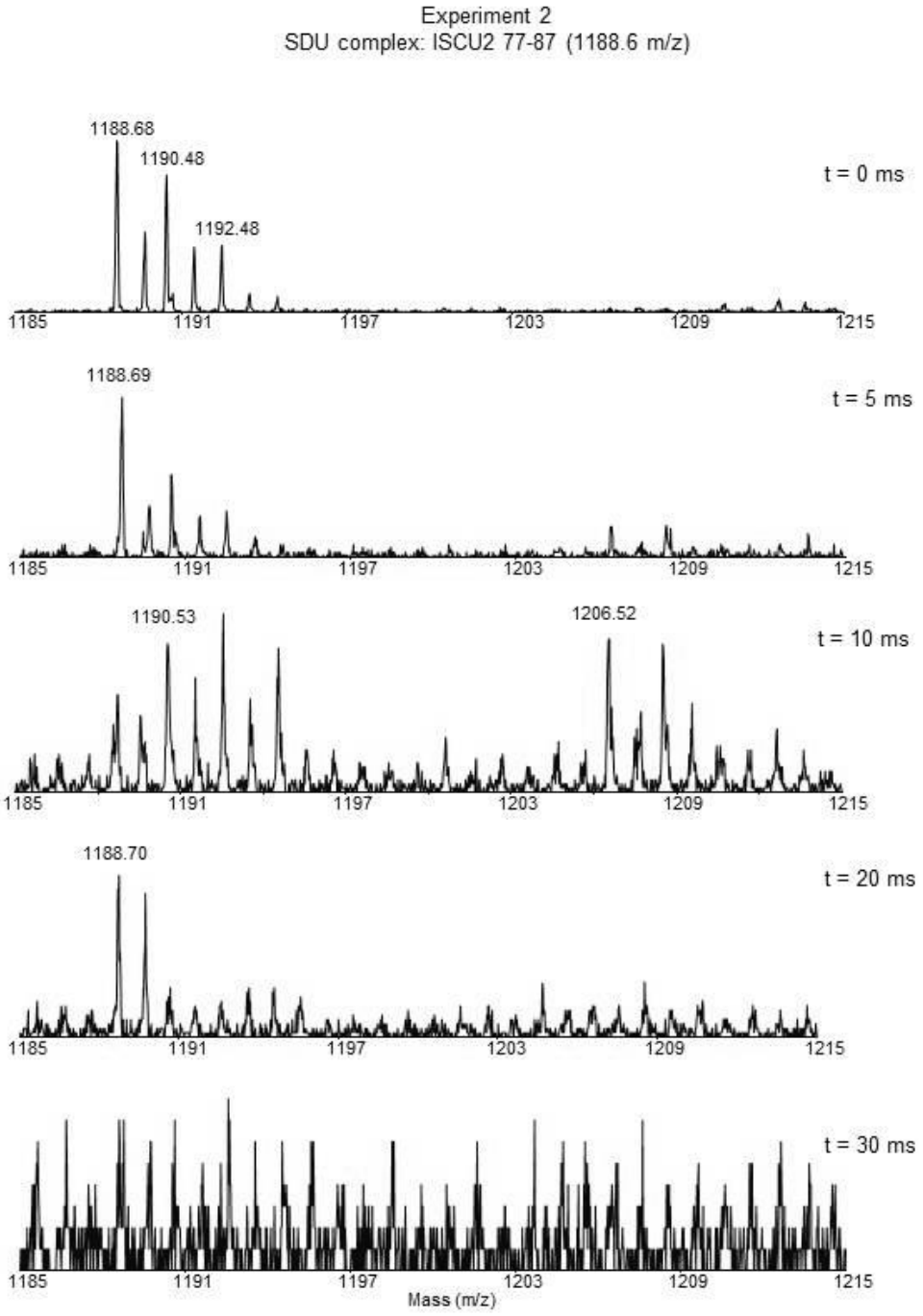

A-35. Mass spectra from SDU, Experiment 2 at various exposure time to hydroxyl radicals.

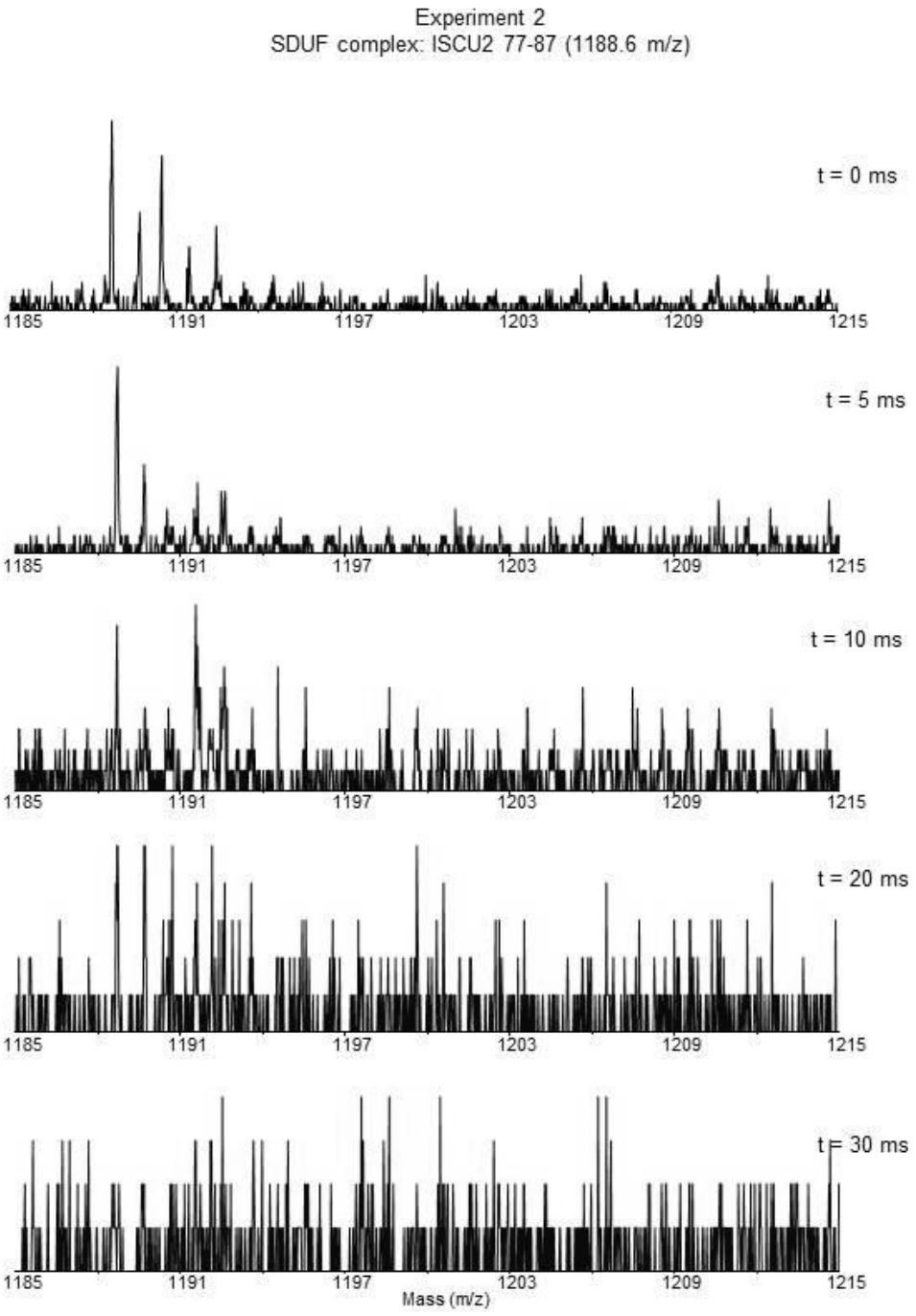

A-36. Mass spectra from SDUF, Experiment 2 at various exposure time to hydroxyl radicals.

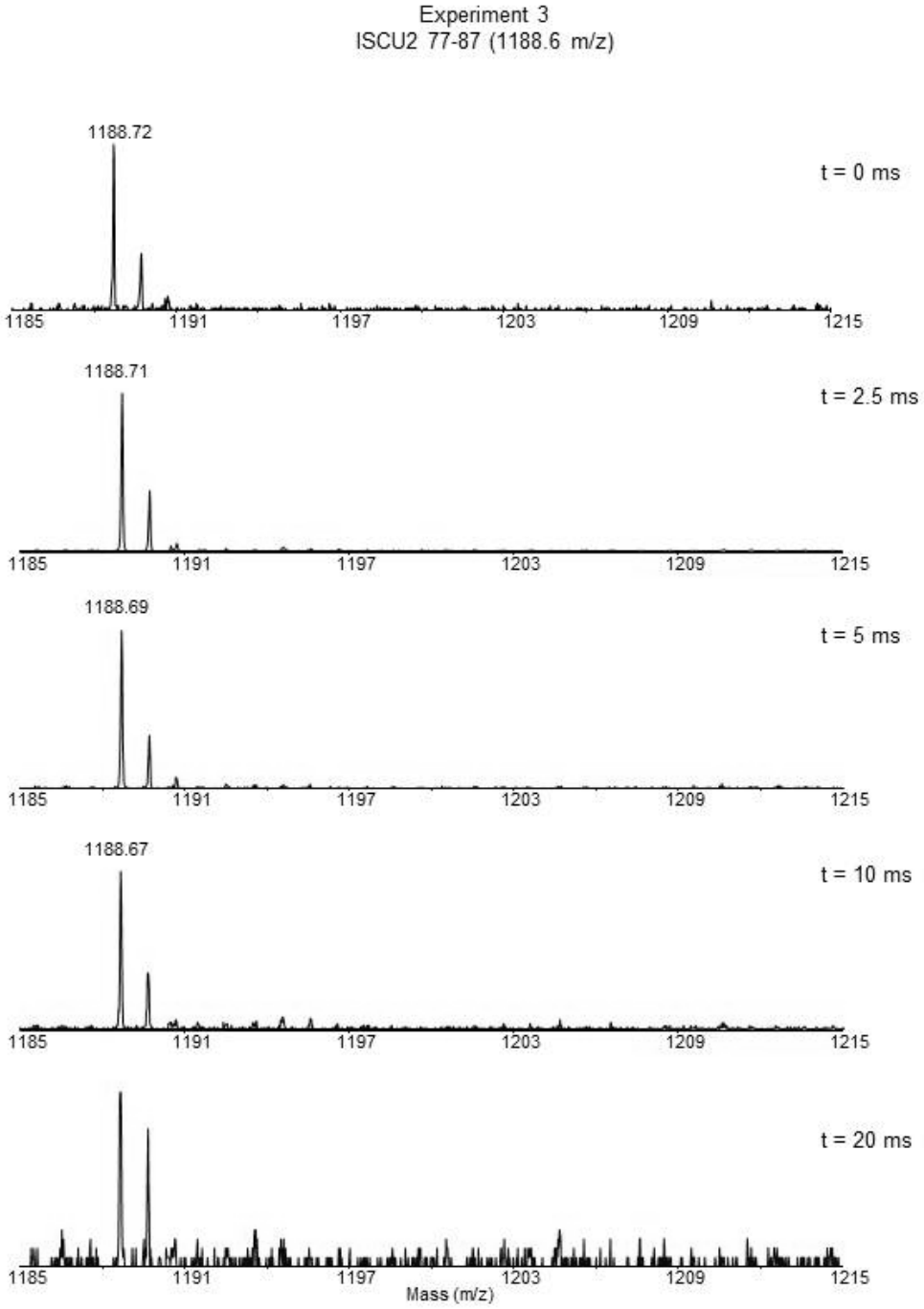

A-37. Mass spectra from ISCU2, Experiment 3 at various exposure time to hydroxyl radicals.

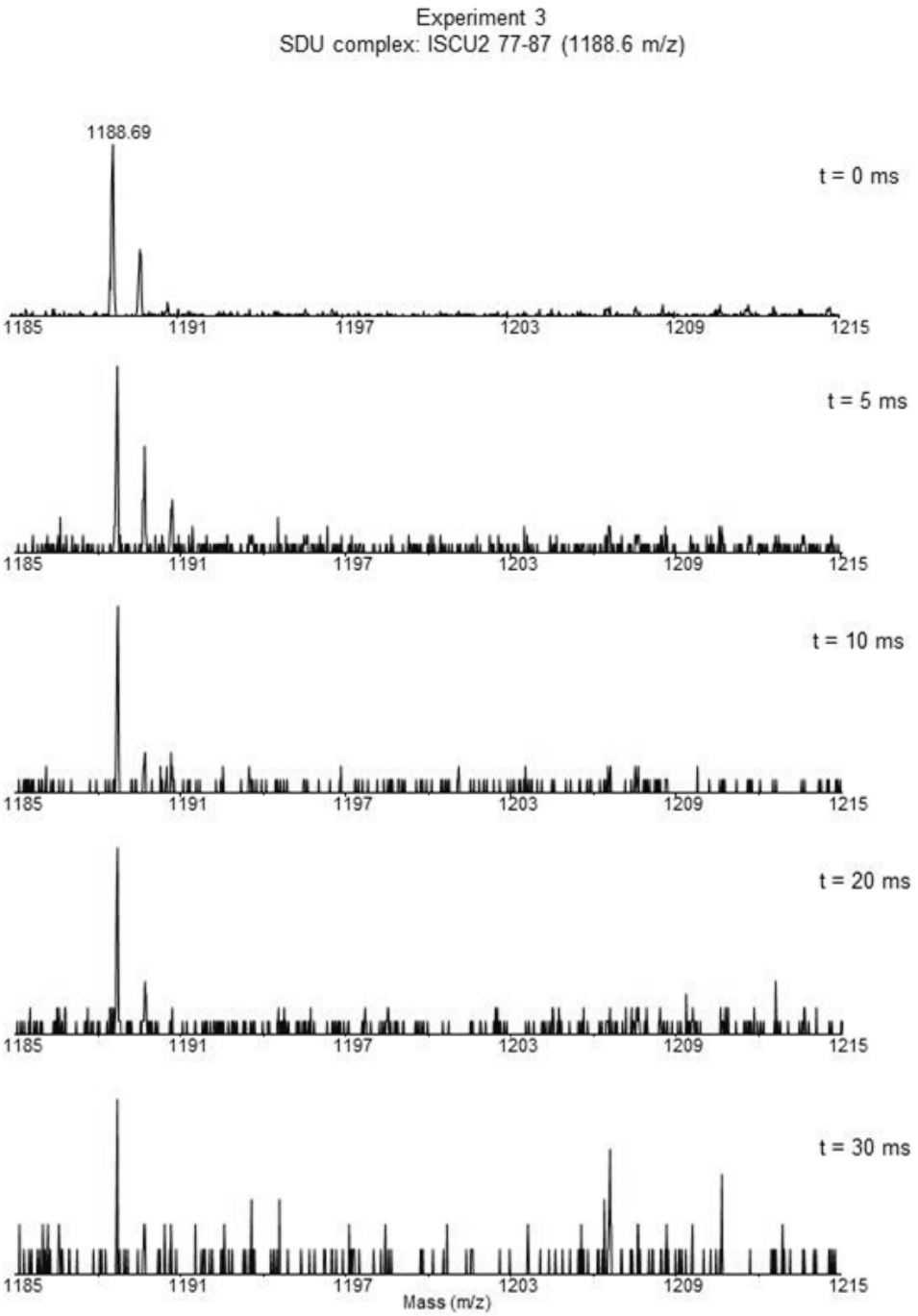

A-38. Mass spectra from SDU, Experiment 3 at various exposure time to hydroxyl radicals.

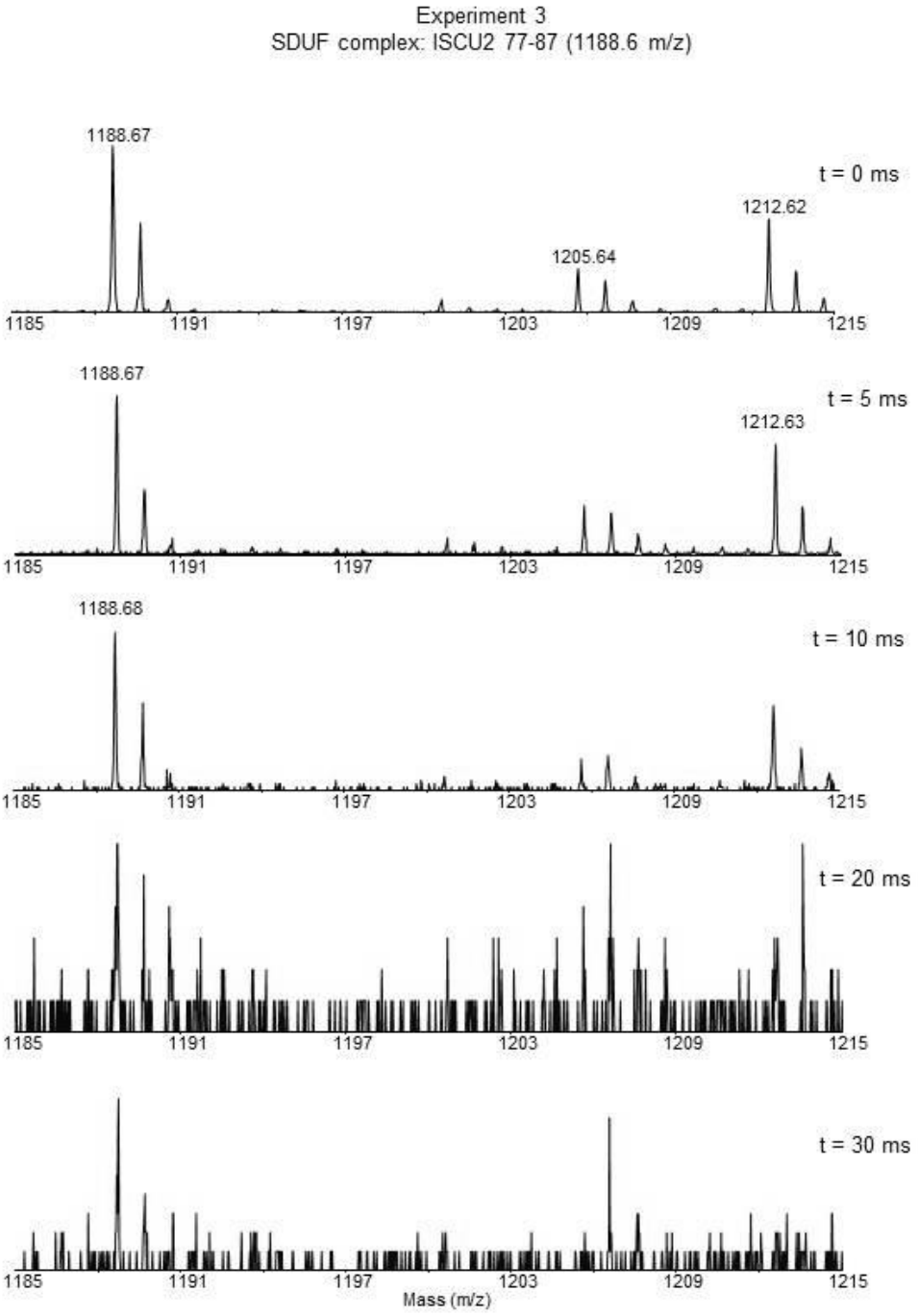

A-39. Mass spectra from SDUF, Experiment 3 at various exposure time to hydroxyl radicals.

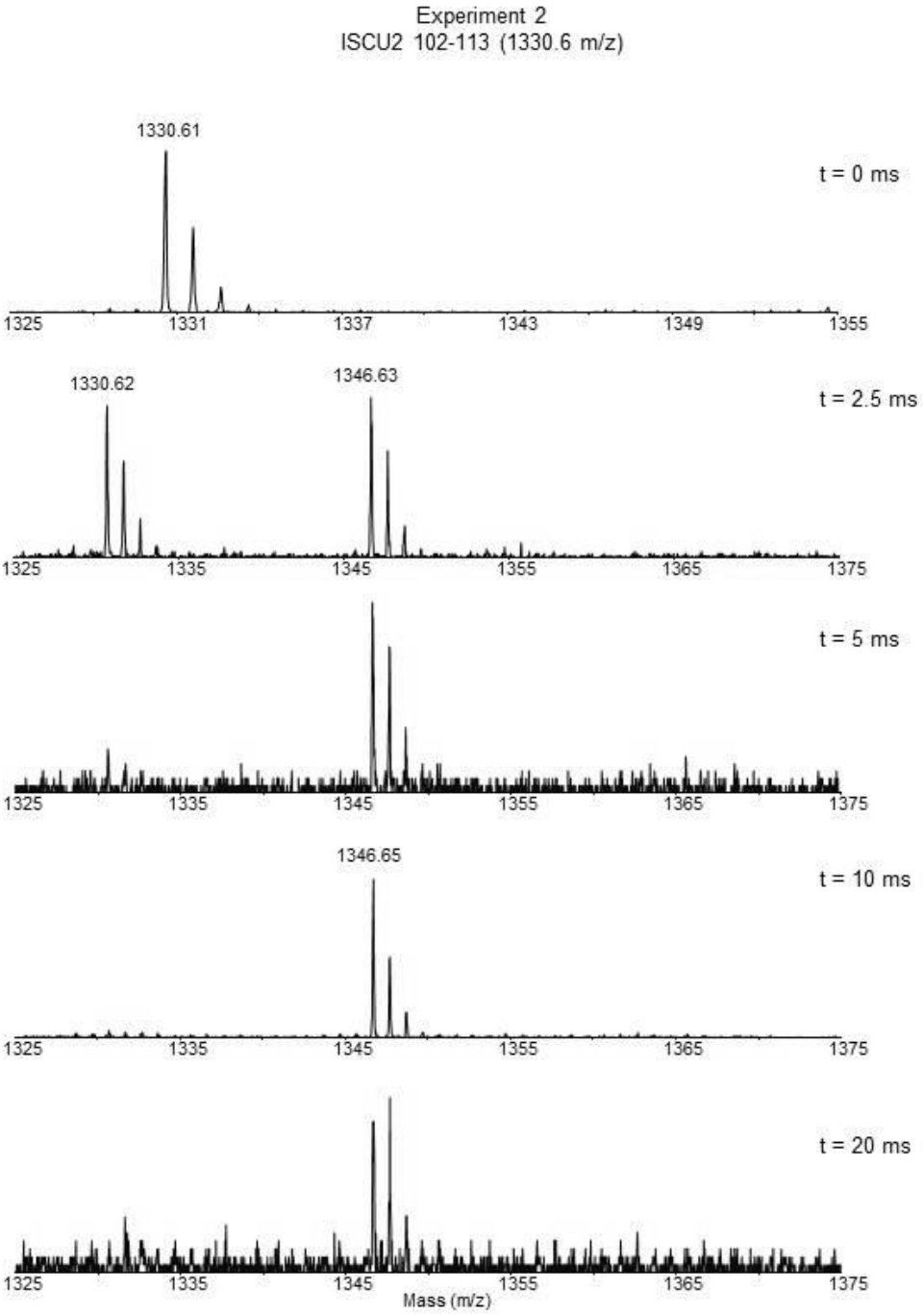

A-40. Mass spectra from ISCU2, Experiment 2 at various exposure time to hydroxyl radicals.

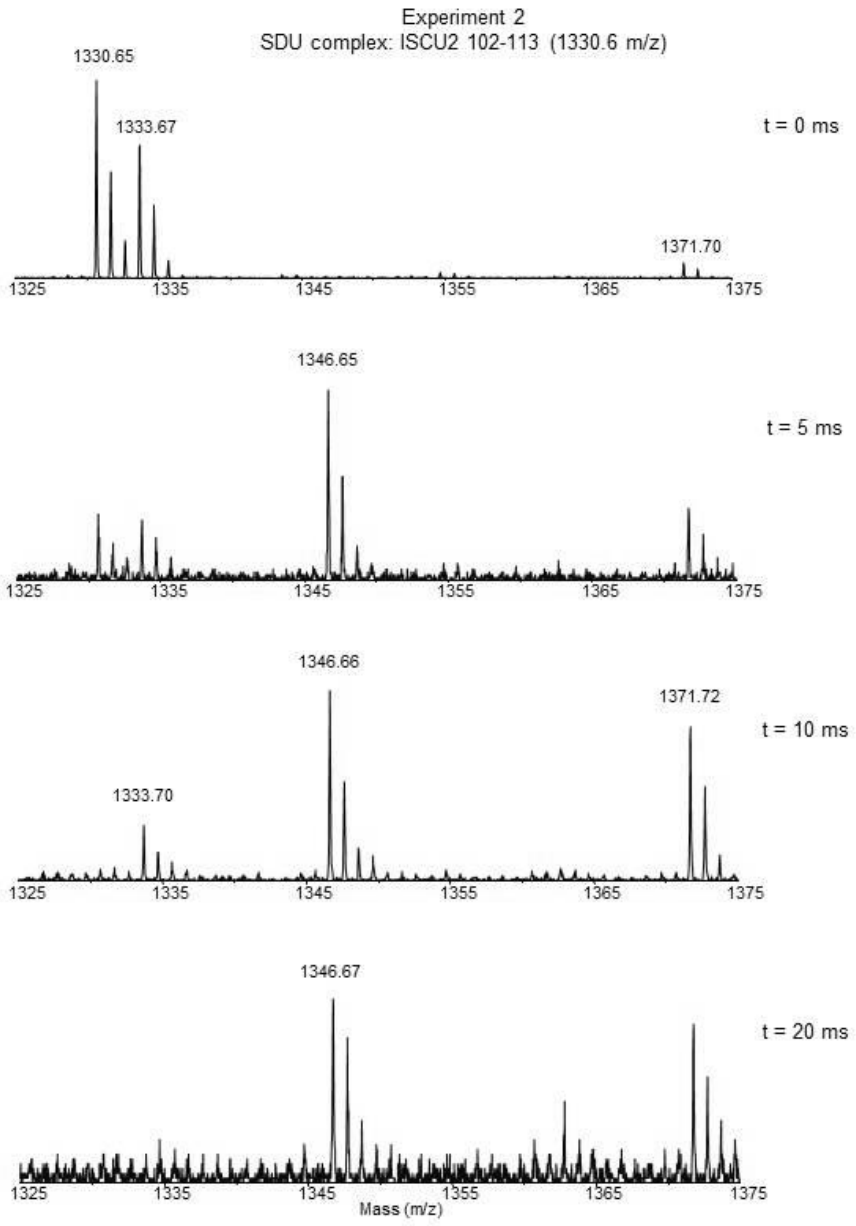

A-41. Mass spectra from SDU, Experiment 2 at various exposure time to hydroxyl radicals.

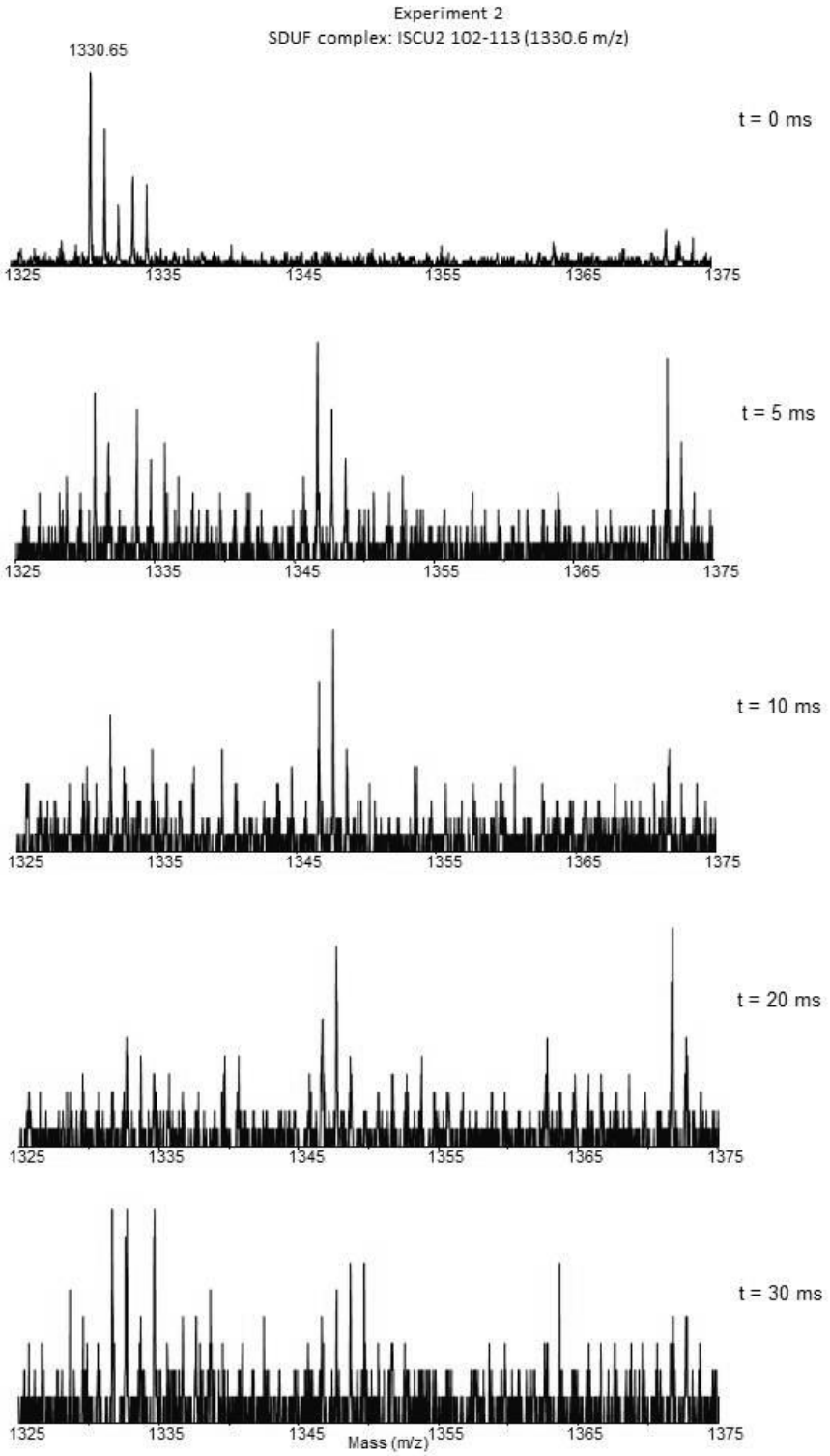

A-42. Mass spectra from SDUF, Experiment 2 at various exposure time to hydroxyl radicals.

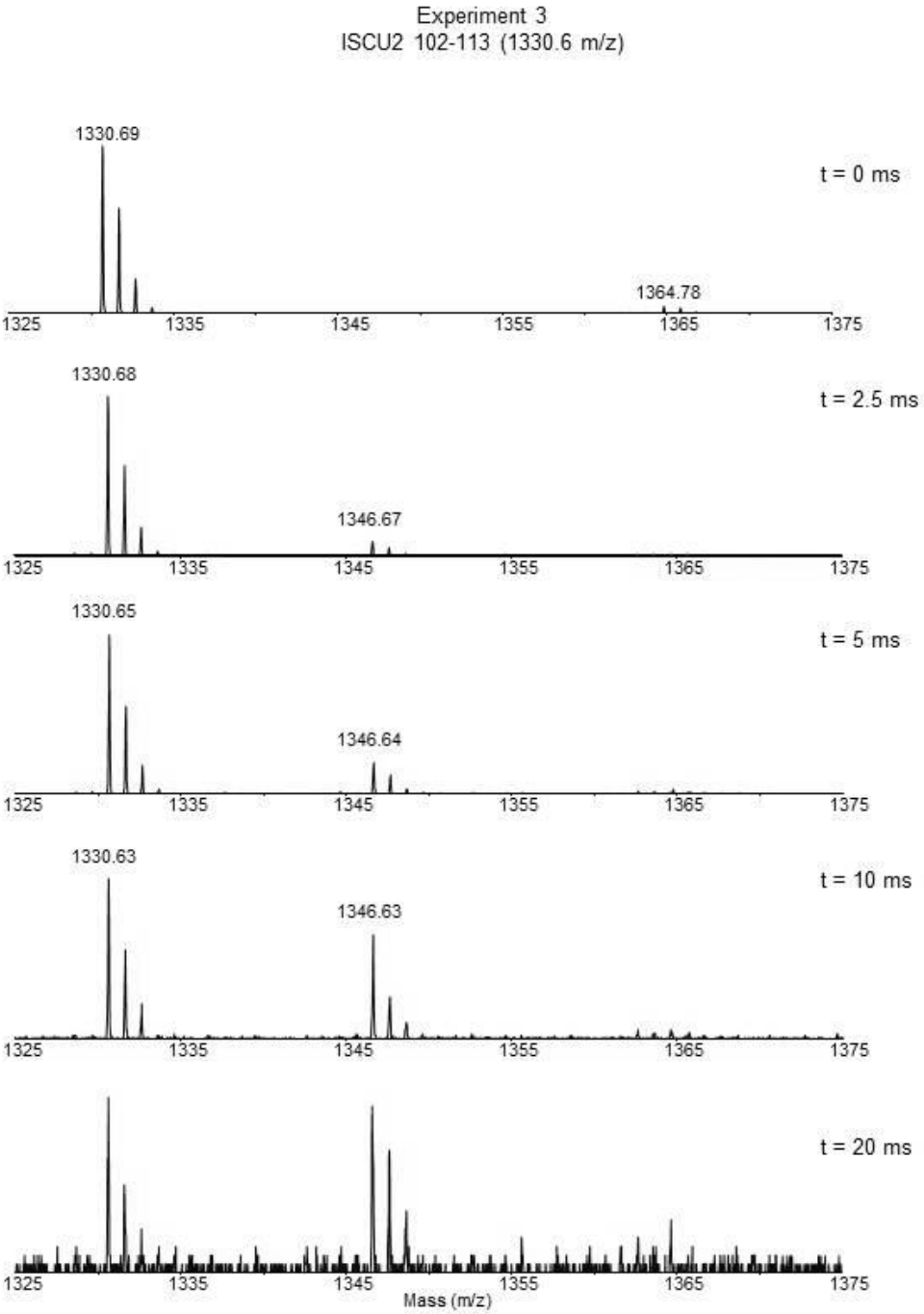

A-43. Mass spectra from ISCU2, Experiment 3 at various exposure time to hydroxyl radicals.

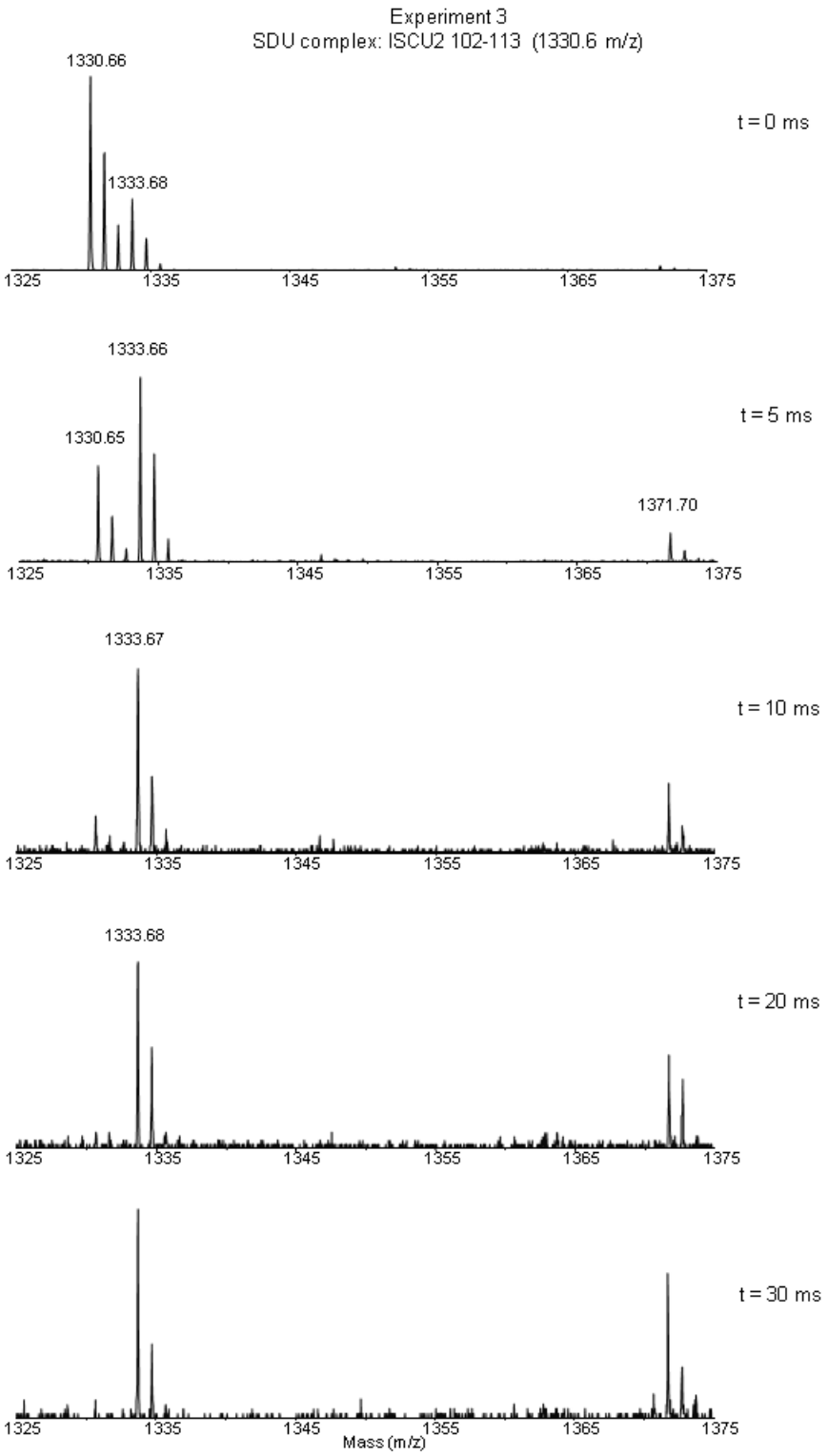

A-44. Mass spectra from SDU, Experiment 3 at various exposure time to hydroxyl radicals.

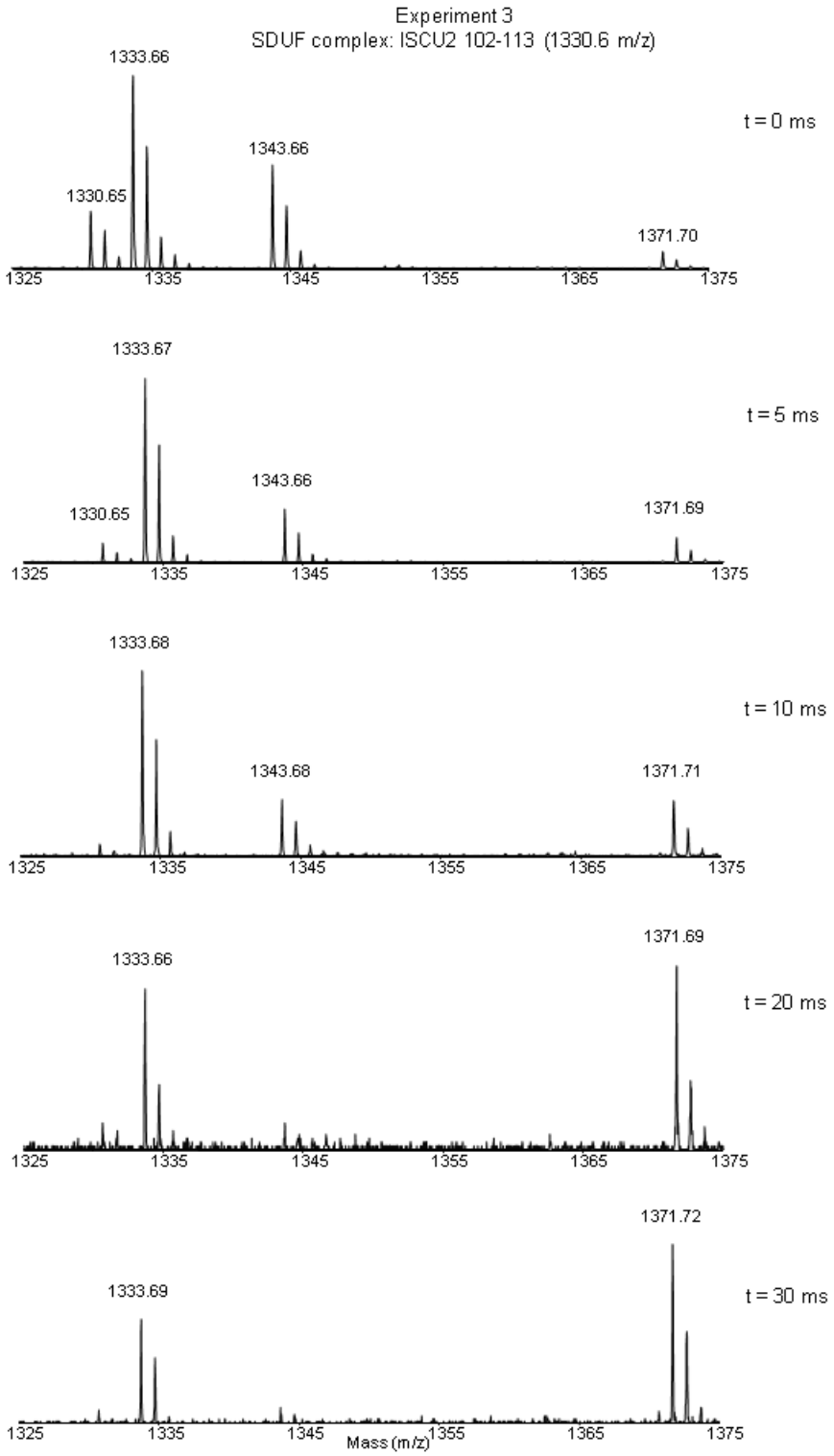

A-45. Mass spectra from SDUF, Experiment 3 at various exposure time to hydroxyl radicals.

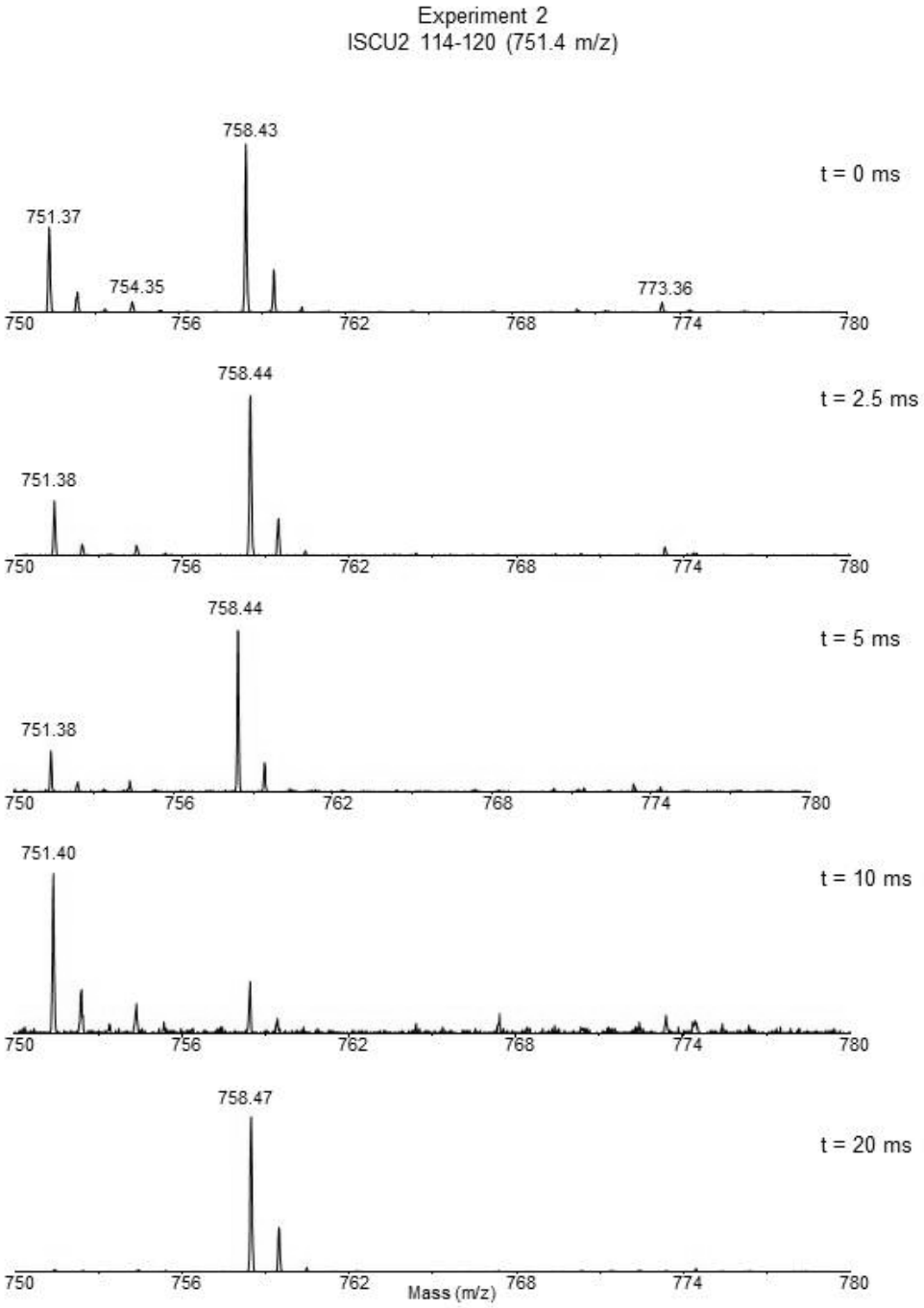

A-46. Mass spectra from ISCU2, Experiment 2 at various exposure time to hydroxyl radicals.

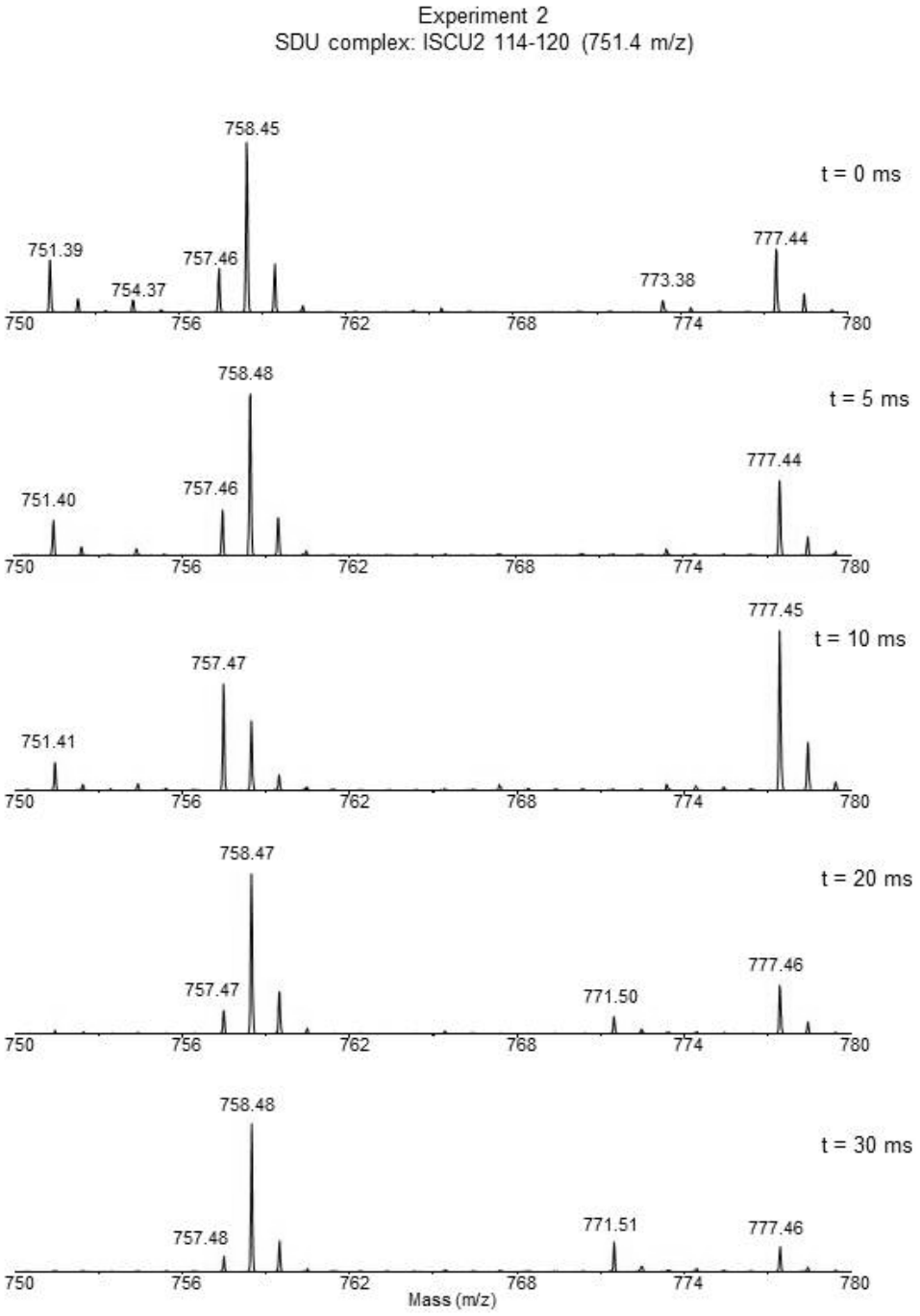

A-47. Mass spectra from SDU, Experiment 2 at various exposure time to hydroxyl radicals.

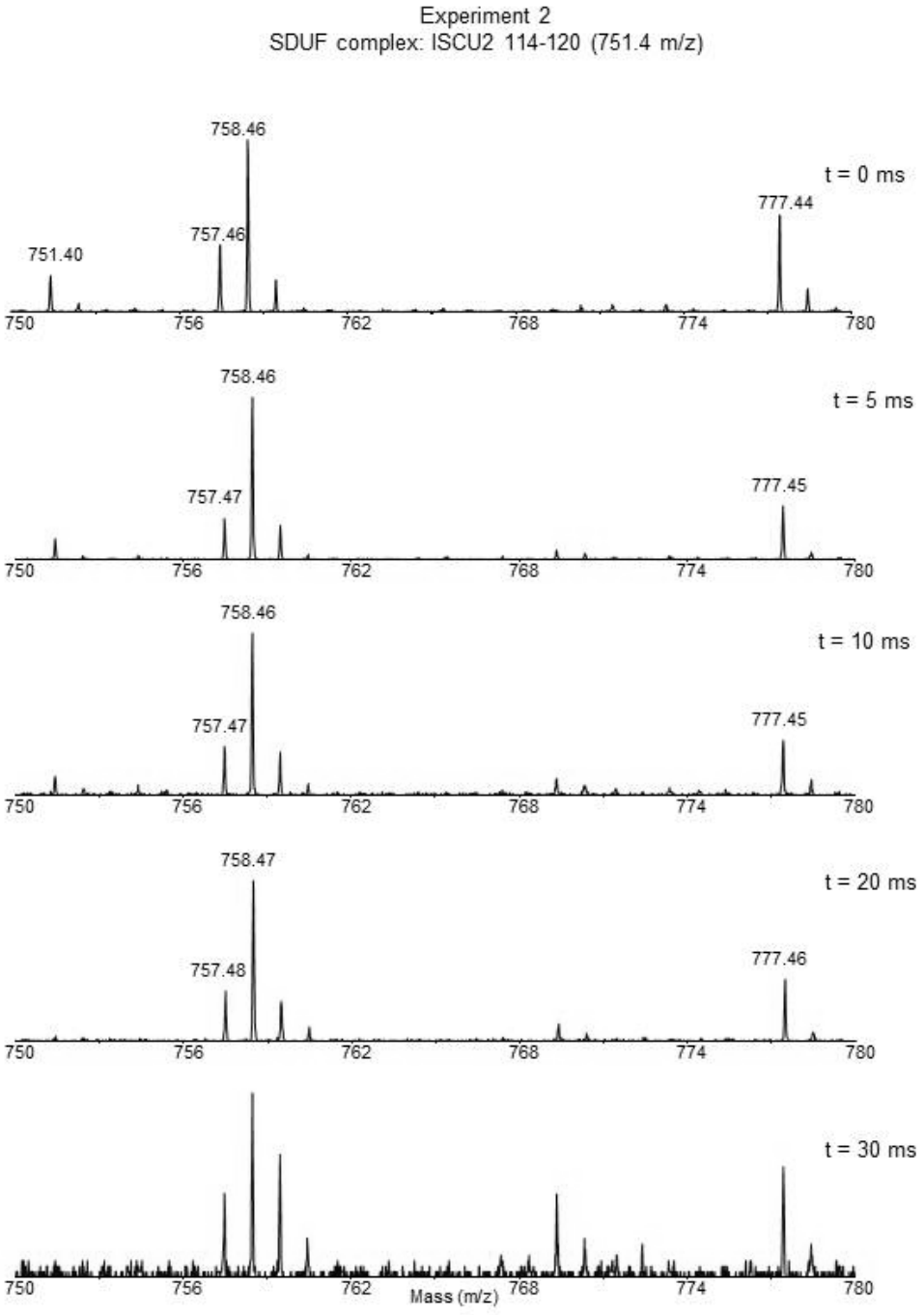

A-48. Mass spectra from SDUF, Experiment 2 at various exposure time to hydroxyl radicals.

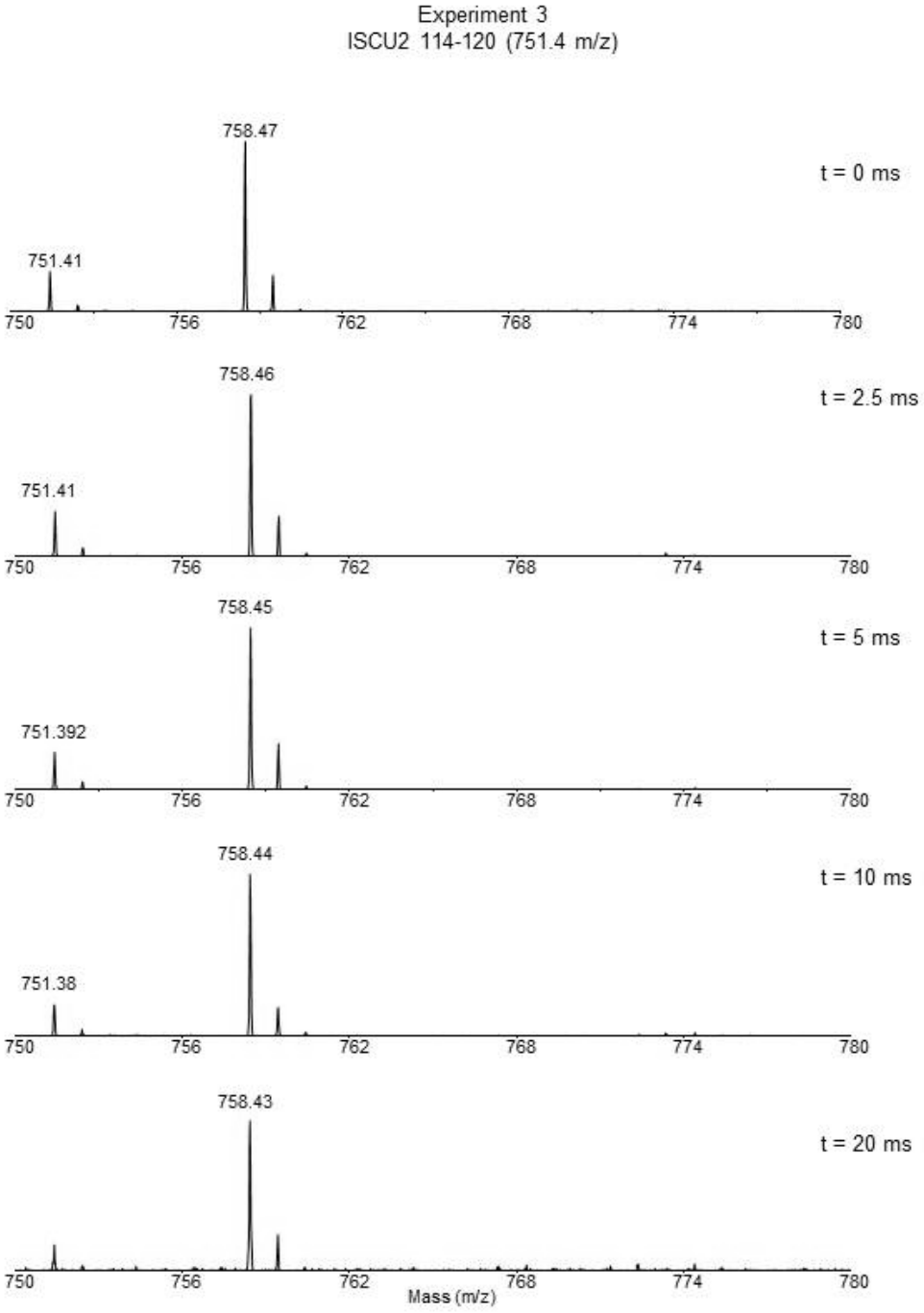

A-49. Mass spectra from ISCU2, Experiment 3 at various exposure time to hydroxyl radicals.

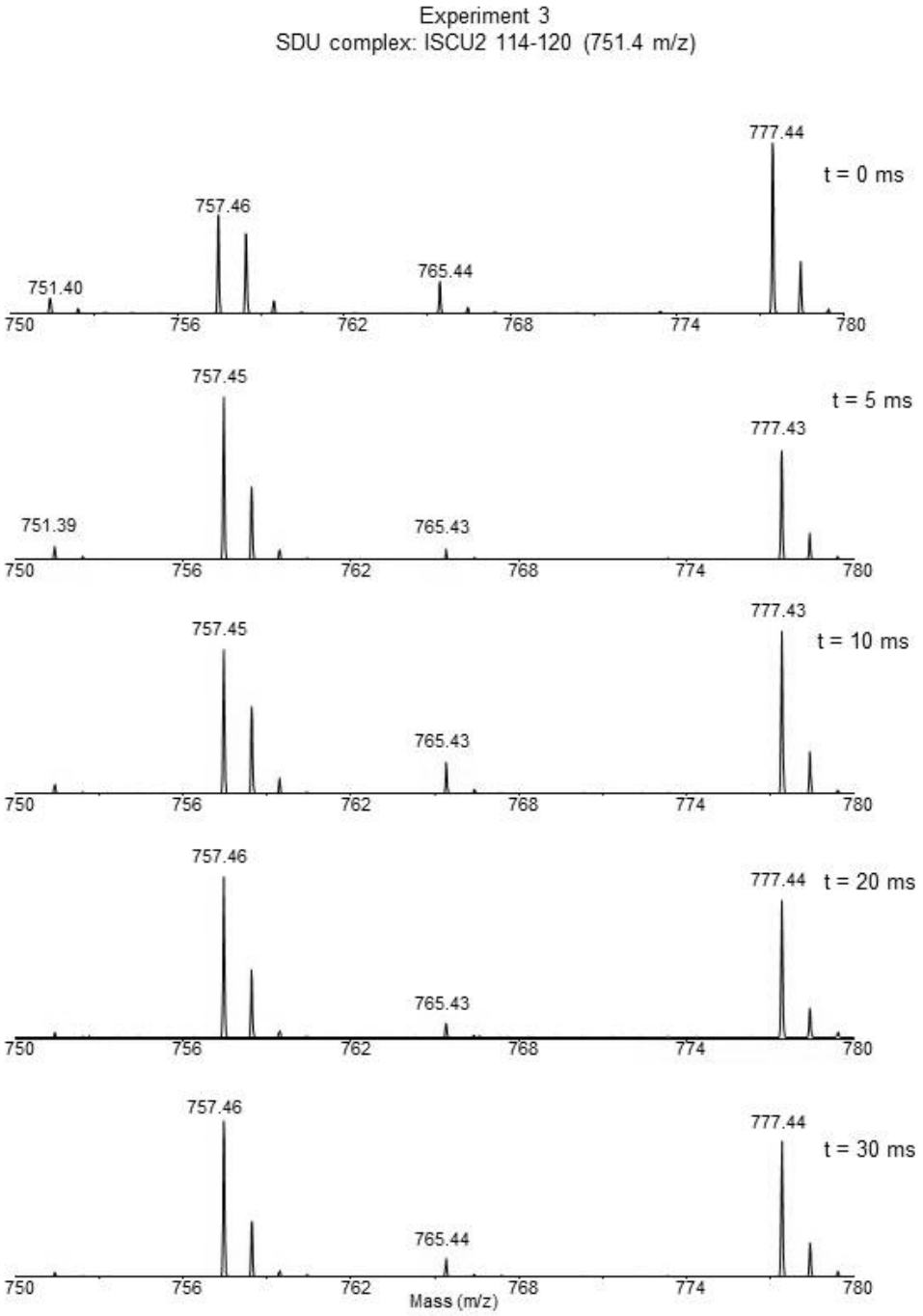

A-50. Mass spectra from SDU, Experiment 3 at various exposure time to hydroxyl radicals.

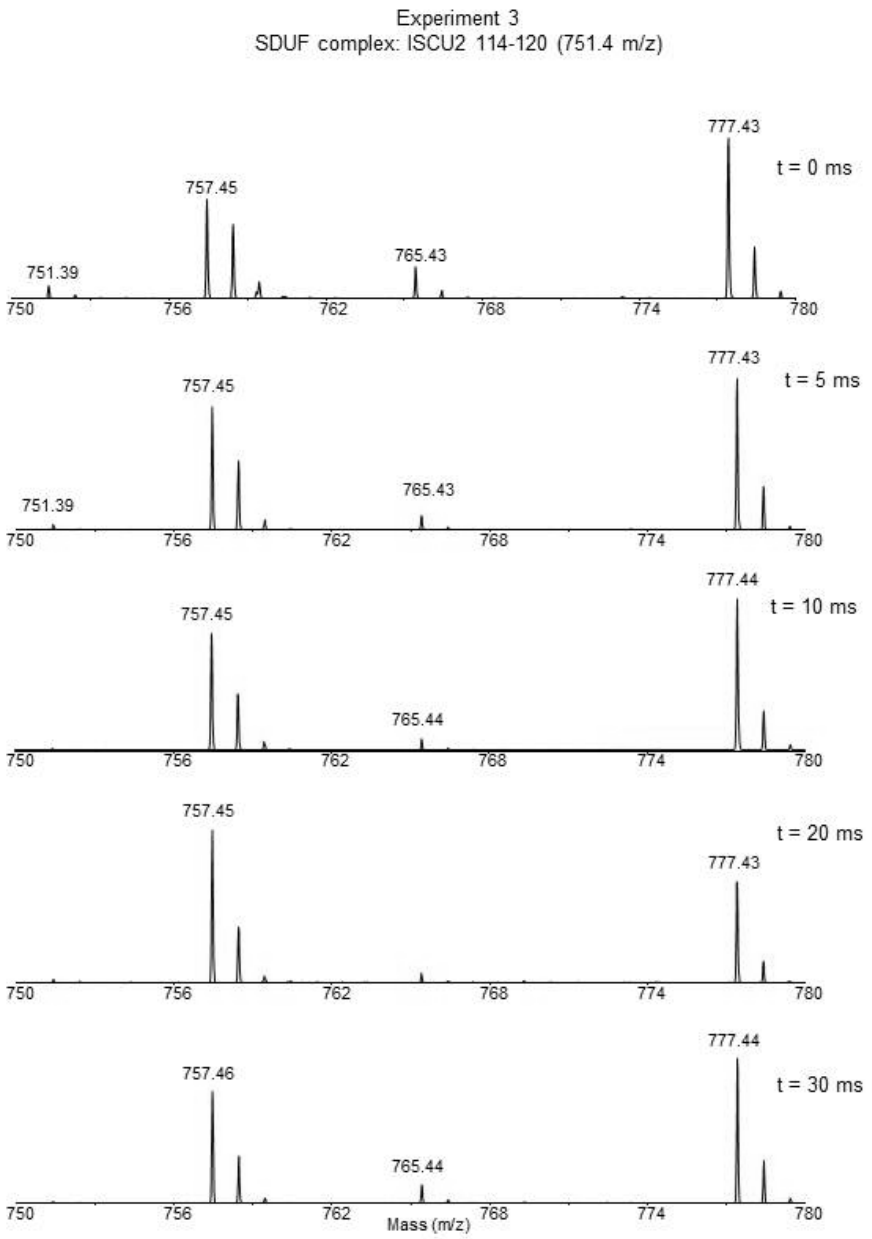

A-51. Mass spectra from SDUF, Experiment 3 at various exposure time to hydroxyl radicals.

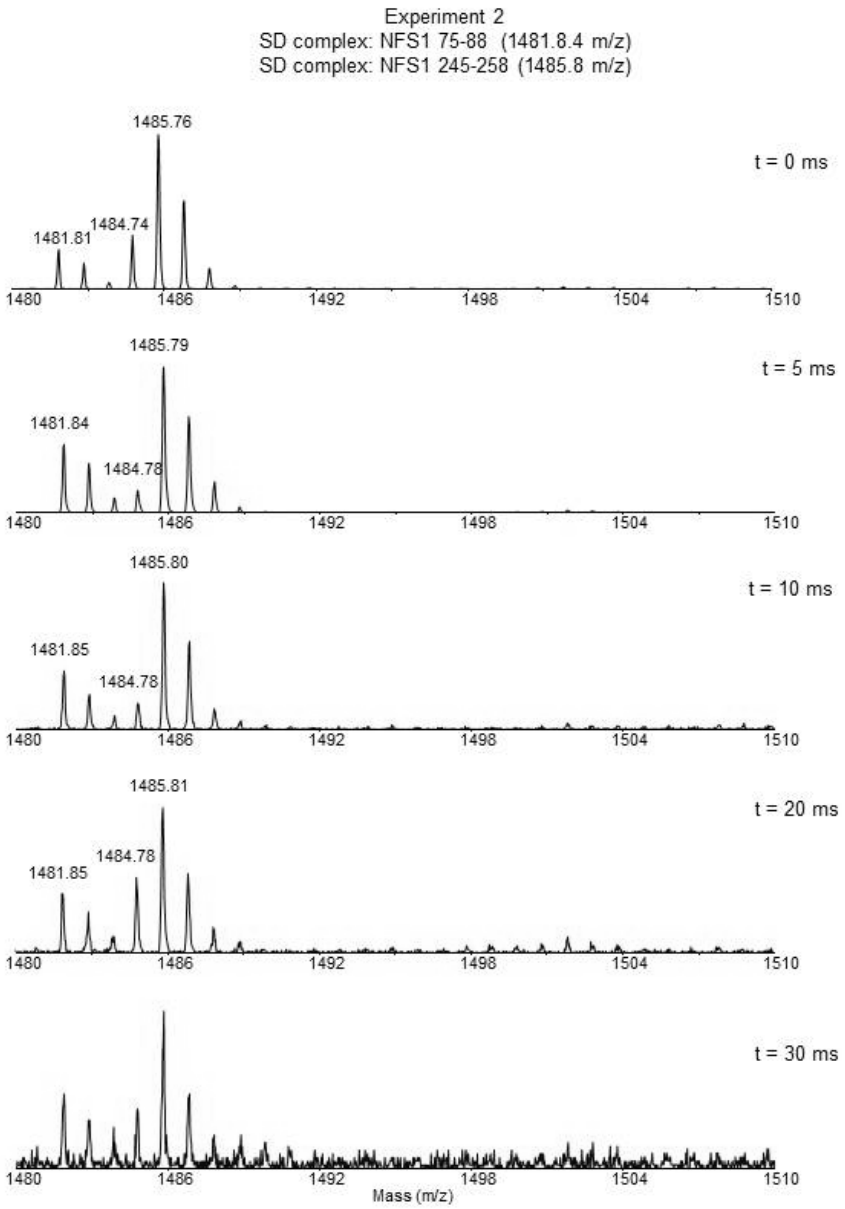

A-52. Mass spectra from SD, Experiment 2 at various exposure time to hydroxyl radicals.

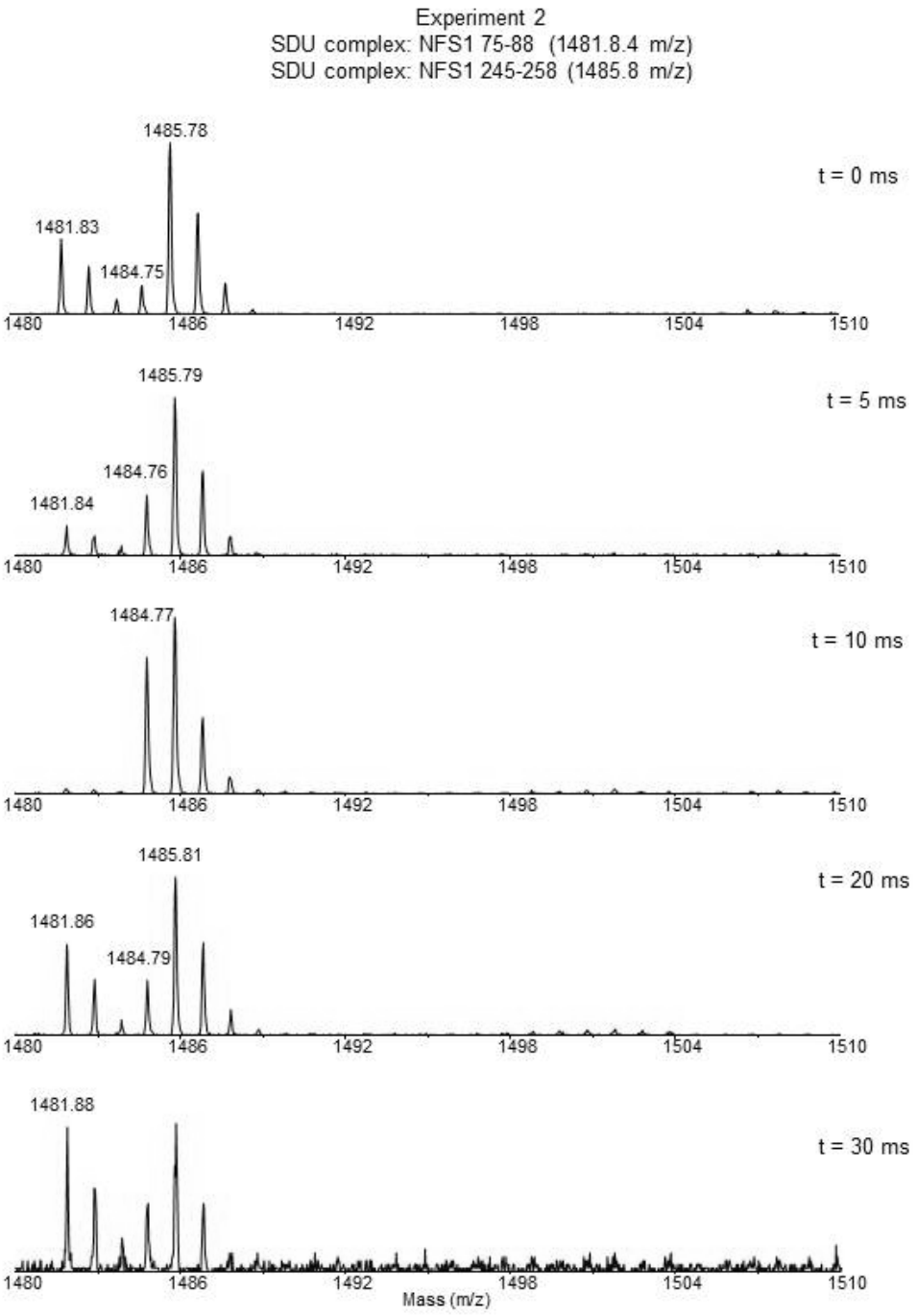

A-53. Mass spectra from SDU, Experiment 2 at various exposure time to hydroxyl radicals.

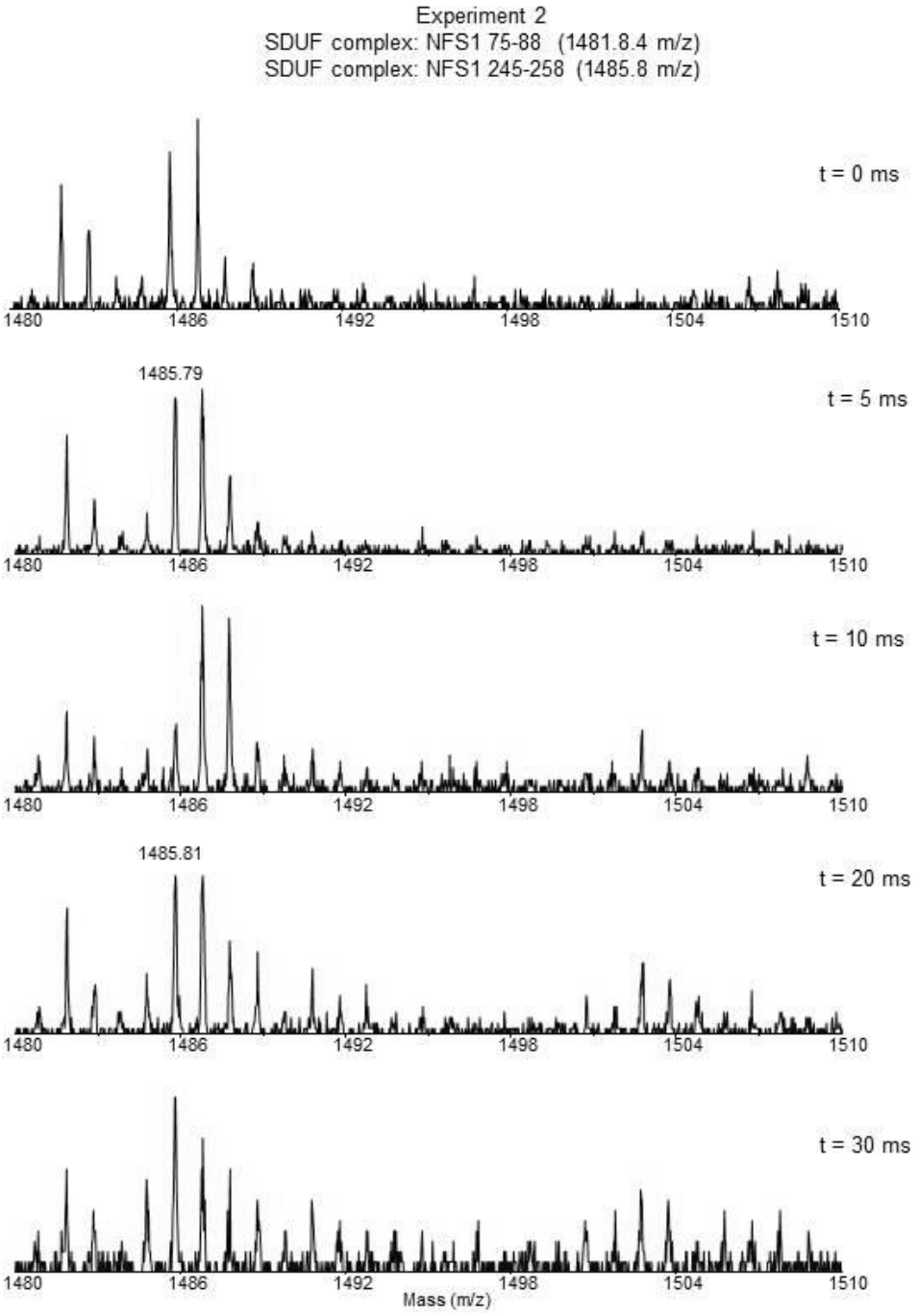

A-54. Mass spectra from SDUF, Experiment 2 at various exposure time to hydroxyl radicals.

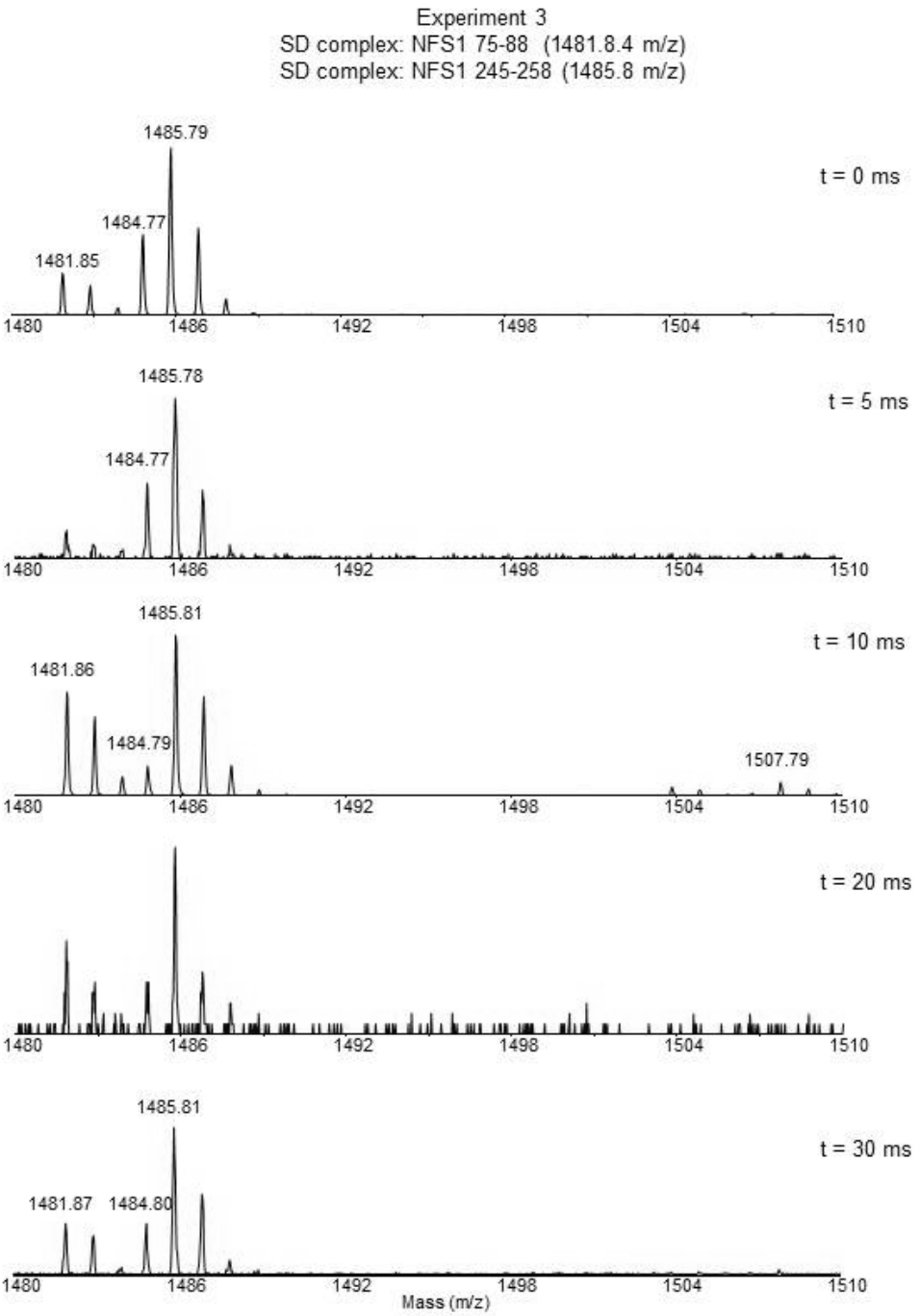

A-55. Mass spectra from SD, Experiment 3 at various exposure time to hydroxyl radicals.

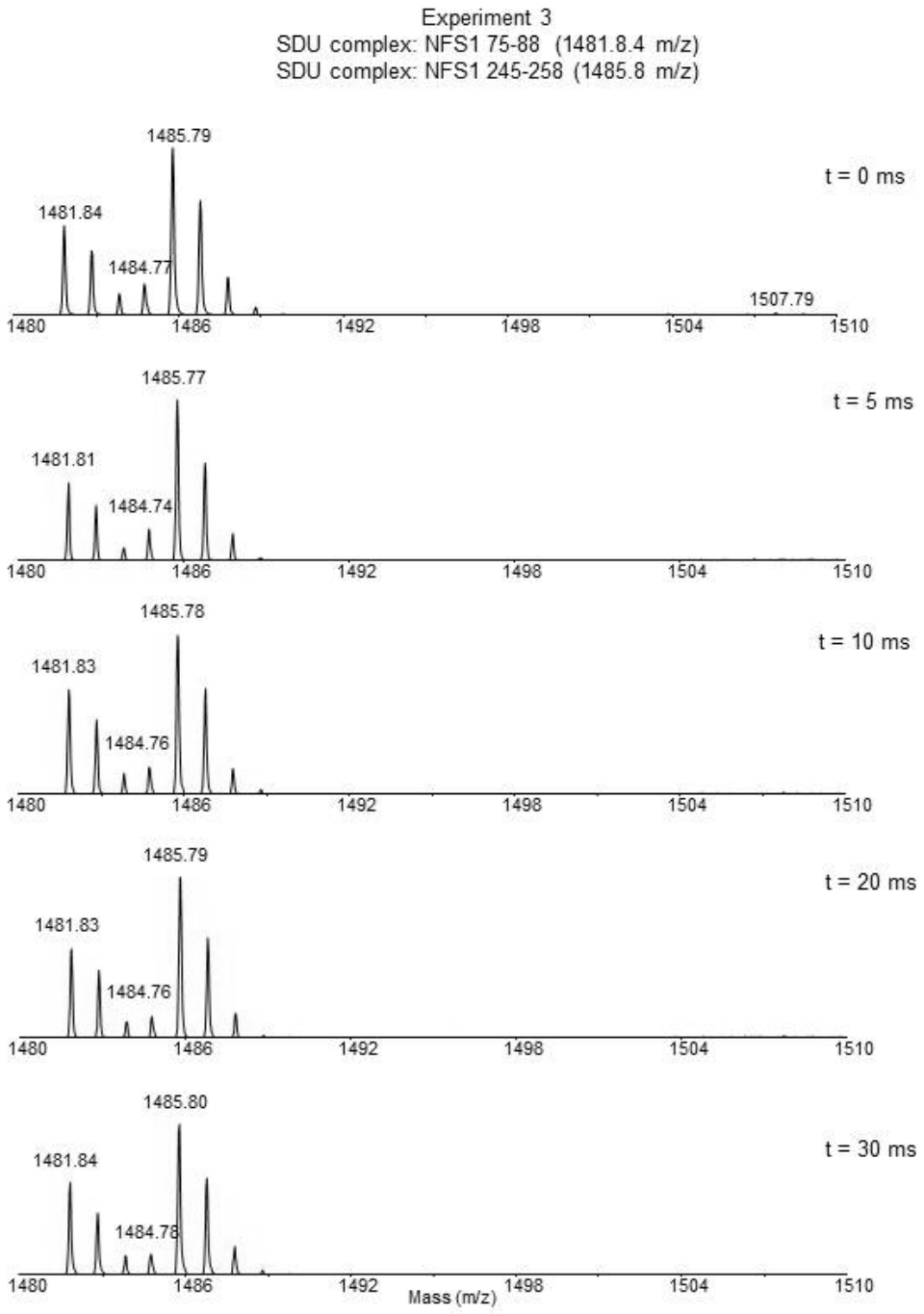

A-56. Mass spectra from SDU, Experiment 3 at various exposure time to hydroxyl radicals.

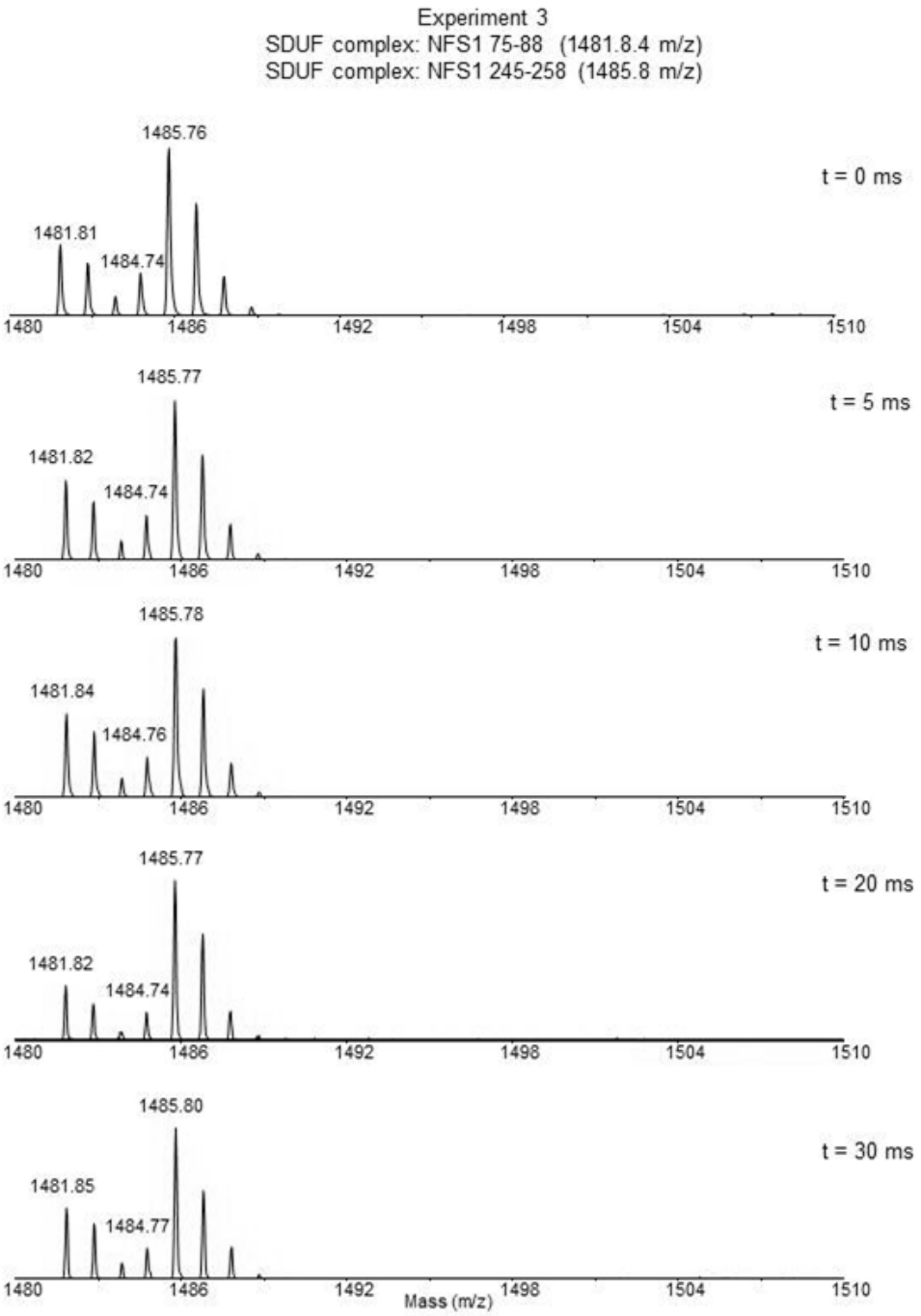

A-57. Mass spectra from SDUF, Experiment 3 at various exposure time to hydroxyl radicals.

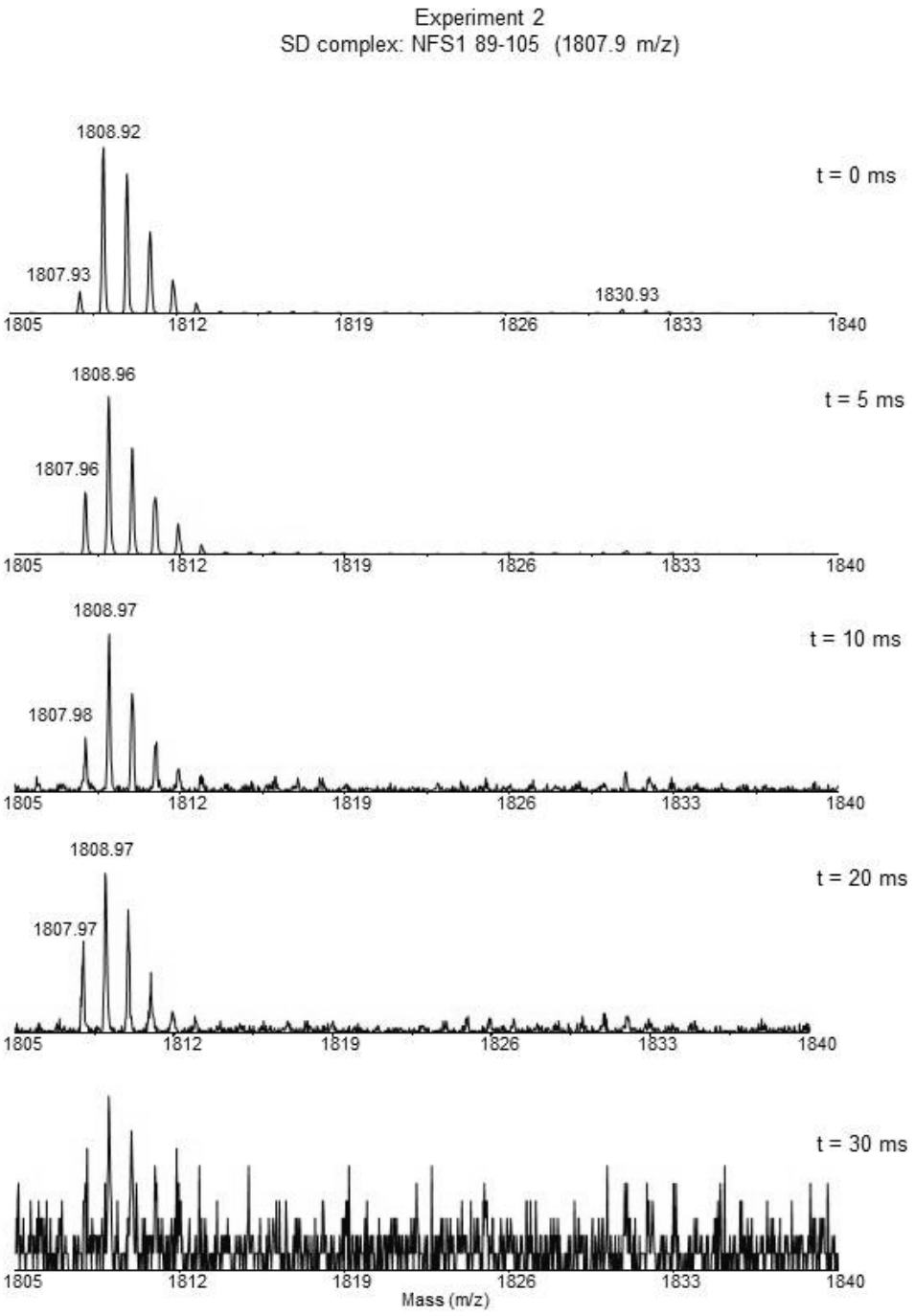

A-58. Mass spectra from SD, Experiment 2 at various exposure time to hydroxyl radicals.

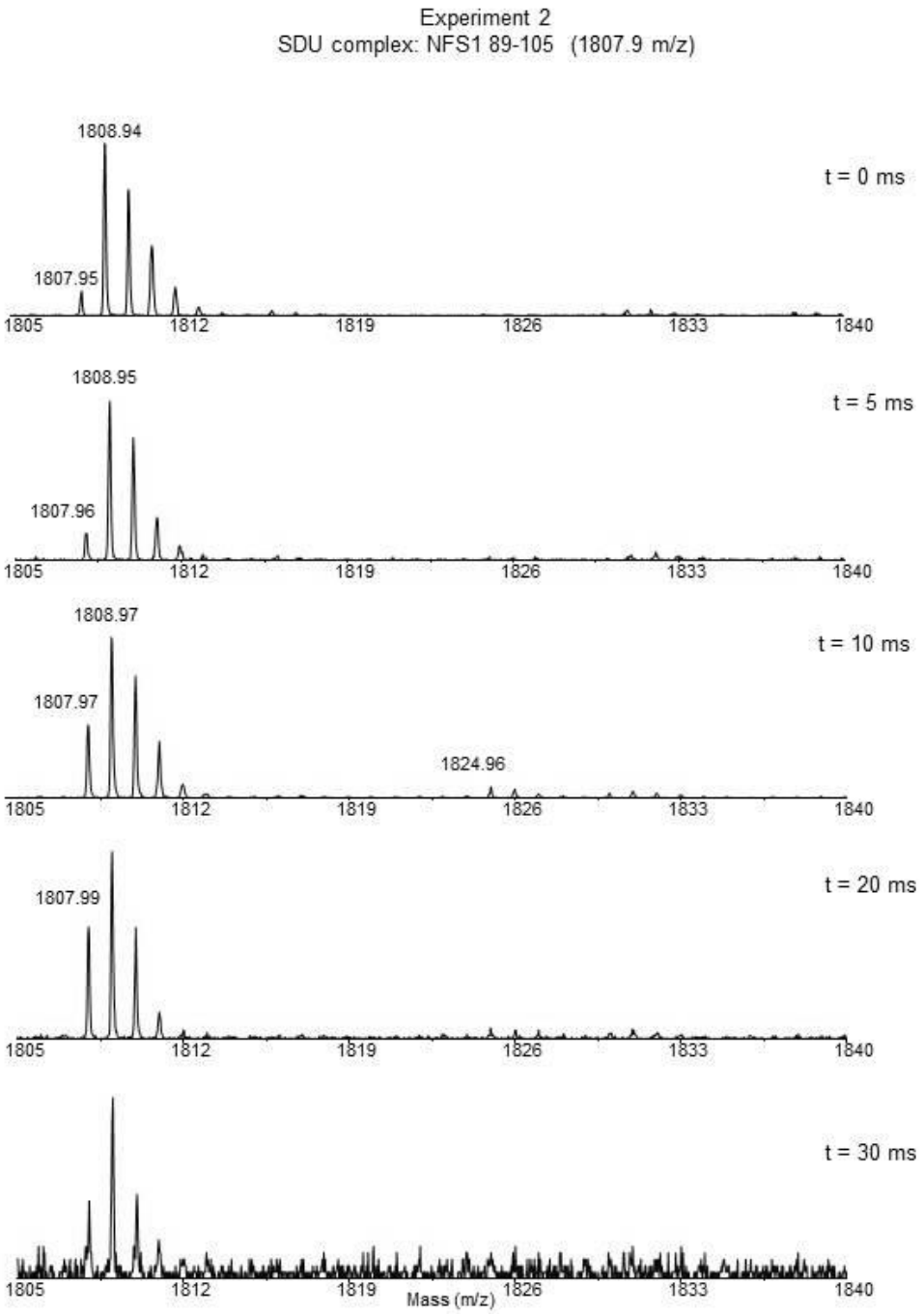

A-59. Mass spectra from SDU, Experiment 2 at various exposure time to hydroxyl radicals.

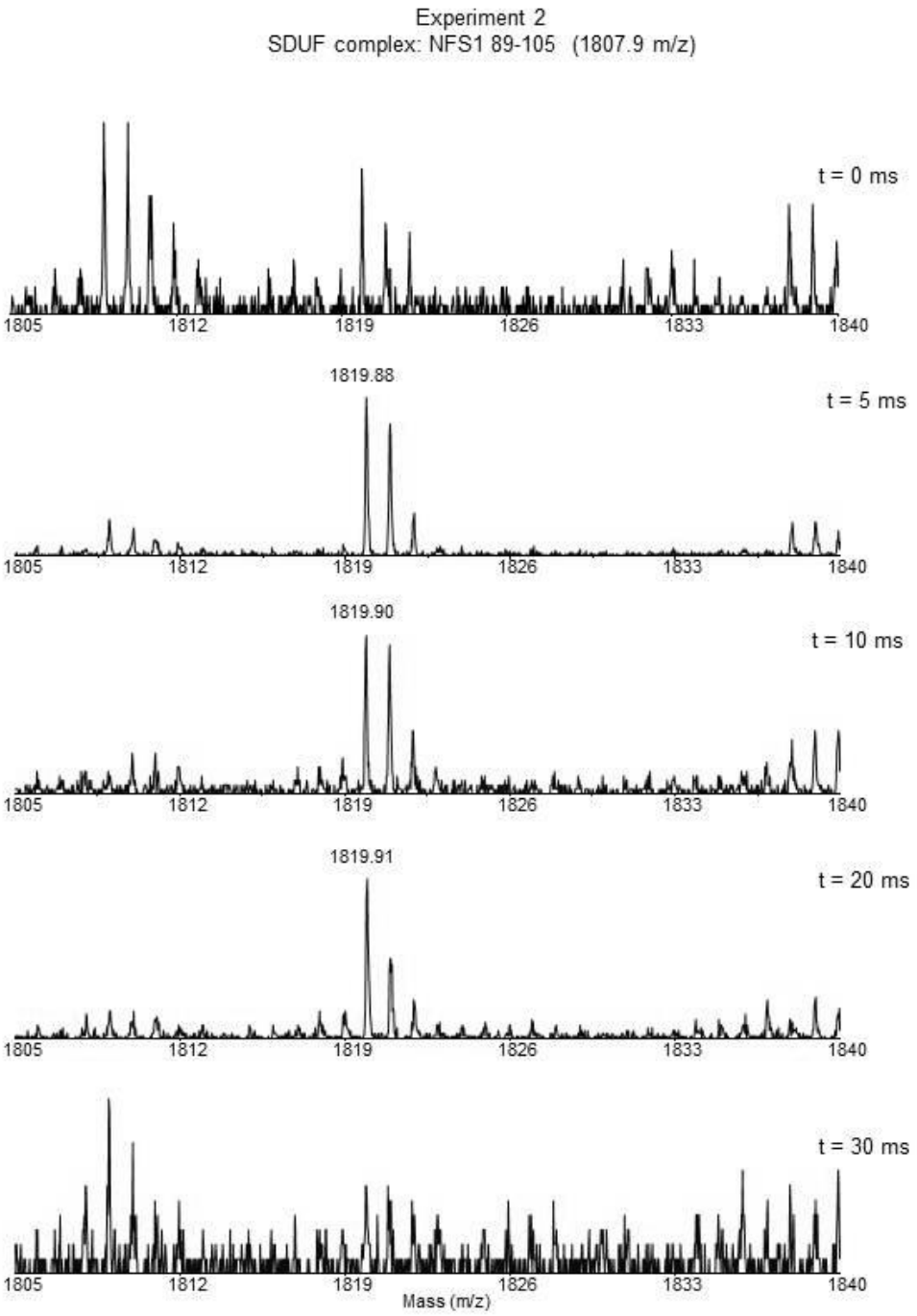

A-60. Mass spectra from SDUF, Experiment 2 at various exposure time to hydroxyl radicals.

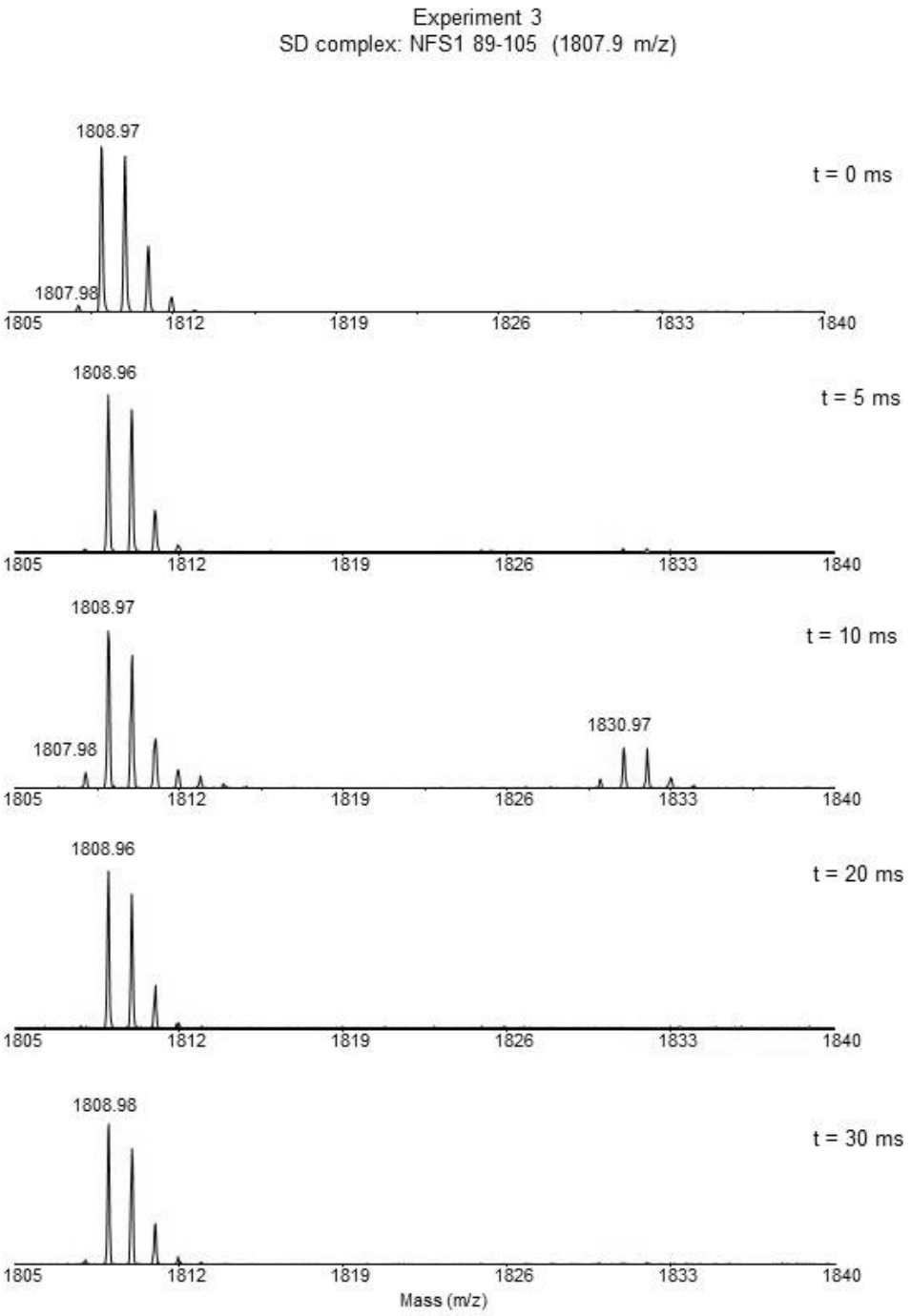

A-61. Mass spectra from SD, Experiment 3 at various exposure time to hydroxyl radicals.

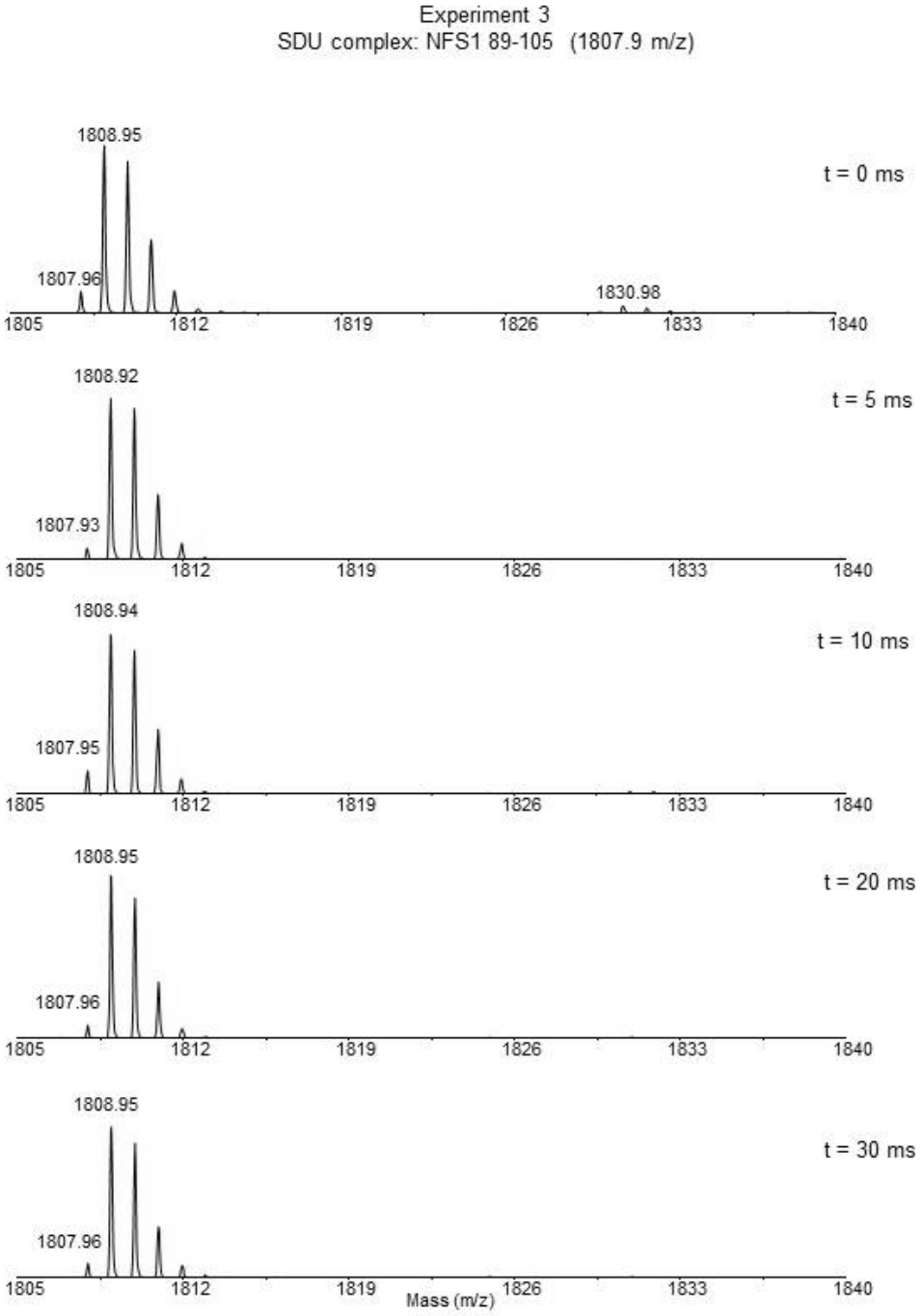

A-62. Mass spectra from SDU, Experiment 3 at various exposure time to hydroxyl radicals.

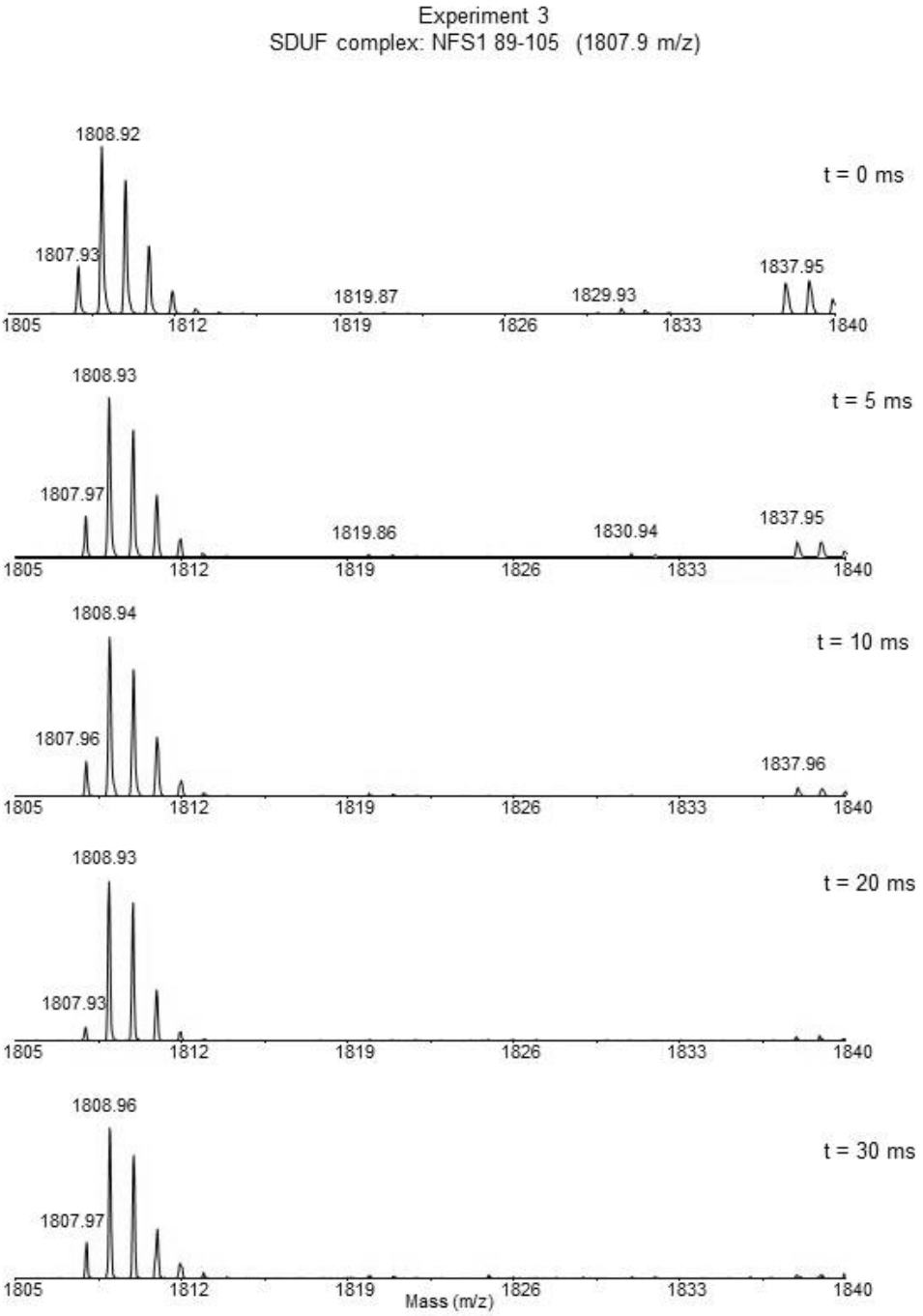

A-63. Mass spectra from SDUF, Experiment 3 at various exposure time to hydroxyl radicals.

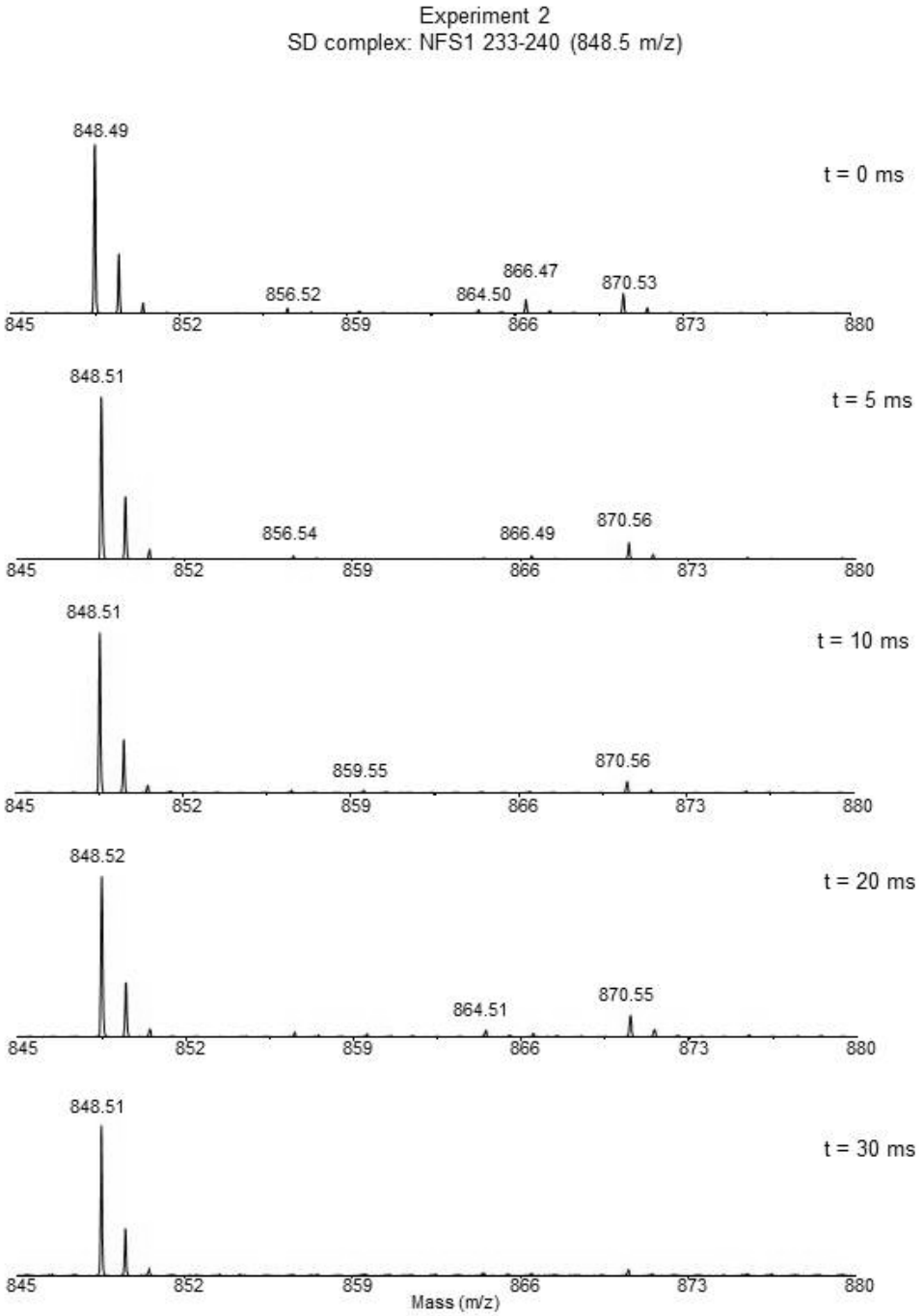

A-64. Mass spectra from SD, Experiment 2 at various exposure time to hydroxyl radicals.

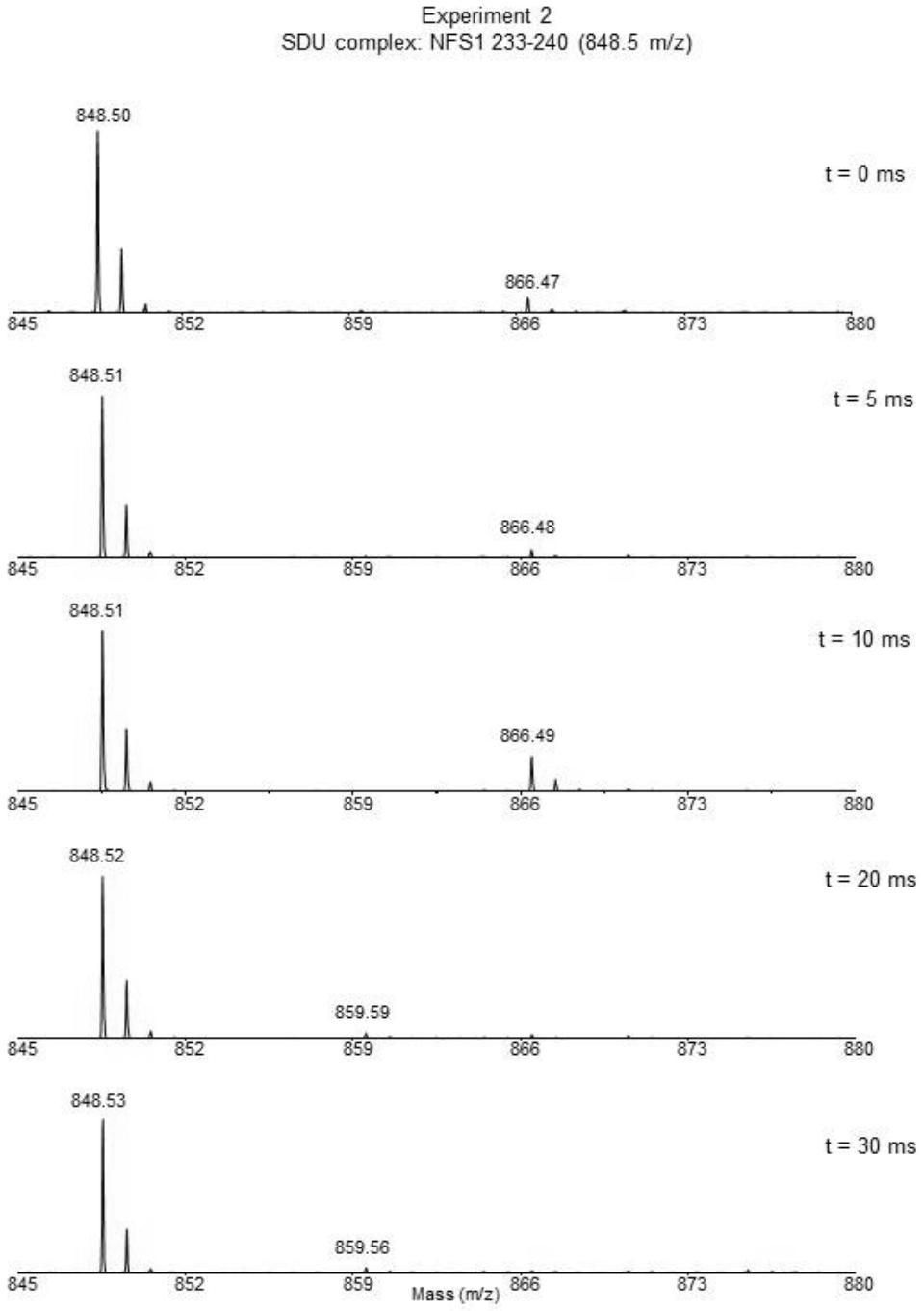

A-65. Mass spectra from SDU, Experiment 2 at various exposure time to hydroxyl radicals.

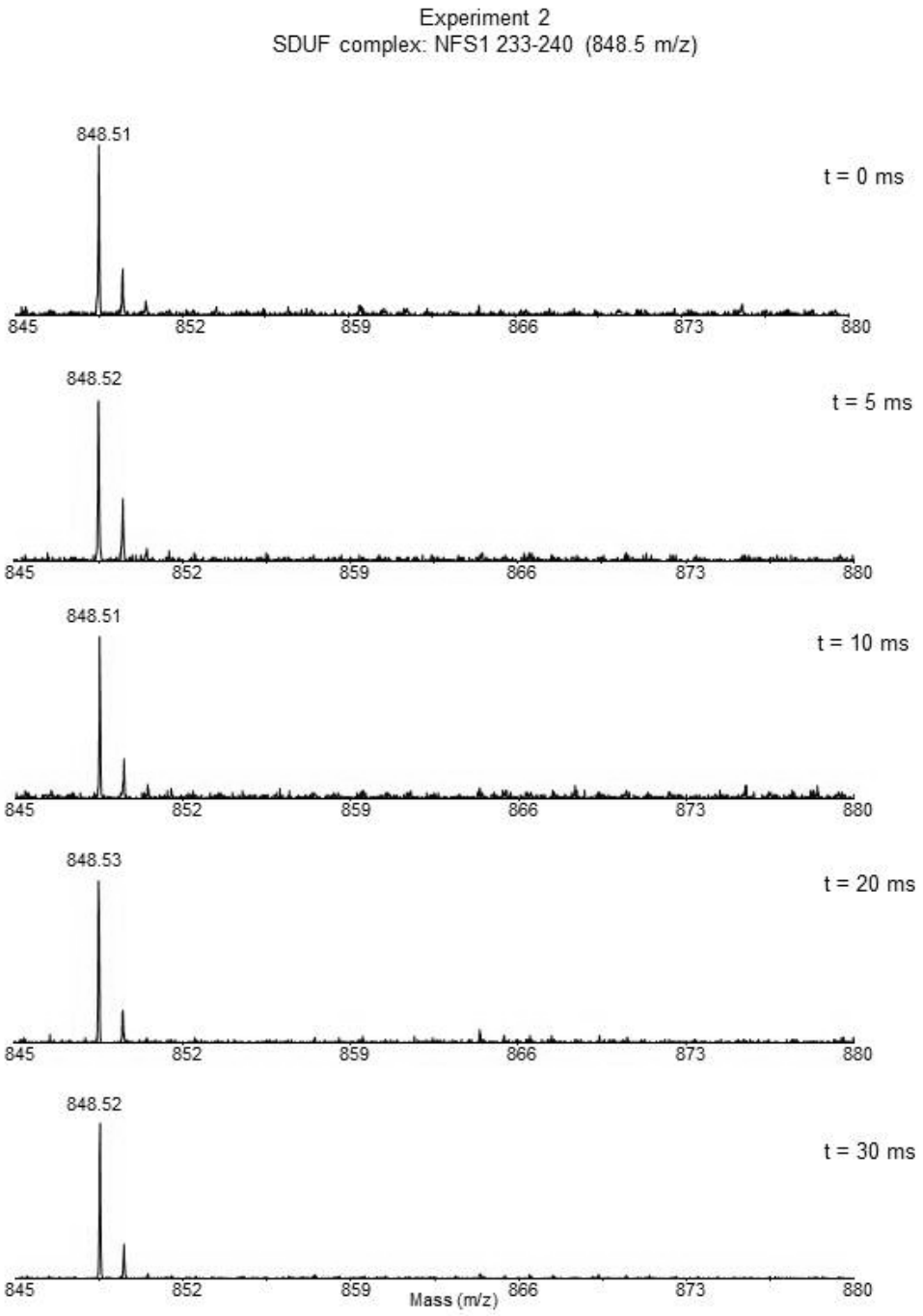

A-66. Mass spectra from SDUF, Experiment 2 at various exposure time to hydroxyl radicals.

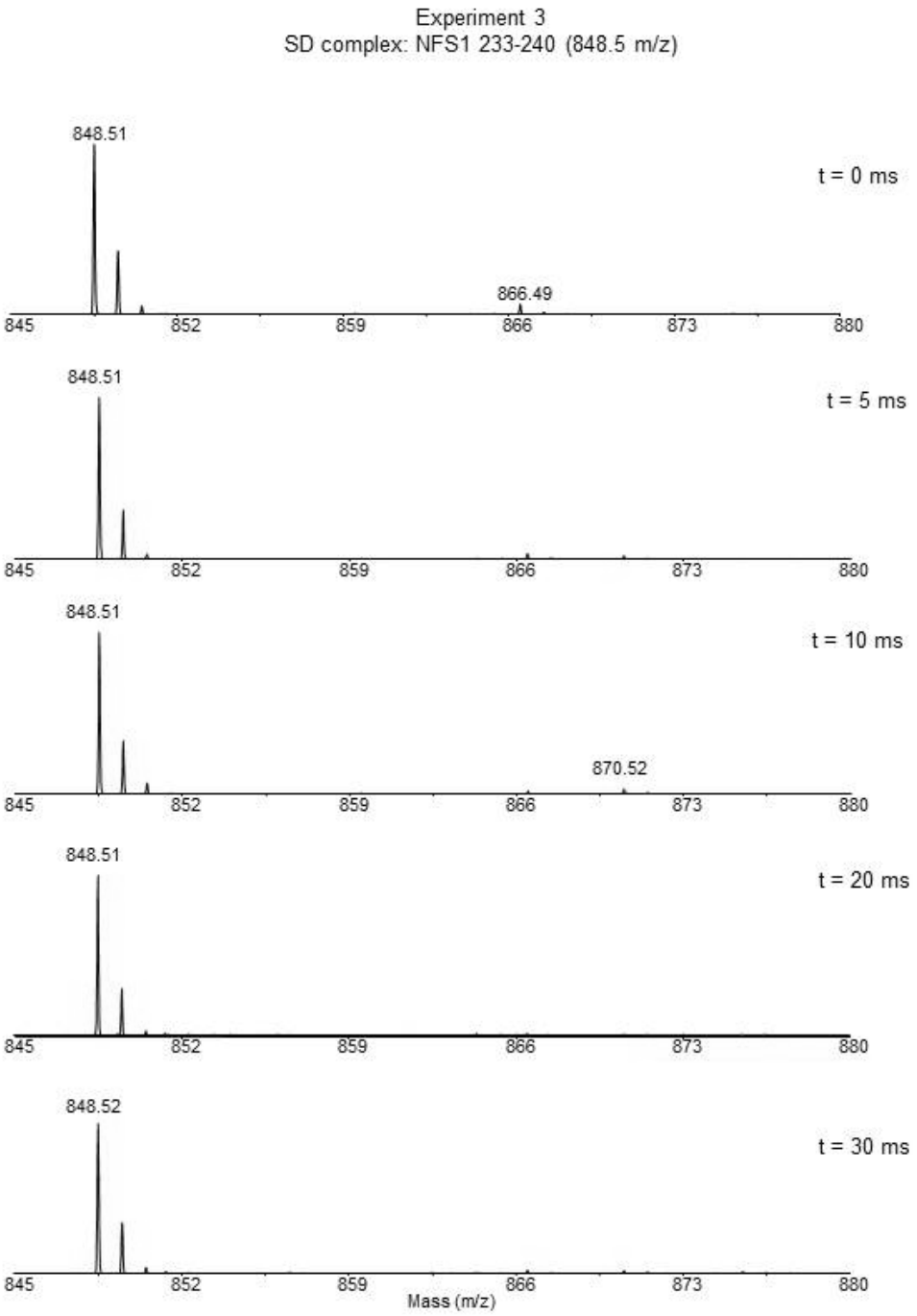

A-67. Mass spectra from SD, Experiment 3 at various exposure time to hydroxyl radicals.

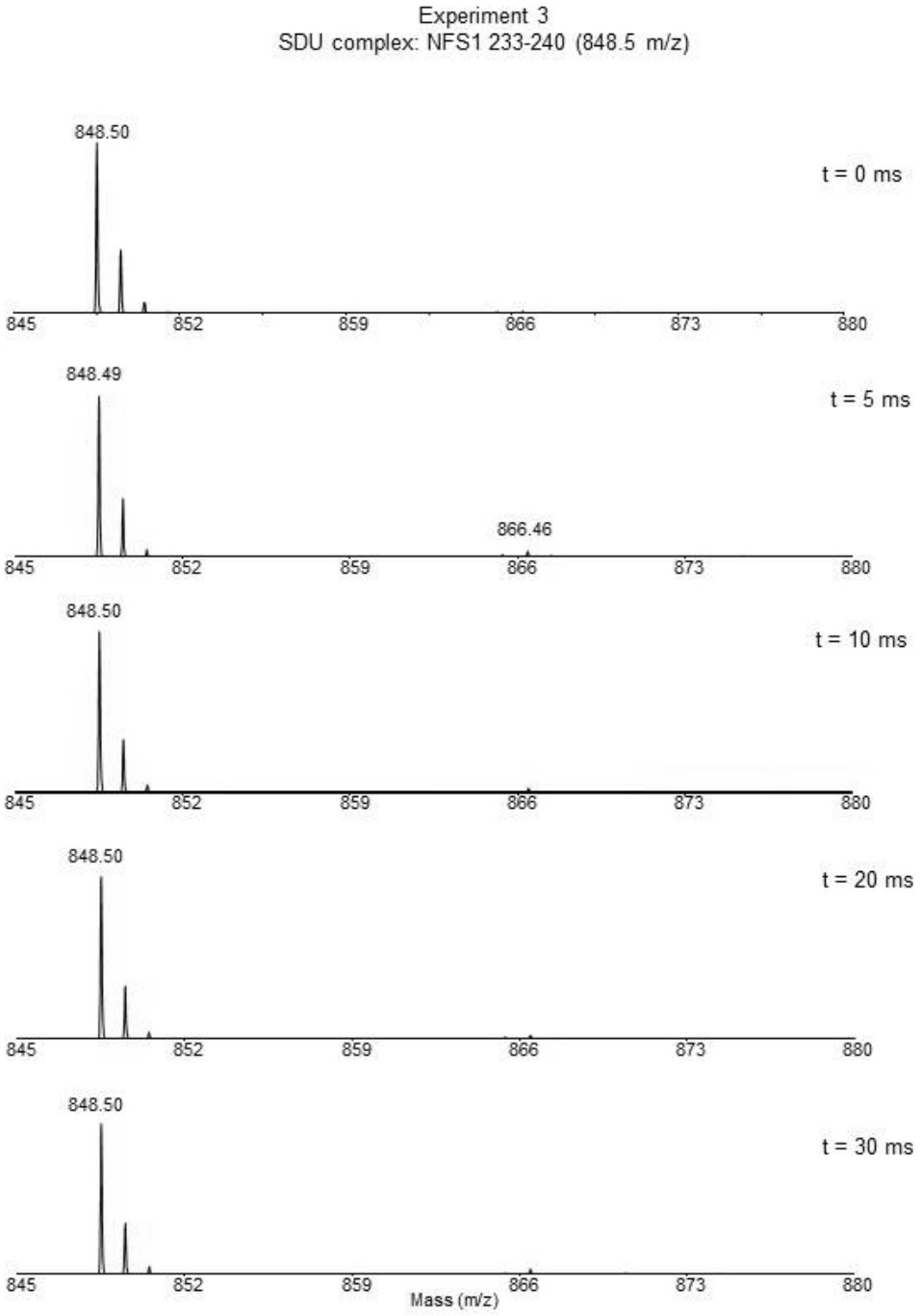

A-68. Mass spectra from SDU, Experiment 3 at various exposure time to hydroxyl radicals.

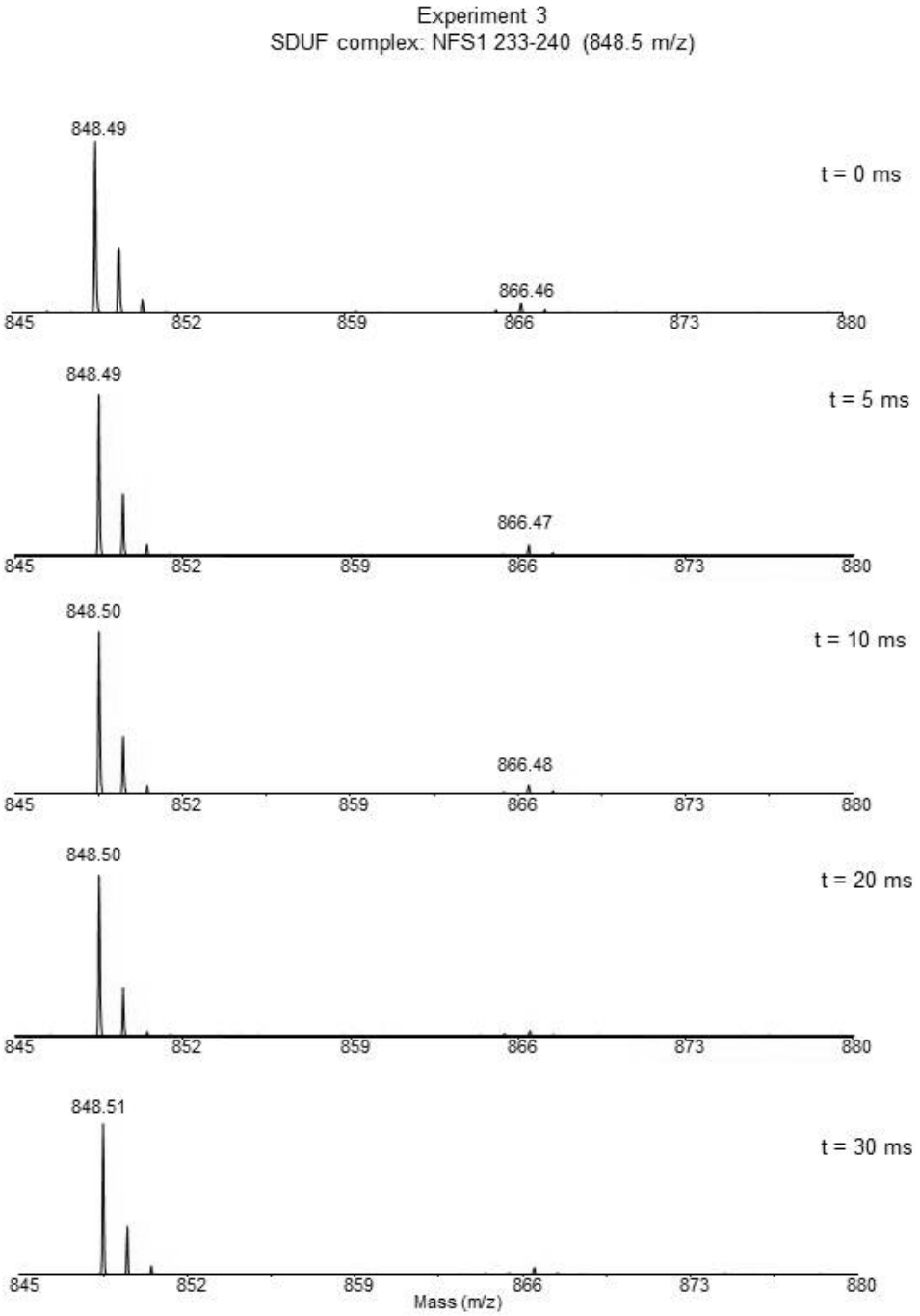

A-69. Mass spectra from SDUF, Experiment 3 at various exposure time to hydroxyl radicals.

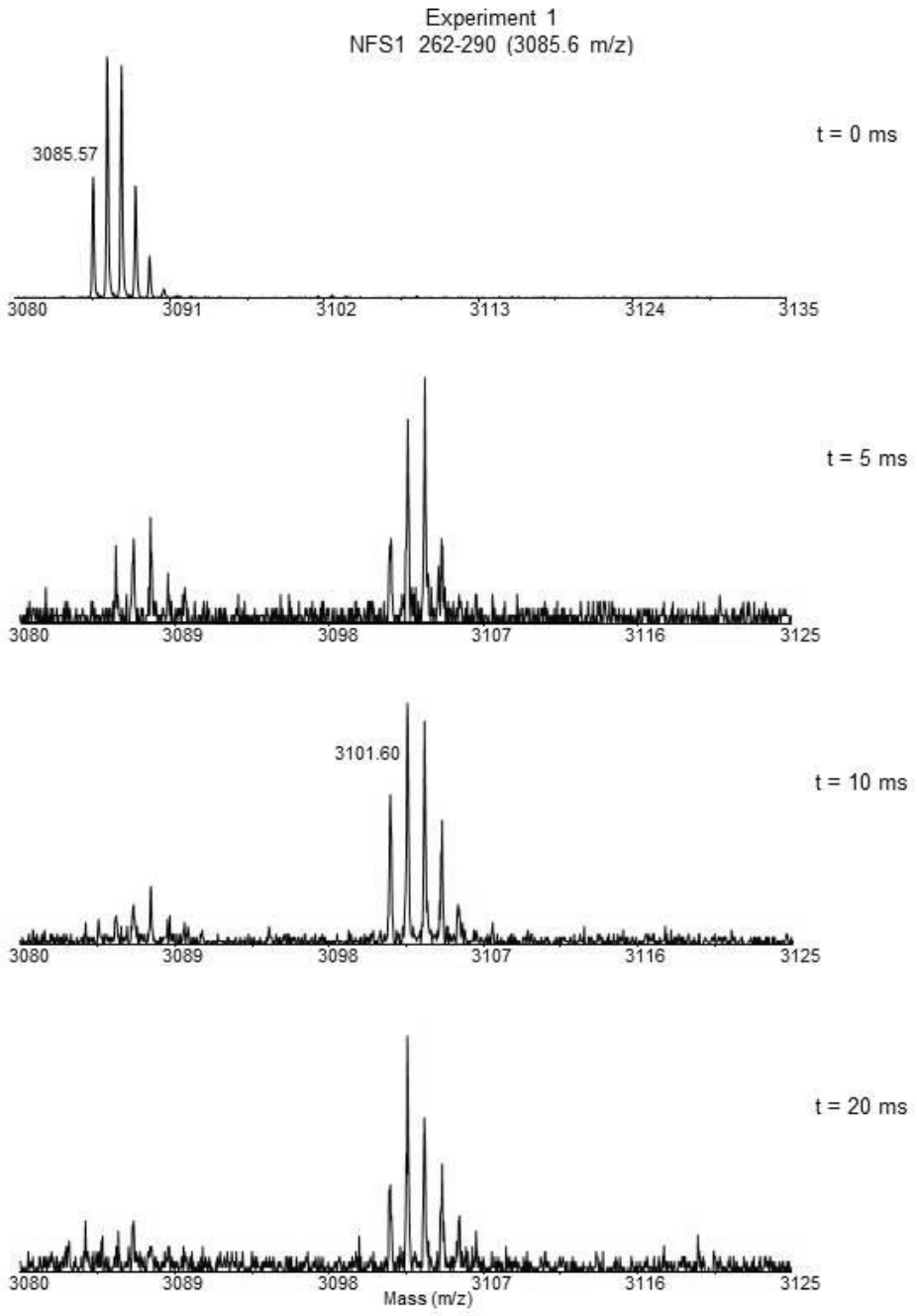

A70. Mass spectra from NFS1, Experiment 1 at various exposure time to hydroxyl radicals.

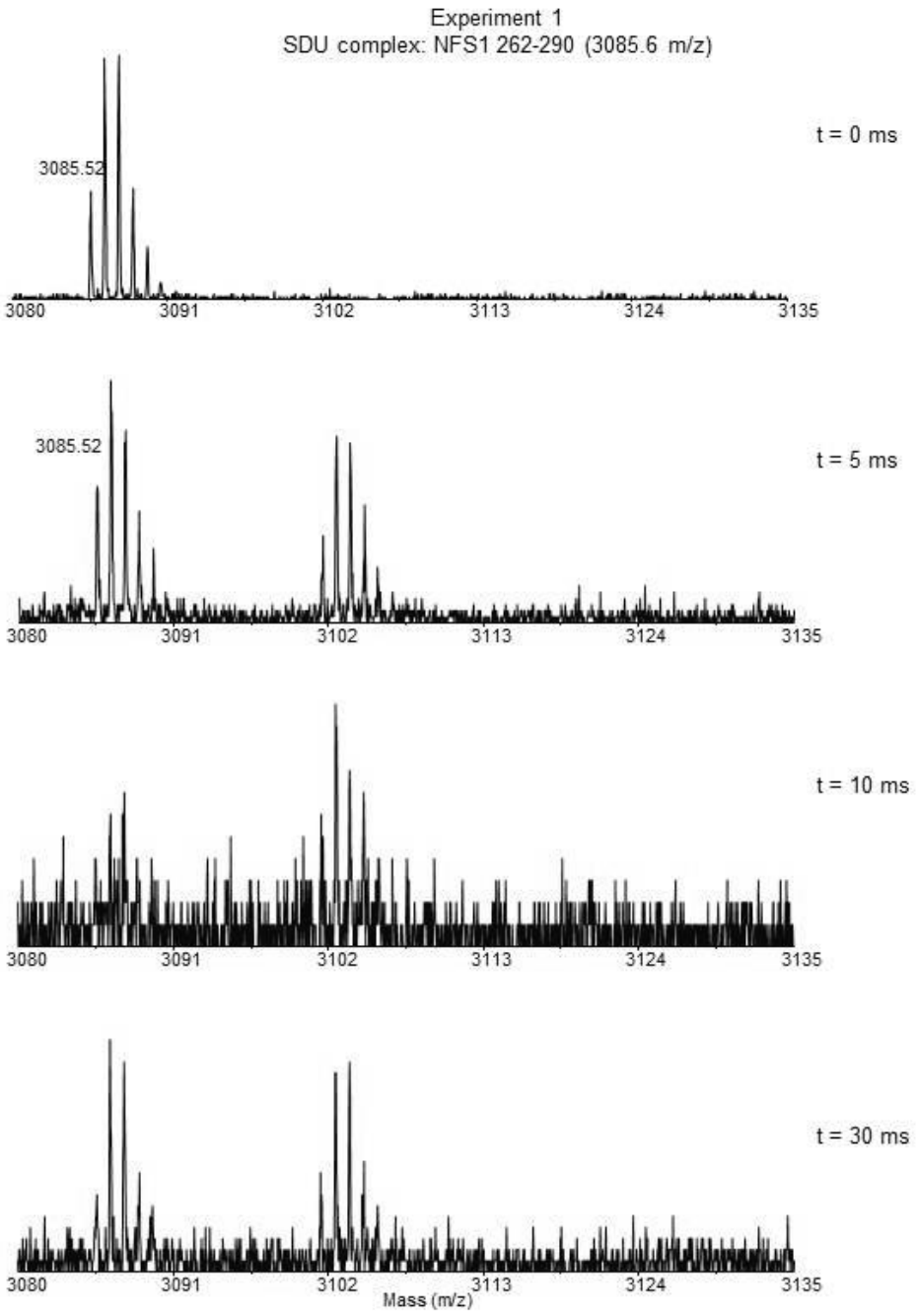

A-71. Mass spectra from SDU, Experiment 1 at various exposure time to hydroxyl radicals.

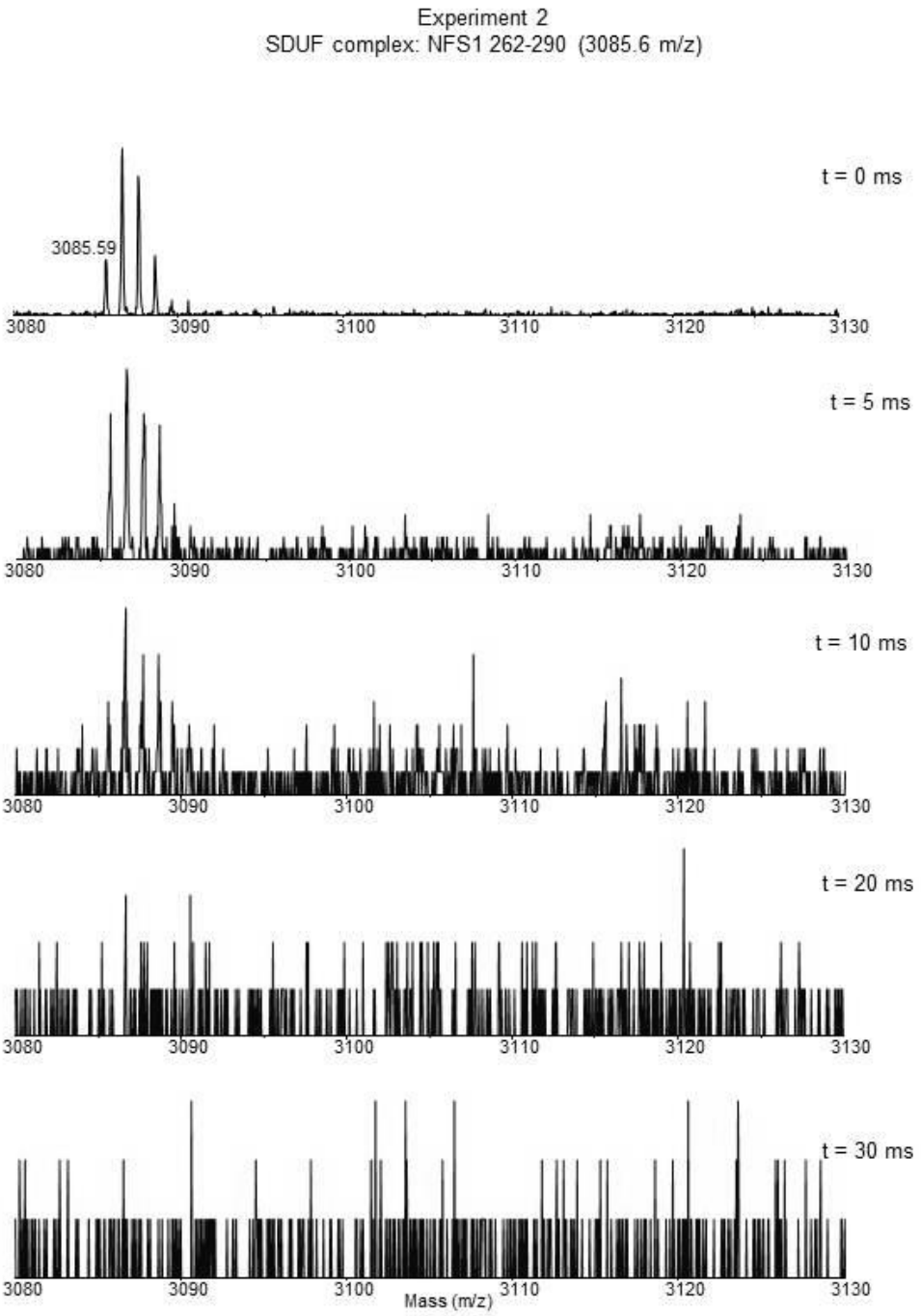

A-72. Mass spectra from SDUF, Experiment 1 at various exposure time to hydroxyl radicals.

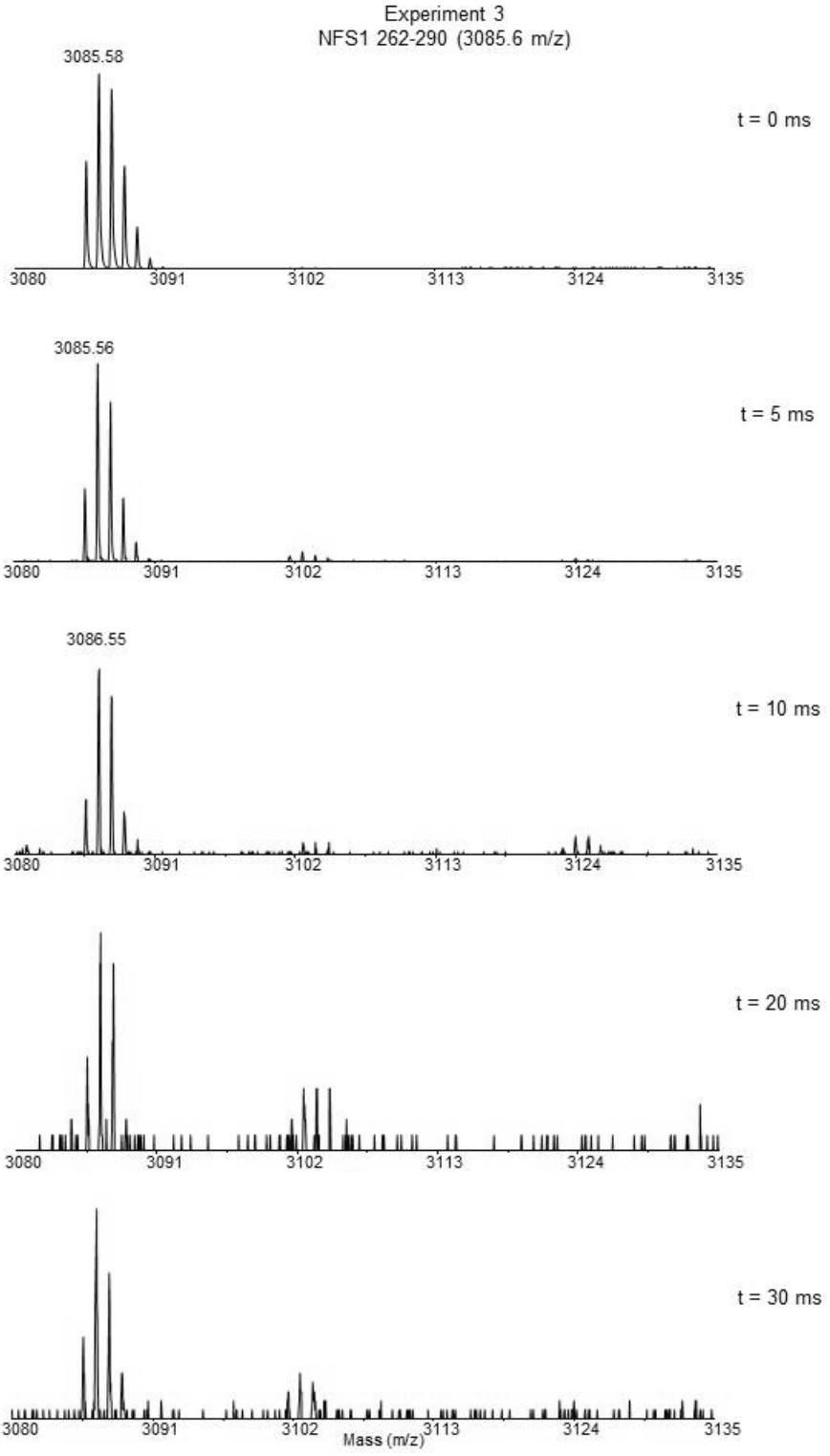

A-73. Mass spectra from NFS1, Experiment 3 at various exposure time to hydroxyl radicals.

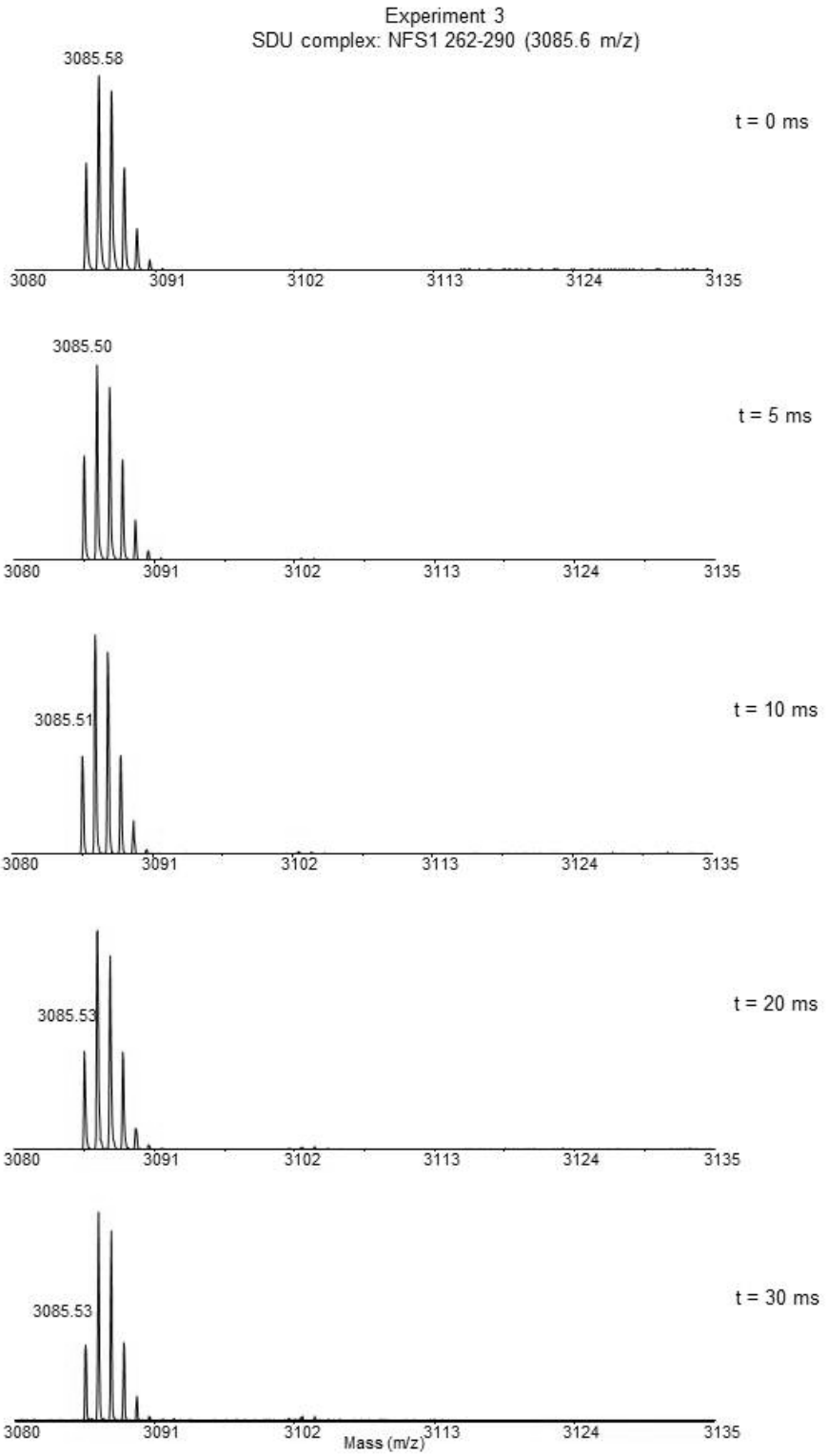

A-74. Mass spectra from SDU, Experiment 3 at various exposure time to hydroxyl radicals.

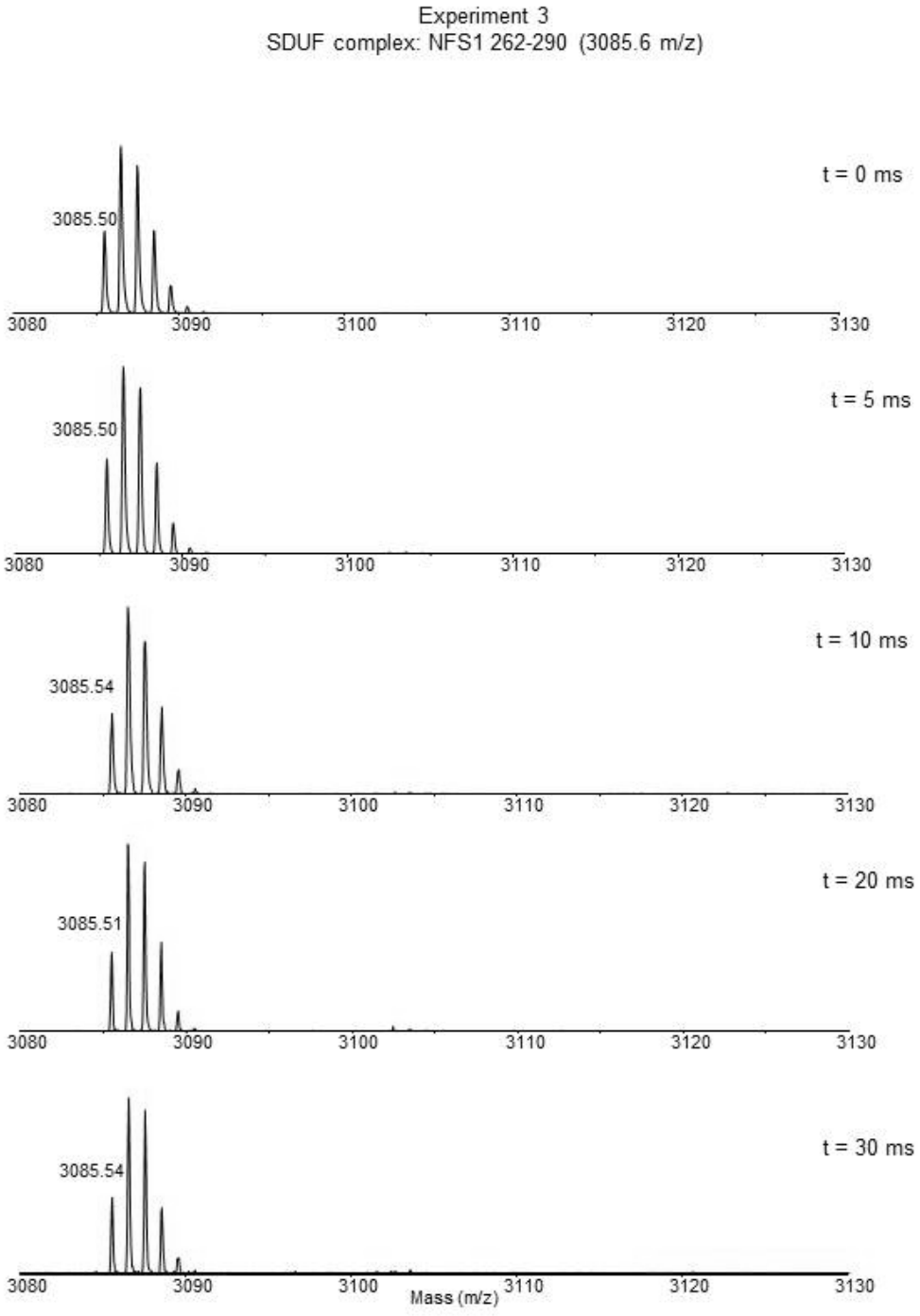

A-75. Mass spectra from SDUF, Experiment 3 at various exposure time to hydroxyl radicals.

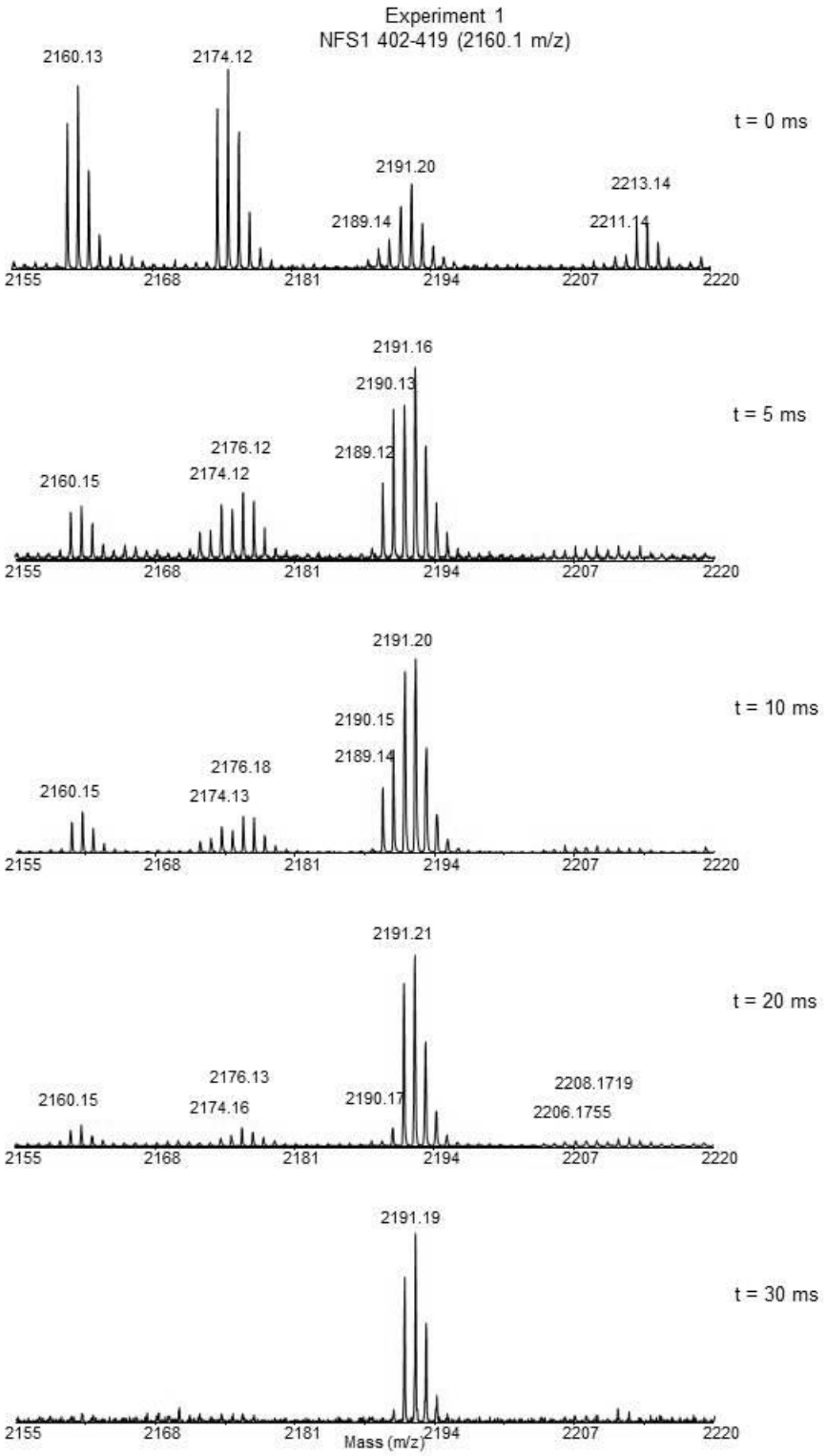

A-76. Mass spectra from NFS1, Experiment 1 at various exposure time to hydroxyl radicals.

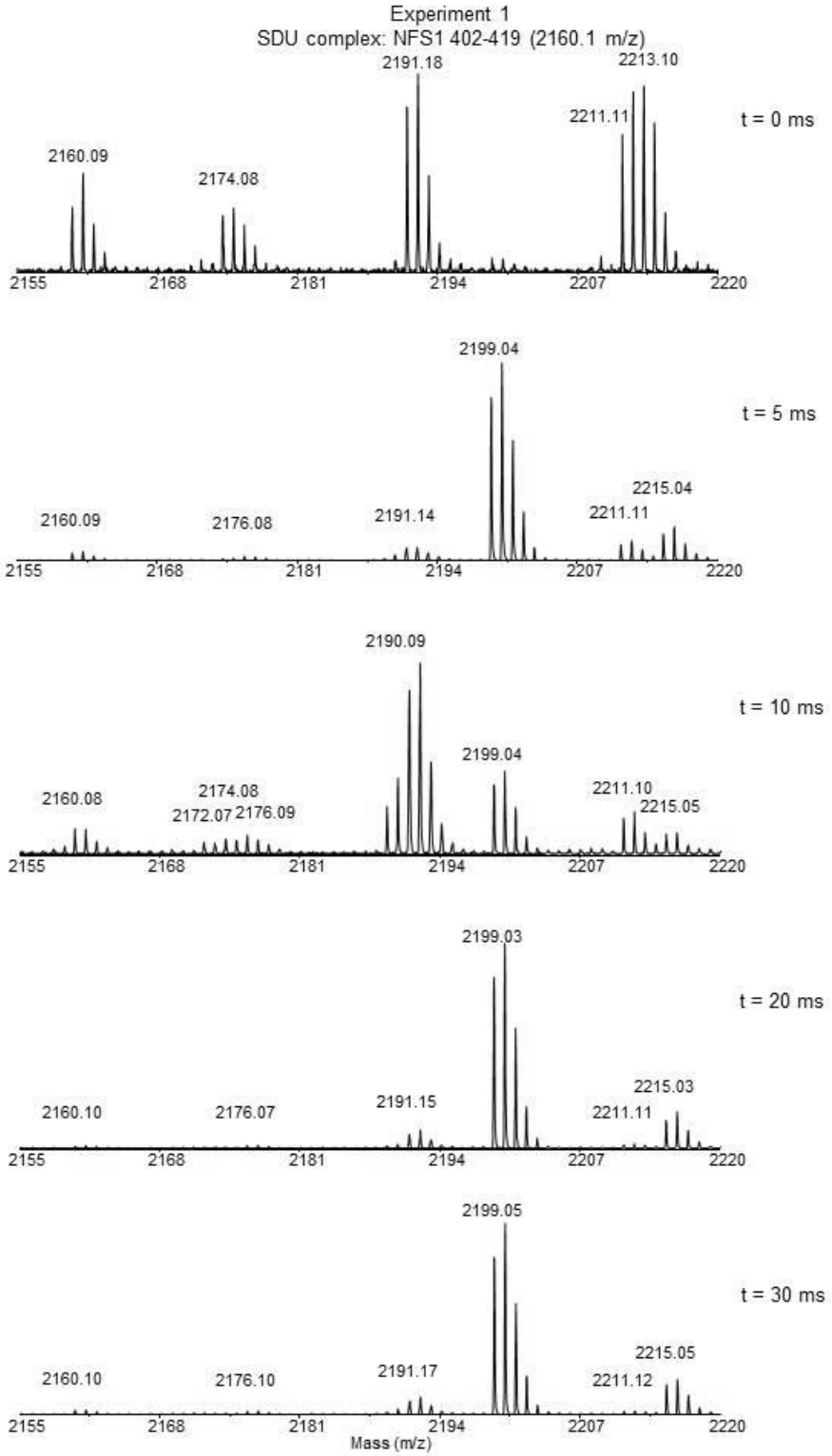

A-77. Mass spectra from SDU, Experiment 1 at various exposure time to hydroxyl radicals.

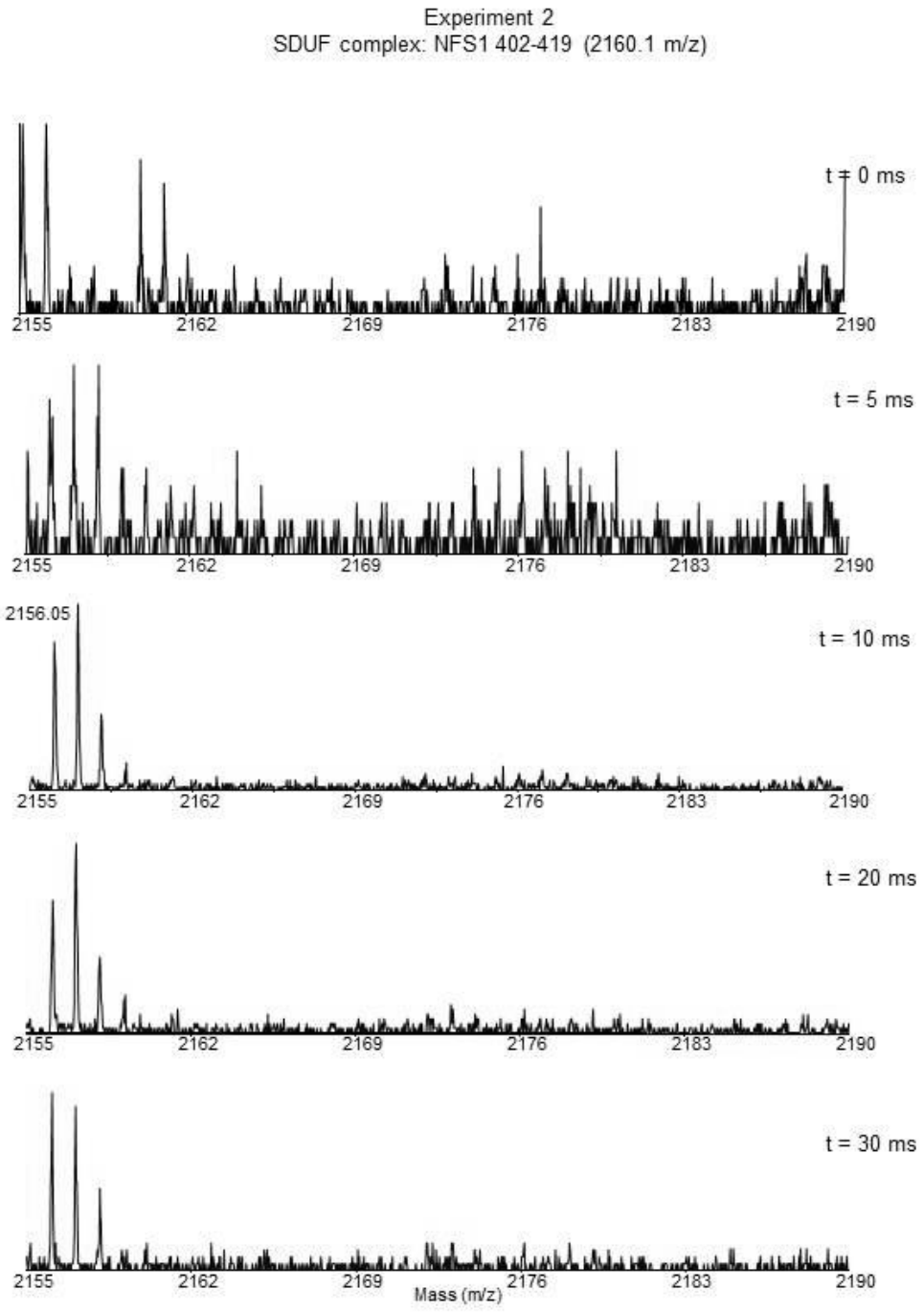

A-78. Mass spectra from SDUF, Experiment 2 at various exposure time to hydroxyl radicals.

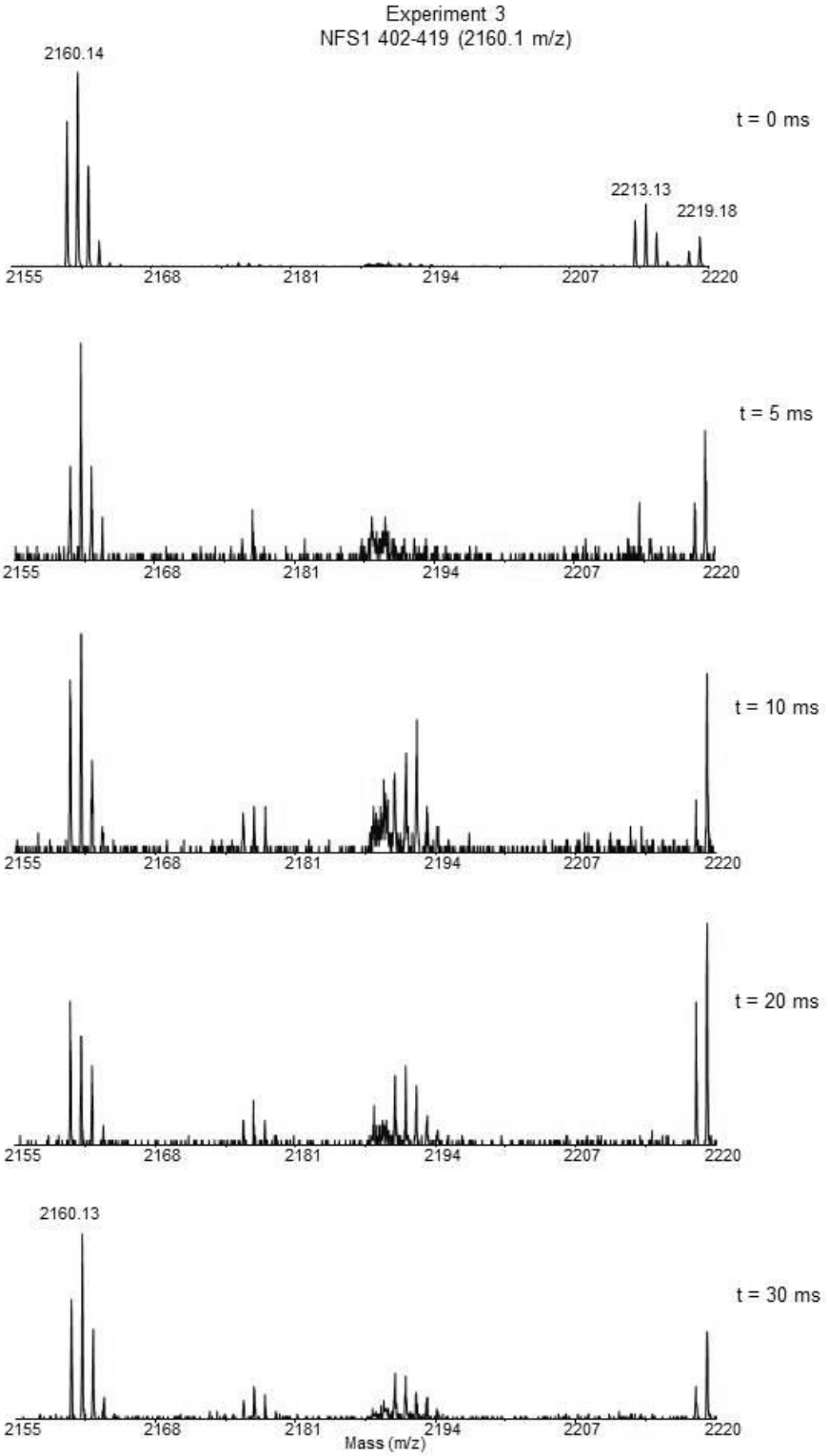

A-79. Mass spectra from NFS1, Experiment 3 at various exposure time to hydroxyl radicals.

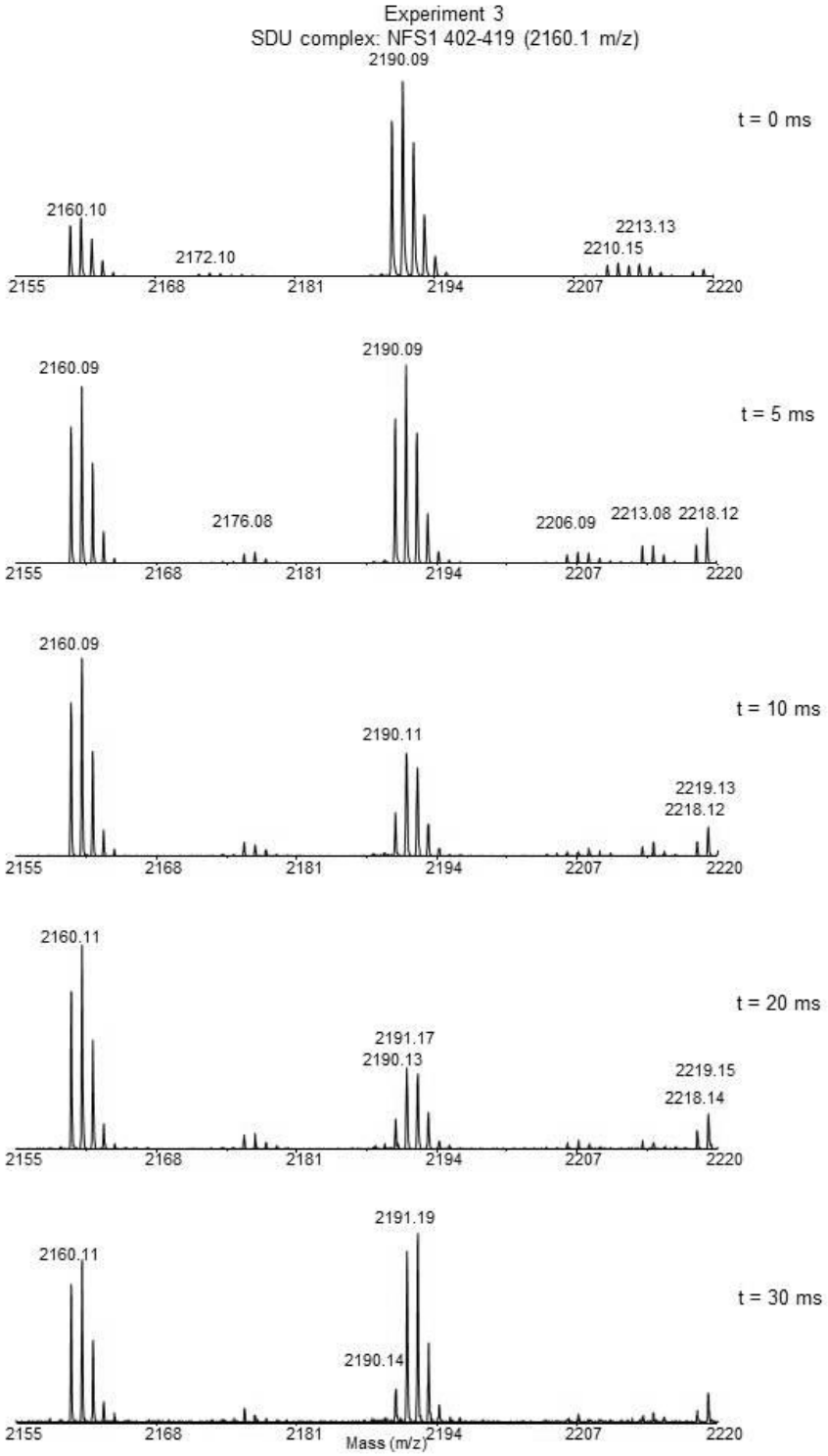

A-80. Mass spectra from SDU, Experiment 3 at various exposure time to hydroxyl radicals.

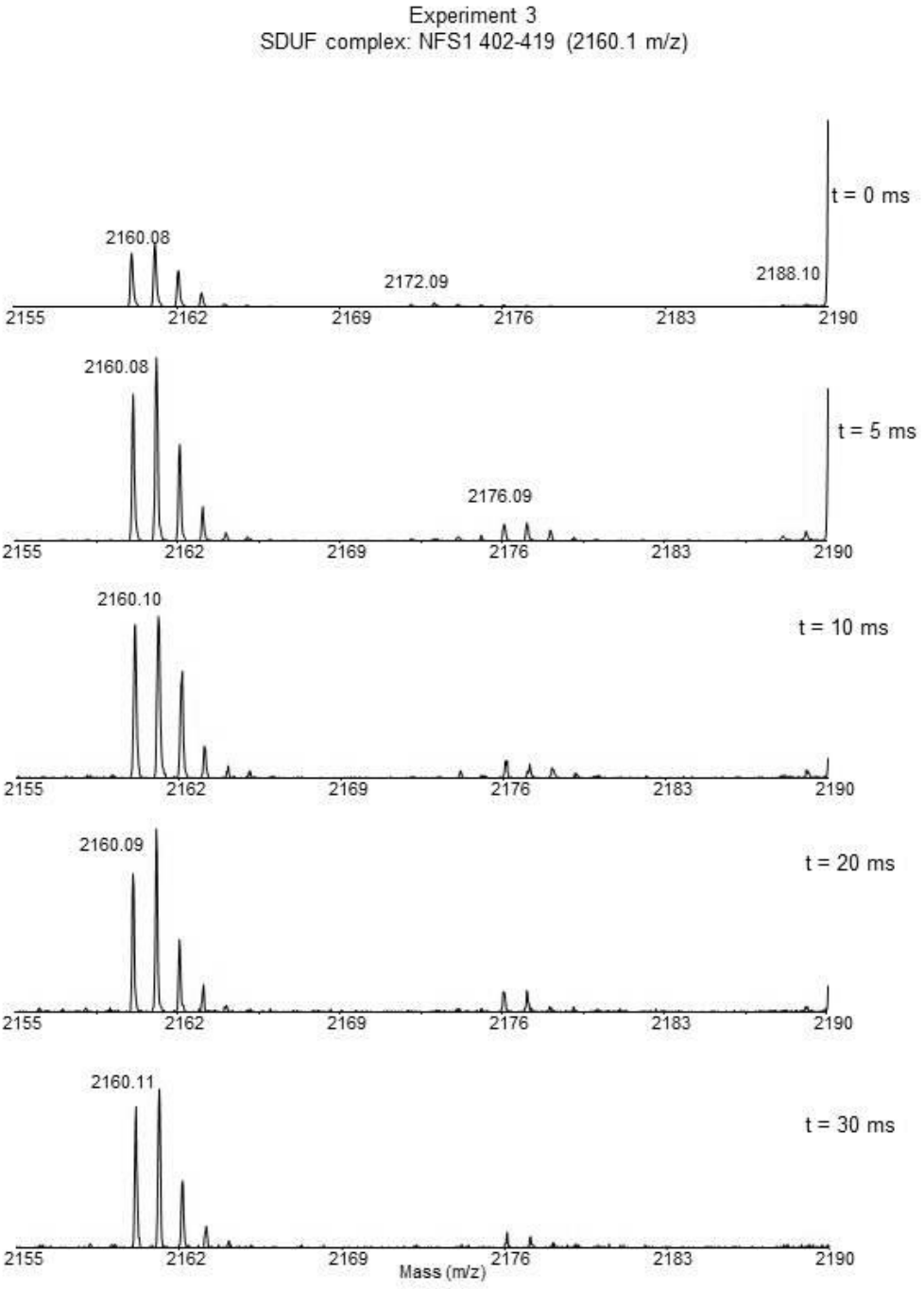

A-81. Mass spectra from SDUF, Experiment 3 at various exposure time to hydroxyl radicals.

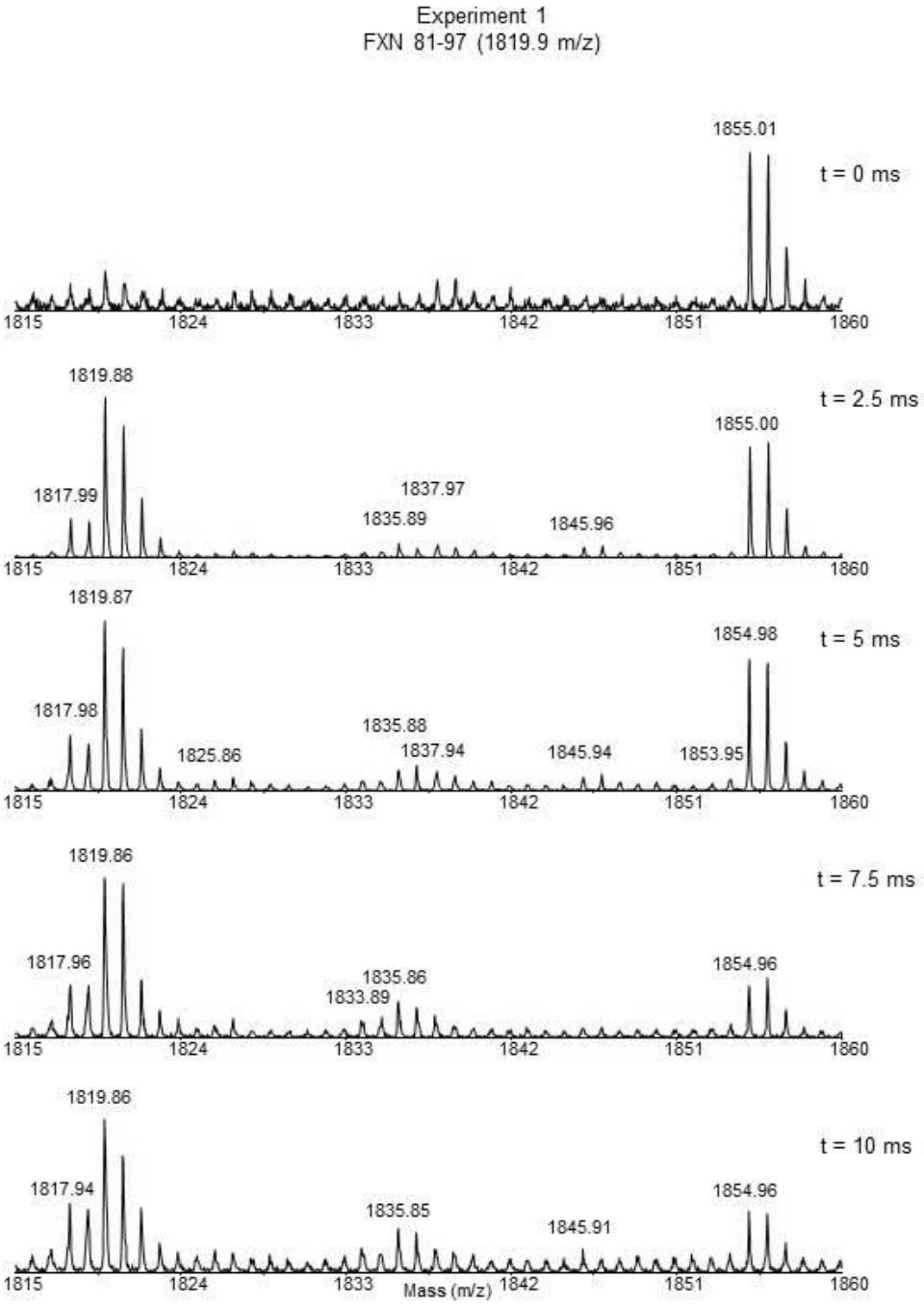

A-82. Mass spectra from FXN, Experiment 1 at various exposure time to hydroxyl radicals.

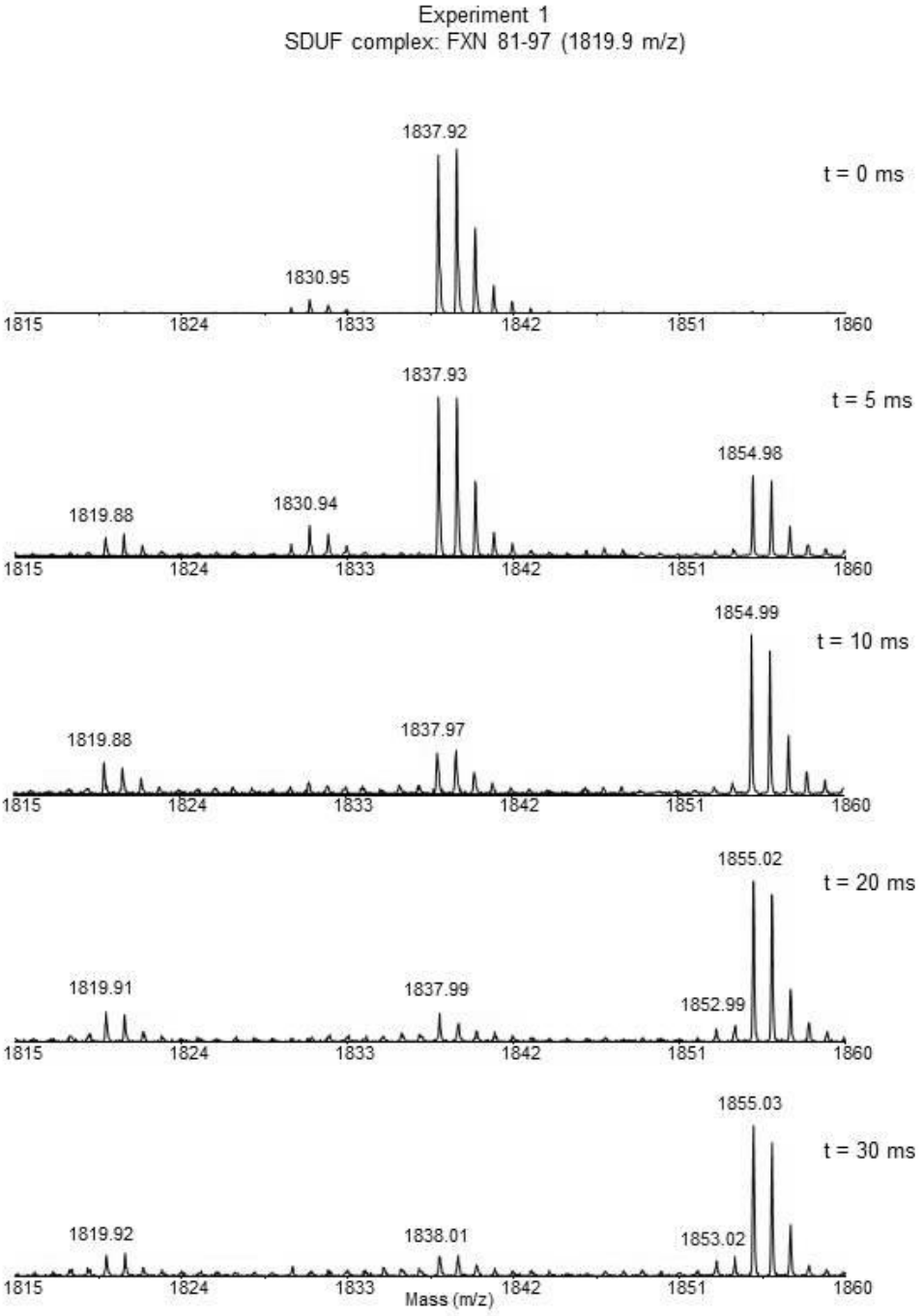

A-83. Mass spectra from SDUF, Experiment 1 at various exposure time to hydroxyl radicals.

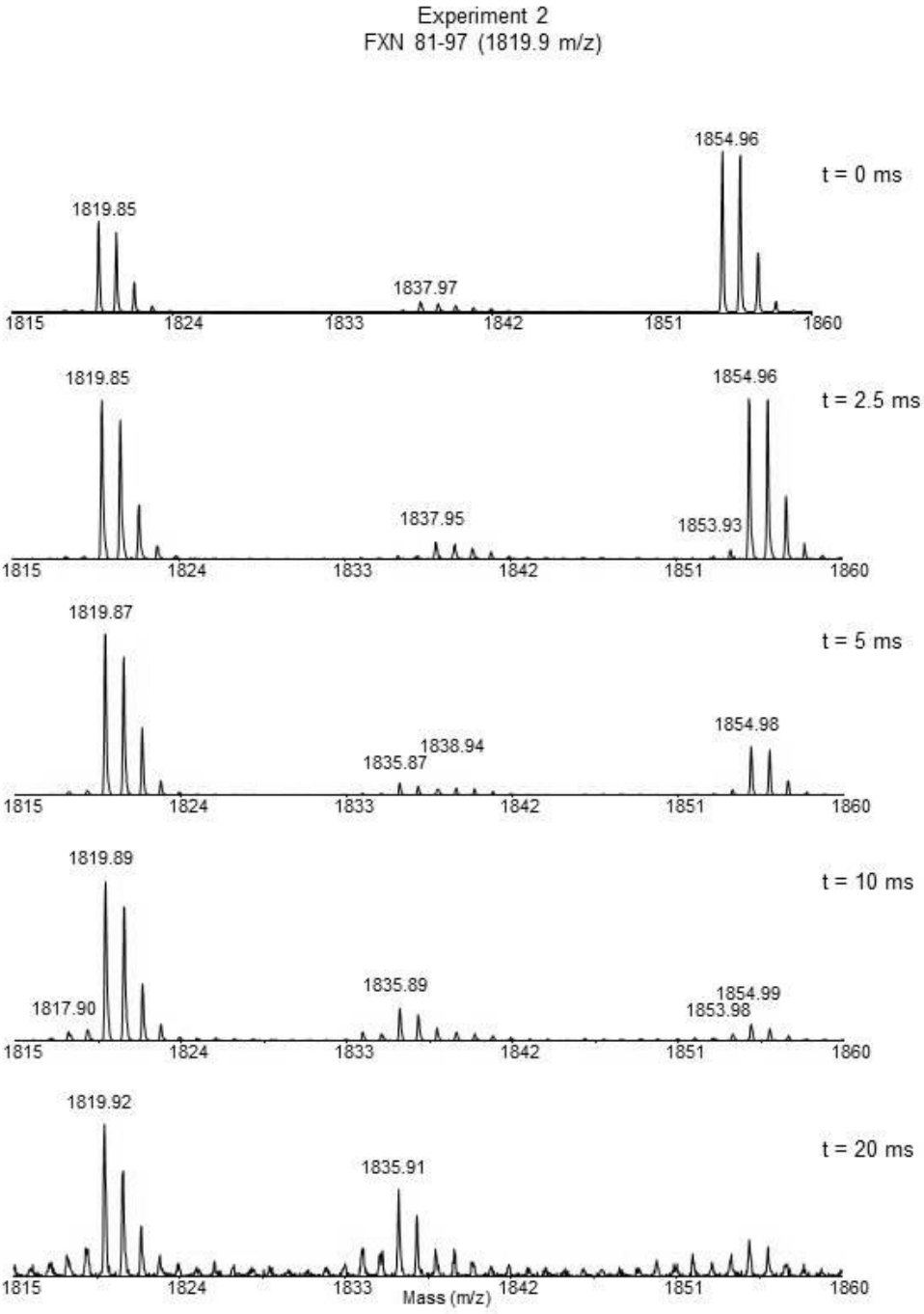

A-84. Mass spectra from FXN, Experiment 2 at various exposure time to hydroxyl radicals.

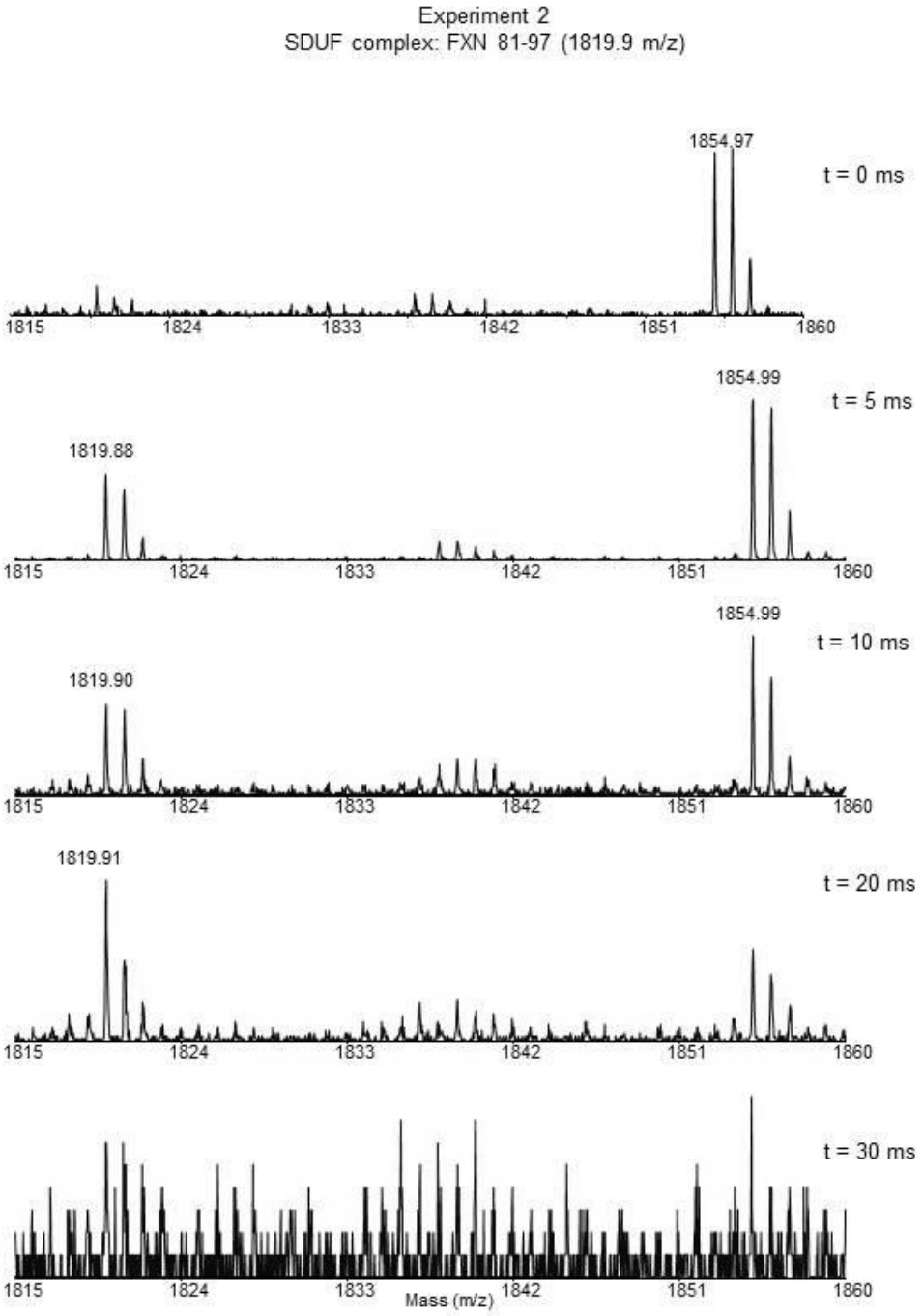

A-85. Mass spectra from SDUF, Experiment 2 at various exposure time to hydroxyl radicals.

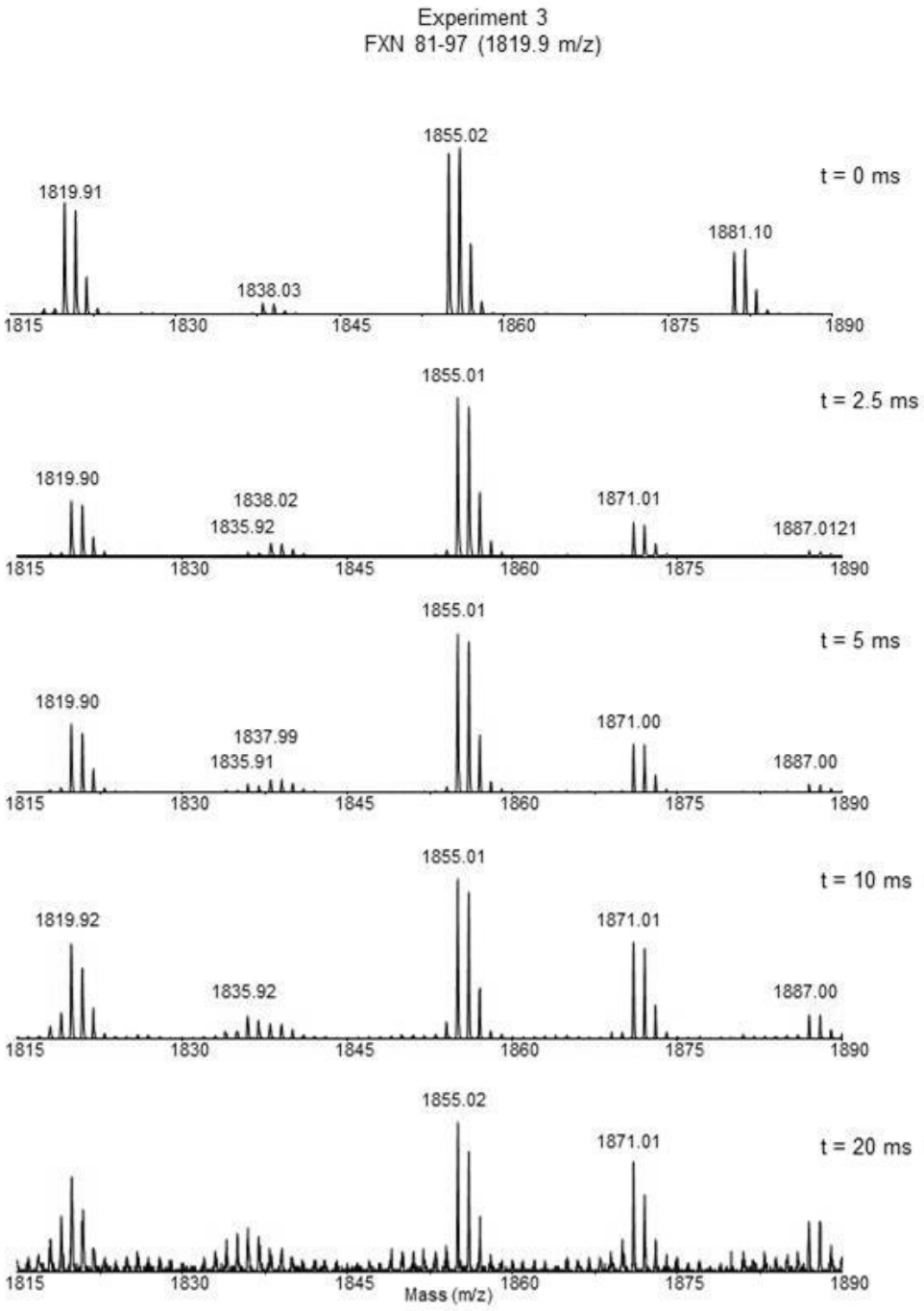

A-86. Mass spectra from FXN, Experiment 3 at various exposure time to hydroxyl radicals.

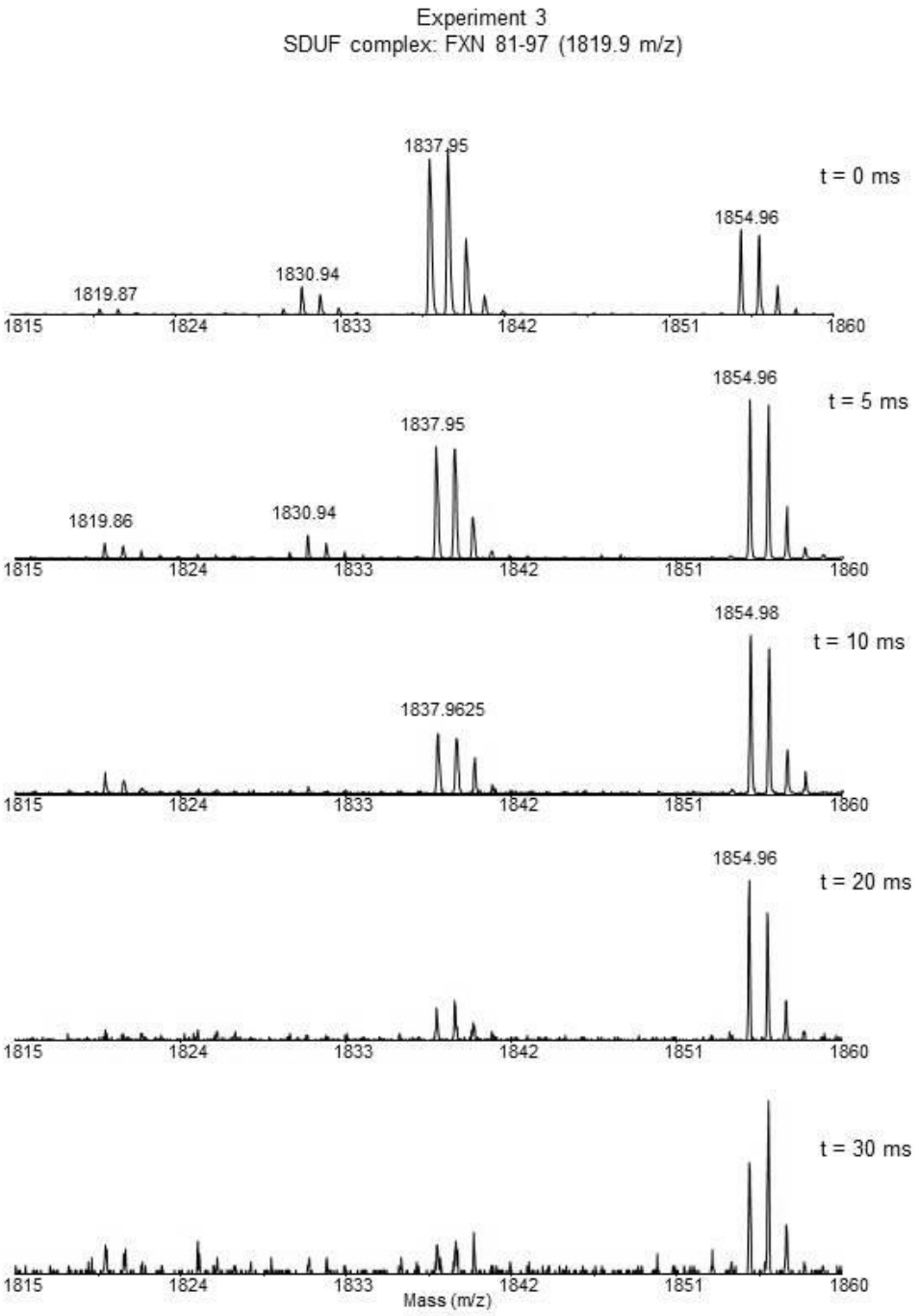

A-87. Mass spectra from SDUF, Experiment 3 at various exposure time to hydroxyl radicals.

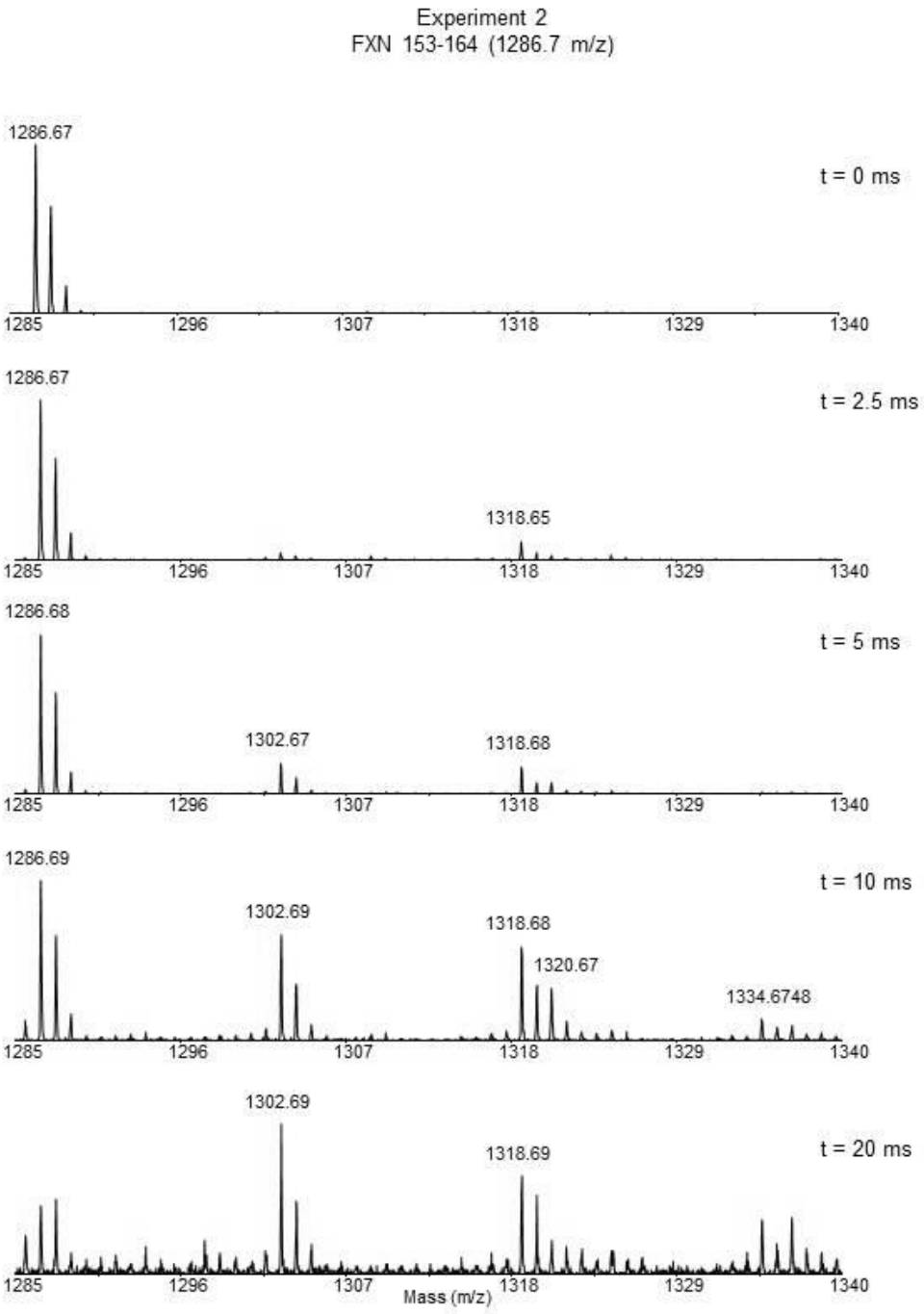

A-88. Mass spectra from FXN, Experiment 2 at various exposure time to hydroxyl radicals.

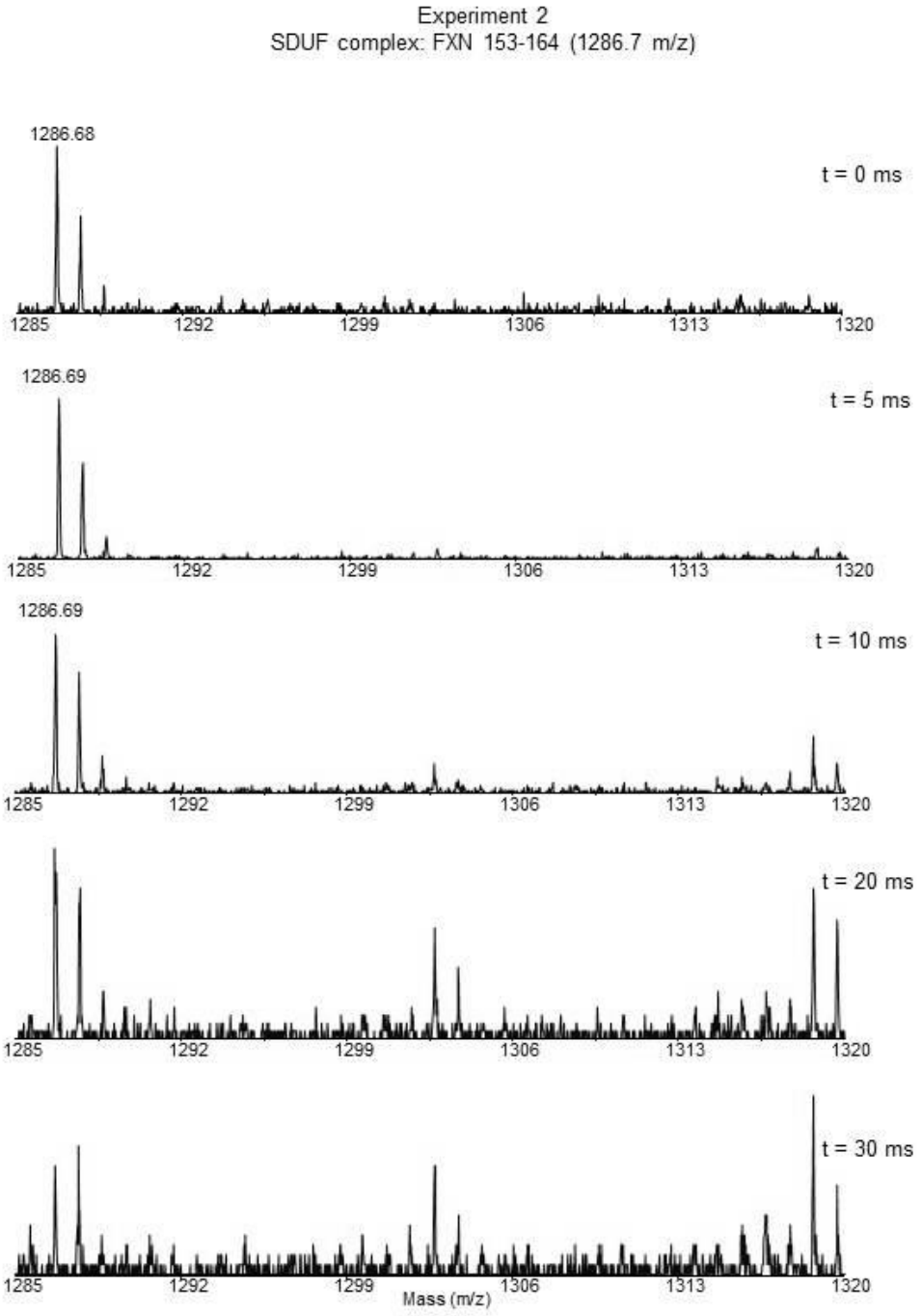

A-89. Mass spectra from SDUF, Experiment 2 at various exposure time to hydroxyl radicals.

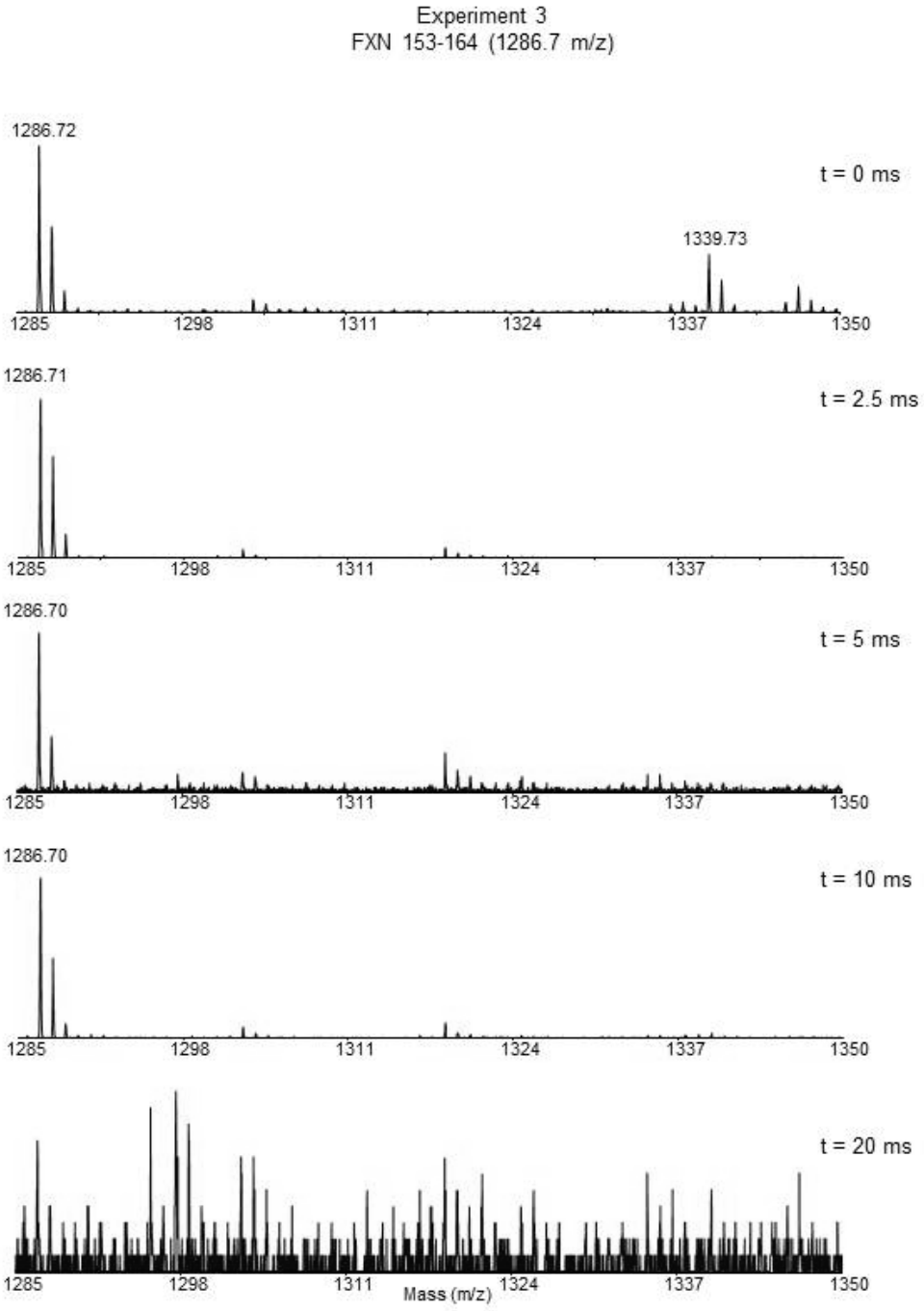

A-90. Mass spectra from FXN, Experiment 3 at various exposure time to hydroxyl radicals.

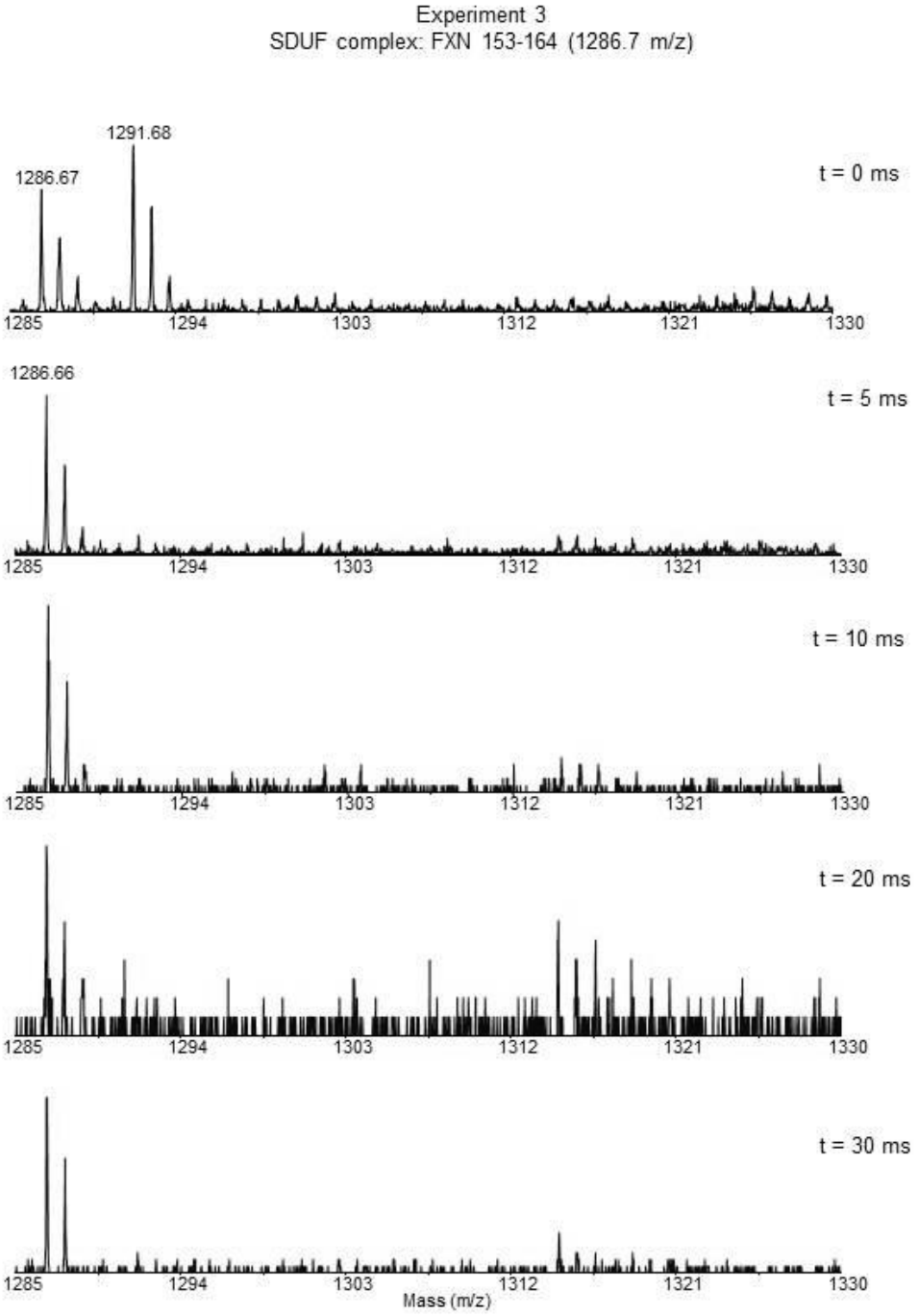

A-91. Mass spectra from SDUF, Experiment 3 at various exposure time to hydroxyl radicals.

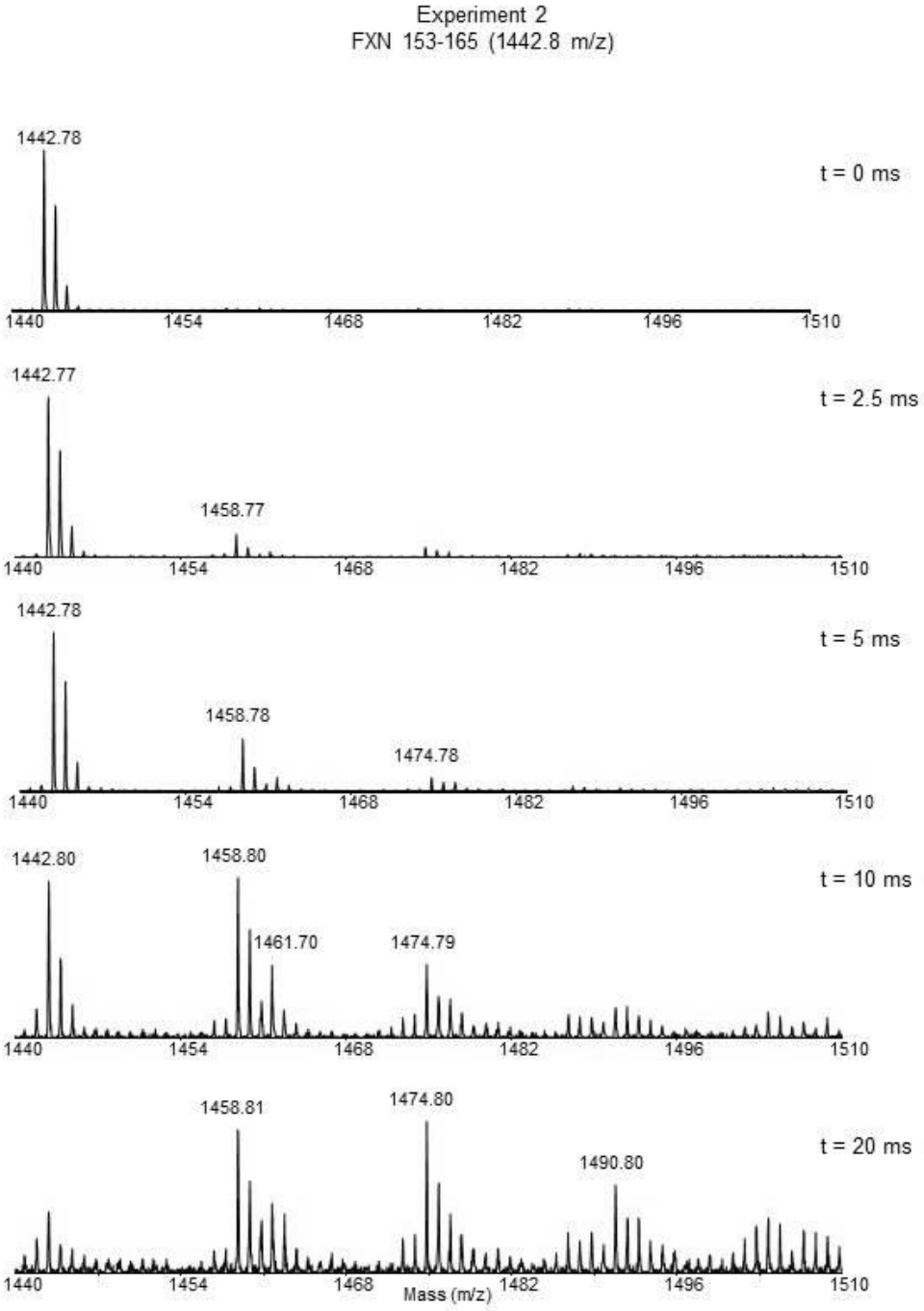

A-92. Mass spectra from FXN, Experiment 2 at various exposure time to hydroxyl radicals.

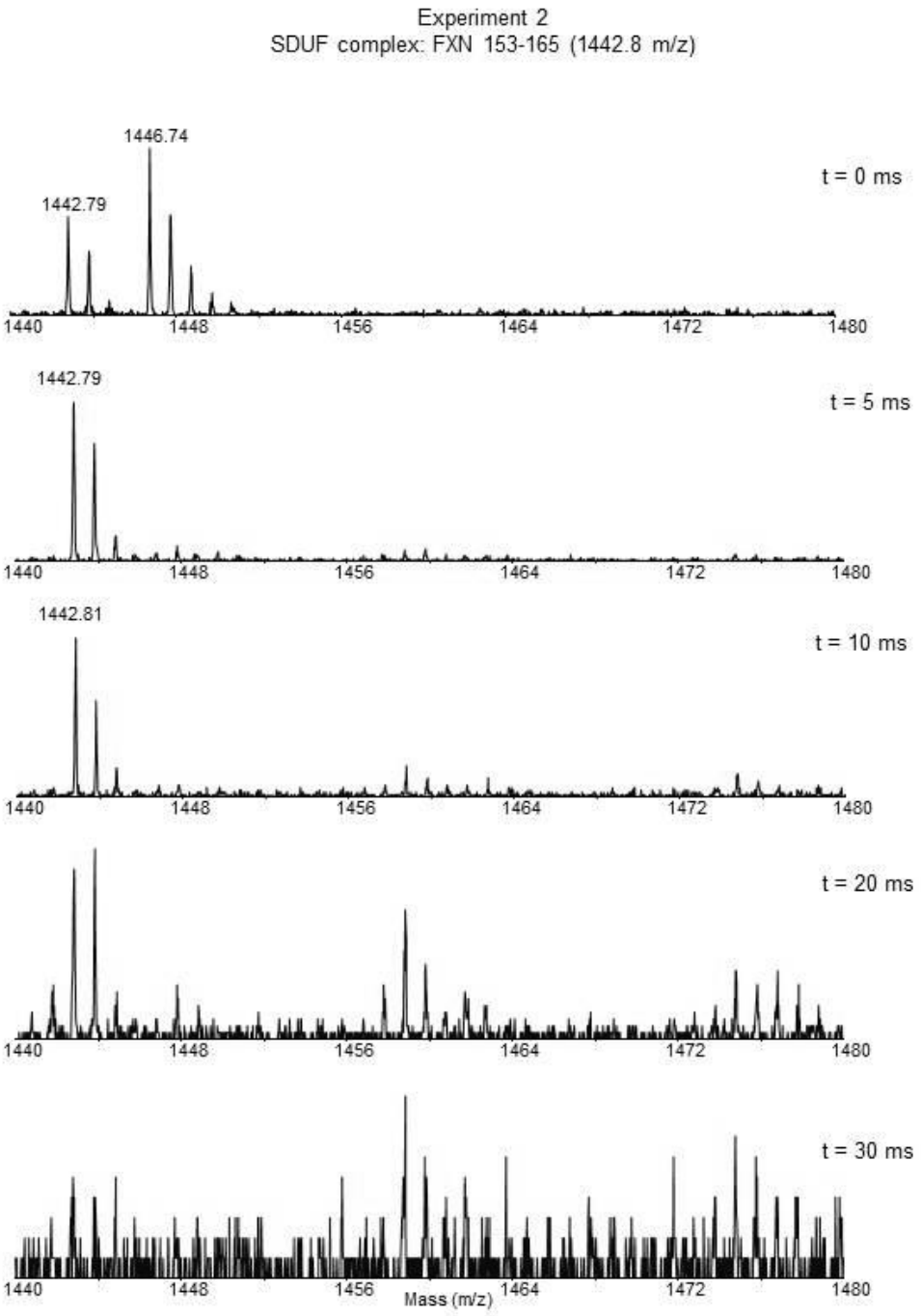

A-93. Mass spectra from SDUF, Experiment 2 at various exposure time to hydroxyl radicals.

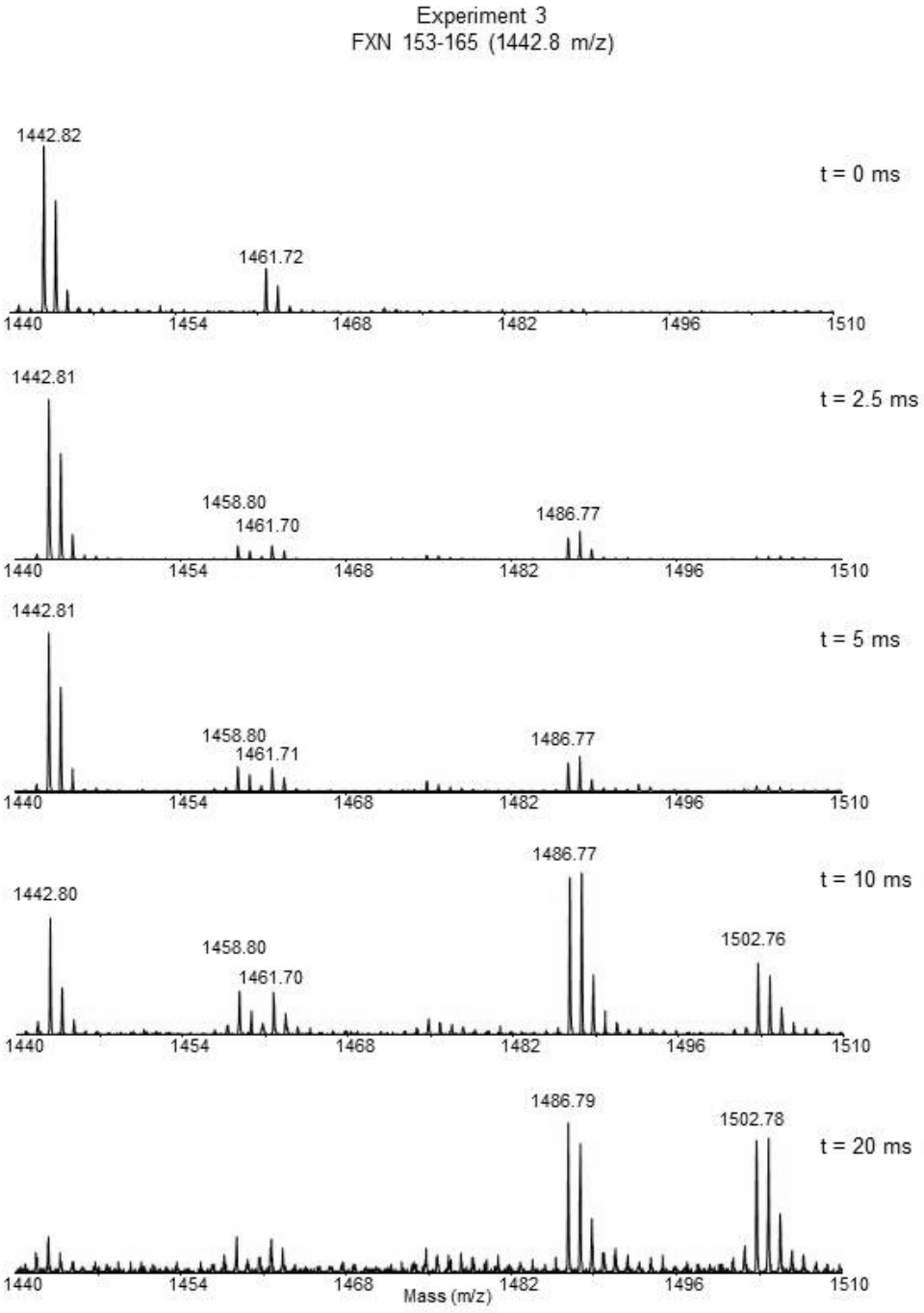

A-94. Mass spectra from FXN, Experiment 3 at various exposure time to hydroxyl radicals.

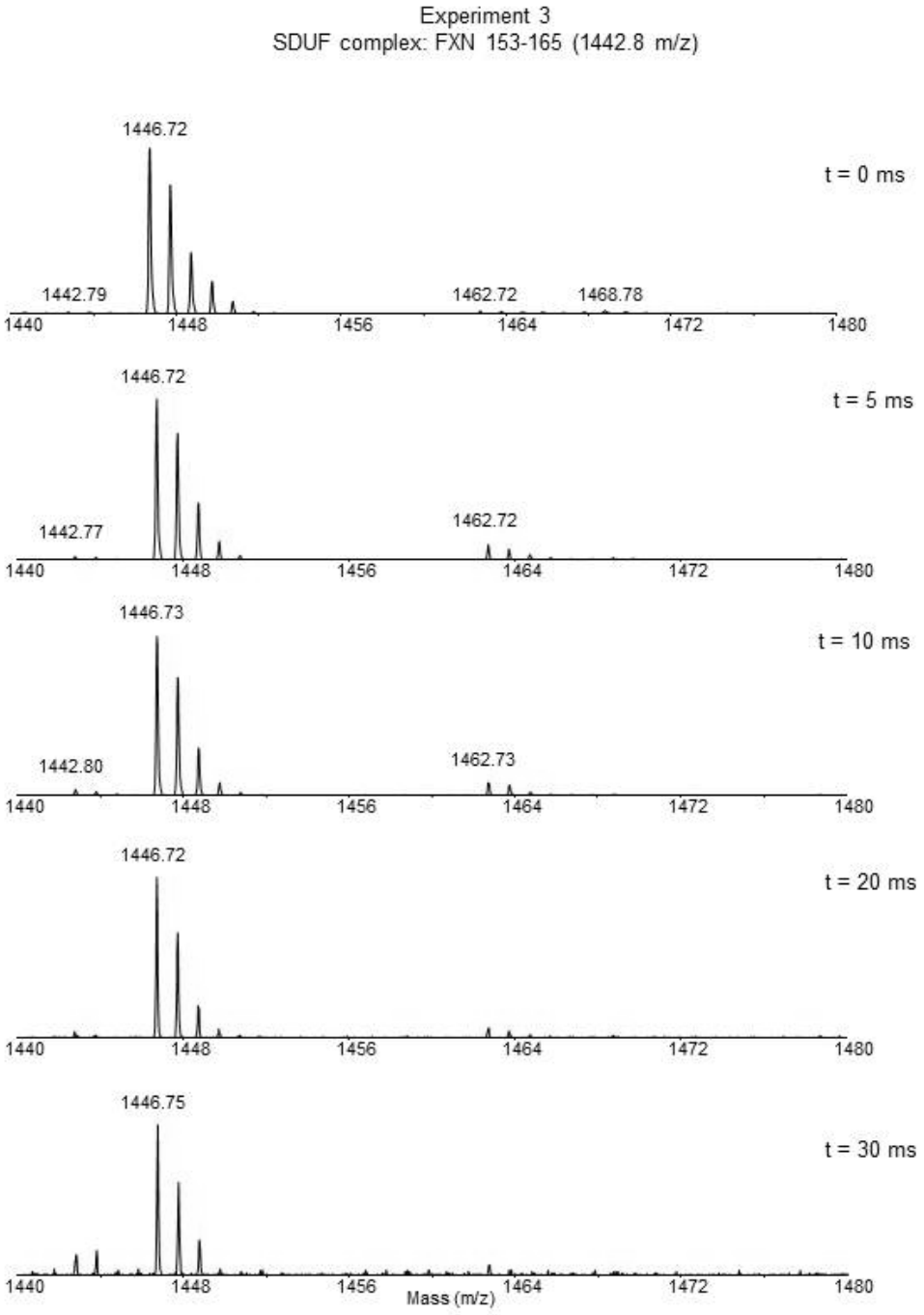

A-95. Mass spectra from SDUF, Experiment 3 at various exposure time to hydroxyl radicals.

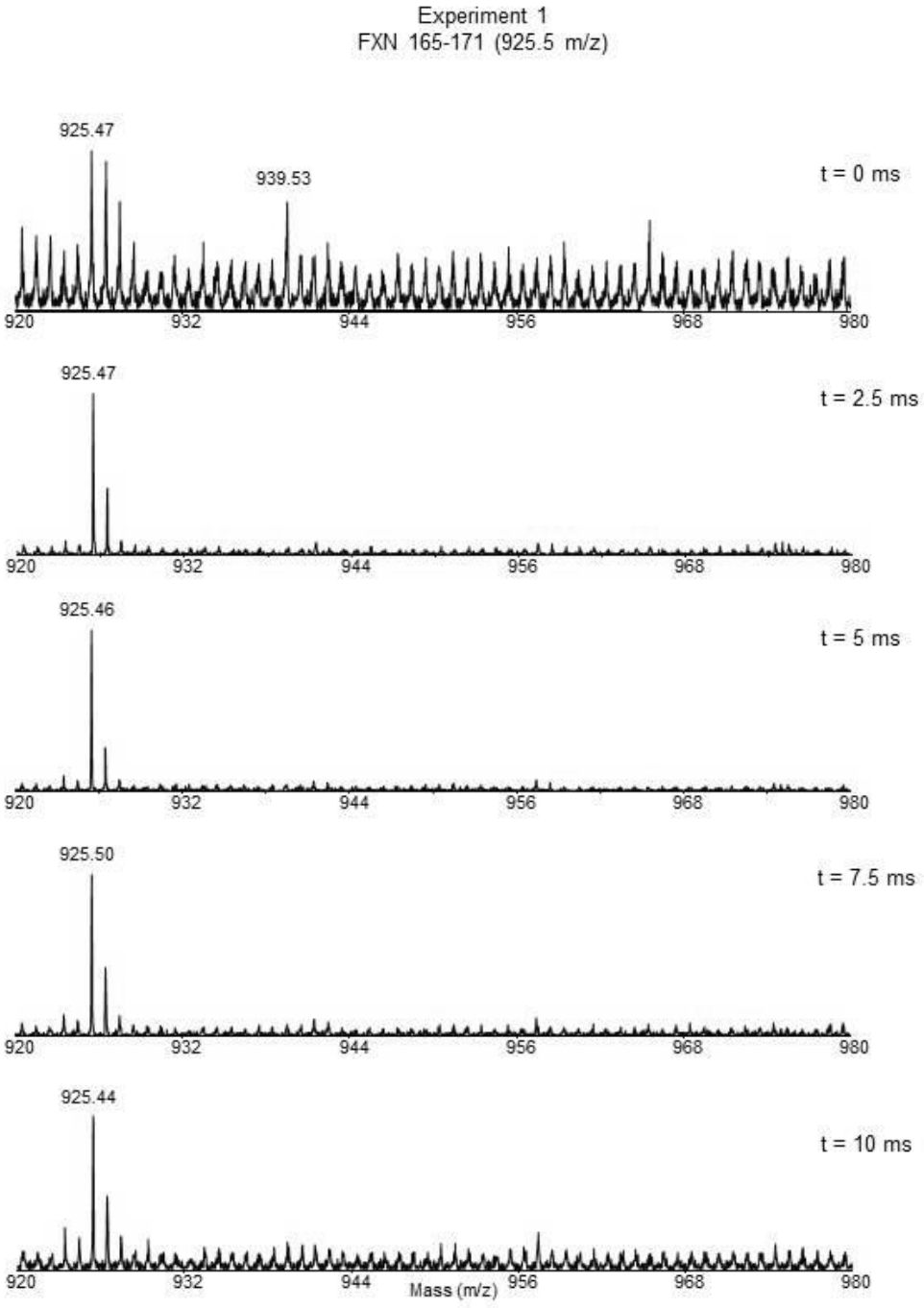

A-96. Mass spectra from FXN, Experiment 1 at various exposure time to hydroxyl radicals.

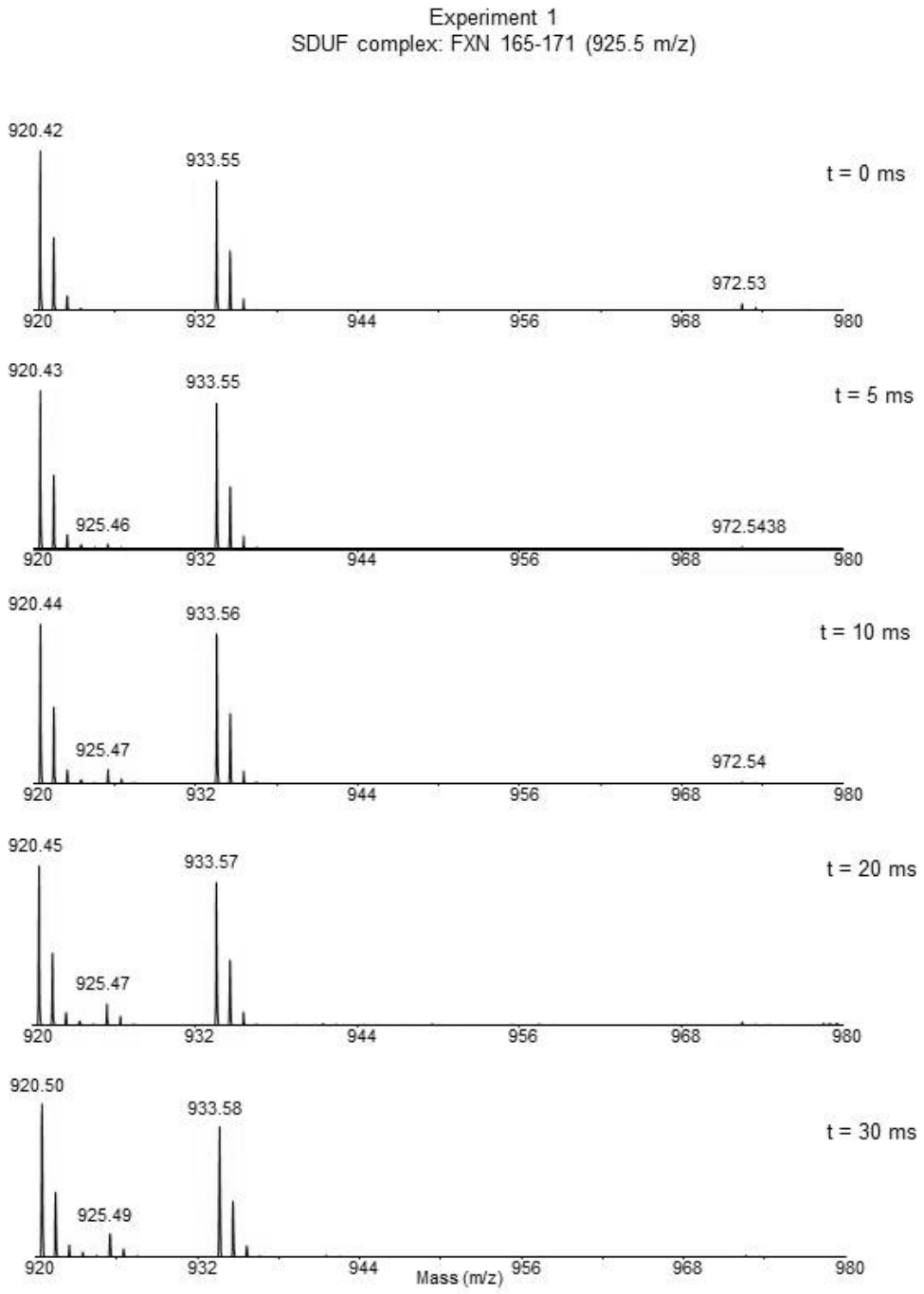

A-97. Mass spectra from SDUF, Experiment 1 at various exposure time to hydroxyl radicals. The peaks at m/z 920.42 and 933.55 are from ISD11.

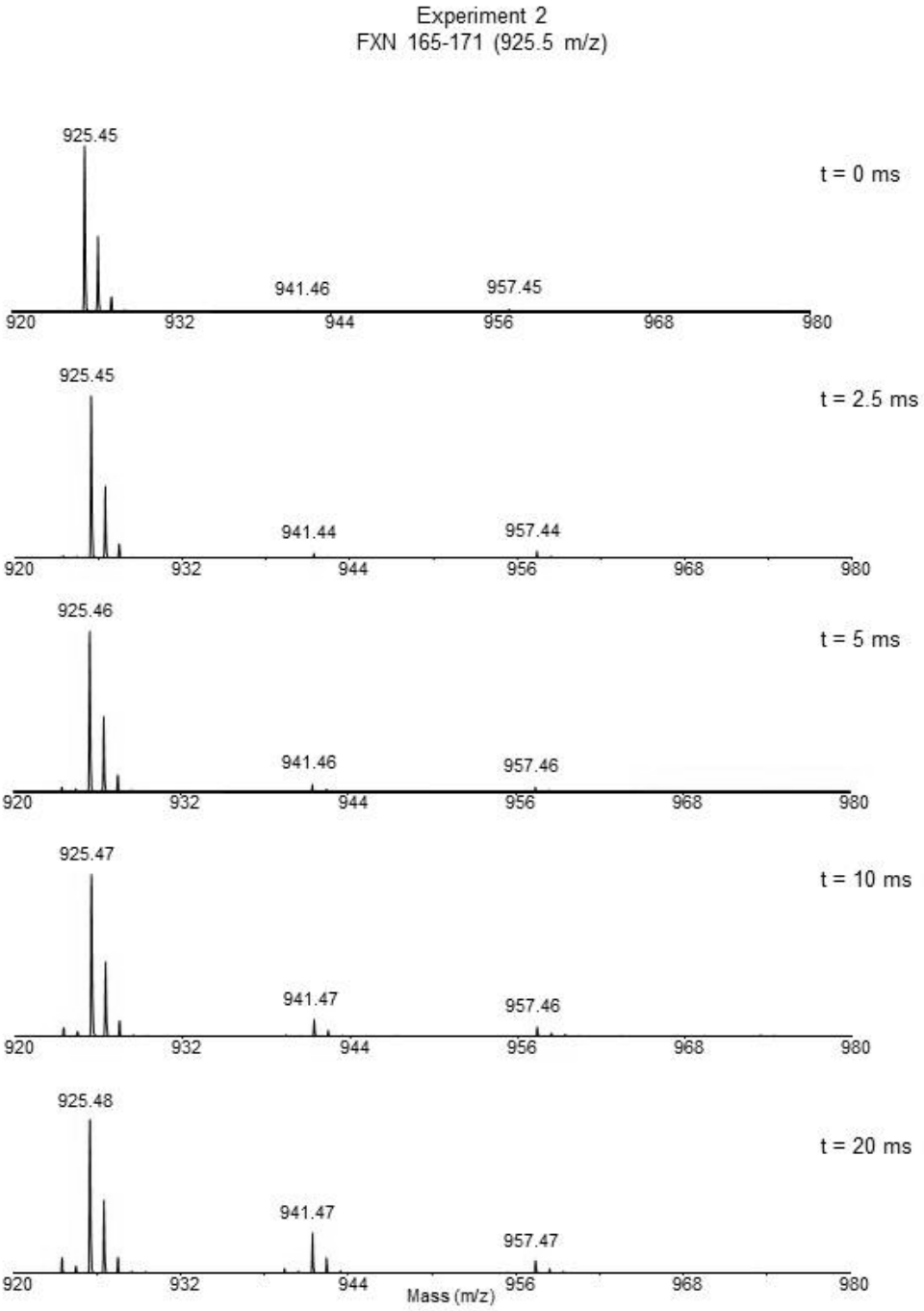

A-98. Mass spectra from FXN, Experiment 2 at various exposure time to hydroxyl radicals.

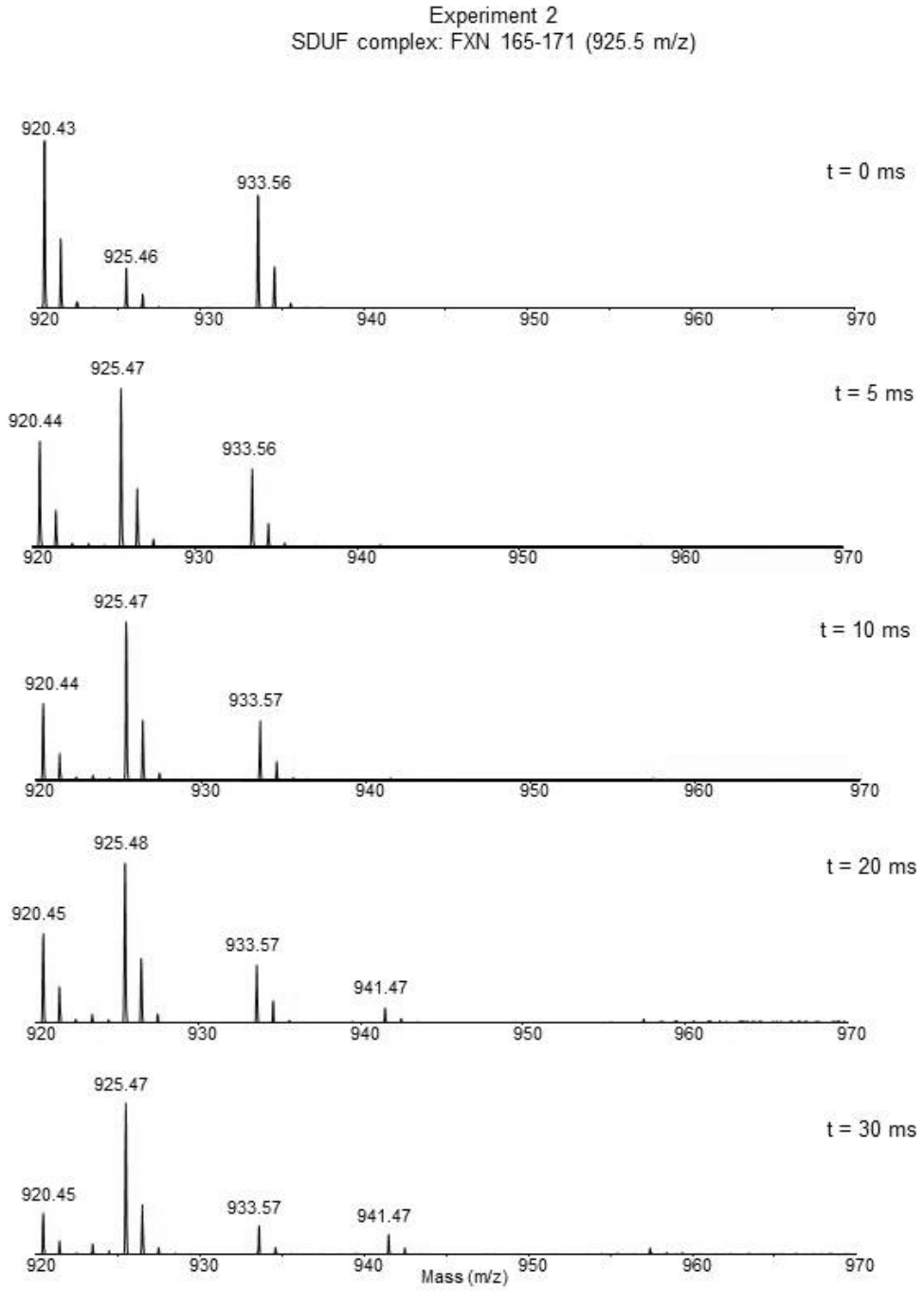

A-99. Mass spectra from SDUF, Experiment 2 at various exposure time to hydroxyl radicals. The peaks at m/z 920.43 and 933.56 are from ISD11.

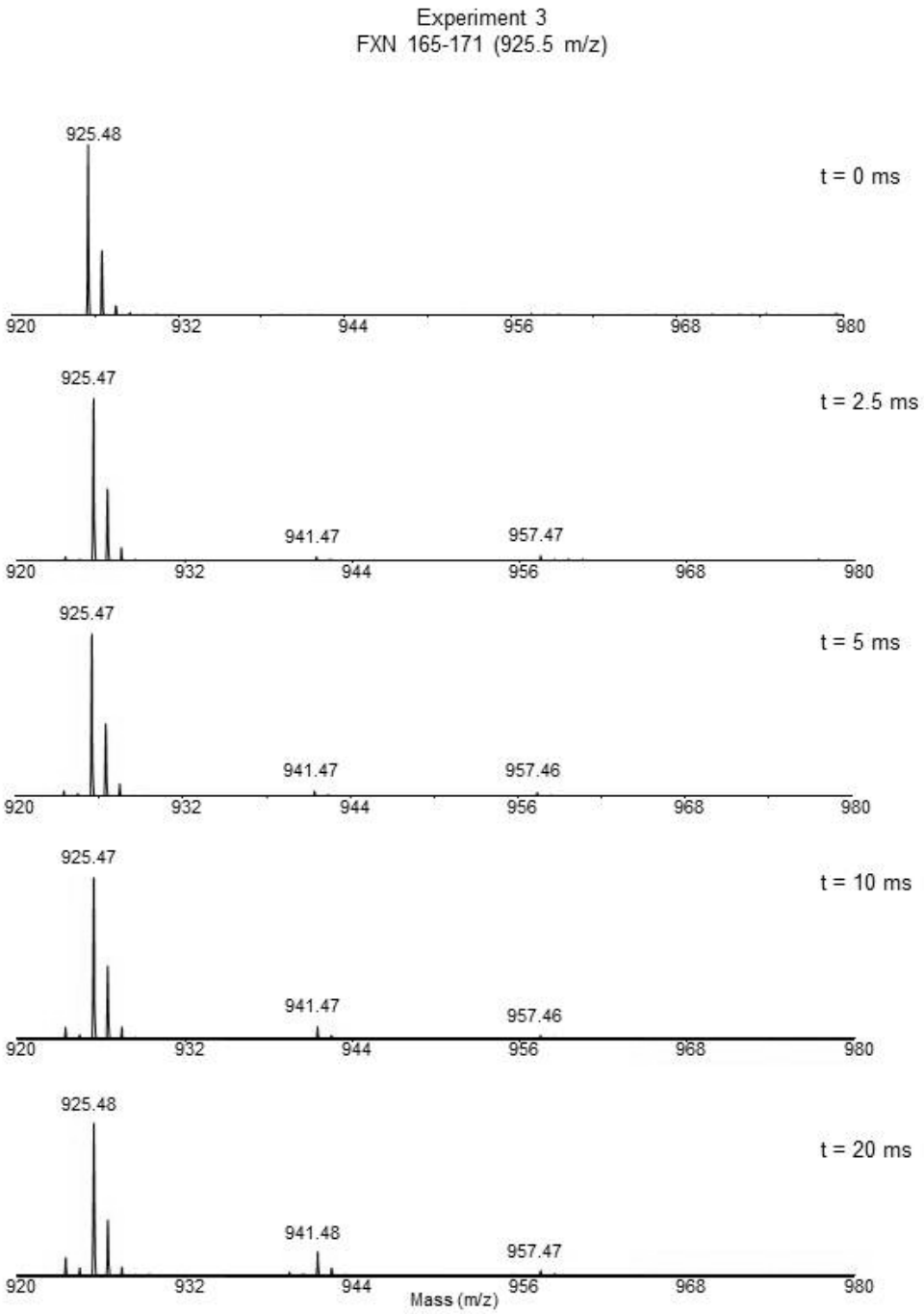

A-100. Mass spectra from FXN, Experiment 3 at various exposure time to hydroxyl radicals.

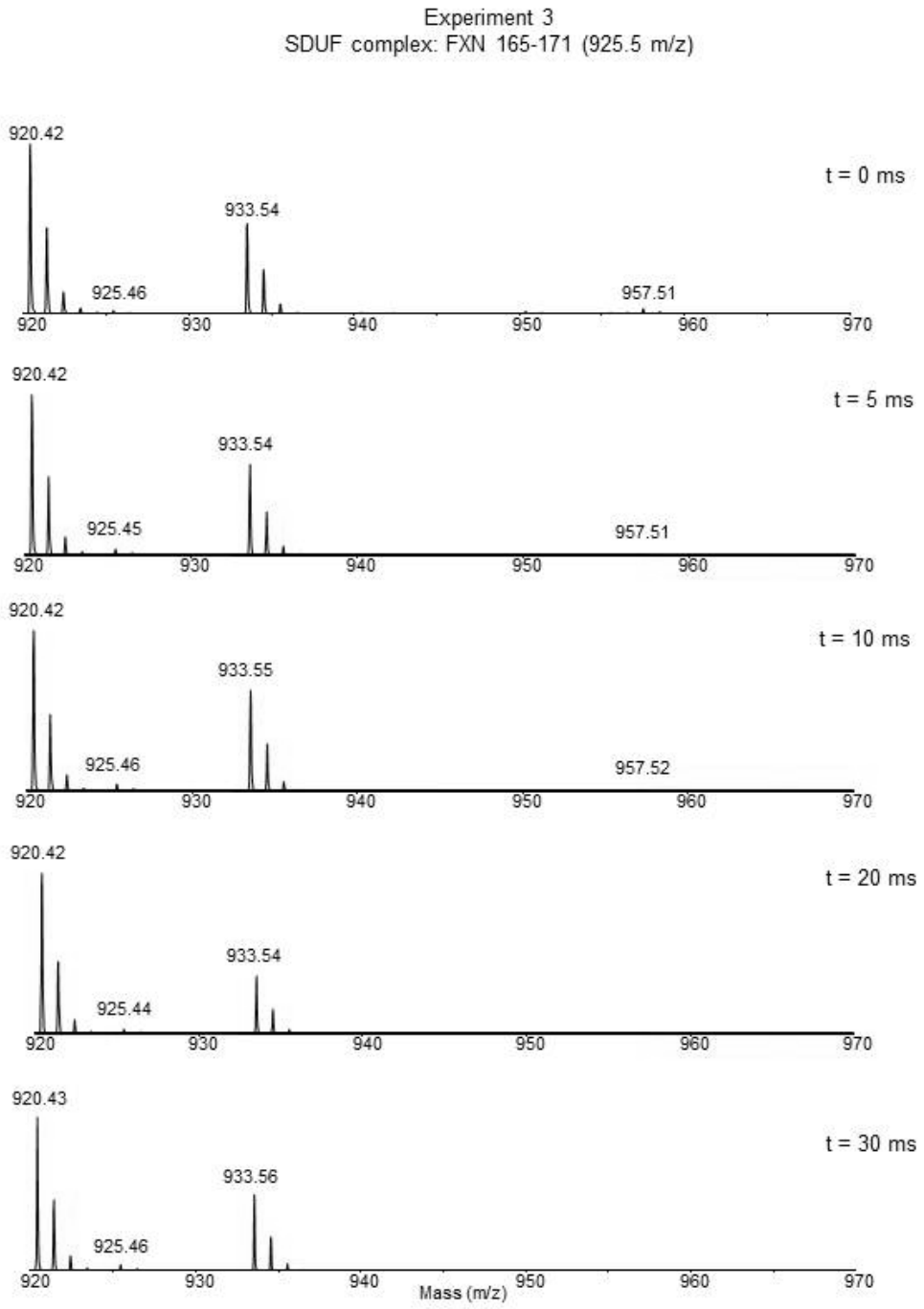

A-101. Mass spectra from SDUF, Experiment 3 at various exposure time to hydroxyl radicals. The peaks at m/z 920.42 and 933.55 are from ISD11.

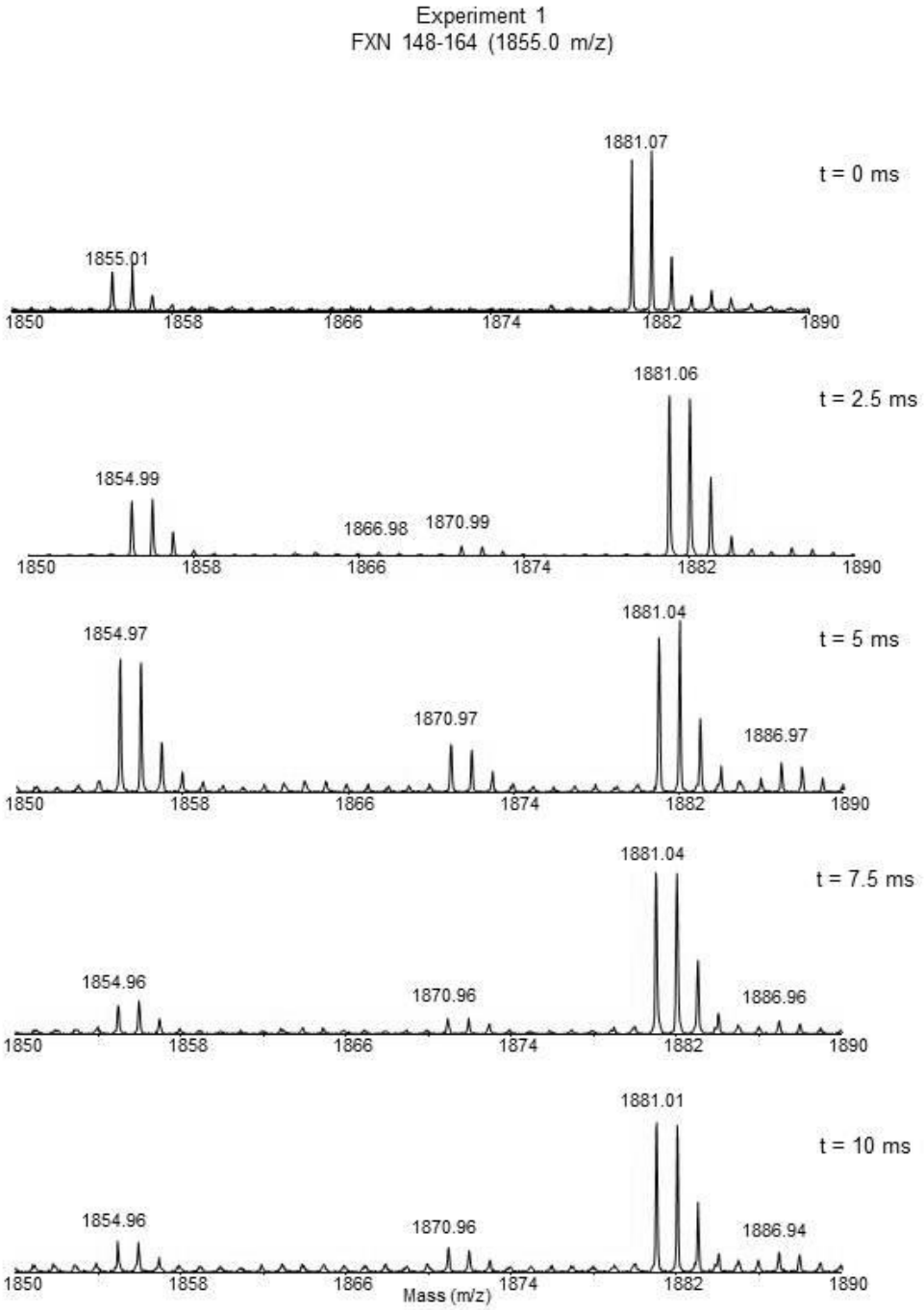

A-102. Mass spectra from FXN, Experiment 1 at various exposure time to hydroxyl radicals.

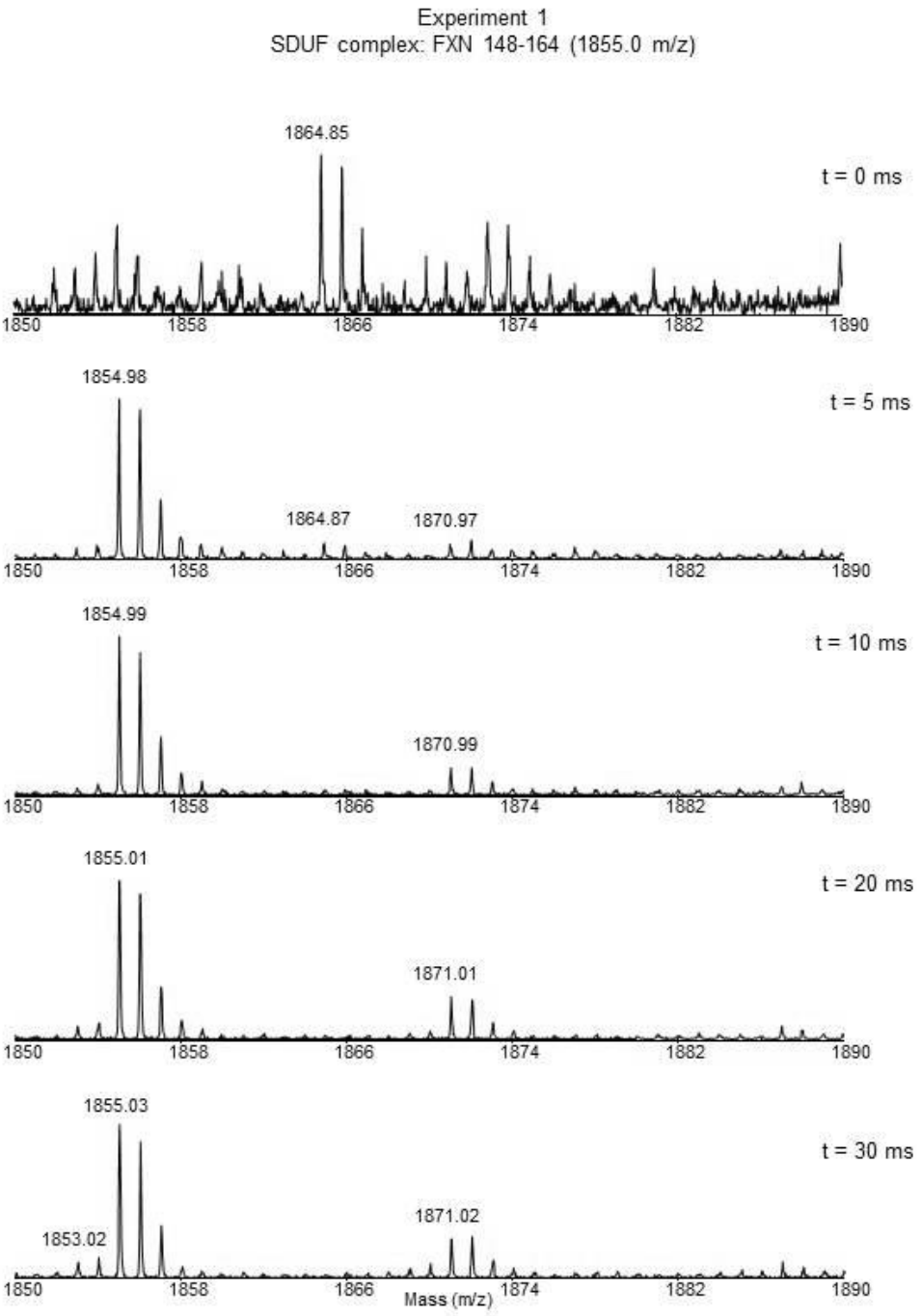

A-103. Mass spectra from SDUF, Experiment 1 at various exposure time to hydroxyl radicals.

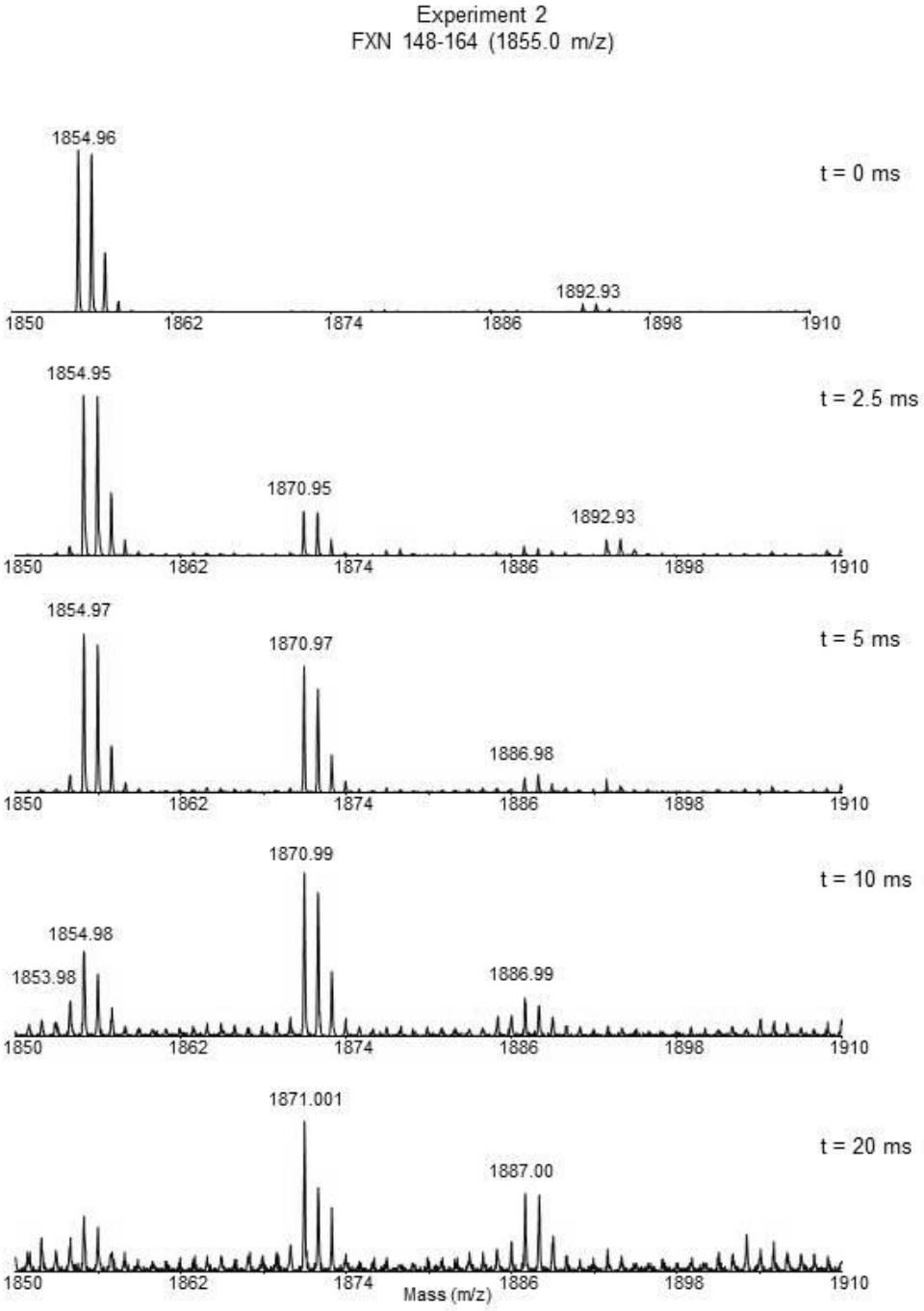

A-104. Mass spectra from FXN, Experiment 2 at various exposure time to hydroxyl radicals.

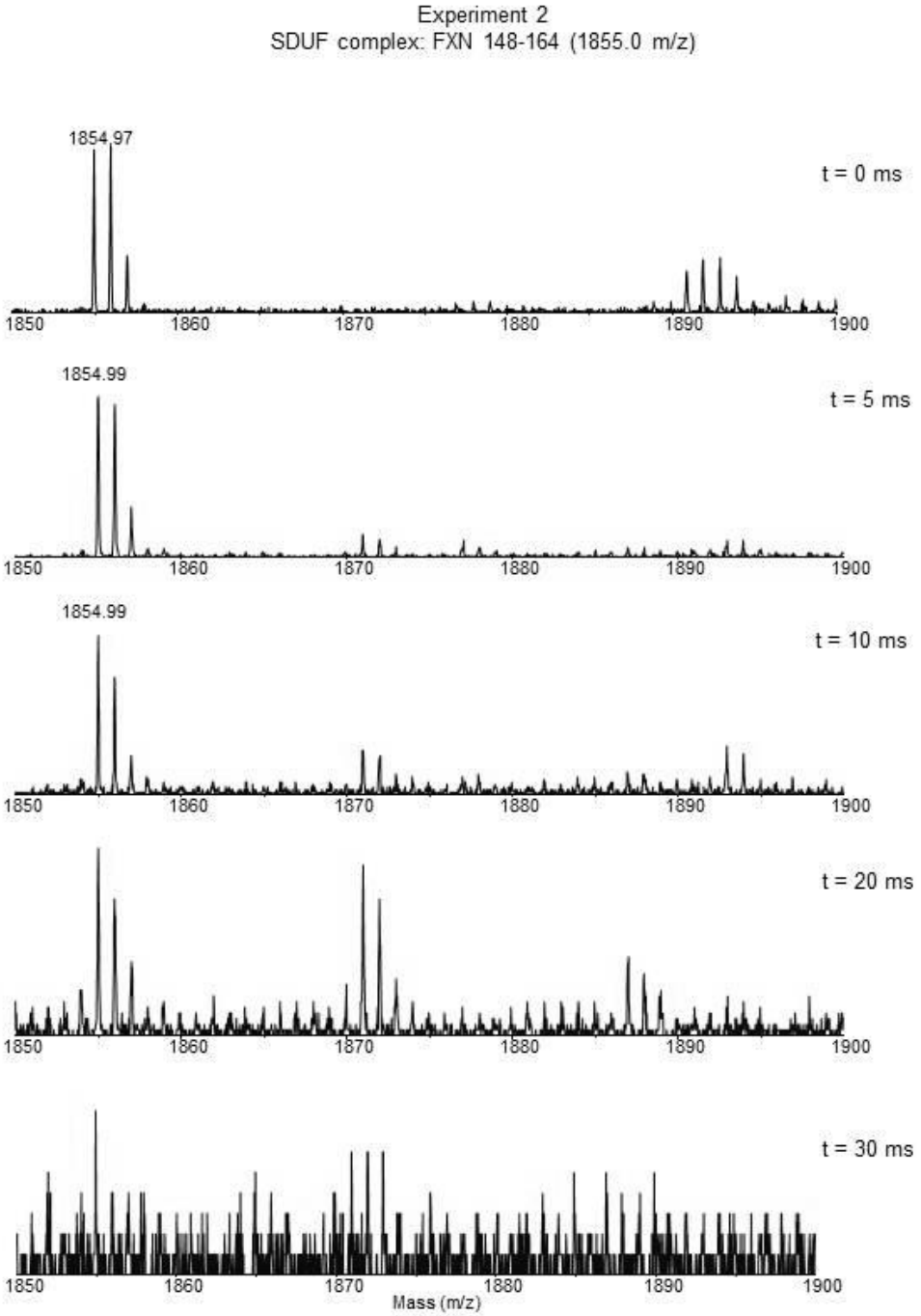

A-105. Mass spectra from SDUF, Experiment 2 at various exposure time to hydroxyl radicals.

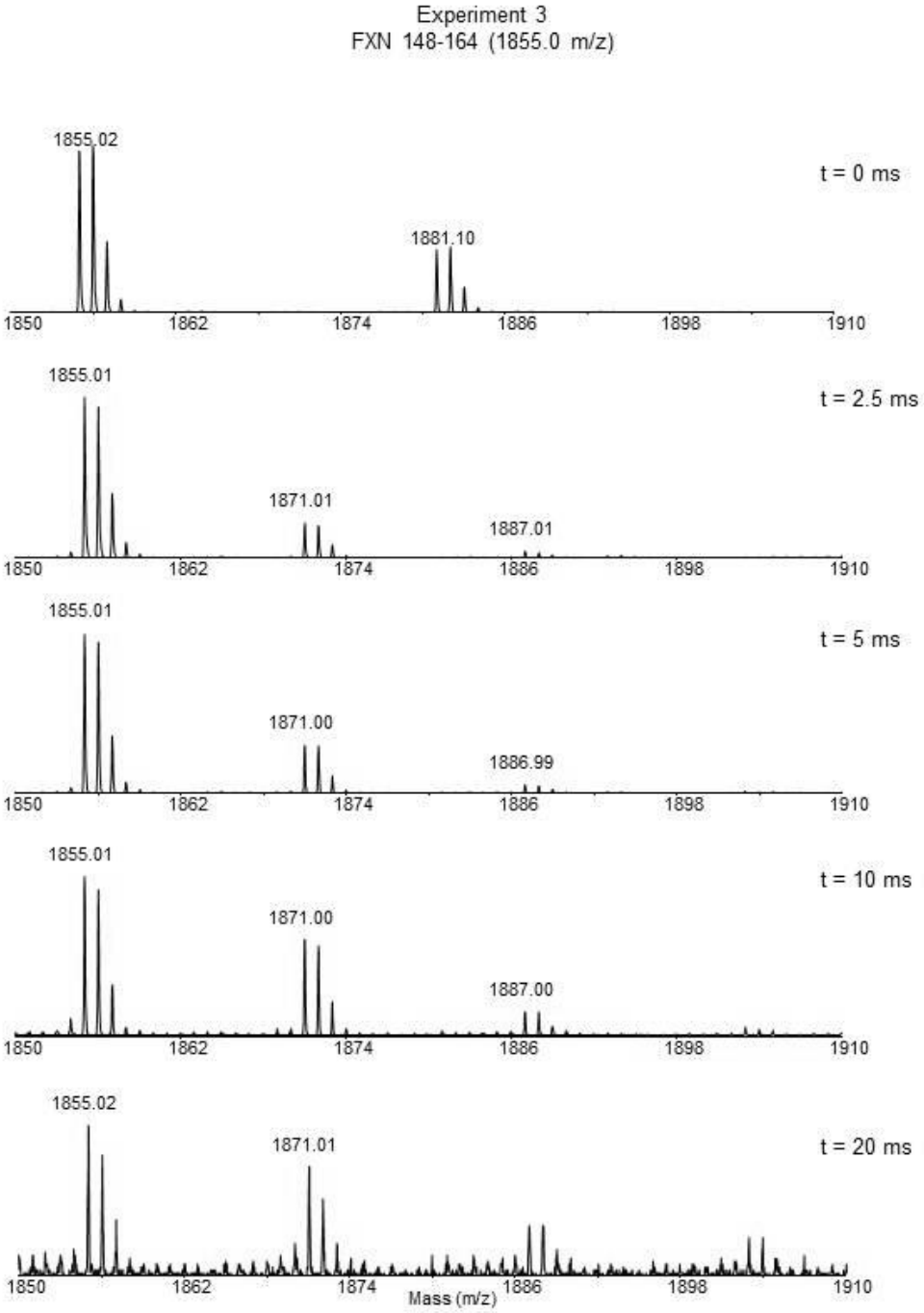

A-106. Mass spectra from FXN, Experiment 3 at various exposure time to hydroxyl radicals.

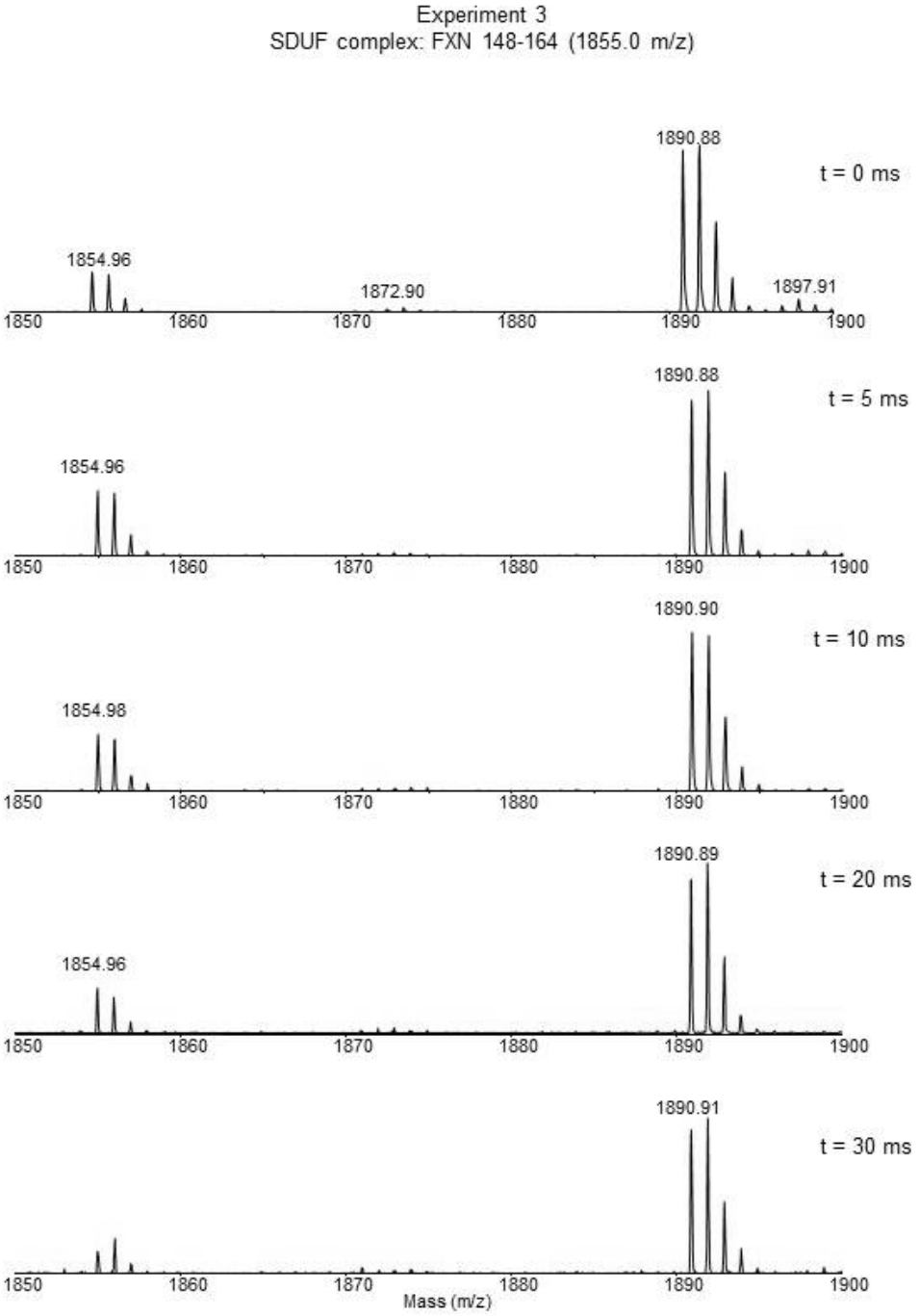

A-107. Mass spectra from SDUF, Experiment 3 at various exposure time to hydroxyl radicals.

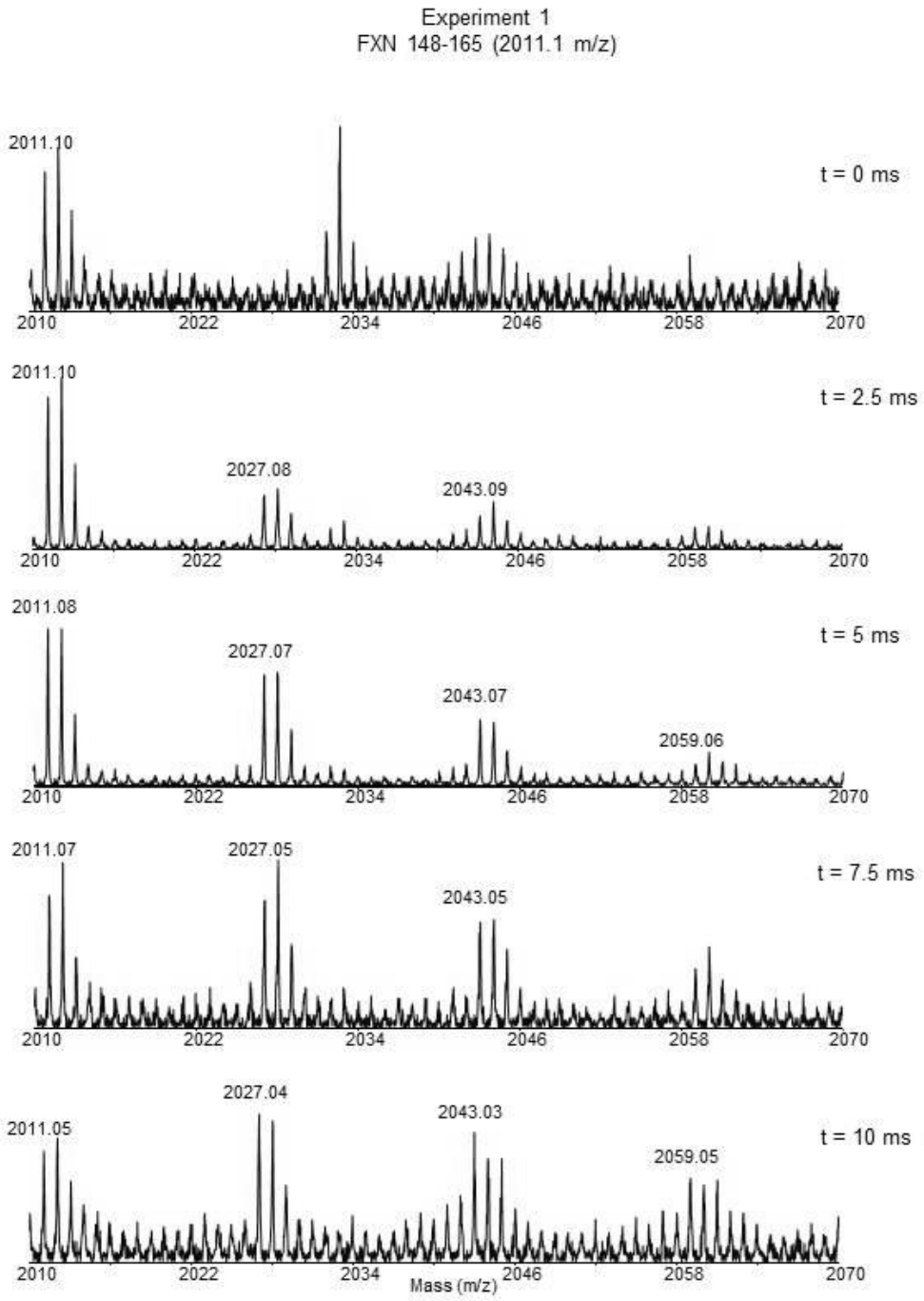

A-108. Mass spectra from FXN, Experiment 1 at various exposure time to hydroxyl radicals.

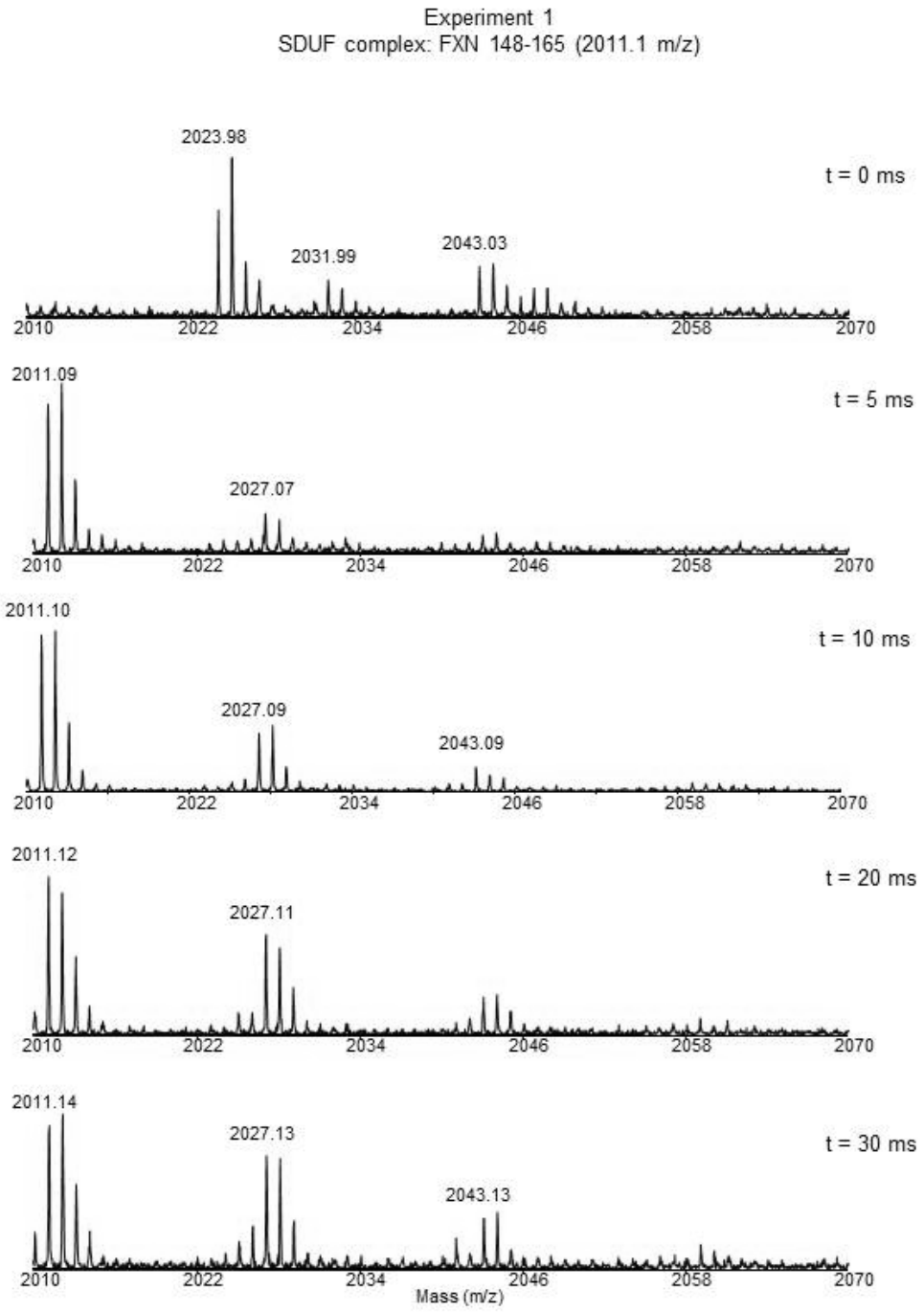

A-109. Mass spectra from SDUF, Experiment 1 at various exposure time to hydroxyl radicals.

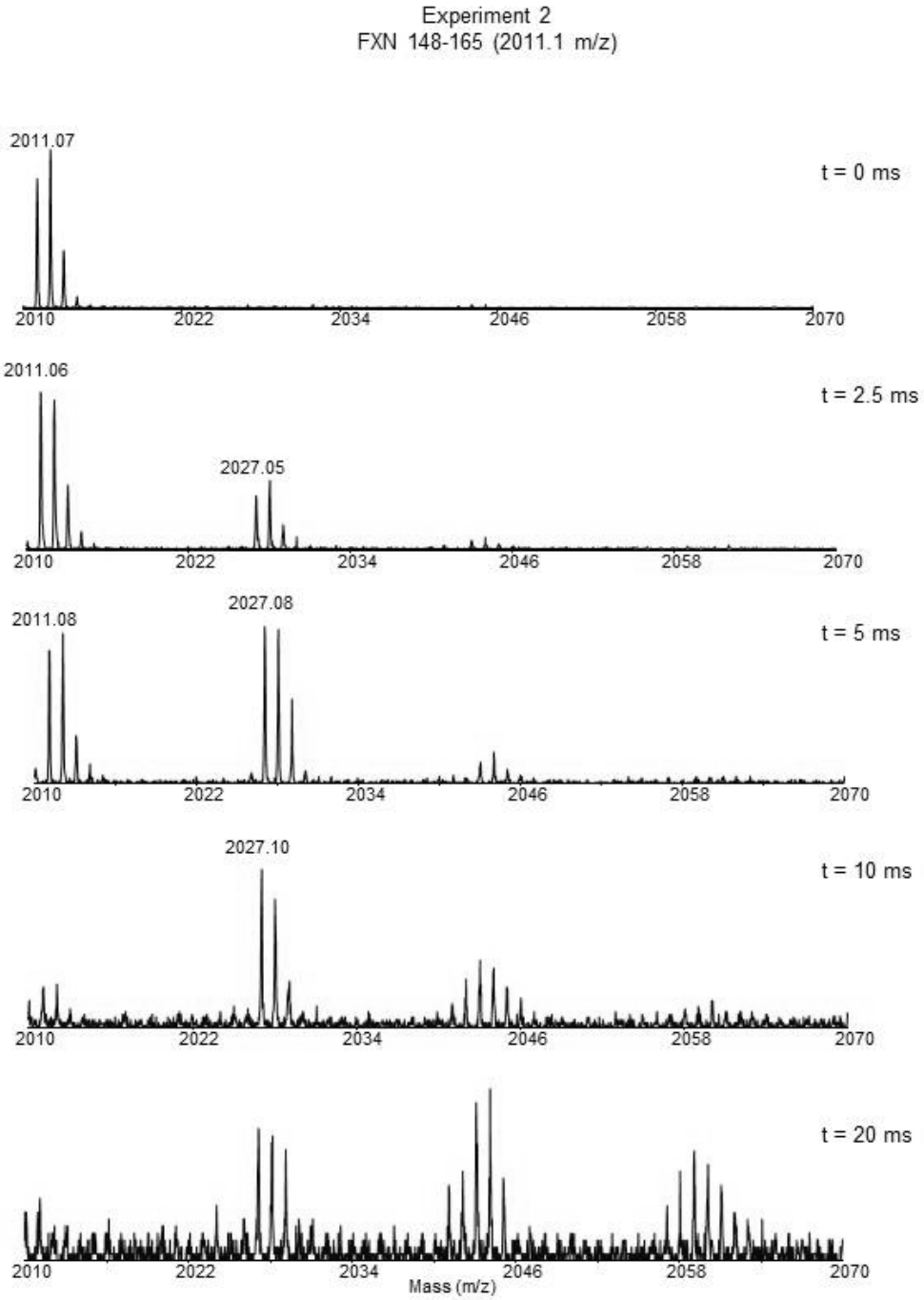

A-110. Mass spectra from FXN, Experiment 2 at various exposure time to hydroxyl radicals.

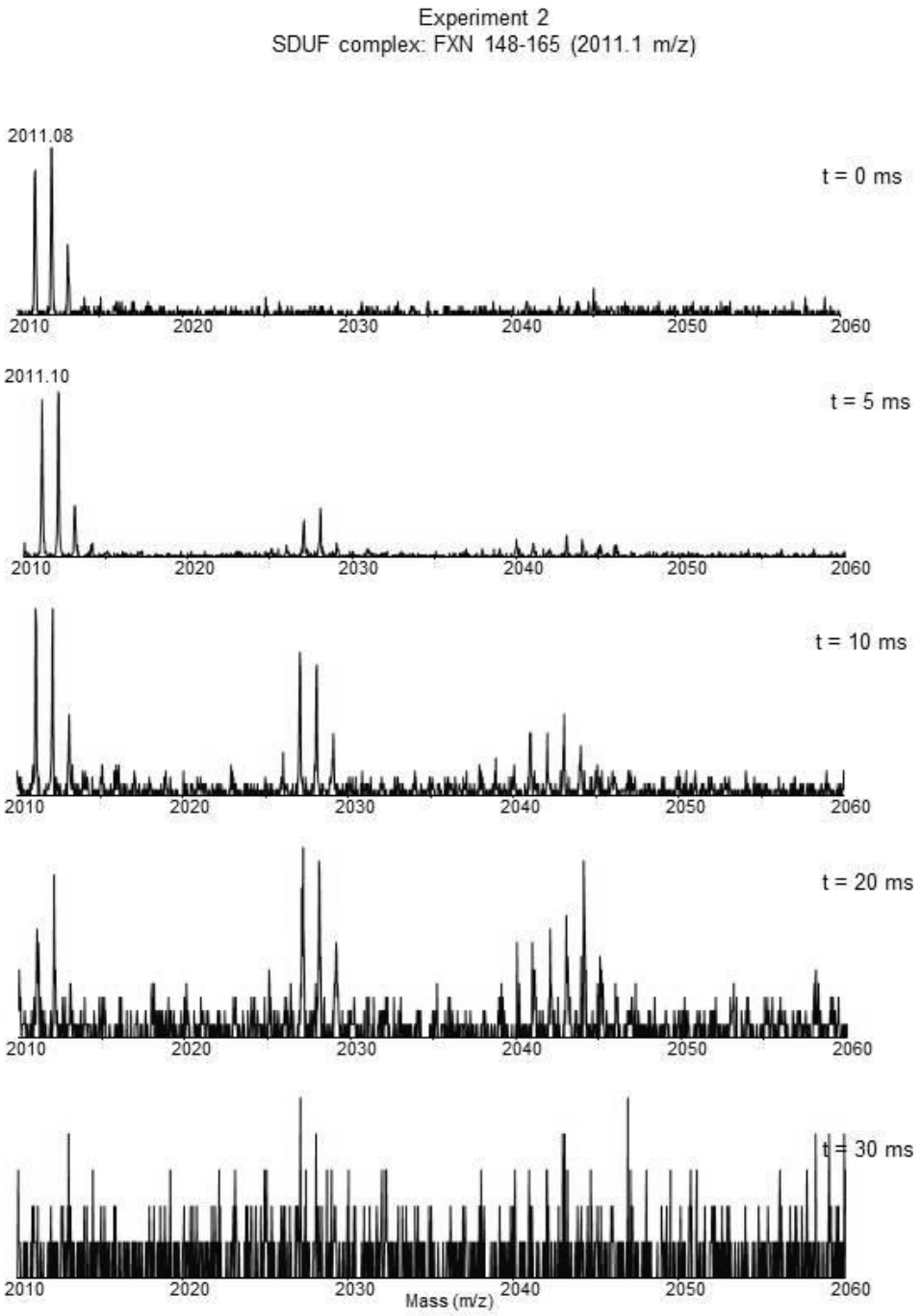

A-111. Mass spectra from SDUF, Experiment 2 at various exposure time to hydroxyl radicals.

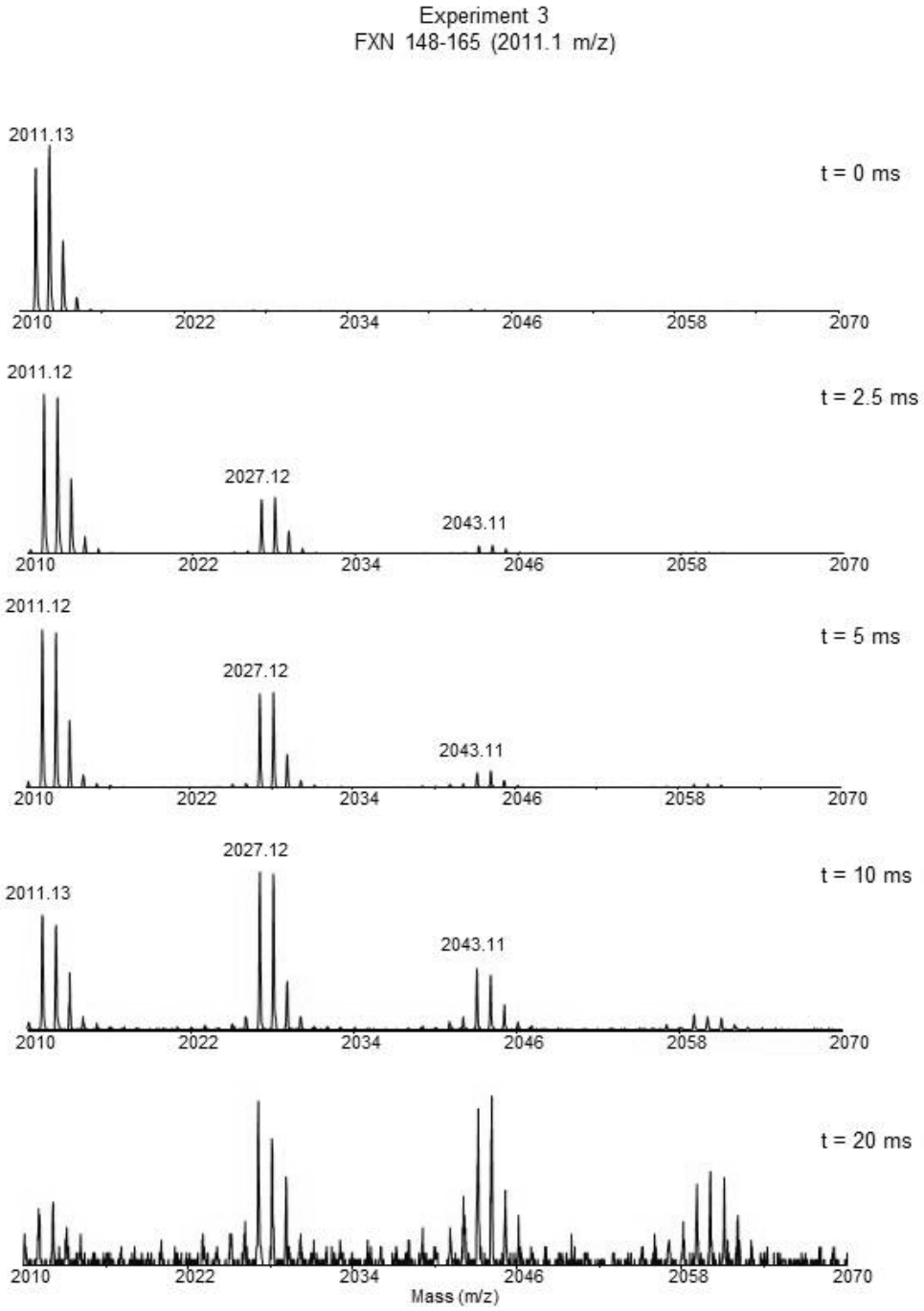

A-112. Mass spectra from FXN, Experiment 3 at various exposure time to hydroxyl radicals.

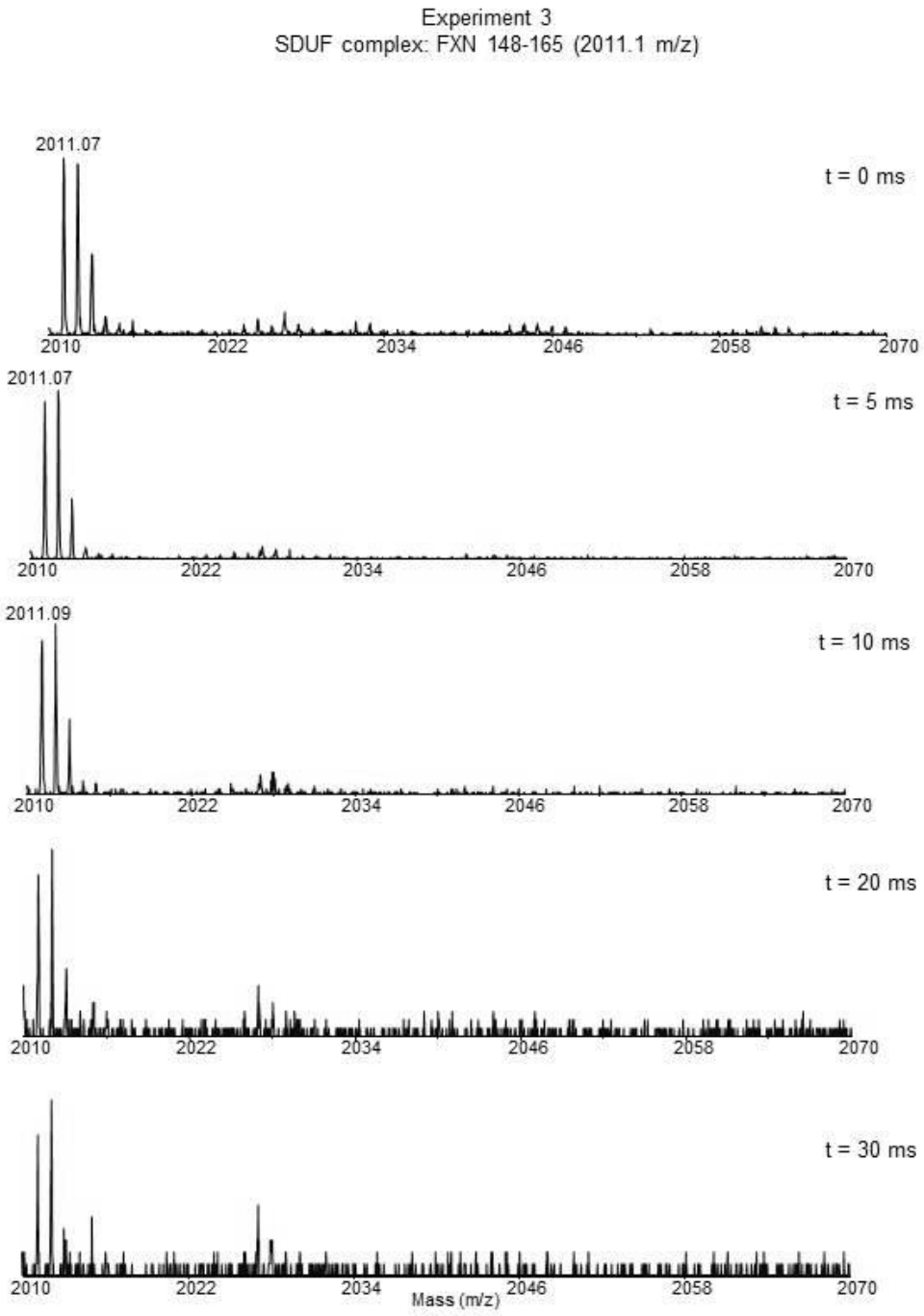

A-113. Mass spectra from SDUF, Experiment 3 at various exposure time to hydroxyl radicals.

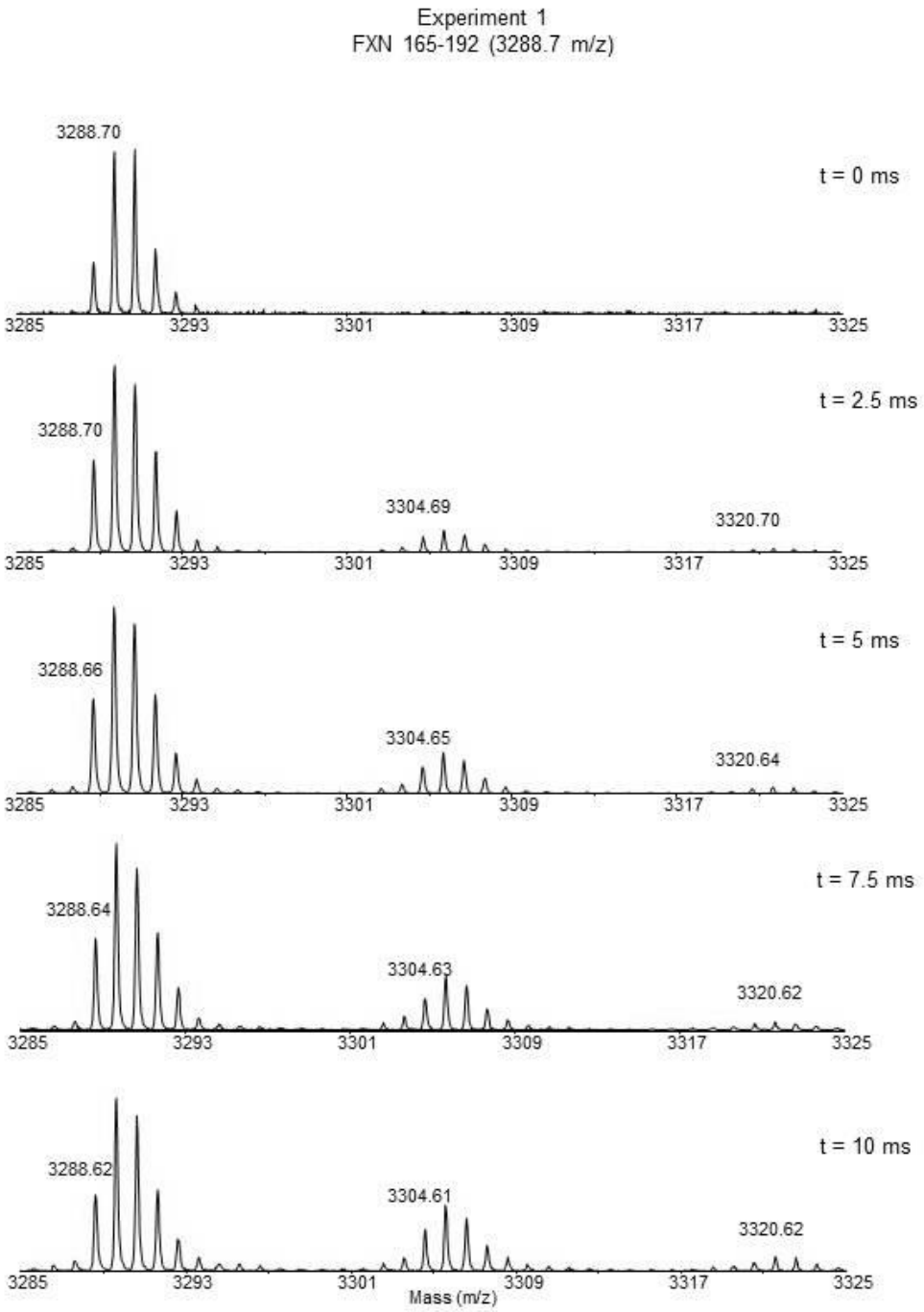

A-114. Mass spectra from FXN, Experiment 1 at various exposure time to hydroxyl radicals.

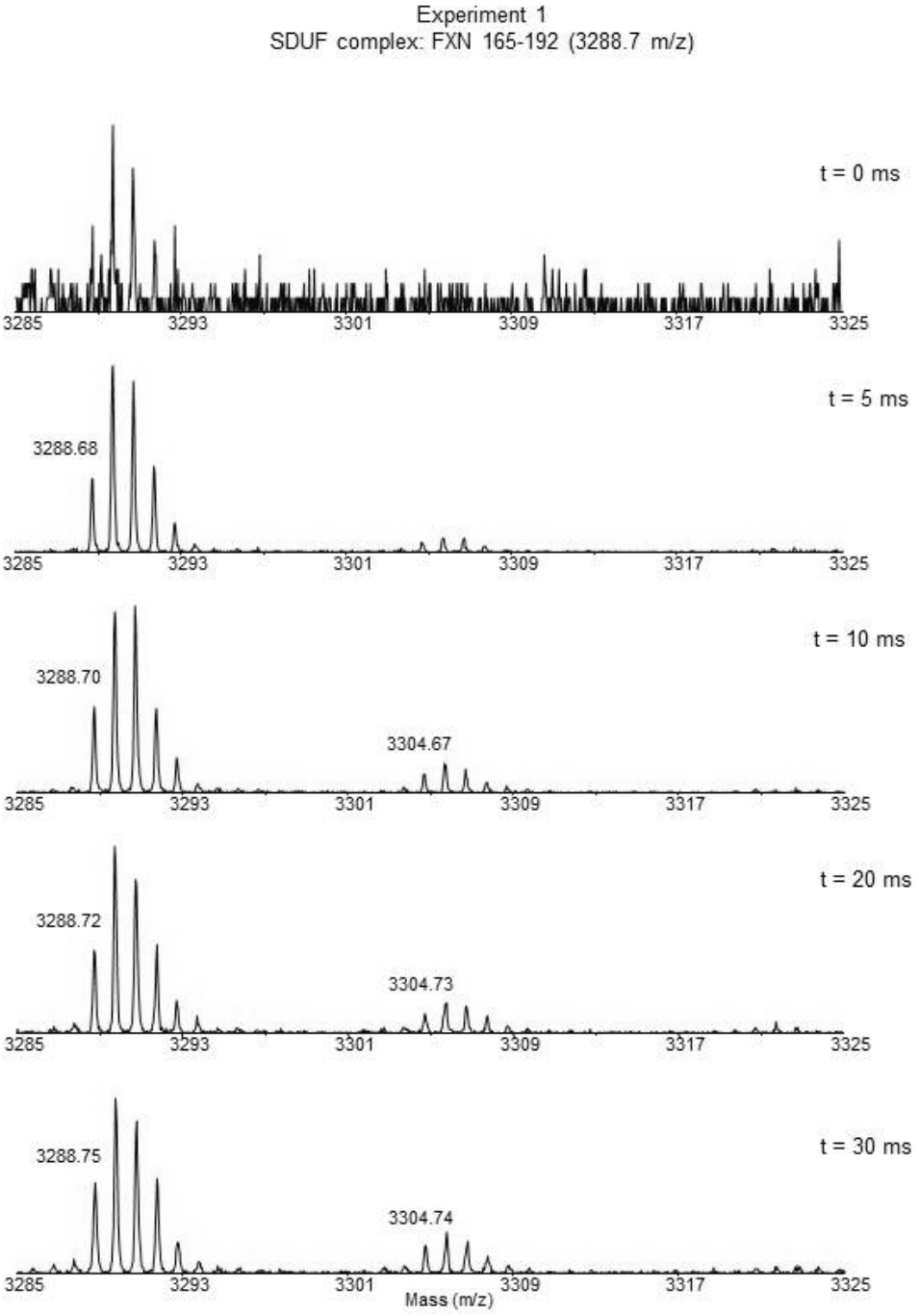

A-115. Mass spectra from SDUF, Experiment 1 at various exposure time to hydroxyl radicals.

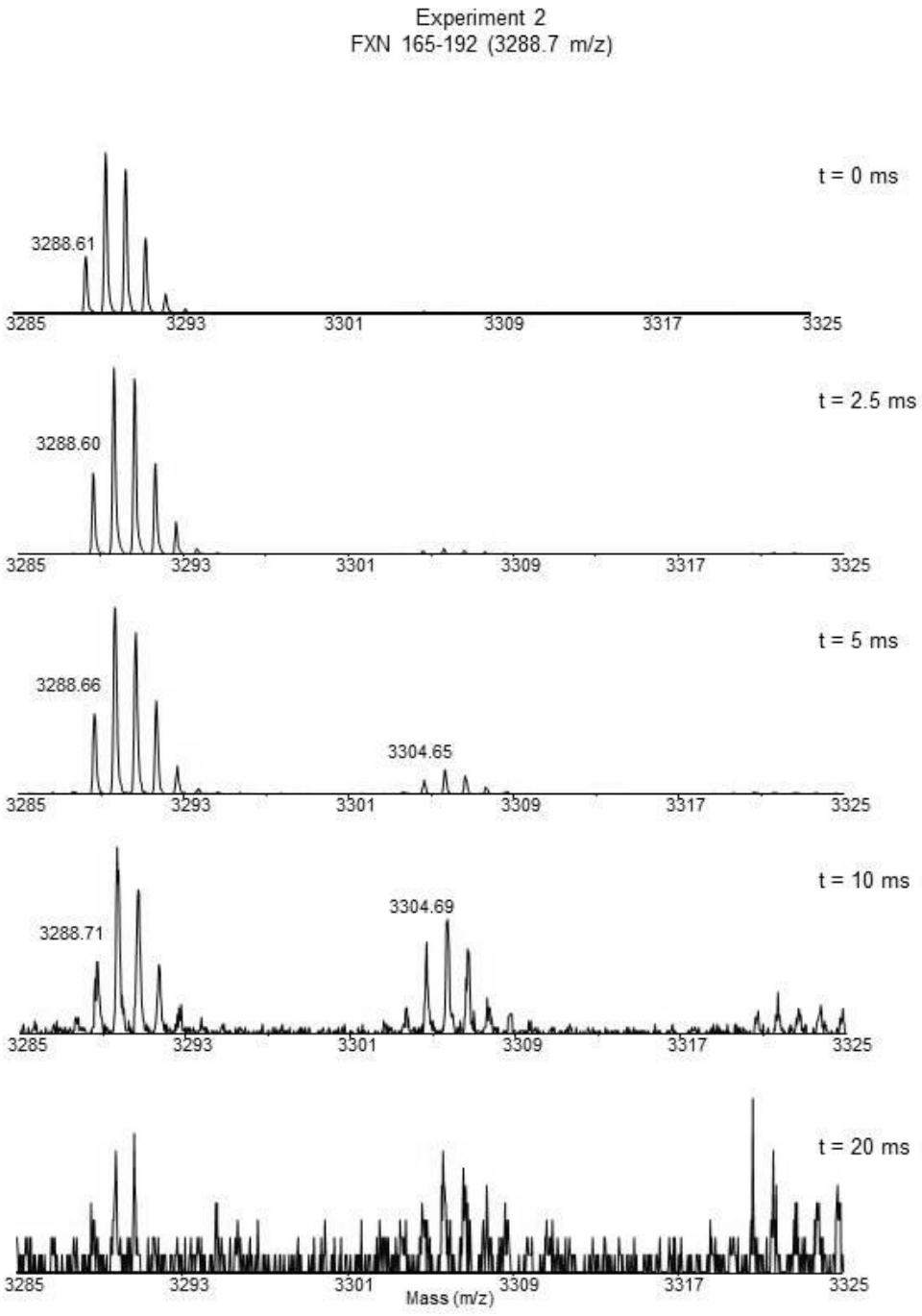

A-116. Mass spectra from FXN, Experiment 2 at various exposure time to hydroxyl radicals.

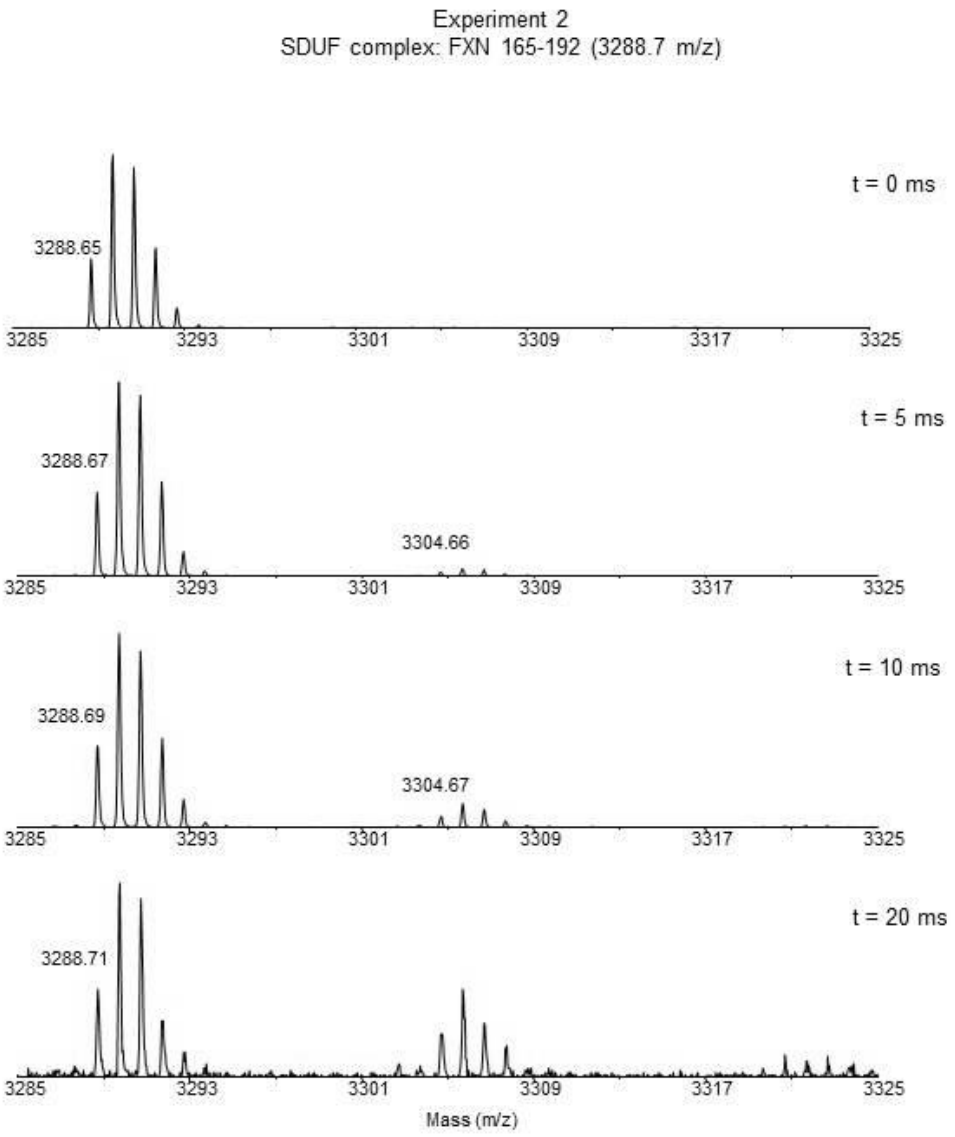

A-117. Mass spectra from SDUF, Experiment 2 at various exposure time to hydroxyl radicals.

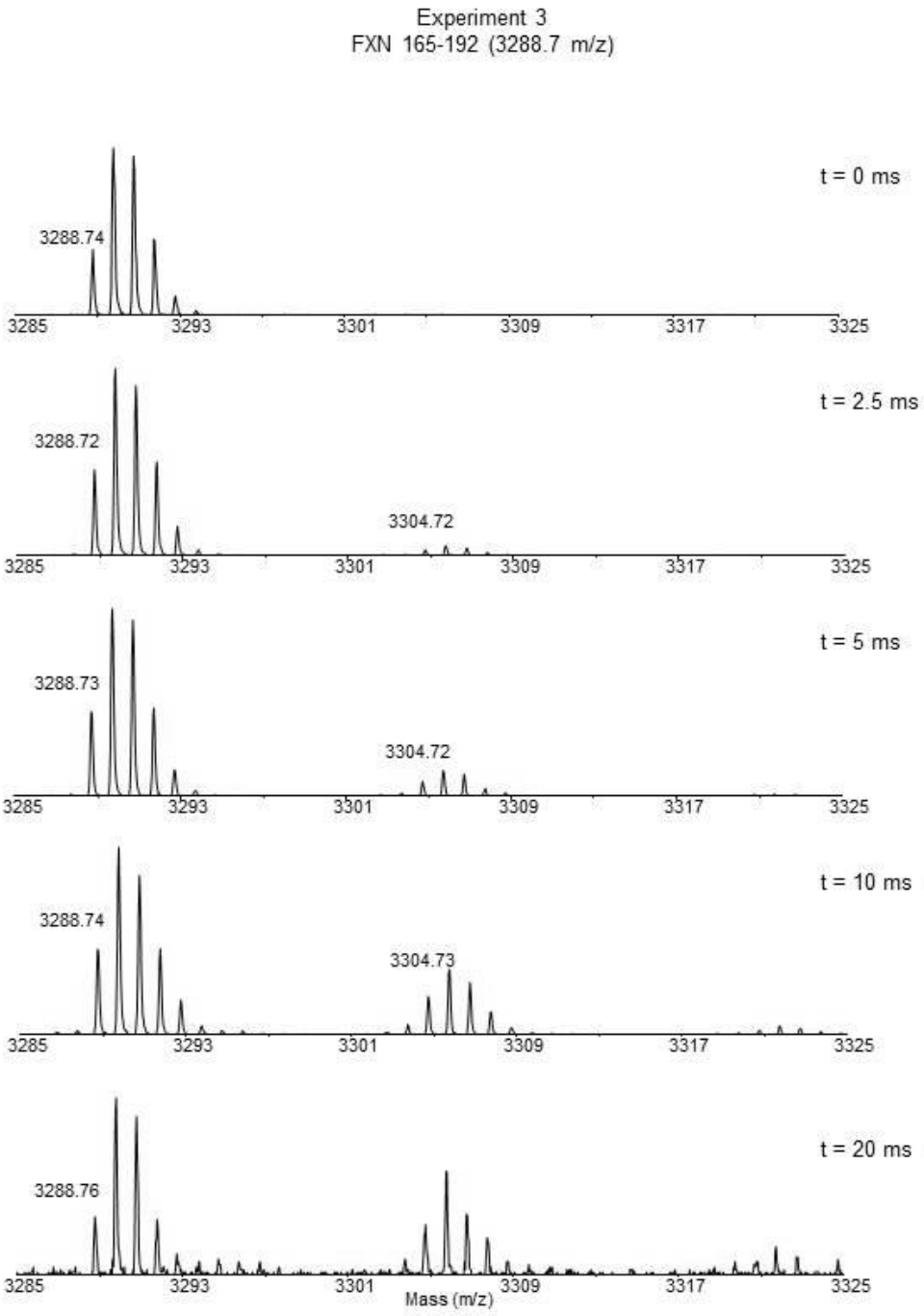

A-118. Mass spectra from FXN, Experiment 3 at various exposure time to hydroxyl radicals.

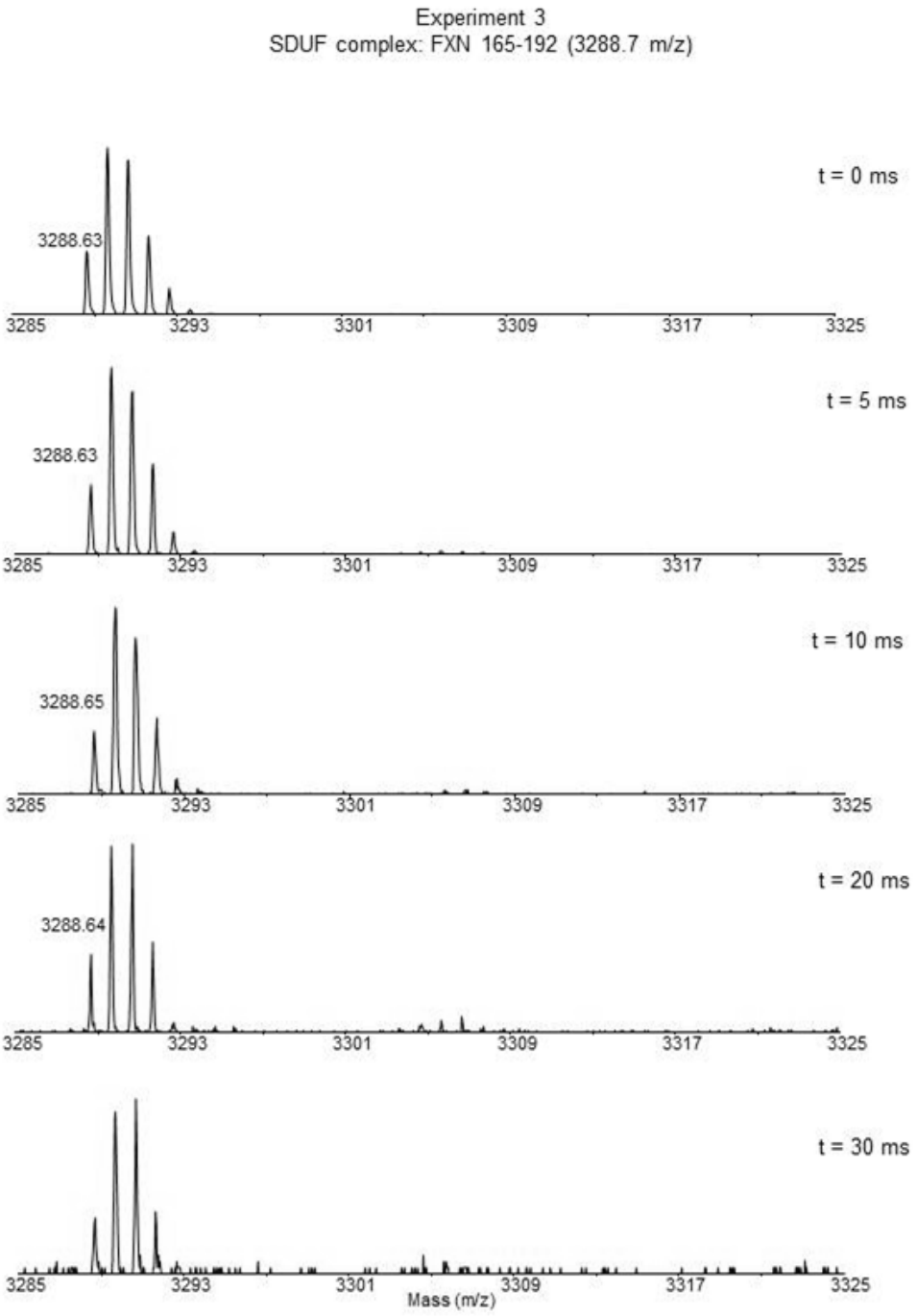

A-119. Mass spectra from SDUF, Experiment 3 at various exposure time to hydroxyl radicals.